PERFORMANCE OF INJECTION-MOULDED CARBON NANO-TUBE POLYPROPYLENE ASYMMETRIC GEARS

A thesis
submitted in partial fulfillment of the
requirements for the degree of

DOCTOR OF PHILOSOPHY

by

A. JOHNNEY MERTENS
(126103014)

DEPARTMENT OF MECHANICAL ENGINEERING
INDIAN INSTITUTE OF TECHNOLOGY GUWAHATI
GUWAHATI–781039
JULY 2016

CERTIFICATE

It is certified that the work contained in the thesis entitled **Performance of Injection-Moulded Carbon Nano-Tube Polypropylene Asymmetric Gears** by **A. Johnney Mertens**, a student in the Department of Mechanical Engineering, Indian Institute of Technology Guwahati, Guwahati, India, for the award of the degree of **Doctor of Philosophy** has been carried out under my supervision and this work has not been submitted elsewhere for the degree.

Dr. S. Senthilvelan
Associate Professor
Department of Mechanical Engineering
Indian Institute of Technology Guwahati
Guwahati – 781039, Assam, India.

ACKNOWLEDGEMENTS

I would like to express my sincere, heartiest thanks and gratitude to my research supervisor and well-wisher, **Dr. S. Senthilvelan** for his valuable guidance and steady encouragement throughout my Ph.D. work. His constant encouragement, enormous goodwill and unruffled patience made me work at ease and kept me highly motivated throughout my stay with him. His innovative ideas and consistent support by extending all the necessary facilities are helpful in successful completion of my research work. I have immensely benefited from each and every moment of my association with him.

I would like to acknowledge **Prof. P. S. Robi, Dr. S. Kanagaraj** and **Prof. G. Pugazhenthi** members of my Doctoral Committee who have directed me in right path by providing comments, suggestions and sharing their expertise at various stages of my experimental work.

I thank the **Honourable Director**, **IIT Guwahati** and the **Head, Department of Mechanical Engineering, IIT Guwahati** for their support during the course of my research work. I extend my sincere thanks to colleague **Mr. M. Kodeeswaran, ISRO-VSSC, Thiruvananthapuram** for his valuable support and suggestions throughout the course of my thesis work.

I would like to thank **Mr. N. K. Das** and his associates for helping me during the fabrication processes in the workshop. Especially I would like to thank **Mr. Mrinal Sarma, Fitting Shop** who patiently helped me throughout my experimental work. I am very grateful to the technical staff of Mechanical Engineering Department, **Mr. Sanjib Sarma, Mr. Jiten Basumatary, Mr. Nip Borah, Mr. Saiffuddin Ahmed, Mr. Pranjol Paul, Mr. Dhruba Jyoti Bordoloi** and **Mr. Rituraj Saikia** for their contribution and help throughout my research work. I am also thankful to the Mechanical Department office staffs **Mr. Nabajyoti Dutta** and **Mr. Raju Talukdar** who have supported me in the academic and administration works.

I am thankful to my seniors and lab colleagues **Mr. R. Kalidasan, Mr. A. Muthuraja, Mr. Nitin S. Sarpe, Mr. Ravi Shankar Shukla, Mr. Anurag Mishra, Ms. Arnika Verma, Ms. Sarita Bharti, Mr. Karthik Pandian** and **Mr. Kishor Kumar Gajrani** for their valuable help in my thesis work**.** I am grateful to the members of Materials Science Lab **Dr. S. Arun, Mr. Avanish Kunwar Verma, Mr. Devarshi Kashyap, Mr. M. Charan** and **Mr. P. Kishore Kumar** for their help throughout the course of experimental work. **Dr. V. Satheesh Kumar** and **Mr. R. Vignesh Babu** needs a special mentioning for providing valuable and timely help during the research work. I also thank my Department colleagues who rendered direct and indirect support in my work.

I owe my gratitude to **Dr. Vimal Katiyar**, **COE-SUSPOL** and his students **Mr. Narendren** and **Mr. Surendra Singh Gaud** for their help in characterisation work. I am also deeply grateful to Chemical Department students **Mr. Manish Kumar, Mr. R. Vinoth Kumar** and **Mr. Kelothu Suresh** for their assistance during the materials characterisation. I thank **Central Instruments Facility, IIT Guwahati** for permitting to utilize their resources throughout the thesis work.

It has been a great pleasure to work with my research colleagues and friends **Mr. N. Sivaramkrishnan, Mr. Hakeem Niyas, Mr. Gururaj Bolar, Mr. P. Vivek Selvan, Mr. Ambesh Kumar, Mr. Rasmi Ranjan Behera, Mr. R. Nithin Narmada, Mr. N. Balasubramani, Mr. K. Vigneshwaran, Mr. M. Vijay, Mr. R. Suresh, Ms. J. Sumitha Banu, Mr. Philip Bernstein Saynik, Ms. Monisha Javadi, Ms. G. Padmavathi** and **Ms. G. Janani,** I thank all of them for helping me directly and indirectly to complete my work.

I wish to extend my deepest gratitude to my parents and brother **Mr. Y. Alexis**, **Mrs. S. Maria Gunaseeli** and **Mr. A. Joyson Albino** for their love, affection and cooperation throughout my research work. Finally, I extend my gratitude to the **Almighty** for giving me this opportunity and good health for the successful completion of this breakthrough in my carrier.

A. Johnney Mertens

ABSTRACT

KEYWORDS: Polymer gear; surface temperature; air cooling; surface topology; tribology; fatigue; carbon nano-tube; asymmetric profile

Polymer composite gears are being utilized in many engineering applications due to their light weight, self-lubrication, cost effectiveness, and mass production capabilities. However, thermal sensitive mechanical properties of the polymers limit their extended usage. During service, polymer gears generate heat caused by repetitive tooth surface interaction and material hysteresis. In this work, an attempt was made to investigate the potential of using air cooling, asymmetric tooth profile and carbon nano-tube (CNT) reinforcement in polypropylene gears to enhance the performance.

Performance of injection-moulded polypropylene (PP) gear was evaluated with and without air cooling, using in-house developed power absorption gear test rig. Measurement of gear weight and periodical measurement of tooth thickness confirmed the enhancement of wear resistance by the air cooling. Continuous measurement of gear tooth surface temperature and worn out gear surface image confirmed significant enhancement of gear life by air cooling. Air cooling has slightly increased transmission efficiency of the gear pair.

The effect of mating gear surface roughness and manufacturing process, wire-cut electric discharge machining (WEDM) and conventional hobbing over the injection-moulded polypropylene gear performance was investigated. Test gear exhibited improved wear resistance when paired with conventional hobbed steel gear compared to the WEDM steel gear. At higher load, thermal fatigue failure and excessive wear was exhibited by test gear when paired with WEDM and hobbed gear respectively.

Injection-moulded asymmetric polypropylene gears were evaluated by pairing with three asymmetric steel gears having different surface roughness. Test gears paired with steel gear having higher surface roughness exhibited higher net surface temperature and inferior wear resistance.

Durability of the injection-moulded symmetric (20/20) and asymmetric (34/20) gears were evaluated to understand the effect of drive side pressure angle. Test gears exhibited wear and plastic tooth deformation at lower and higher loads respectively. The increased radial distance of highest point of single tooth contact point and decreased contact ratio contributed to the poor performance of asymmetric gears.

The mechanical, tribological, and thermal behaviour of various (1–5 wt%) carbon nano-tube reinforced polypropylene was evaluated. Hardness and wear resistance has increased upto 1 wt% CNT-PP and decreased beyond 1 wt% due to the agglomeration. 1 wt% CNT–PP composite gear was injection-moulded and its performance was compared with unreinforced polypropylene gear. 1 wt% CNT–PP gears exhibited lower surface temperature and slightly higher transmission efficiency. Carbon nano-tube reinforcement has improved the test gear wear resistance and fatigue life.

TABLE OF CONTENTS

ACKNOWLEDGEMENTS ..... **i**

ABSTRACT ..... **iii**

LIST OF FIGURES ..... **xi**

LIST OF TABLES ..... **xxi**

LIST OF EQUATIONS ..... **xxiii**

ABBREVIATIONS ..... **xxv**

NOTATIONS ..... **xxvii**

CHAPTER 1 INTRODUCTION

1.1 Overview on Polymer and Polymer Composite Gears 1

1.2 Motivation 2

1.3 Objectives 3

1.3.1 Methodology 3

1.4 Organisation of the Thesis 4

CHAPTER 2 LITERATURE SURVEY

2.1 Introduction 7

2.2 Polymer Gear 8

2.3 Polymer Composite Material 11

2.4 Polymer Composite Gear 11

2.5 Carbon Nano-Tube Based Polymer Material 14

2.5.1 Mechanical Properties 14

2.5.2 Tribological Properties 15

2.6 Carbon Nano-Tube Based Polypropylene Material 17

2.7 Surface Roughness Effect on the Polymer and Polymer Gear Tribology 19

2.8 Asymmetric Gear 22

2.9 Summary 24

CHAPTER 3 MATERIALS AND METHODOLOGY

3.1 Introduction 27

3.2 Materials and Processing Conditions 27

3.3 Polymer Composite Performance 29

3.4 Polymer and Polymer Composite Gear 30

3.4.1 Gear Test Rig Details 32

3.4.2 Gear Test Details 33

3.5 Summary 34

CHAPTER 4 EFFECT OF AIR COOLING ON POLYMER GEAR PERFORMANCE

4.1 Introduction 35

4.2 Methodology 35

4.3 Gear Surface Temperature 37

4.4 Gear Tooth Wear 42

4.4.1 Gear Tooth Profile Wear 44

4.4.2 Worn out Morphology of Test Gear at Various Stages of Service 45

4.4.3 Effect of Air Cooling over the Worn out Morphology of the Test Gear 46

4.5 Transmission Efficiency 50

4.6 Summary 52

CHAPTER 5 EFFECT OF MATING STEEL GEAR MANUFACTURING PROCESS OVER THE PERFORMANCE OF INJECTION-MOULDED POLYPROPYLENE GEAR

5.1 Introduction 53

5.2 Methodology 55

5.3 Surface Morphology 56

5.4 Micro Hardness 61

5.5 Gear Surface Temperature 62

5.6 Gear Tooth Wear 66

5.7 Worn out Surface Morphology 67

5.8 Summary 70

CHAPTER 6 EFFECT OF MATING STEEL GEAR SURFACE OVER THE PERFORMANCE OF INJECTION-MOULDED POLYPROPYLENE GEAR

6.1 Introduction 71

6.2 Methodology 72

6.3 Surface Morphology of Gears 74

6.4 Gear Surface Temperature 78

6.5 Gear Tooth Wear 80

6.6 Worn out Surface Morphology 80

6.7 Friction and Wear Performance of Polypropylene 83

6.8 Summary 87

CHAPTER 7 INJECTION-MOULDED ASYMMETRIC POLYPROPYLENE GEAR PERFORMANCE

7.1 Introduction 89

7.2 Methodology 90

7.3 Gear Surface Temperature 91

7.4 Gear Tooth Wear 93

7.4.1 Symmetric Vs Asymmetric – Tooth Wear 94

7.4.2 Worn out Morphology of Test Gears 96

7.4.3 Gear Tooth Profile Wear 98

7.5 Plastic Deformation 99

7.5.1 Symmetric Vs Asymmetric – Plastic Deformation 102

7.6 Performance 105

7.7 Static Gear Tooth Deflection 106

7.8 Summary 107

CHAPTER 8 MECHANICAL AND TRIBOLOGICAL PERFORMANCE OF CNT–PP COMPOSITES

8.1 Introduction 109

8.2 Methodology 109

8.3 Mechanical Properties 111

8.3.1 Structural Properties 111

8.3.2 Fractography of Tensile Specimen 114

8.3.3 Hardness 118

8.4 Tribological Properties 119

8.4.1 Friction and Wear Measurements 119

8.4.2 Wear Morphology 123

8.4.3 Frictional Heating 127

8.5 Thermal Characteristics 131

8.5.1 Thermal Conductivity 134

8.6 Summary 135

CHAPTER 9 SURFACE DURABILITY OF INJECTION-MOULDED CARBON NANOTUBE–POLYPROPYLENE SPUR GEARS

9.1 Introduction 137

9.2 Methodology 137

9.3 Properties of Test Gear Materials 138

9.4 Gear Surface Temperature 139

9.5 Transmission Efficiency 142

9.6 Gear Tooth Wear 143

9.7 Gear Tooth Profile Wear 144

9.8 Performance 147

9.9 Gear Damage Morphology 148

9.10 Summary 153

CHAPTER 10 SUMMARY AND CONCLUSIONS

10.1 Summary 155

10.2 Conclusions 155

10.3 Future Scope 157

REFERENCES 159

LIST OF PUBLICATIONS BASED ON THE RESEARCH WORK 177

CURRICULUM VITAE 179

LIST OF FIGURES

Figure	Title	Page No.
3.1	Injection-mouldable pellets (a) Master batch CNT–PP, (b) PP, (c) PP–g–MA, and (d) developed CNT–PP composite (1 wt% CNT–PP)	28
3.2	Test gear geometry and dimension	31
3.3	Injection-moulding die	31
3.4	In-house developed power absorption gear test rig	32
3.5	Schematic of power absorption gear test rig	32
4.1	In-house developed power absorption gear test rig: (a) overall view and (b) close-up view of gear mesh and compressed air supply in the test rig	36
4.2	Thermograph of the test gear during testing (3 Nm, without cooling)	37
4.3	Measured surface temperature of the test gear through IR camera and sensor (3 Nm, with cooling)	38
4.4	Effect of load on the surface temperature of the test gear	38
4.5	Surface temperature of the test gear with and without cooling (3 Nm)	39
4.6	Effect of cooling on the surface temperature of the test gear	40
4.7	Gear tooth surface temperature: predicted and measured	41
4.8	Gear tooth thickness reduction during testing	42
4.9	Effect of cooling on the wear resistance of the test gear	43

4.10 Gear tooth profile observed under profile projector: (a) 2 Nm after 10×10^5 cycles and (b) 2.5 Nm after 7.2×10^5 cycles 44

4.11 Surface of test gear tooth loaded at 2.5 Nm (without cooling) after (a) 1.4×10^5 cycles, (b) 2.8×10^5 cycles, (c) 4.3×10^5 cycles, (d) 5.7×10^5 cycles, and (e) 7.2×10^5 cycles..... 46

4.12 Surface of gear tested at 2 Nm after 10×10^5 cycles: (a) test gear without cooling, (b) close-up view of test gear without cooling, (c) test gear with cooling, and (d) close- up view of test gear with cooling..... 47

4.13 Surface of gear tested at 2.5 Nm after 7.2×10^5 cycles: (a) test gear without cooling, (b) close-up view of test gear without cooling, (c) test gear with cooling, and (d) close-up view of test gear with cooling..... 48

4.14 Surface of gear tested at 3 Nm after 1.4×10^5 cycles: (a) test gear without cooling, (b) close-up view of test gear without cooling, (c) test gear with cooling, (d) close-up view of test gear with cooling, (e) abrasive wear marks on gear tested without cooling, and (f) plastic deformation near the pitch region of gear tested without cooling..... 49

4.15 Transmission efficiency of test gear pair with and without cooling tested at (a) 2 Nm, (b) 2.5 Nm, and (c) 3 Nm..... 51

5.1 Mating gear tooth surface manufactured by (a) conventional machining, (b) wire-cut electric discharge machining, and (c) Injection-moulded polypropylene gear showing tooth profile..... 56

5.2 Scanning electron micrographs of gear tooth surface manufactured by (a–b) conventional machining and (c–d) wire-cut electric discharge machining 57

5.3 XRD spectrum of conventional machined and WEDM surface..... 58

5.4 Micro graph of gear tooth surface (a–b) machined surface and (c–d) WEDM surface 59

5.5 Three dimensional profiler image of (a) conventional machined gear tooth surface and (b) gear tooth surface manufactured by WEDM 59

5.6 Bearing ratio curve of mating steel gears 60

5.7 Measured micro hardness of the considered counter gear surface 61

5.8 Measured surface temperature of the test gears when paired with conventional machined gear and WEDM gear at (a) 2 Nm, (b) 2.5 Nm, and (c) 3 Nm 63

5.9 Schematic view of gear tooth contact stress 65

5.10 Measured gear tooth wear 66

5.11 Measured weight loss of the polymer gear 67

5.12 Worn out of test gear at 2 Nm against (a) conventional machined gear (after 10.08×10^5 cycles) and (b) WEDM gear (after 4.32×10^5 cycles) 68

5.13 Worn out of test gear at 2.5 Nm against (a) conventional machined gear (after 7.20×10^5 cycles) and (b) WEDM gear (after 2.88×10^5 cycles) 68

5.14 Worn out of test gear at 3 Nm against (a) conventional machined gear (after 1.44×10^5 cycles) and (b) WEDM gear (after 1.54×10^5 cycles) 69

5.15 Close-up view of the test gear at 3 Nm against (a) conventional machined gear (after 1.44×10^5 cycles) and (b) WEDM gear (after 1.54×10^5 cycles) 69

6.1 Test gear details 72

6.2 View of the machined steel gears (a) newly machined gear, (b) run against polymer gear for 5×10^5 cycles, and (c) run against polymer gear for 10×10^5 cycles 73

6.3 (a) Surface profile of injection-moulded polypropylene gear tooth, (b) surface profile of steel gear A tooth, (c) surface profile of steel gear B tooth, and (d) surface profile of steel gear C tooth 75

6.4 (a) Three-dimensional surface image of steel gear C tooth, (b) two-dimensional surface depth of steel gear C tooth, and (c) estimated bearing ratio curve of steel gear C tooth 76

6.5 Bearing ratio curve of the steel gears A, B, and C tooth 77

6.6 (a) Measured surface temperature of polymer gear at 2.5 Nm load and (b) maximum surface temperature of polymer gears when paired with different steel gears A, B, and C 79

6.7 Gear tooth thickness reduction 80

6.8 Worn out polymer gear when paired with (a) steel gear A, (b) steel gear B, and (c) steel gear C at 2 Nm after 48×10^3 cycles (3600 s and 800 rev/min) 81

6.9 Worn out polymer gear when paired with (a) steel gear A, (b) steel gear B, and (c) steel gear C at 2.5 Nm after 48×10^3 cycles (3600 s and 800 rev/min) 82

6.10 Worn out polymer gear when paired with (a) steel gear A, (b) steel gear B, and (c) steel gear C at 3 Nm after 48×10^3 cycles (3600 s and 800 rev/min) 83

6.11 View of counter steel disc A and B 83

6.12 (a) Surface profile of injection-moulded polypropylene specimen, (b) surface profile of steel disc A, and (c) surface profile of steel disc B 84

6.13 Bearing ratio curve of discs A and B 85

6.14 Net surface temperature of polypropylene pin when slid against steel disc A and B 85

6.15 Friction coefficient of polypropylene pin against steel disc A and B 86

6.16 (a) Worn out surface of polypropylene pin when slid against steel disc A and (b) worn out surface of polypropylene pin when slid against steel disc B 87

7.1 Injection-moulded symmetric and asymmetric test gears 90

7.2 Gear tooth deflection test rig 91

7.3 Measured surface temperature of the test gears at (a) 3–4.5 Nm and (b) 2–2.5 Nm 92

7.4 Measured gear tooth thickness across three teeth of the test gears 93

7.5 Gear tooth engagement of (a) symmetric gear pair and (b) asymmetric gear pair 94

7.6 Worn out gear tooth surface of (a) symmetric gear and (b) asymmetric gear after 1.45×10^5 cycles, 2 Nm 96

7.7 Worn out gear tooth surface of (a) symmetric gear and (b) asymmetric gear after 1.45×10^5 cycles, 2.5 Nm 96

7.8 Coast side gear tooth surface of (a) symmetric gear after 4.32×10^5 cycles and (b) asymmetric gear after 1.45×10^5 cycles, 2 Nm 97

7.9 Coast side gear tooth surface of (a) symmetric gear after 2.88×10^5 cycles and (b) asymmetric gear after 1.45×10^5 cycles, 2.5 Nm 97

7.10 Final profile of the test gears (a) symmetric gear tooth profile tested at 2 and 2.5 Nm after 4.32×10^5 and 2.88×10^5 cycles; (b) asymmetric gear tooth profile tested at 2 and 2.5 Nm after 1.44×10^5 cycles 98

7.11 Failure morphology of (a) symmetric gear (1.34×10^5 cycles), (b) asymmetric gear (0.85×10^5 cycles) at 3 Nm, (c) close-up view of Figure 7.11(a) showing tooth deformation, and (d) close-up view of Figure 7.11(b) showing tooth deformation 100

7.12 Failure morphology of (a) symmetric gear (23.44×10^3 cycles) and (b) asymmetric gear (10.23×10^3 cycles) at 3.5 Nm 101

7.13 Failure morphology of (a) symmetric gear (2.67×10^3 cycles) and (b) asymmetric gear (1.88×10^3 cycles) at 4 Nm 101

7.14 Failure morphology of (a) symmetric gear (1.14×10^3 cycles) and (b) asymmetric gear (0.96×10^3 cycles) at 4.5 Nm 101

7.15 HPSTC load position of (a) symmetric gear and (b) asymmetric gear 103

7.16 Load angle and load radius 104

7.17 Life of the symmetric and asymmetric gears at various loads 105

7.18 Gear tooth deflection of symmetric gear and asymmetric gear 106

7.19 Schematic of symmetric gear and asymmetric gear with loading 107

8.1 (a) Tensile and (b) pin specimens of polypropylene, 0.5, 1, 3, 5 wt% CNT–PP composites 110

8.2 Surface profile of counter steel disc 111

8.3 Stress–strain plot of the tested CNT–PP composites 112

8.4 Yield strength and Young's modulus of the CNT–PP composites 112

8.5 XRD plot of the CNT–PP composites 113

8.6 Fractured surface of the 1wt% CNT–PP that shows (a) agglomerates and (b) the dispersion of CNTs in the PP 115

8.7 Fractured surface of the 5wt% CNT–PP that shows (a) agglomerates and (b) the dispersion of CNTs in the PP 116

8.8 Fractured surface of the polypropylene that shows no agglomerates 117

8.9 Hardness of the considered CNT–PP composites 118

8.10 Online wear of the tested CNT–PP composites 120

8.11 Surface of the counter disc after test (a) polypropylene and (b) 1 wt% CNT–PP 120

8.12 Wear rate of the considered CNT–PP composites 121

8.13 Friction coefficient of the tested CNT–PP composites 121

8.14 Average friction coefficient and weight loss of the CNT–PP composite 123

8.15 Worn out surface of the polypropylene material that shows the sliding direction and deeper wear tracks 124

8.16 Worn out surface of the 1wt% CNT–PP composite that shows the sliding direction and mild wear tracks 124

8.17 Optical profilometer image of the worn out surface of (a) unreinforced polypropylene, (b) 1wt% CNT–PP, and (c) 5wt% CNT–PP 126

8.18 (a) Schematic of the test specimen with the temperature measurement locations, (b) Various regions of the temperature measurement during sliding wear of 5 wt% CNT–PP, and (c) Measured temperatures at various regions of the 5 wt% CNT–PP while sliding 128

8.19 Thermograph of (a) polypropylene, (b) 1 wt% CNT–PP, and (c) 5 wt% CNT–PP at 50 N load and sliding speed of 56.54 m/min 129

8.20 Surface temperature of the tested CNT–PP composites while sliding 129

8.21 Measured surface temperature of the tested CNT–PP composites 130

8.22 DSC melting curve of polypropylene and CNT–PP composites 132

8.23 TGA plot of the CNT–PP composites 133

8.24 Thermal conductivity of the considered CNT–PP composites 134

9.1 Injection-moulded polypropylene and 1 wt% CNT–PP gears 138

9.2 Measured surface temperature of test gear at 2 and 2.5 Nm 140

9.3 Measured surface temperature of test gear at 3 and 3.5 Nm 141

9.4 Measured surface temperature of test gear at 4 and 4.5 Nm 142

9.5 Transmission efficiency of test gear at 2.5 Nm 143

9.6 Measured gear tooth thickness across three teeth of the test gears 143

9.7 Worn out gear profile of test gear at 2 Nm after 1.4×10^5 cycles 145

9.8 Worn out tooth profile of test gear at (a) 2 Nm after 8.64×10^5 cycles and (b) 2.5 Nm after 5.76×10^5 cycles 146

9.9 S-N curve of polypropylene and 1 wt% CNT–PP gears at various loads 147

9.10 Tooth surface of test gear subjected to 2.5 Nm (a) polypropylene after 1.44×10^5 cycles, (b) 1 wt% CNT–PP after 1.44×10^5 cycles, (c) polypropylene after 5.76×10^5 cycles, (d) 1 wt% CNT–PP after 5.76×10^5 cycles, (e–f) SEM image of polypropylene gear after

5.76×10^5 cycles, and (g–h) SEM image of 1 wt% CNT–PP after 5.76×10^5 cycles 149

9.11 Tooth surface of test gear subjected to 2 Nm (a) polypropylene after 1.44×10^5 cycles, (b) 1 wt% CNT–PP after 1.44×10^5 cycles, (c) polypropylene after 5.76×10^5 cycles, and (d) 1wt% CNT–PP after 5.76×10^5 cycles 151

9.12 Test gear failure showing all teeth, 2 Nm: (a) polypropylene and (b) 1 wt% CNT–PP 151

9.13 Test gear failure showing all teeth, 3 Nm: (a) polypropylene and (b) 1 wt% CNT–PP 152

9.14 Test gear failure showing all teeth, 4 Nm: (a) polypropylene and (b) 1 wt% CNT–PP 152

LIST OF TABLES

Table	Title	Page No.
3.1	Test gear parameters	30
6.1	Test gear parameters	72
9.1	Mechanical and thermal properties of the test gear materials	139

LIST OF EQUATIONS

Equation No.	Title	Page No.
4.1	Gear body temperature rise using modified MAO model	40
4.2	Specific gravity of air as per gas law	41
4.3	Transmission efficiency	50
5.1	Scherrer's equation	58
5.2	Vickers hardness	61
5.3	Hertzian contact stress	64
5.4	Hertzian contact width	64
5.5	Contact diameter of equivalent cylinders	64
5.6	Load normal to the tooth	64
5.7	Load tangential to the tooth	64
7.1	Contact ratio	95
7.2	Arc of contact	95
7.3	Path of contact	95
7.4	Maximum sliding velocity	99
7.5	Path of approach/recess	99
7.6	Location of HPSTC	102
7.7	Operating pressure angle	102
7.8	Transverse base pitch	102
7.9	Pressure angle at the load application point	103
7.10	Load angle	103
7.11	HPSTC radius	103

7.12 Virtual load radius 103

8.1 Wear rate 120

8.2 Percentage crystallinity 132

ABBREVIATIONS

AFM	Atomic Force Microscope
AMMA	Polyacrylonitrile-methylmethacrylate
CF	Carbon Fibre
CNT	Carbon Nanotube
EDM	Electric Discharge Machining
FEA	Finite Element Analysis
HPSTC	Highest Point Single Tooth Contact
IR	Infrared
MWCNT	Multi-wall Carbon Nanotube
PA	Polyamide
PEEK	Polyetheretherketone
PI	Polyimide
PMDC	Permanent magnet direct current
PMMA	Polymethylmethacrylate
POM	Polyoxymethylene
PP	Polypropylene
PP-g-MA	Polypropylene-grafted-Maleic anhydride
PPS	Polyphenylene Sulphide
PS	Polystyrene
PTFE	Polytetrafluoroethylene
PU	Polyurethane

SiC	Silicon Carbide
SiC/Ca-OCA	Silicon Carbide/Calcium salt of Octacosanoic Acid
TGA	Thermogravimetric analysis
TLCP	Thermotropic Liquid Crystal Polyester
UHMWPE	Ultra High Molecular Weight Polyethylene
WEDM	Wire-cut electric discharge machining
XRD	X-ray Diffraction
ZFDA	Silane coupling agent

NOTATIONS

English Symbols

a	Crystal size (nm)
B	Semi-width of contact between cylinders (m)
b	Gear face width (m)
C_p	Specific heat capacity of the air (J/kg.K)
C_r	Operating centre distance (mm)
$D_1\ and\ D_2$	Contact diameter of driver and driven equivalent cylinders (m)
d	Arithmetic mean of two diagonal in Vickers hardness tester (mm)
$d_1(or)d_2$	Pitch circle diameter of the driver and driven gear (m)
$E_1\ and\ E_2$	Young's modulus of driver and driven gear (Pa)
F	Applied load in Vickers hardness tester (kgf)
ΔH_m	Measured heating enthalpy (J/g)
ΔH_m°	Melting enthalpy of 100% crystalline polypropylene (209 J/g)
L	Sliding distance (m)
N	Applied load (N)
P_a	Absolute pressure (N/m^2)
P_b	Transverse base pitch (mm)
R	Specific gas constant (J/kg.K)
T	Applied torque (Nm)
t	Absolute temperature of the air (K)
Δt	Gear body temperature rise (K)

$R\ and\ r$	Pitch circle radius of driver and driven gear (mm)
$R_a\ and\ r_a$	Radius of outer or addendum circle of driver and driven gear (mm)
$R_b\ and\ r_b$	Base radius of driver and driven gear (mm)
r_{nb}	Virtual base radius (mm)
r_{nL}	Virtual load radius (mm)
r_{nW}	HPSTC radius (mm)
S_n	Normal circular tooth thickness (mm)
V	Wear volume loss (mm^3)
W_n	Load normal to the tooth (N)
W_f	Weight fraction of the filler
W_t	Load tangential to the tooth (N)
X_c	Percentage crystallinity
$Z_1\ and\ Z_2$	Number of teeth in driver and driven gear

Greek Symbols

β	Full-width at half maximum
$\gamma_1\ and\ \gamma_2$	Poisson's ratio of the driver and driven
θ	Diffracted angle (deg)
λ	Wave length of X-ray (0.15406 nm)
μ	coefficient of friction
ρ	Specific density of air (kg/m^3)
σ_C	Maximum contact stress (Pa)
$\emptyset_n$	Standard normal pressure angle (deg)

$\emptyset_{nW}$	Pressure angle at the load application point (radian/deg)
$\emptyset_{nL}$	Load angle (radian)
$\emptyset_r$	Operating transverse pressure angle (deg)
$\omega_1 \; and \; \omega_2$	Angular velocity of driver and driven gear (rad/s)
ω	Wear rate ($mm^3N^{-1}m^{-1}$)

CHAPTER 1

INTRODUCTION

1.1 OVERVIEW ON POLYMER AND POLYMER COMPOSITE GEARS

Majority of the machines utilize gears for motion and power transmission applications. Polymer and polymer composite gears are replacing metallic gears in many applications due to their noise reduction, self-lubrication, light weight, cost effectiveness and mass production capabilities. However, thermal sensitive mechanical properties of the polymers limit their wide engineering application (Yousef *et al.*, 1973; Koffi *et al.*, 1985; Hooke *et al.*, 1993). However, no work has been carried out on the effect of external cooling over the performance of polymer gears. Researchers utilized compressed air cooling techniques to improve the productivity of machining processes (Dixit *et al.*, 2012; Sarma and Dixit 2007; Sharma *et al.*, 2009).

Many researchers investigated the surface effect on the friction and wear performance of polymer materials (Barrett *et al.*, 1992; Wieleba 2002; Hohn *et al.*, 2006; Tzanakis *et al.*, 2013). Investigations have been carried out on the surface roughness effect by different manufacturing processes on the contact area and gear profile deviation (Bergseth *et al.*, 2012; Gupta and Jain 2014). Limited work has been carried out on the polymer gear performance with respect to surface roughness (Akkurt 1995). However, no work has been carried out on the effect of mating gear tooth surface over the test gears.

For the past one-decade, asymmetric gear tooth profile (different pressure angle at drive and coast side) has been considered and numerically investigated by many researchers for improving the bending stress capability (Litvin *et al.*, 2000; Cavdar *et al.*, 2005; Karpat, Ekwaro-Osire and

Khandaker, 2008; Muni *et al.*, 2007). Even though sufficient amount of works have been carried out on asymmetric gear design, very limited experimental work has been carried out (Kapelevich 2000; Mohan and Senthilvelan 2014).

Sufficient works have been carried out to understand the effect of reinforcements on gear performance (Kurokawa *et al.*, 1999; Kurokawa *et al.* 2000a; Kurokawa *et al.* 2000b; Kurokawa *et al.* 2003; Senthilvelan and Gnanamoorthy, 2004a; Senthilvelan and Gnanamoorthy, 2004b; Senthilvelan and Gnanamoorthy, 2009), directional shrinkage (Weale *et al.*, 1999; Senthilvelan and Gnanamoorthy, 2006; Senthilvelan and Gnanamoorthy, 2008; Hakimian and Sulong, 2012), directional mechanical (Bernasconi *et al.*, 2007; Goel *et al.*, 2009; Bernasconi *et al.*, 2015) and tribological properties (Sung and Suh, 1979; Cirino *et al.*, 1988; Kim *et al.*, 2012). However, carbon nano-tube (CNT) based polymer materials which does not have directional shrinkage (Prashantha *et al.*, 2009) and directional mechanical (Prashantha *et al.*, 2009) properties have not been considered for the gear applications.

In the present work, an attempt has been made to improve the durability of polymer and polymer composites gears by improved service conditions (external cooling), gear design (asymmetric tooth profile) and new material (CNT based polypropylene). In addition, the effect of manufacturing process and surface condition of mating steel gears over polymer gears have also been investigated.

1.2 MOTIVATION

Gear tooth surface interaction and material hysteresis of the polymer generates heat during the service of polymer gear. Thus, thermal sensitive mechanical properties of polymer gear motivate to investigate the effect of external air cooling over the performance of polymer based gears.

Various reinforcements (glass, carbon, and kevlar) are generally used to increase the mechanical and tribological properties of polymeric materials, whereas these fibres caused directional shrinkage. Carbon nano-tube can be used as an alternative in which the directional shrinkage properties can be reduced. Thus, absence of directional properties motivate to investigate carbon nano-tube based polymer gears.

Prior numerical works on asymmetric gears exhibited superior bending fatigue performance. However, absence of surface durability investigation on asymmetric polymer gears motivate to carry out the same.

Complex shaped asymmetric gear tooth profiles are generally manufactured by wire-cut electric discharge machining process. Unlike conventional machining process, followed by grinding and secondary finishing process, the surface quality of this complex shape tooth profile cannot be improved further. Thus, this limitation of wire-cut electric discharge machining of mating steel gear motivates to investigate the effect of mating steel gear tooth surface over the durability of injection-moulded asymmetric polymer gears.

1.3 OBJECTIVES

The main objectives of the present work is to improve the durability of the polymer gears by air cooling, asymmetric tooth design concept and carbon nano-tube reinforcement.

1.3.1 Methodology

Following methods were carried out to achieve the main objectives mentioned above

- Mechanical, friction, and wear properties of the gear material (unreinforced polypropylene and carbon nano-tube reinforced polypropylene) were investigated using standard servo hydraulic tensile test facility and pin-on-disc configuration.

- The surface durability evaluation of unreinforced polypropylene gear with and without compressed air cooling using power absorption test rig.
- The effect of manufacturing processes of the mating metal gear on the performance of unreinforced polypropylene gear.
- The effect of surface roughness of the mating metal gear on the performance of unreinforced polypropylene gear.
- Evaluation of pressure angle at the drive side of the gear over the surface durability of polypropylene gear.
- Mechanical, friction, and wear properties evaluation of carbon nano-tube reinforced polypropylene.
- Surface durability evaluation of carbon nano-tube reinforced polypropylene gear.

1.4 ORGANISATION OF THE THESIS

First chapter briefly discusses the motivation of the present work which includes research on polymer and polymer composite gears, asymmetric gear, limitation of fibre reinforcement and benefits of CNT reinforcement. Objective and major methodology adopted is outlined in this chapter.

Brief literatures on polymer and polymer composite gear were discussed in the second chapter. Prior work related to CNT based polymer material and surface roughness effect on the polymer gear tribology were also discussed in this chapter.

Third chapter deals with the materials used to develop gears, test rig details and methodology adopted for evaluating mechanical, tribological, and gear performance were discussed.

Compressed air is used to reduce the surface temperature of polypropylene gear. Wear resistance and transmission efficiency with and without air cooling were reported in the fourth chapter.

The effect of mating steel gear manufacturing processes on the polypropylene gear durability was discussed in the fifth chapter. The modification made by the wire-cut electric discharge machining process on the metal gear surface was also discussed in this chapter.

Sixth chapter deals with the effect of asymmetric mating steel gear surface roughness over the asymmetric polypropylene gear performance. Standard pin-on-disc test under different surface roughness condition was also discussed in this chapter which was used to correlate the surface roughness effect with the frictional force.

The asymmetric polypropylene gear durability against asymmetric metal gear was discussed in the seventh chapter. Improved bending strength of asymmetric gear was also reported in this chapter using in-house developed experimental test rig.

Eighth chapter deals with the evaluation of mechanical and tribological performance of the CNT–PP (0.5, 1.0, 3.0, and 5.0 wt%) composites developed using the melt compounding technique. Thermal characterization of the developed composites were also discussed in this chapter.

Ninth chapter deals with the development of CNT reinforced polypropylene gear and evaluated for its durability.

Major conclusions drawn from the work and scope for the future work are the outline of the last chapter.

CHAPTER 2

LITERATURE SURVEY

2.1 INTRODUCTION

Utilization of thermoplastic materials in the engineering applications has increased due to their excellent chemical resistance, superior damping properties, and mass production capabilities. Among thermoplastic materials, polypropylene (PP) materials are used in many engineering applications because of their low density, easy processability, low cost, and reasonable mechanical strength. The load carrying capacity of the polymer gear can be improved by fibre reinforcement. Carbon nanotubes are replacing microfibres (glass and carbon fibres) in polymer composites because of their higher aspect ratio, absence of directional shrinkage, directional mechanical, and tribological properties. CNT addition improves mechanical, flexural, and fatigue properties of the polymers. In the recent years, the importance of gears with advanced tooth forms have increased mainly due to the advancement in the manufacturing industries. By altering standard tooth forms, bending/contact load carrying capacity and tooth sliding characteristics can be altered as desired. Asymmetric gear design is one of the effective tooth form which will improve the bending load capacity at the drive side of the gear.

Research and development of composite spur gears have progressed significantly in the last few decades. Present work attempted to widen the scope of using polymer gears with compressed air cooling, carbon nanotube reinforcement, and asymmetric gear design concept. Since there is a need to review the prior work to understand the relevant behaviours of polymer, polymer composite gear, and nano-fibre reinforcement which are presented in this chapter. Shrinkage and

heat generation due to fibre reinforcement and surface interactions are crucial issues in the composite gear performance evaluation. So, prior work with reinforcement to reduce shrinkage and improve heat dissipation is also discussed in this chapter.

2.2 POLYMER GEAR

During running, the polymer gear tooth surface temperature significantly influenced the gear life. Polymer gears generate heat due to the tooth sliding friction and material hysteresis (Yousef *et al.*, 1973). Koffi *et al.* (1985) proposed a model to predict the heat generation in thermoplastic polymer spur gears. The proposed model predicts the generated heat with less computing effort than the exact one. Breeds *et al.* (1993) investigated the durability of Acetal and Nylon gear pairs. At lower loads (upto 7 Nm), the life was decided by wear; whereas at higher load (beyond 7 Nm), life was limited by the maximum permissible surface temperature of the gear material. Hooke *et al.* (1993) measured the wear and surface temperature of the polymer gears using back to back test configuration. When the load increases from 3 to 20 Nm, surface temperature increased from 35 to 175 °C. Taburdagitan and Akkok (2000) investigated the tooth surface temperature in spur gear meshing due to frictional heat using coupled thermo-elastic finite element analysis (FEA). From the investigation, they concluded that the surface temperature rises on spur gear teeth pair along the pressure line were highest at the beginning of meshing and by profile modification at the tooth tip could reduce that surface temperature during initial contact.

Walton *et al.* (2002a) and Walton *et al.* (2002b) evaluated the influence of various materials and geometries on the efficiency of polymer gear pairs and found to be dependent on the load and speed. Senthilvelan and Gnanamoorthy (2006) investigated the effect of teeth fillet radius on the life performance of Nylon 6/6 gear made with the fillet radius of 0.25 and 0.75 mm against steel gear using power absorption gear test rig. Gears with low gear tooth fillet radius exhibited higher

deflection and higher hysteresis loss results in higher surface temperature. Kim (2006) proposed two design modifications for improving the durability of plastic spur gears. In one design, series of holes were made at the intersection of base circle and tooth centreline. In another design, steel pins were inserted after making the holes at the intersection of base circle and tooth centreline. Presence of the holes decreased the accumulated heat and presence of pins reduced hysteretic heat generation. Presence of holes as well as pins reduced the surface temperature about 5–10 °C (depends on load) and increased the gear wear resistance.

Senthilvelan and Gnanamoorthy (2007) investigated the effect of rotational speed on the performance of polyamide (PA) gears. At higher rotational speed, gears exhibited higher surface temperature due to the increased frictional and material hysteresis losses. Lin and Kuang (2008) investigated the interactions between the dynamic loads and the tooth profile wear of polyoxymethylene (POM) and Nylon 66 plastic gear pairs using a dynamic model which incorporates the effects of position-varying tooth mesh stiffness, damping ratio, load sharing, tooth profile wear, and temperature on the dynamic contact loads. Simulation results indicated that the tooth profile variation caused by cumulative sliding wear had a significant influence on the contact loads and as the running cycle proceeds, the interactions between dynamic contact loads and cumulative wear gradually increases.

Imrek (2009) increased the gear tooth face width of Nylon gears at single tooth contact region to attain uniform contact stresses. Modified gear tooth reduced the heat generation and gear tooth wear. Duzcukoglu (2009) modified the polyamide gears by making cooling holes across the face width of the pitch circle as well as well below the root circle. Modified gear exhibited 5–20 °C (depends on load) lower surface temperature and improved the wear resistance when compared to that of standard gear. Senthilvelan and Gnanamoorthy (2009) examined the transmission

efficiency of polyamide gears. Gear surface temperature and transmission efficiency decreased with increase in number of cycles. Tooth wear as well as reduction of gear tooth stiffness contributed to this reduction of transmission efficiency.

Mao *et al.* (2010) evaluated the durability of the Acetal gears at various loads (7–6 Nm) and measured tooth wear and gear temperature (30–150 °C). Letzelter *et al.* (2010) investigated the thermal characteristics of polyamide gear pairs at different loads and speeds. With the increase in load (0–10 Nm), the gear tooth surface temperature increased from 10 to 15 °C. Karimpour *et al.* (2010) investigated the contact behaviour of polymeric gear using ABAQUS (FEA) and analytical compared with BS ISO 6336 rating standard. From the investigation, they concluded that the contact path extensions were occurred at the beginning (premature contact) and end (extension contact) which causes large tooth deflection as a result of lower stiffness than metallic gears. And also they interpret that the premature contact caused pitch line tooth fractures and extended contact caused extreme wear. Li *et al.* (2011) investigated the friction and wear behaviour of various dissimilar gears.

Hoskins *et al.* (2014) investigated the rolling contact fatigue performance of polyetheretherketone (PEEK) material. As the load increased, both the coefficient of friction and temperature increased. At higher load conditions, surface melting and contact fatigue failures were predominant. Pogacnik and Tavcar (2015) proposed an accelerated multi-level test procedure for polymer gears by applying step level loads. Form the developed test rig the performance of unreinforced PA and POM along with glass fibre reinforced PA and POM were investigated. It was found that about 5-10 °C less temperature was exhibited by the reinforced gear than unreinforced gear for the considered load and speeds. Mao *et al.* (2015) investigated the continuous wear of injection-moulded and machined polymer composite gears.

2.3 POLYMER COMPOSITE MATERIAL

Sung and Suh (1979) investigated the effect of fibre orientation on the frictional wear performance of unidirectional and particulate composites. Cirino *et al.* (1988) investigated the effect of fibre orientation of thermoplastic and thermoset composites. Bernasconi *et al.* (2007) investigated the fatigue strength of glass fibre reinforced polyamide with different fibre orientations under tension-tension mode. Goel *et al.* (2009) investigated the fatigue behaviour of glass fibre reinforced polypropylene at various frequencies to understand the influence of fibre orientation.

Unal and Mimaroglu (2012) investigated the friction and wear performance of polyamide 6 and graphite composites. The addition of graphite (5–15 wt%) reduced the coefficient of friction (30–60%) and wear rate. However, the measured surface temperature increased (20–85%) for the test conditions (50–100 N – normal load, 0.4–1.6 m/s – sliding velocity and 4,000 m – sliding distance). Kim *et al.* (2012) investigated the friction and wear performance of polyamide and glass fibre composites to understand the orientation of reinforced fibres. The addition of glass fibres (10–50 wt%) reduced the coefficient of friction (15–30%) and the wear rate. However, the surface temperature measured with an infrared (IR) thermal sensor confirmed an increase in the temperature (10–15%) due to the addition of the glass fibres for the test conditions (100–900 N – normal load, 23.6 cm/s – sliding velocity and 7,000 m – sliding distance). Bernasconi *et al.* (2015) investigated the fatigue strength of short glass fibre reinforced polyamide plate at various fibre orientations.

2.4 POLYMER COMPOSITE GEAR

Crippa and Davoli (1995) investigated the fatigue-life behaviour of injection-moulded Nylon 6 gears with different reinforcements using back-to-back test configuration. The tests were carried out under various lubrication mode such as dry, grease, and splash oil and different meshing

combination such as plastic/plastic and steel/plastic gears. Weale *et al.* (1999) investigated the fibre orientation in injection-moulded polymer composite gears using imaging techniques. Kurokawa *et al.* (1999) and Kurokawa *et al.* (2000) investigated and found that PEEK reinforced with high modulus carbon fibre exhibited superior wear resistance than that of PEEK and PEEK reinforced with high strength carbon fibres. Kurokawa *et al.* (2000) studied the tribological properties and gear performance of POM composites reinforced with silicon carbide/calcium salt of octacosanoic acid (SiC/Ca-OCA) using pin-on-disc and power absorption test rig. POM/SiC/Ca-OCA composite possessed lower coefficient of friction and wear rate which makes it to withstand higher load capability than the unfilled POM.

Teisuke *et al.* (2001) studied the wear distribution on the gear teeth on various combinations of injection-moulded plastic gears such as Nylon 66, polyacetal, PEEK and glass fibre reinforced Nylon, polyacetal, polyphenylene sulphide (PPS). From the investigation, the highest level of wear was recorded for unreinforced Nylon and glass fibre reinforced polyacetal gears and the lowest level of wear were recorded for the unfilled PEEK and polyacetal gears. Wright and Kukureka (2001) experimentally proposed the co-ordinate wear measurement techniques for polymer composite gears as a function of load, sliding speed, roll angle, and slip ratio. The moderate correlation was obtained between the proposed techniques with the simple test configuration such as disc roll/slide test and pin-on-disc results. Kurokawa et al. (2003) studied the gear performance of injection-moulded carbon fibre reinforced polyamide 12 and compared with carbon fibre reinforced polyamide 6, 66, and 46 using power absorption test rig. From the investigation, they concluded that PA12/carbon fibre (CF) gear possessed high load capability, excellent noiseless property, and lowest water absorption properties among all polyamides.

Senthilvelan and Gnanamoorthy (2006) investigated the damping characteristics of unreinforced, 20% glass, and 20% carbon reinforced Nylon 6/6 spur gears against steel gear using power absorption test rig. Addition of fibres to the polymer matrix reduces the damping characteristics of the composite and increases the gear mesh noise than the unreinforced gears. But fibre reinforcement reduces the internal heat generation capacity and thus gear reinforced with high modulus fibres shows lower heat generation during service. Senthilvelan and Gnanamoorthy (2006) investigated the shrinkage characteristics of injection-moulded short glass fibre reinforced polyamide gears and correlated with the gate location. Mao (2007) evaluated the performance of Acetal and glass fibre reinforced Nylon gear pairs. Rapid wear beyond the critical load (8 Nm) was observed due to the rise in surface temperature, which is close to the melting point of the gear material, 175 °C. Mao also proposed a model to predict gear tooth surface temperature by considering heat generation as well as dissipation during the gear service. Senthilvelan and Gnanamoorthy (2008) investigated the effect of reinforcement on gear metrology for the injection-moulded unreinforced and 20% short glass fibre reinforced Nylon 6/6 spur gear using computer aided simulation and gear-measuring centre. Presence of hard glass fibres across the tooth section affected material homogeneity, surface smoothness and hence the involute profile form is deviated.

Hossan and Hu (2008) investigated the stress-strain behaviour of a 20% short glass fibre reinforced Nylon 66 and unreinforced Nylon 66 gear tooth under various dynamic loads using three-dimensional finite element model. From the investigation, they concluded that the tooth root region of the gear usually experiences high stress and potential to failure. Kirupasankar *et al.* (2012) investigated the transmission efficiency of nanoclay (0, 3, and 5 wt%) reinforced polyamide gears paired with steel gear. The addition of nanoclay increased the stiffness and lowered the viscous component of the gear material. Thus, the transmission efficiency of polyamide nanocomposite

gear was superior compared to the pristine polyamide gear. Hakimian and Sulong (2012) investigated the shrinkage and warpage behaviour of fibre reinforced micro gears to understand the influence of fibre orientation. Hossan and Hu (2013) numerically evaluated the strength of short carbon fibre reinforced Nylon spur gears by 3D finite element model using ANSYS. From the investigation, they concluded that the composite gear manufactured by properly controlled injection-moulding process provide better strength and performance.

Yousef *et al.* (2013) investigated the mechanical and wear properties of CNT (1 wt%) reinforced Acetal gears. In addition to the strength and stiffness improvement, the wear resistance of the CNT–POM gears also increased because of the CNT addition. Yousef *et al.* (2015) evaluated 0.02 wt% CNT reinforced Acetal gear material and investigated spur, helical, bevel, and worm gear performance. CNT–Acetal spur, helical, bevel, and worm gears exhibited improved wear resistance by 28%, 35%, 44%, and 47% compared to the pure Acetal gears.

2.5 CARBON NANO-TUBE BASED POLYMER MATERIAL

2.5.1 Mechanical Properties

Kim *et al.* (2009) investigated the mechanical, rheological, and thermal properties of the CNT (0.5–1.5 wt%) reinforced thermotropic liquid crystal polyester (TLCP) prepared using the melt blending method. The thermal stability, rheological, and mechanical properties of the TLCP increased as the CNT content increased. The tensile strength and modulus of the CNT–TLCP composites increased by 41% and 34% respectively, for the 1.5 wt% CNT–TLCP composite compared to the pristine TLCP. Kang *et al.* (2010) investigated thermal, electrical, rheological, and mechanical properties of CNT–PP, (0.5–5 wt%) composites prepared using the melt compounding process. The thermal conductivity and tensile strength of the composite increased as the CNT content increased.

Suresha *et al.* (2010) investigated the effect of nanofillers on the mechanical and tribological properties of polyamide 66 and PP. Improvements in mechanical and tribological behaviours were observed with the addition of the fillers. Chen *et al.* (2011) produced highly aligned polyimide and polyimide nanocomposite fibres (1–5 wt%) containing carbon nanotubes using the electrospinning process. A tensile strength evaluation and dynamic mechanical analysis were performed. Liu *et al.* (2013) investigated the mechanical, electrical, and thermal behaviours of polyurethane reinforced with the CNTs (0.2–2 wt%).

2.5.2 Tribological Properties

Chen *et al.* (2003) investigated the tribological properties of various CNT–polytetrafluoroethylene (PTFE) composites with the aid of a block-on-ring test configuration in a dry condition. The presence of the CNTs significantly improved the wear resistance of the PTFE and decreased the coefficient of friction. As the CNT content increased, the wear rate decreased upto 20% volume content, beyond which the wear rate increased. The worn out surface of the pure PTFE was very rough due to the adhesive and ploughing phenomenon, which was reduced by adding CNTs. Cai *et al.* (2004) developed a polyimide (PI)–CNT composite by polymerization and investigated the tribological performance in a dry sliding condition. The PI-CNT composite exhibited low frictional coefficient, reduced wear losses, and reduced adhesion and scuffing of the PI matrix.

Yang *et al.* (2005) developed CNT–polymethylmethacrylate (PMMA) composites by polymerization and investigated the tribological performance. The wear rate and coefficient of friction decreased as the CNT content increased. Scuffing and adhesion wear were observed for the pure PMMA and the wear was reduced by adding the CNTs. Yang *et al.* (2005) developed the polystyrene (PS) CNT composites through polymerization and investigated the wear and micro hardness. The self-lubricating characteristics of CNTs increased the wear resistance and hardness

of the polystyrene composite and reduced the friction coefficient. The worn out surface of the pure PS showed traces of adhesion and abrasive wear and the wear was considerably reduced by adding the CNTs.

Wang *et al.* (2008) developed polyacrylonitrile-methylmethacrylate (AMMA)–CNT composite by polymerization and evaluated the micro hardness and wear performance in the dry-sliding condition. A significant wear resistance improvement was observed because of the improved mechanical properties and lubricating characteristics of the CNTs. Cho (2008) investigated the flexural and tribological performance of a multi-wall carbon nanotube (MWCNT)–polyphenylene sulphide (PPS) composite. A thick and grainy transfer film formed on the counter face (hardened tool steel) when sliding over neat PPS. However, the transfer film was thin and uniform with the addition of the CNTs to the PPS. The specific wear rate of the composite decreased as the MWCNT content increased to 2 wt%, and beyond this content, the wear rate increased.

Park *et al.* (2013) developed CNT–ultra high molecular weight polyethylene (UHMWPE) composites using an in-situ polymerization processes and evaluated the mechanical and wear resistance. The CNT–UHMWPE composite exhibited superior wear resistance; ploughing and micro cracks were observed on the worn out surfaces of the neat and CNT reinforced UHMWPE composites. Solonin *et al.* (2014) investigated the mechanical and tribological properties of fluoroplastic–MWCNT composites (1–10 wt%). The Young's modulus and hardness of the composite increased significantly at 3 wt%, while the wear loss was reduced by two orders compared to the unreinforced material. Roy *et al.* (2015) investigated the mechanical behaviour of a CNT-reinforced (0.4–1.2 wt%) Nylon 12 processed by plasma treatment. A significant improvement in the tensile strength, Young's modulus, elongation at break, and storage modulus

were observed due to the addition of 1.2 wt% CNT because of strong interfacial adhesion and homogeneous dispersion.

2.6 CARBON NANO-TUBE BASED POLYPROPYLENE MATERIAL

Sandler *et al.* (2003) developed CNT–PP composites using melt compounding and solution techniques to evaluate crystallization characteristics. Yang *et al.* (2008) investigated the effect of compatibilizer on the mechanical properties of MWCNT–PP composites. The effective CNT and PP–g–MA content was 1 wt% and 0.6 wt% respectively. With the addition of CNT, the Young's modulus, tensile strength, and toughness of the PP increased by upto 118%, 117%, and 141% respectively. Prashantha *et al.* (2008) investigated the mechanical properties of multi-walled CNT filled PP by promoting the CNTs dispersion using polypropylene-grafted-maleic anhydride (PP-g-MA) by melt compounding with a twin-screw extruder. A PP-MWCNT composite was developed by mixing PP with a 20 wt% master batch of the CNT–PP along with PP-g-MA in a co-rotating twin-screw extrusion. The weight fraction of CNTs (1–5 wt%) and PP-g-MA (1–3 wt%) were varied and good adhesion of the CNTs and PP at 2 wt% PP-g-MA was observed.

Prashantha *et al.* (2009) investigated the rheological and mechanical properties of CNT-reinforced PP (1–5 wt%) prepared by diluting a PP-MWCNT master batch using the melt compounding process. Significant improvement in the mechanical behaviour was observed by adding CNTs to the PP matrix. As the CNT content increased, the tensile modulus and yield stress of the developed composite increased by 68% and 25% respectively. Thiebaud and Gelin (2009) analysed the mechanical behaviour of PP/MWCNT composites for the percentage such as 1, 2, 4, and 8 wt%. Young's modulus and the stress at fracture increases with the MWCNT level while the strain to failure decreases significantly. Prashantha *et al.* (2009) investigated the shrinkage and warpage

properties of injection-moulded PP/MWCNT composites. Shrinkage reduction upto 48% whereas more than 55% warpage reduction were obtained in the flow direction.

Zaikov *et al.* (2010) investigated the thermal degradation behaviour of melt compounded MWCNT–PP (1, 3, and 5 wt%) composites. An increased (30–35%) in thermal conductivity was observed for CNT–PP composites as the CNT content increased (0 to 5 wt%). Pan *et al.* (2010) correlated the CNT dispersion with the electrical conductivity of a MWCNT–PP composite prepared by melt compounding. Muller *et al.* (2011) investigated the influence of feeding conditions in the twin-screw extrusion of two different MWCNT–PP composites on the electrical and mechanical properties by feeding them in the hopper and side feeder. The other extrusion conditions (e.g. rotation speed, feeding rate, and temperature profile) remained constant.

Xin and Li (2012) investigated the role of a silane coupling agent (ZFDA, 0–100%) on the electrical, mechanical, and thermal properties of 10 wt% CNT–PP composite. An optimum of 20 wt% ZFDA was found to improve the tensile modulus of the CNT–PP composites without sacrificing the tensile strength because the ZFDA reduced the percolation threshold value. Novais *et al.* (2012) investigated the effect of processing parameters (screw speed and feed rate) on the dispersion of 4 wt% CNT–PP composite. Higher screw speed and lower feed rate were found to improve the CNT dispersion.

Wang *et al.* (2013) developed a CNT–PP composite by solvent dispersion followed by extrusion (twin screws). The influence of the CNTs on the mechanical and interfacial properties of PP was evaluated by tensile, impact, and micro-droplet pull-out tests and the corresponding internal damage was measured using a correlated electrical resistance technique. Loos *et al.* (2013) investigated the fatigue behaviour (tension-tension) of polyurethane (PU)–CNT (0.3 wt%)

composites at various loads. The addition of CNTs increased the fatigue life by approximately 250% in the low-cycle regime.

Gandhi *et al.* (2013) investigated the role of CNT on the wear properties of PP in the dry sliding condition for various sliding speeds, loads, and compositions. The wear resistance increased as the CNT content increased. Lee *et al.* (2014) investigated the frictional behaviour of various CNT–PA composites having different lengths of reinforcement. The CNT–PA exhibited lower surface temperature (188 °C to 168 °C) as a result of its superior thermal conductivity (0.334 to 0.405 W/mK). Patti *et al.* (2015) developed various CNT–PP (0.5–2.5 vol%) composites using the melt blending technique. The effect of functionalization of carbon nanotubes on flexural behaviour of the developed composite was examined. PP–0.5 vol% CNT exhibited maximum flexural strength and modulus. Beyond 0.5 vol% CNT, strength and modulus deteriorated as a consequence of agglomeration.

2.7 SURFACE ROUGHNESS EFFECT ON THE POLYMER AND POLYMER GEAR TRIBOLOGY

Few research investigations have been carried out to understand the friction wear performance of polymer against steel surface. Hisakado (1977) investigated the abrasive wear of soft material (copper, cadmium, lead, and zinc) against a hard metal surface (carbon steel). Coefficient of friction and wear were found to increase with increase in surface roughness of the hard surface. Eiss *et al.* (1979) investigated the wear performance of low density polyethylene against steel with the aid of pin on disc test configuration. Bearing ratios of the disc were found to affect the transfer of polymer to the disc. With the increase in bearing ratio, penetration depth of the polymer layer was found to increase. The penetrating depth of a polymer for a specific change in the bearing ratio was found to be larger for a rough disc than a smooth disc. Barrett *et al.* (1992) investigated the

influence of mating surface roughness over the friction wear performance of ultra-high molecular weight polyethylene using pin on disc configuration. An increase in coefficient of friction was observed at higher surface roughness for all the investigated sliding speed.

Ovaert and Ramachandra (1995) investigated the effect of counter face topography on PAI and HDPE polymers wear. Oriented scribing patterns were generated on the counter face. A stable and well adhered polymer transfer film was formed at lower surface roughness disc whereas unstable polymer layer was formed at higher surface roughness disc. Torrance (1997) proposed a method to predict the friction of the lubricated surface from various parameters of the Abbott-Firestone curve.

Wieleba (2002) investigated the tribological performance of PTFE composites against steel counter faces with different roughness under dry conditions. The coefficient of friction and wear rate were found to be significantly influenced by the surface roughness parameter including asperity shape. Franklin and Kraker (2003) investigated the effect surface topography on the wear of POM-PTFE composite. The roughness of the steel counter face was varied in the range of 0.01–0.70 µm using grinding and grit blasting. Transfer layer formed on the steel surfaces depend on the surface roughness height and roughness orientation.

Hohn *et al.* (2006) considered different surfaces of disc including circumferential grinding, transverse grinding, transverse structured and evaluated mean film thickness, pressure distribution with the aid of FZG twin disc test rig. The contact pressure was found to increase with increase in surface roughness of the counter disc. Xiao *et al.* (2007) investigated the wear performance of steel rollers at various loads and slide to roll ratios. Coefficient of friction decreased with the decrease in surface roughness. Menezes *et al.* (2008) prepared various surface textures of steel plates and

investigated the influence of 25 different roughness parameters. Among all the parameters, the average slope of the profile was found to have maximum correlation with coefficient of friction.

Litwin (2011) manufactured various bush materials (polyamide, polyethylene teraphathalate) through turning and broaching. For all the test condition, broached bearing exhibited higher friction than that of turned bearing due to its inferior surface condition. Tzanakis *et al.* (2013) investigated PTFE composites against steel having different surface roughness (R_a= 0.12, 0.25, 0.50, and 0.70 µm). The coefficient of friction and surface temperature increased upto a particular surface roughness (0.25 µm), and then decreased due to the thermal softening.

The effect of manufacturing processes over gear performance has been investigated by few researchers. Micro geometry of the metal gear can significantly influence the friction-wear performance of polymer gears due to their superior hardness. Akkurt (1995) investigated the effect of surface roughness (R_a=9, 11, 26, and 56 µm) of mating metal gear over the wear of Acetal gear. The volume loss exhibited by the test gears after 4 h (6.5 Nm and 1000 rev/min) was 6, 3, 1.5, and 1 mm^3 when paired with metal gears having surface finish of 56, 26, 11, and 9 µm respectively. Acetal gears exhibited higher wear when meshed with the higher surface roughness gears. Wear rate as well as wear mechanism were influenced by the surface roughness of the steel gear. Tung and Cheng (1998) experimentally simulated the grease lubricated polymer-steel worm gear interface with the aid of pin on disc tribometer.

Kim *et al.* (2012) evaluated the performance of steel worm gear meshed with Nylon 6 worm wheel. The efficiency of the worm gear found to increase with the increase in load due to the adhesion shearing theory. Moorthy and Shaw (2013) investigated the contact fatigue performance of grounded and coated gears. Coated gears exhibited superior resistance against pitting damage when compared to that of ground gears.

2.8 ASYMMETRIC GEAR

Kapelevich (2000) developed the basic geometric gear design for the asymmetric involute spur gear to increase load carrying capacity and to reduce weight and vibration. Symmetric helical gears were compared with asymmetric spur gears having a larger pressure angle at drive and coast side. Litvin *et al.* (2000) investigated asymmetric spur gear with the aid of finite element analysis. From the investigation, it is concluded that the asymmetric gear with the larger pressure angle at the drive side exhibited less contact and bending stress when compared to the symmetric gear. Cavdar *et al.* (2005) investigated the bending stress and contact ratio of the gear tooth profile when the pressure angle on the drive side is larger than that of the coast side using the developed computer program and finite element analysis.

Muni *et al.* (2007) optimized the asymmetric spur gear drives for its maximum bending stress by considering several sets of the addendum pressure angles for the required contact ratio of pinion and gear using direct gear design method and FEM (ANSYS). Eight–noded quadratic plane 82 element is used for the analysis. Dynamic behaviour of asymmetric spur gear was investigated by Karpat *et al.* (2008). With an increase in drive side pressure angle, single tooth contact zone and dynamic load-carrying capacity were found to be increased. Karpat *et al.* (2008) investigated the asymmetric gears for micro electric mechanical system. Gear root stress was computed for four different asymmetric gear configurations. Karpat and Ekwaro-Osire (2008) investigated the impact of tip relief modification on the wear of asymmetric spur gear teeth by using FEM. The wear depth was determined from the instantaneous contact loads and Hertzian pressures. From the investigation, they concluded that the wear depth was decreased with respect to tip relief increment. Kumar *et al.* (2008) used finite element method to optimize the asymmetric gear tooth

to improve bending load capacity. The optimum value of the rack cutter shift was suggested for asymmetric gear.

Costopoulos and Spitas (2009) considered one sided involute asymmetric spur gear with circular fillet at the root of the working side. The generating rack has a straight line on the coast side and standard 20° involute on the drive side. Finite element analysis was carried out for various gears (11–60 number of teeth) and confirmed the superior bending capacity of asymmetric gear than that of symmetric gear. Kumar *et al.* (2009) studied the performance of injection-moulded polypropylene asymmetric gears against steel gear using power absorption test rig and compared with symmetric gears. From the investigation, they concluded that superior gear pair efficiency and less surface temperature were obtained for the asymmetric gears compared to symmetric gears. Spitas *et al.* (2009) investigated the reduction of root fillet stress by asymmetric half-involute gear teeth using FEA (NISA II) and fillet stress decrement of 28% was observed for asymmetric gear when compared to that of symmetric gear.

Pedersen (2010) confirmed that bending stress can be reduced significantly by using asymmetric gear teeth. In addition, shape optimization of gear by changing the tool geometry was also attempted. Alipiev (2011) proposed a method for geometric design of symmetric and asymmetric involute meshing in which the contact ratio of the gear drive is equal and potential based on realized potential method. By assigning the gear drive potential and teeth number, geometry of the rack-cutter, and gears, involute meshing were determined. Ekwaro-Osire *et al.* (2011) performed photo elastic analysis with various profiles of asymmetric gears.

Marimuthu and Muthuveerappan (2014) investigated the influence of drive and coast sides pressure angle of asymmetric gear using multi pair contact finite element analysis. From the investigation, it was concluded that the maximum fillet stress initially decreases upto the threshold

point and increases subsequently. Marimuthu and Muthuveerappan (2014) investigated the effect of addendum height, teeth number, and module on the load sharing ratio and stress analysis of asymmetric spur gear using ANSYS. An eight nodded quadrilateral 2D-PLANE 82 element was used for the analysis. From the investigation, it is concluded that the bending stress decreases with the increase in teeth number and module. Mohan and Senthilvelan (2014) evaluated the single tooth bending fatigue performance of injection-moulded asymmetric polymer gears. Increased critical width contributed to improve the bending fatigue performance of asymmetric gear.

Marimuthu and Muthuveerappan (2016) developed a ANSYS parametric design language code which is used to find the load sharing ratio, maximum fillet and contact nondimensional stress and the influence of gear drive parameters such as drive and coast side pressure angles, top-land thickness coefficients, contact ratio, coefficient of asymmetry, gear ratio, and teeth number on the load carrying capacity which were investigated and compared with that of the conventional designed gears. Marimuthu and Muthuveerappan (2016) carried out a parametric study on the asymmetric high contact ratio spur gears and determine the nondimensional fillet and contact stresses that quantify the improvement in load carrying capacity using multi-pair finite element model using ANSYS tool. A six noded higher order triangular element (PLANE82) is selected for the investigation. From the investigation, they concluded that the nondimensional fillet and contact stresses of asymmetric HCR spur gear were lesser than that of the symmetric HCR spur gears.

2.9 SUMMARY

Research works have been carried out to improve the wear resistance of polymer gear with reinforced gear material, tooth modification, and lubricants. However, effect of air cooling on polymer gear performance is not yet evaluated. Literature review has been carried out on the gear surface roughness and manufacturing process which significantly affects the surface durability of

the gears. However, effect of manufacturing processes on the surface roughness of the mating metal gear over the polymer gear performance is not yet investigated. Sufficient numerical and analytical works have been carried out on asymmetric gear performance. However, experimental investigation on the asymmetric gear profile is not yet studied. The addition of fibre reinforcement to the polymer gear material tends to orient the fibres along the melt flow direction, which results in directional shrinkage and CNT reinforcements can be as an alternative over micro fibres in injection-moulded thermoplastic composite gears to avoid directional shrinkage. The effect of CNT reinforcement in polymers on mechanical, thermal, fatigue, friction, and wear performance were observed by many researchers at specimen level and few works have been conducted on gears. However, effect of CNT on the gear performance is not comprehensively evaluated.

CHAPTER 3

MATERIALS AND METHODOLOGY

3.1 INTRODUCTION

Easy processability and low density properties of polypropylene (PP) makes it to use in many engineering applications. Significant improvement in the mechanical and rheological properties was observed from the master-batch diluted CNT–PP composites (Prashantha *et al.*, 2009). Dispersion of CNT in PP can be improved by adding a small percentage of PP-g-MA as a compatibilizer (Prashantha *et al.*, 2008). Significant reduction in directional shrinkage and warpage properties was observed in CNT–PP composite when compared to glass/carbon fibre reinforced polymers (Prashantha *et al.*, 2009). Due to these advantages PP and CNT–PP were considered for gear application. Material processing conditions, gear test rig details, and performance evaluation including tensile strength, hardness, surface roughness, crystallinity, gear tooth wear, gear life, surface temperature of test gear, friction, and wear properties were reported in this chapter.

3.2 MATERIALS AND PROCESSING CONDITIONS

A commercial masterbatch CNT–PP (PLASTICYL PP2001, Nanocyl, Belgium) containing 20 wt% Multi-wall Carbon nanotubes was proposed to use for the development of nanocomposite (Figure 3.1(a)). To achieve the desired percentage of CNT, this masterbatch was further processed through melt-intercalation with Polypropylene (M110 Haldia Petrochemical Ltd) which is shown in Figure 3.1(b) using co-rotating twin screw extruder (SPECIFIQ zv20). Test materials were dried

at 80 °C for 4 h before compounding. The molecular weight of the considered polypropylene is 42.08 g/mol. The melt flow index of PP is 11 g/10min at 230 °C and the density is 0.90 g/cm^3.

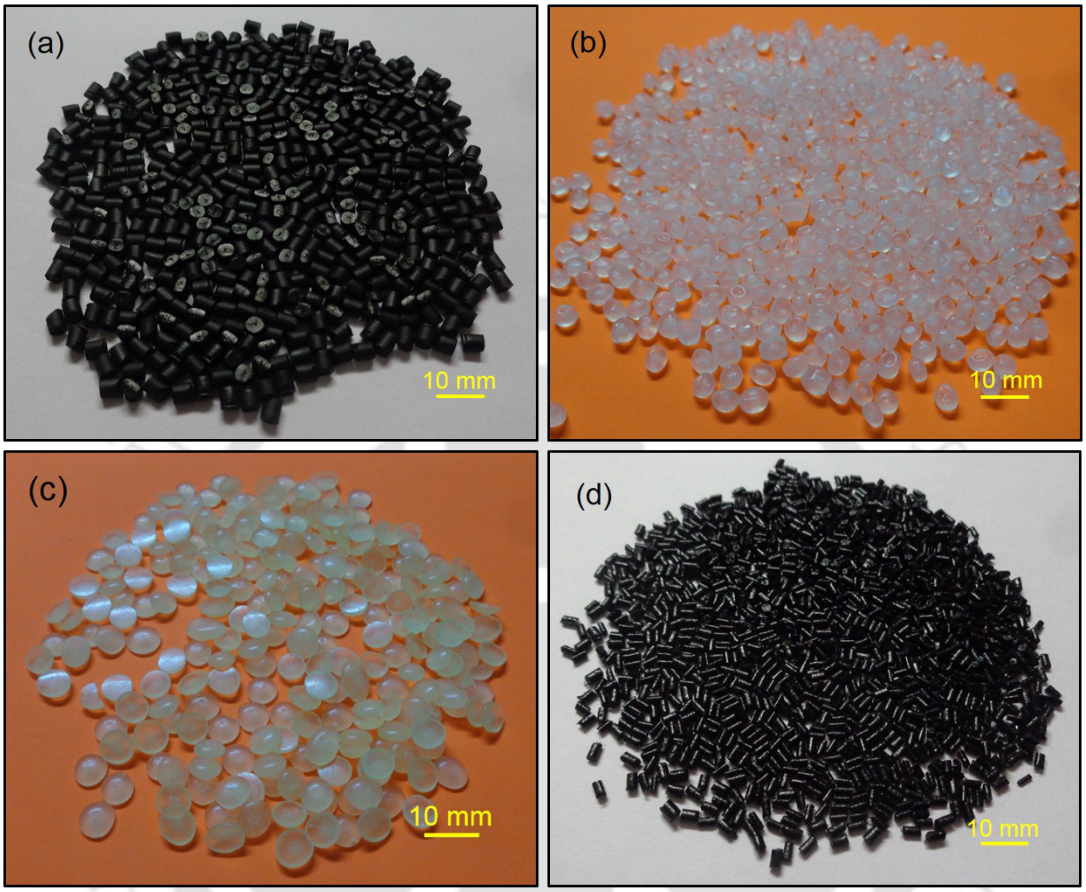

Figure 3.1 Injection-mouldable pellets (a) Master batch CNT–PP, (b) PP, (c) PP–g–MA, and (d) developed CNT–PP composite (1 wt% CNT–PP)

Compounding was carried out in the extruder at a barrel temperature of 195–210 °C and a screw speed of 60 rev/min. The extruded material was further quenched in cold water and then pelletized into granules (Figure 3.1(d)). The strong intermolecular van der walls interactions among the nanotubes in combination with its high surface area and high aspect ratio commonly causes significant agglomeration and prevents transfer of its superior properties to the matrix. To improve

dispersion and bonding strength between fibre and matrix compatibilizer (2 wt% of PP-g-MA, ALDRICH Chemistry) was used which is shown in Figure 3.1(c).

Developed composites (1–5 wt% CNT–PP) were further injection-moulded into tensile specimen at 230 °C as per ASTM D638 dimensions using Texair JTS-40 injection-moulding machine. Materials were dried at 80 °C for 4 h before injection-moulding to remove the moisture content. Injection pressure of 9 MPa was used and temperature maintained in three zones of the barrel was 210 °C, 230 °C, and 250 °C.

3.3 POLYMER COMPOSITE PERFORMANCE

Tensile strength of the developed composites was evaluated using servo hydraulic testing machine (INSTRON 8801) as per ASTM D638. From the test results stress–strain behaviour, yield strength, and tensile modulus of the developed composites were determined. Failure morphology of the tensile test specimens were analysed using scanning electron microscope (Zeiss, Sigma). The hardness of the injection-moulded sample was measured as per ASTM D2240 using Shore-D-Durometer.

XRD (Panalytical, Xpert Powder) analysis was performed on the test materials to understand the effect of CNTs on the crystalline size. The thermal properties such as melting temperature and degree of crystallinity of the developed composites was determined using differential scanning calorimeter (Perkin-Elmer, STA 8000) in an argon environment. The test materials were heated from 30 °C to 230 °C at a heating rate of 10 °C/min. The thermal degradation behaviour of the test materials was evaluated by thermogravimetric analysis (Perkin-Elmer, STA 8000) in an argon environment by heating the samples from 30 °C to 800 °C at a heating rate of 10 °C/min. The

thermal conductivity of the developed composites was measured using a Decagon Devices KD2 Pro Thermal Property Analyser with an accuracy of ±0.01 W/mK.

Tribological performance of the developed material was carried out with the standard pin-on-disc friction and wear testing apparatus (DUCOM TR-201). Test specimens with a 10 mm diameter were slid against a hardened steel disc. Tests were performed at a normal load of 50 N and at a sliding speed of 56.54 m/min in accordance with ASTM G99. The surface roughness of the counter disc was measured with the aid of stylus type perthometer (MitutoyoSurftest SJ-401). The test samples were weighed before and after the test using a digital electronic balance (Sartorius, BSA224S-CW) having an accuracy of 0.0001 g. The worn out surface morphology of the samples was observed under noncontact optical profilometer (Taylor & Hobson, CCI MP) and scanning electron microscope (Zeiss, Sigma). During testing the surface temperature of the test specimen near the contact region was measured using a noncontact infrared (IR) camera (Infratec, Vario CAM), which had an accuracy of ±1.5 K.

3.4 POLYMER AND POLYMER COMPOSITE GEAR

Table 3.1 Test gear parameters

Parameters	Test and mating gear
Pressure angle (°)	20
Module (mm)	3
Number of teeth	18
Pitch circle diameter (mm)	54
Face width (mm)	4/12
Root fillet radius (mm)	1.14

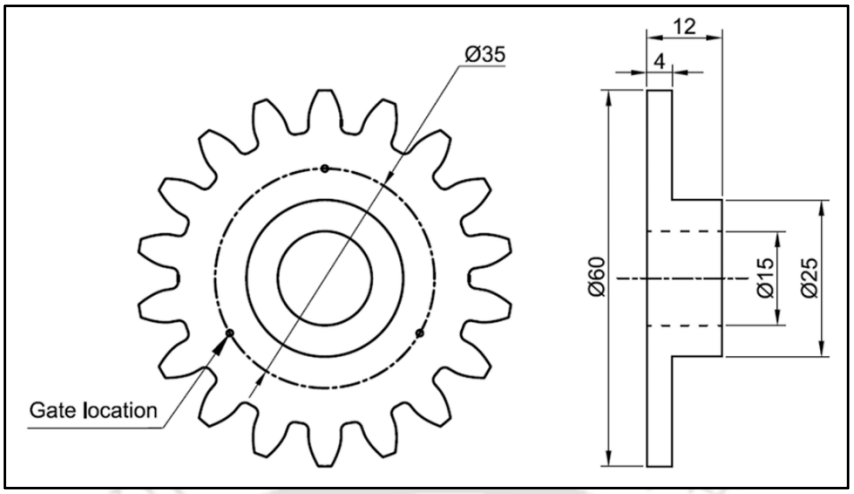

Figure 3.2 Test gear geometry and dimension

The optimum percentage of CNT–PP composite was selected from mechanical and tribological test and the corresponding percentage of composite gear was developed using twin-screw extruder (SPECIFIQ, zv20) for the same process conditions. The test gear details and the gear parameters are shown in Table 3.1 and Figure 3.2.

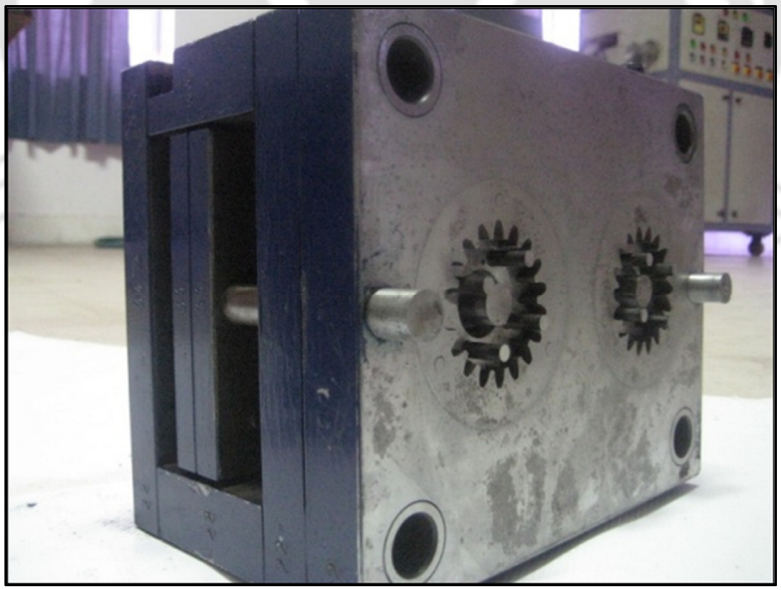

Figure 3.3 Injection-moulding die

The durability of the CNT–PP gear was evaluated using in-house developed power absorption gear test rig and compared with PP gear performance. The injection-moulding die used to manufacture the gear is shown in Figure 3.3. Both the symmetric and asymmetric gear is manufactured during the single injection of molten PP.

3.4.1 Gear Test Rig Details

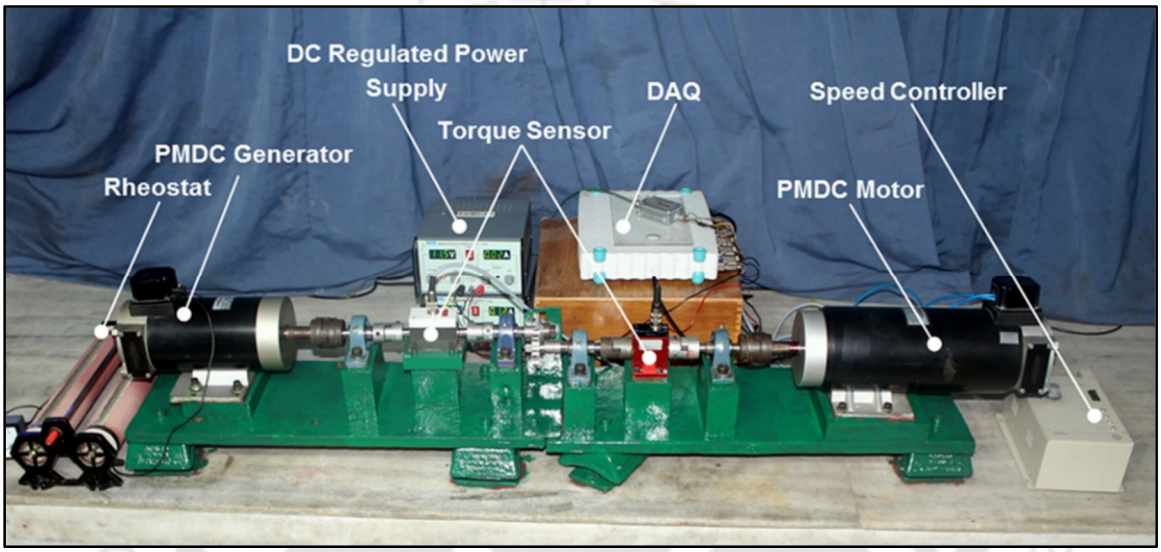

Figure 3.4 In-house developed power absorption gear test rig

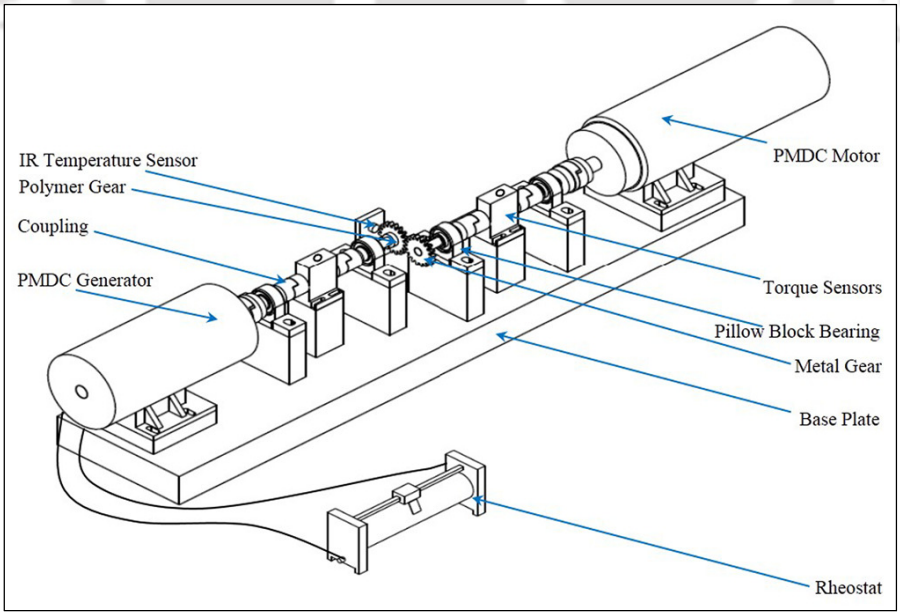

Figure 3.5 Schematic of power absorption gear test rig

The power absorption gear test rig was developed in-house to evaluate the performance of polymer based gears (Figure 3.4). The schematic view of the power absorption gear test rig is shown in Figure 3.5. Test gear was connected to a permanent magnet direct current (PMDC) generator (1 kW) meshed with identical standard metallic gear (SS 316) having 12 mm face width. Standard gear was driven by the PMDC motor (1.5 kW) and could be run at any speed upto 1500 rev/min. Test gears were loaded by generator through rheostat. The torque available at both the driver and driven side was measured with inline torque sensors (HBM, T20WN) of ±0.2% accuracy. Surface temperature of the test gear was measured using the noncontact infrared (IR) temperature sensor (Raytek, MID10LT) with an accuracy of ±1 °C. An IR camera (Infratec, VarioCAM) with an accuracy of ±1.5 °C was also used to measure the surface temperature of the test gear.

3.4.2 Gear Test Details

The gear tests were performed at a constant speed of 800 rev/min and at various loads (2, 2.5, 3, 3.5, 4, and 4.5 Nm) until failure or 10×10^5 cycles, whichever occurred first. All the tests were carried out under the room conditions (Temperature: 25–28 °C and Humidity: 50–60%). A personal computer-based data acquisition system (HBM, Spider 8) was used to continuously record the gear temperature, and torque at the driver and driven gear. The base tangent length across three teeth at three locations equally spaced along the circumference was measured periodically (for every 3 h) to monitor gear tooth wear using gear tooth flange digital micrometre. The gear weight loss was measured by weighing the test gear before and after the test using weighing balance (0.1 mg accuracy). Worn out gear tooth profile after test was observed under vertical profile projector (PP400TE Optomech, linear encoder resolution: 0.001 mm) at 20X magnification. About 70 points were chosen to measure coordinates from the tip to root of the involute profile. Periodically (for every 3 h) gear tooth surface condition was observed and image

was acquired with the aid of digital microscope (Celestron, Digital Microscope Pro). And also the tested tooth was observed under scanning electron microscope (Zeiss, Sigma) to determine the type of wear mechanism occurred during the course of operation.

3.5 SUMMARY

Injection-moulding and twin screw extrusion process condition used for preparing the test specimens and gears were discussed. Materials and test methodology of both the specimen and gear were highlighted in this chapter. Methods for evaluating the tensile strength, crystallinity, tribological, and thermal characteristics were discussed. Details of the gear test rig and various methods of evaluating wear, fatigue performance, and fracture were also highlighted.

CHAPTER 4

EFFECT OF AIR COOLING ON POLYMER GEAR PERFORMANCE

4.1 INTRODUCTION

Polymer gears can replace metallic gears in many engineering applications; however thermal sensitive mechanical properties of the polymers limit their wide application. Gear tooth surface interaction as well as material hysteresis generate heat in the gear operation (Yousef *et al.*, 1973; Koffi *et al.*, 1985). There have been many attempts to improve the gear performance by design modifications (Imrek, 2009; Duzcukoglu, 2009) as well as with new materials (Mao, 2007; Senthilvelan and Gnanamoorthy, 2009; Kirupasankar *et al.*, 2012) to withstand against thermal damages. In machining, air cooling is used to reduce the friction between the tool and work piece which will enhance the tool life and performance (Sarma and Dixit, 2007; Sharma *et al.*, 2009; Dixit *et al.*, 2012). The present work attempts to utilize air cooling to improve the performance of polymer gears and compressed air is used to reduce the surface temperature of polymer gear, thereby wear resistance and transmission efficiency can be improved.

4.2 METHODOLOGY

Polypropylene (M110, Haldia Petrochemical Ltd.) was injection-moulded (Texair, JTS 40) to spur gears at 230 °C. Moulding conditions, details, and parameters of the test gears are explained in Section 3.2 and Section 3.4 (CHAPTER 3). The gear tests were carried out at a constant speed of 800 rev/min and at various torques (2, 2.5, and 3 Nm). To understand the effect of air cooling, the

gears were run with and without compressed air cooling for the same fixed number of cycles. An air compressor (Stanley, 1.5 kW) was used to supply the compressed air for gear cooling and the full view of the test rig with compressor is shown in Figure 4.1(a). The surface temperature of the test gear was measured using an IR temperature sensor (Raytek, MID10LT) with an accuracy of ±1 °C. An IR camera (Infratec, Vario CAM) having an accuracy of ±1.5 °C was also used to measure the gear surface temperature of the test gear. The jet of compressed air was delivered near the gear mesh region (Figure 4.1(b)).

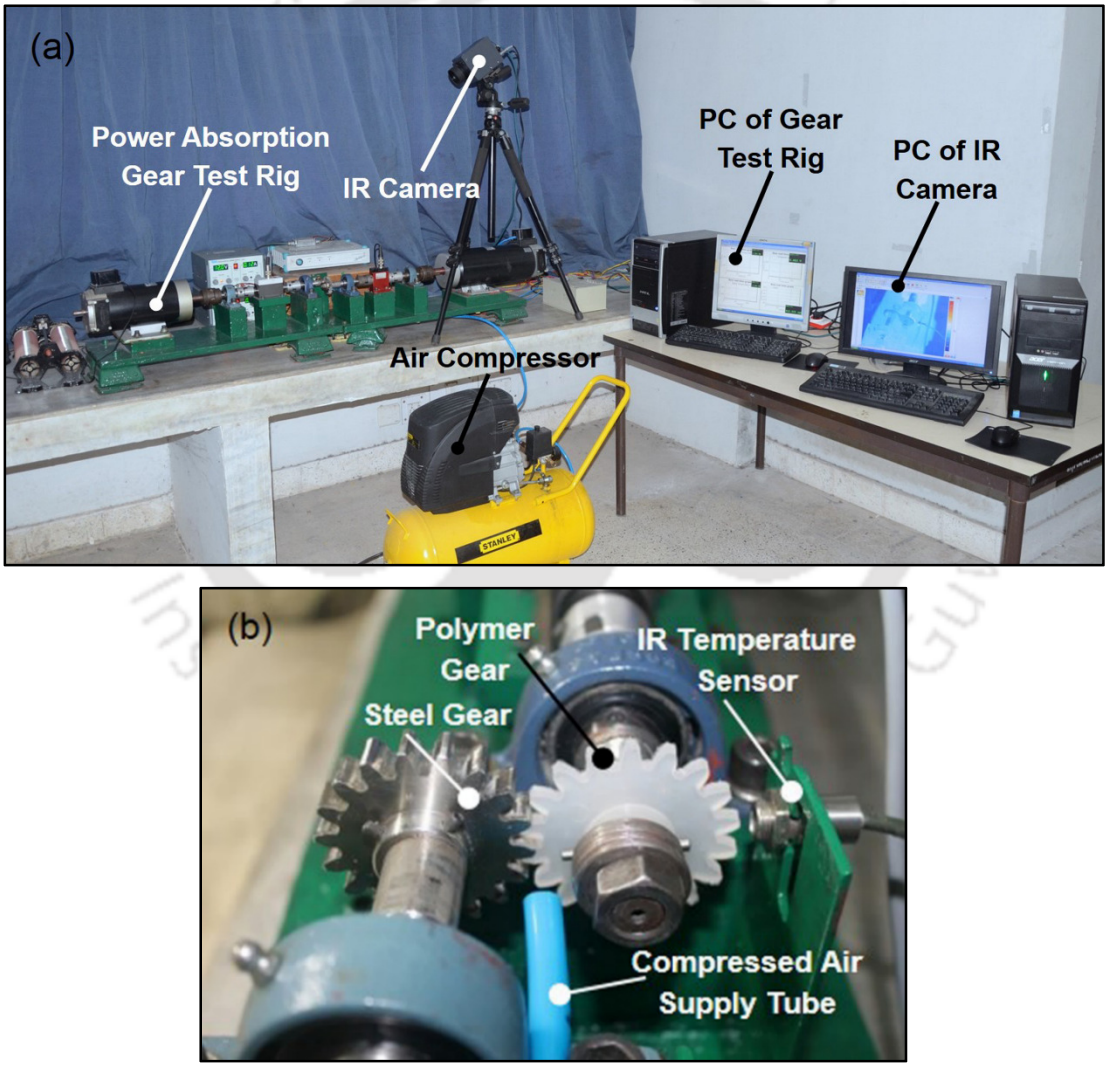

Figure 4.1 In-house developed power absorption gear test rig: (a) overall view and (b) close-up view of gear mesh and compressed air supply in the test rig

Test gears were subjected to 2, 2.5, and 3 Nm torque and run upto 10×10^5, 7.2×10^5, and 1.4×10^5 cycles respectively. All the tests were carried out under the room conditions. Compressed air of 0.3 MPa pressure was continuously delivered near the gear mesh region through a pipe of 8 mm diameter and the temperature, torque at the driver and driven gear were recorded by the data acquisition system (HBM, Spider 8).

4.3 GEAR SURFACE TEMPERATURE

The surface interaction between the gears and material hysteresis causes raise to the gear surface temperature during test. The thermograph of test gear at 3 Nm without air cooling is shown in

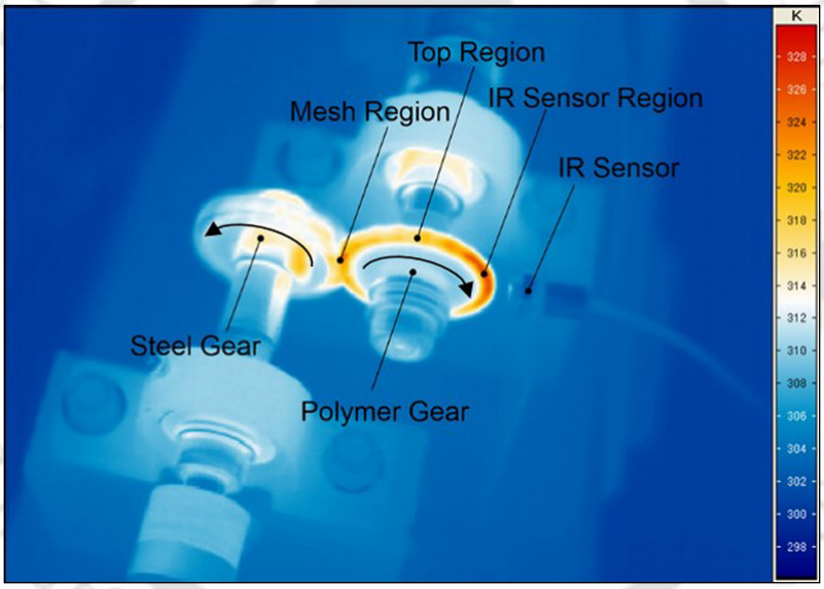

Figure 4.2 Thermograph of the test gear during testing (3 Nm, without cooling)

Figure 4.2. The measured surface temperature of test gear with IR camera as well as the IR sensor during cooling is shown in Figure 4.3. From the Figure 4.3, it is observed that the surface temperature of test gear measured by the IR camera is almost same at both the mesh region and top region. An increase of about 4 °C is observed on the IR sensor region side when compared to the other regions. This is due to the absence of jet of compressed air at this point.

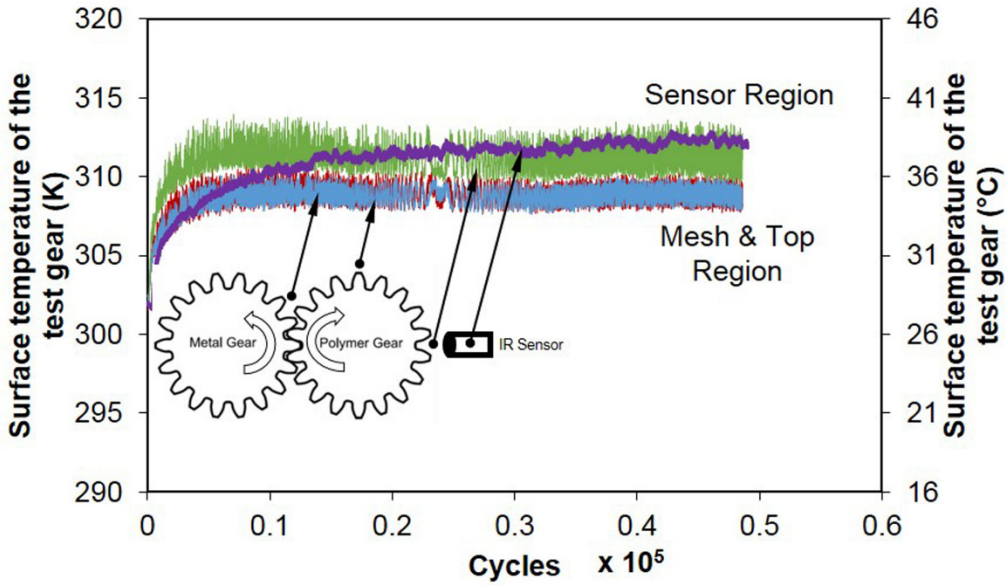

Figure 4.3 Measured surface temperature of the test gear through IR camera and sensor (3 Nm, with cooling)

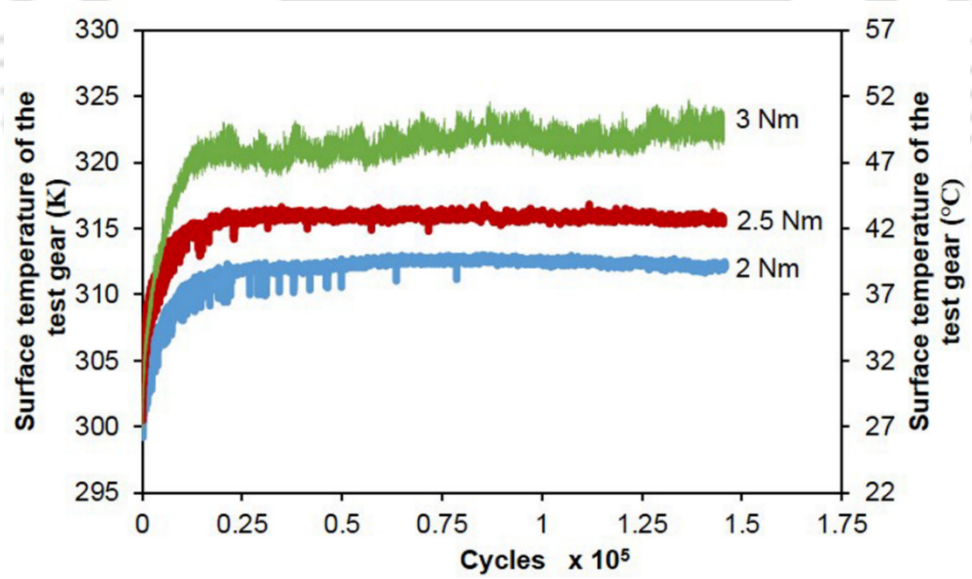

Figure 4.4 Effect of load on the surface temperature of the test gear

The measured surface temperature of the test gears at 2, 2.5, and 3 Nm loads is shown in Figure 4.4. There is a gradual rise in the beginning, and then temperature reaches a steady value once the equilibrium is reached between the heat generation and heat dissipation. With increased load,

surface temperature of the test gear increased due to increased heat generation by contact stress and gear tooth deflection. Similar load sensitive gear surface temperature was also observed by Senthilvelan and Gnanamoorthy (2006), Senthilvelan and Gnanamoorthy (2007), Duzcukoglu (2009), and Kim (2006).

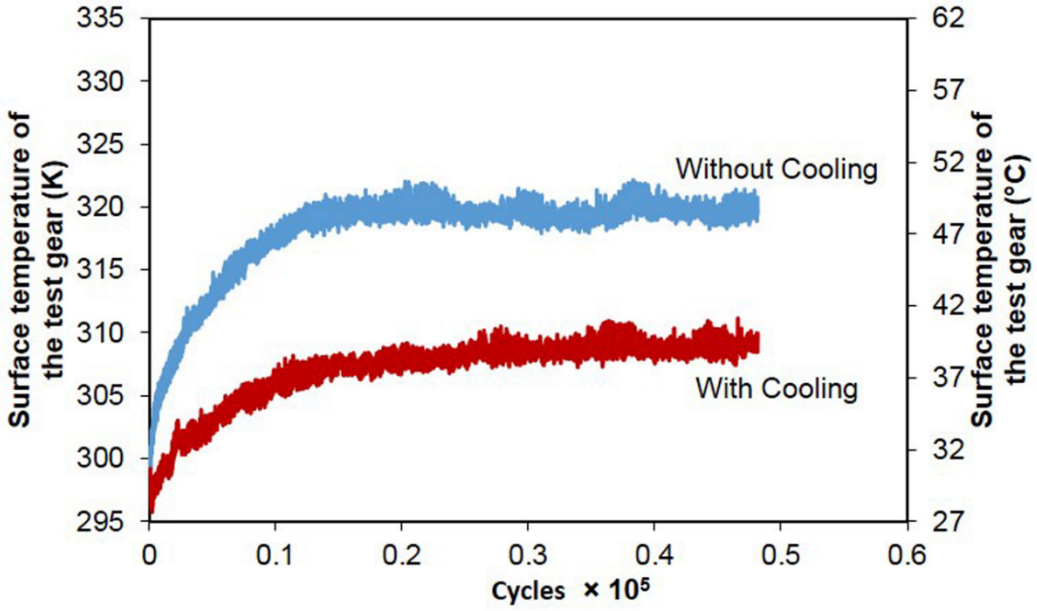

Figure 4.5 Surface temperature of the test gear with and without cooling (3 Nm)

The online measured surface temperature and maximum surface temperature of test gear while running with and without compressed air are shown in Figure 4.5 and Figure 4.6 respectively. A temperature drop of 6–10 °C is observed when the compressed air is delivered near the gear mesh region during the test. Test gears subjected to 2, 2.5, and 3 Nm reduced its surface temperature by 16, 17, and 23% by the air cooling. Due to the forced convection, heat dissipation improved which reduces the net gear surface temperature and the effect of cooling is significant at higher loads. Measured gear tooth surface temperature is the net surface temperature after equilibrium between heat generation and heat dissipation during gear test.

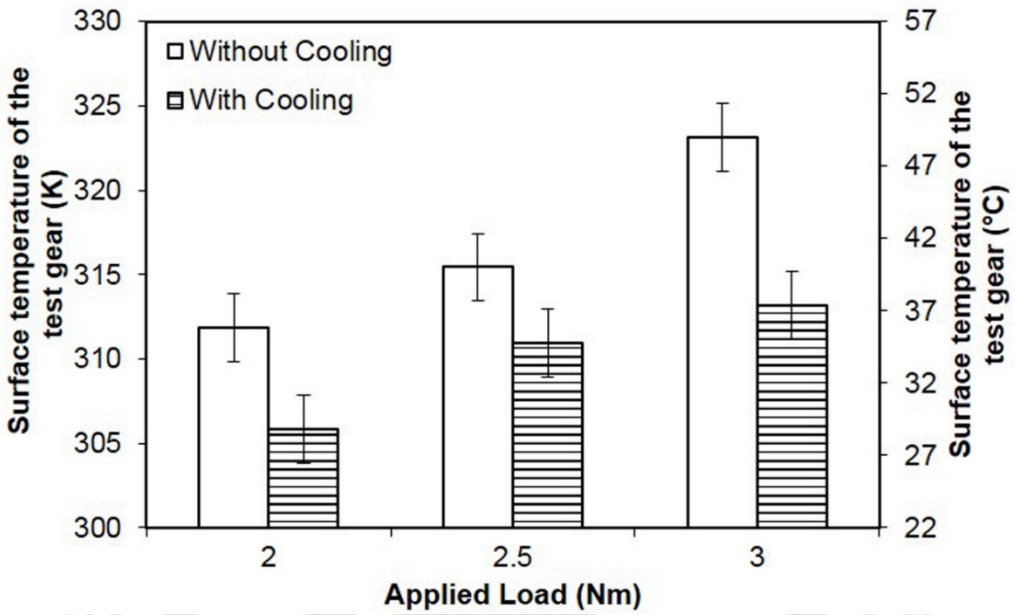

Figure 4.6 Effect of cooling on the surface temperature of the test gear

Mao (2007) proposed a gear heat transfer model, wherein the airflow between gear teeth gap is pumped from one side of the contact region to the other. The pockets of air are trapped between gear teeth during meshing and heated. The heated air is moved around the gear and expelled outside during meshing operation and replaced by fresh air. The temperature of hot air within each pocket is close to that of the gear surface temperature and the turbulence in each pocket will ensure that the noncontact gear surface is heated to contact surface temperature. From the Mao model, gear body temperature rise Δt can be evaluated,

$$\Delta t = \frac{0.625\mu T}{C_p \rho Z b (r_a^2 - r^2)} \tag{4.1}$$

where μ is the coefficient of friction, T is the applied torque (Nm), ρ is the specific density of air (kg/m^3), C_p is the specific heat capacity of the air (J/kg.K), Z is the teeth number, b is the gear face width (m) of driven gear, r_a and r are the radius of addendum and pitch circle (m) of driven gear.

To predict the surface temperature of gear body during air cooling, the specific density is replaced in the following manner as per gas law,

$$\rho = \frac{P_a}{Rt} \tag{4.2}$$

where P_a is the absolute pressure (N/m^2), R is the specific gas constant (J/kg.K), and t is the absolute temperature of the air (K). The perfect load sharing between the gear teeth contact ratio of 1.5 was assumed in this model. In the standard condition (without air cooling), atmospheric pressure and temperature were used. In the air cooling condition, air delivery pressure of 0.3 MPa and theoretical temperature of 27 °C were considered for the surface temperature prediction. Coefficient of friction for both dry running as well as compressed air cooling was assumed as 0.25. However, in reality, thermoplastic polymers exhibit slightly higher coefficient of friction due to the material softening and enhanced the real contact area.

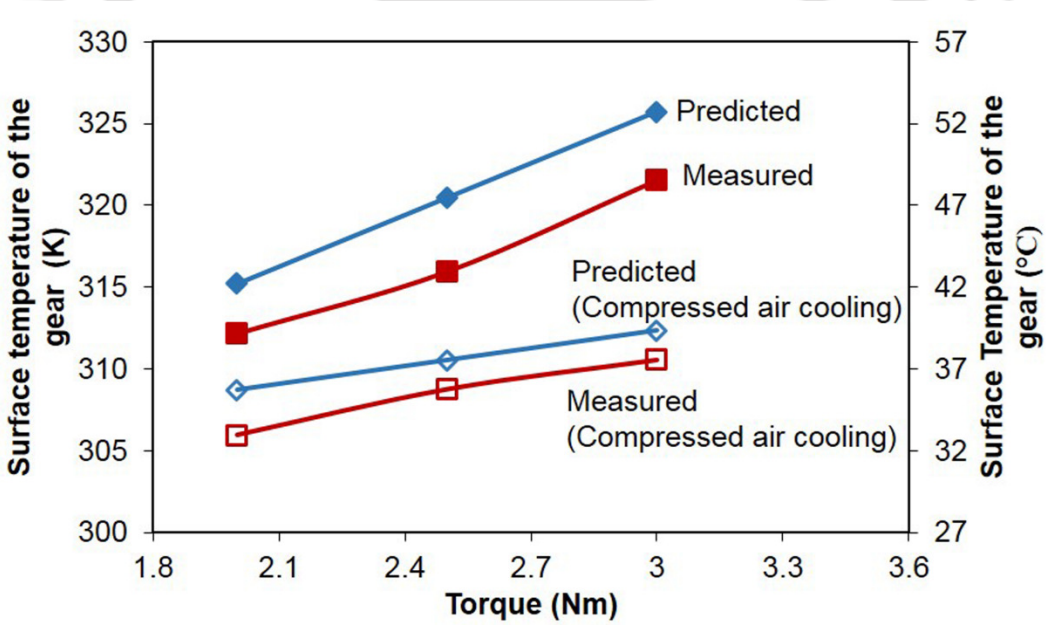

Figure 4.7 Gear tooth surface temperature: predicted and measured

Figure 4.7 shows the predicted gear surface temperature based on the modified Mao model for the load levels of 2, 2.5, and 3 Nm and compared with the measured temperature. A good agreement (2% deviation) is observed between the model and experiment.

4.4 GEAR TOOTH WEAR

Test gear tooth thickness reduction by base tangent length measurement as described in Subsection 3.4.2 (Section 3.4; CHAPTER 3) was measured periodically (every 3 h) to understand the wear

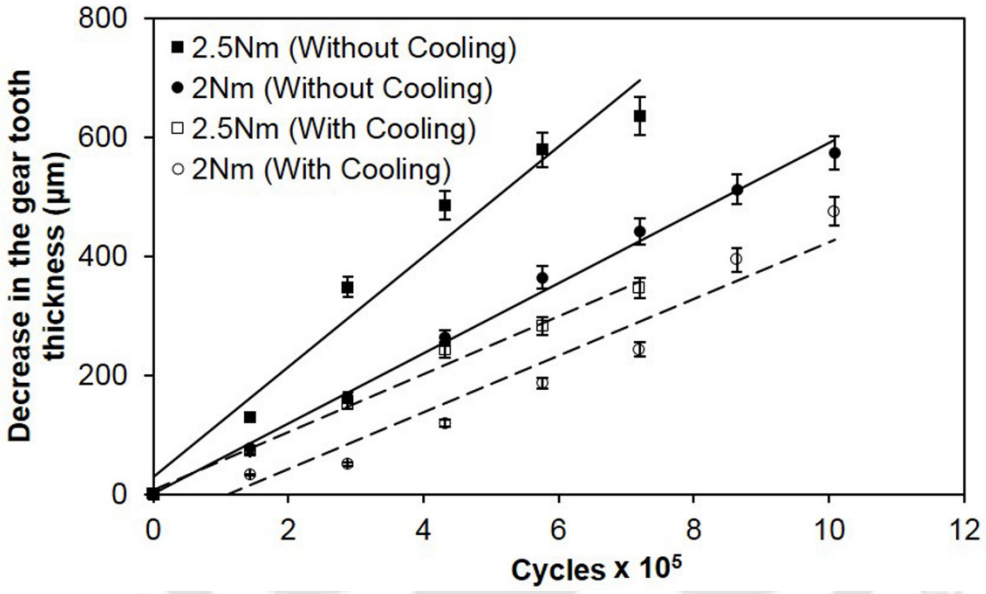

Figure 4.8 Gear tooth thickness reduction during testing

resistance. Figure 4.8 shows the gear tooth wear with and without compressed air cooling. For all the loads, gears cooled with compressed air exhibit less wear and the slope of the curve indicates the wear rate. At higher loads and without cooling, higher surface temperature softened the gear material and provided less wear resistance. With air cooling, a 50% life enhancement is observed when gears are subjected to 2 Nm when base tangent length of gear tooth reduced by 0.3 mm. Similarly, a 100% life enhancement is observed when gears are subjected to 2.5 Nm for the 0.3 mm reduced base tangent length.

Similar to tooth wear, weight loss of the test gear per 1×10^5 cycles were measured and shown in Figure 4.9. With the increased load, gear tooth wear increased due to the higher contact pressure. For all the test loads, test gears cooled with compressed air exhibited less wear after a finite number

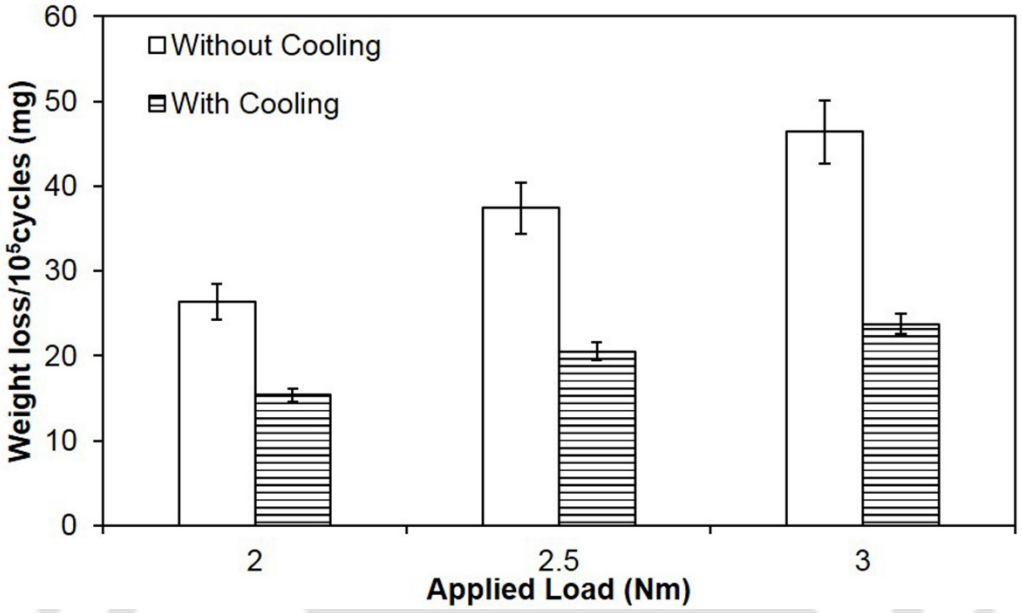

Figure 4.9 Effect of cooling on the wear resistance of the test gear

of cycles. Similar to the surface temperature of the test gear, the effect of cooling on the gear wear is significant at higher loads. At elevated temperature, polymeric materials exhibited high coefficient of friction and high wear (ASM handbook, 1992). This behaviour is due to the change in friction mechanism from abrasion to adhesion. Increased surface temperature of test gear softened the gear tooth and offered less resistance to the wear. Duan *et al.* (2009) also observed similar behaviour in the sliding wear performance of polyphenylene sulfide, polyethersulfone, and polysulfone under dry, forced air, and water cooling environment. Both air and water cooling reduced friction coefficient and improve wear resistance. From the wear morphology, it is revealed that considerable amount of plastic deformation occurred at dry sliding, while the amount of plastic deformation was reduced by the cooling processes.

4.4.1 Gear Tooth Profile Wear

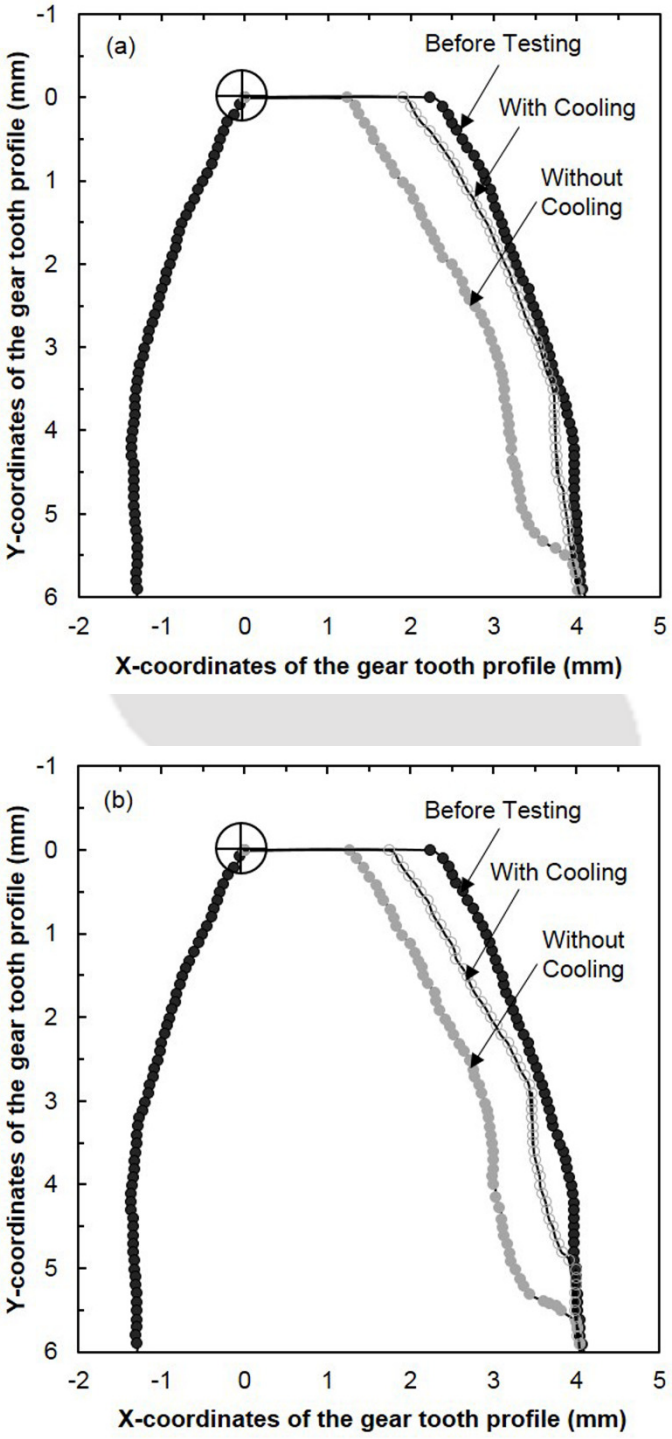

Figure 4.10 Gear tooth profile observed under profile projector: (a) 2 Nm after 10×10^5 cycles and (b) 2.5 Nm after 7.2×10^5 cycles

The final involute profile of a gear tooth tested at 2 and 2.5 Nm after 10×10^5 and 7.2×10^5 cycles were measured as per the procedure described in Subsection 3.4.2 (Section 3.4; CHAPTER 3) and shown in Figure 4.10(a)–(b) and compared with the untested gear. For the measurement of worn out gear tooth surface, origin was taken on the coast side tip of the gear. Test gears loaded at 2 Nm after 10×10^5 cycles with and without air cooling is shown in Figure 4.10(a). Similarly, Figure 4.10 (b) shows the profile of test gear loaded at 2.5 Nm after 7.2×10^5 cycles with and without air cooling. From both the test conditions, superior wear resistance under air cooling is observed. With increased loading, tooth wear increase is also clearly observed. However, slightly more wear was observed near the tip and root region for all the test conditions and detailed discussion of this behaviour will be presented in Subsection 7.4.3 (Section 7.4; Chapter 7).

4.4.2 Worn out Morphology of Test Gear at Various Stages of Service

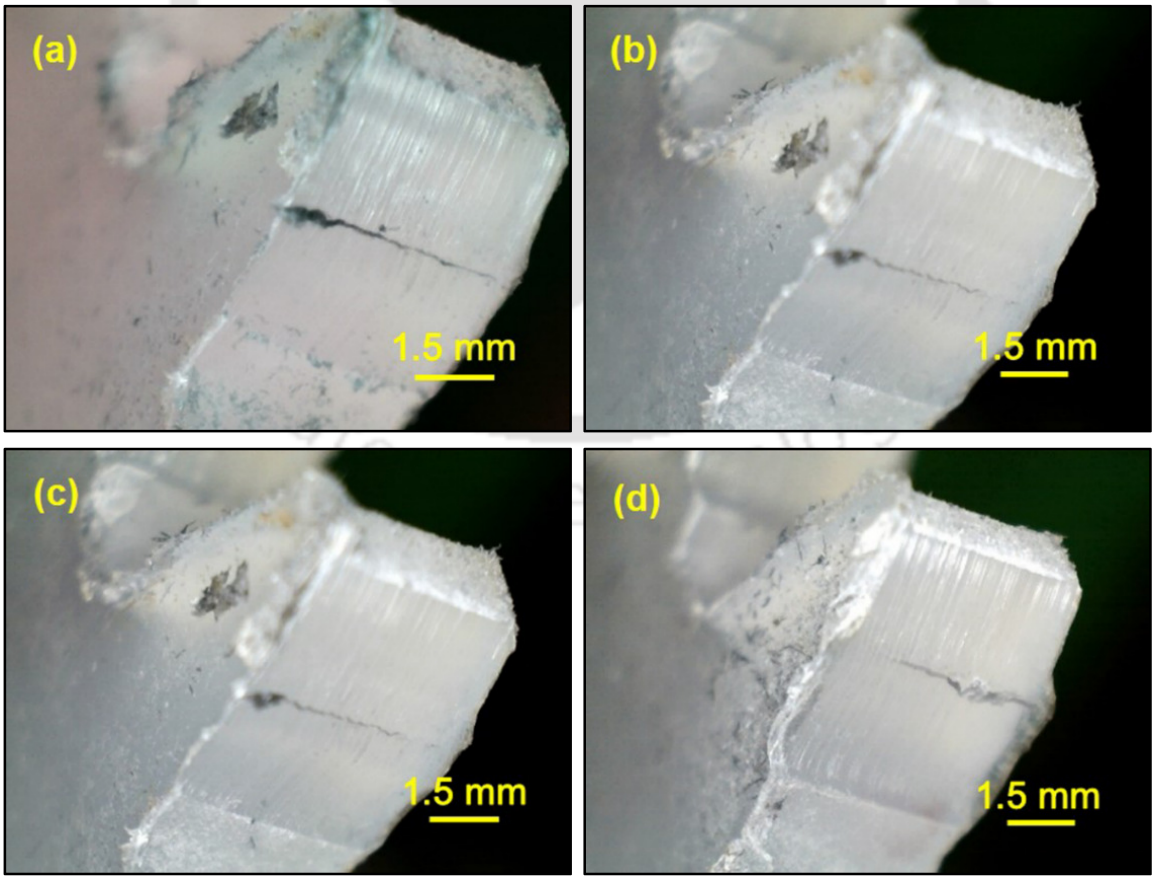

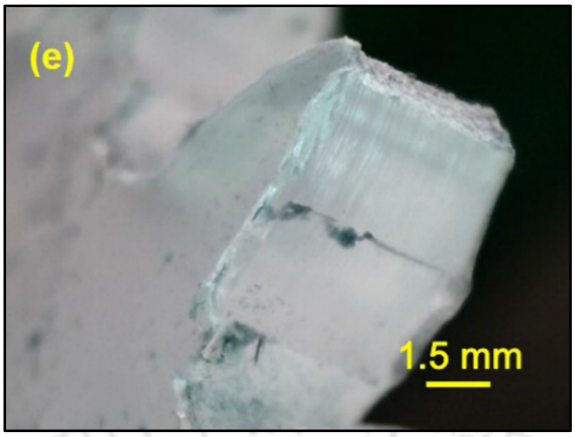

Figure 4.11 Surface of test gear tooth loaded at 2.5 Nm (without cooling) after (a) 1.4×10^5 cycles, (b) 2.8×10^5 cycles, (c) 4.3×10^5 cycles, (d) 5.7×10^5 cycles, and (e) 7.2×10^5 cycles.

To determine the effect of load cycles on the gear tooth wear, the worn out surface of the test gear at various number of cycles and at same load condition (2 Nm) was observed (Figure 4.11(a–e)) using digital microscope (Celestron, Digital Microscope Pro). With increased number of cycles, surface damage of the gear tooth increased.

4.4.3 Effect of Air Cooling over the Worn out Morphology of the Test Gear

Generally, wear, scoring, plastic flow, pitting, and tooth fracture are some of the common failure modes of the polymer gears due to fatigue.

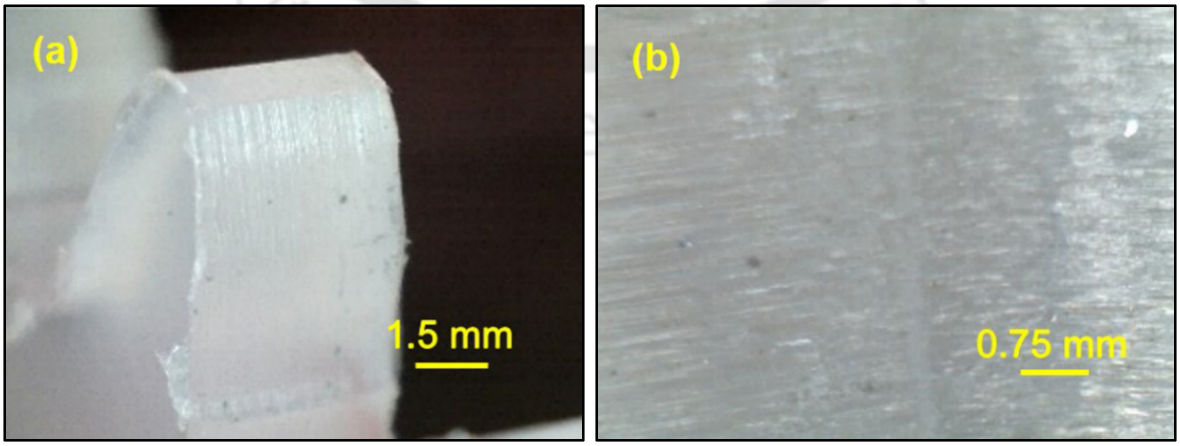

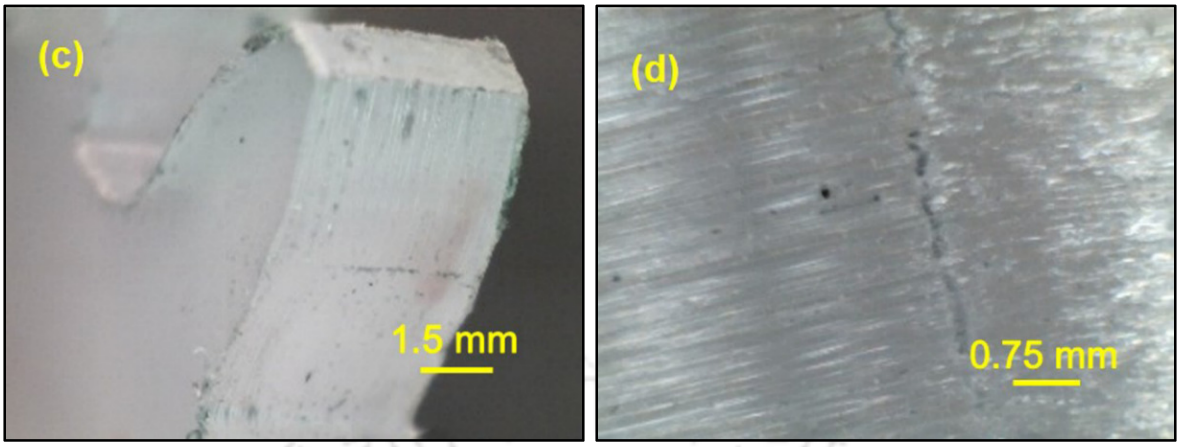

Figure 4.12 Surface of gear tested at 2 Nm after 10×10^5 cycles: (a) test gear without cooling, (b) close-up view of test gear without cooling, (c) test gear with cooling, and (d) close- up view of test gear with cooling

Figure 4.12(a–d) shows the abrasive marks on tooth surface when the gears were tested at 2 Nm; change in the direction of sliding on pitch line is observed. Figure 4.12(a) and Figure 4.12(b) show the test gear wear without cooling and Figure 4.12(c) and Figure 4.12(d) show the test gear wear with cooling. At this low load condition, no significant difference between with and without cooling is observed, though measurement of gear tooth thickness and weight loss exhibited a significant difference.

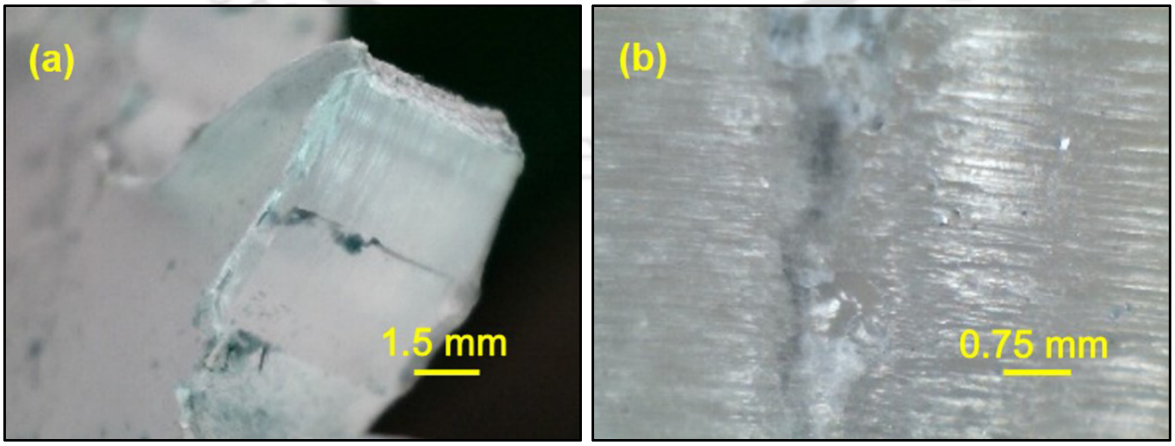

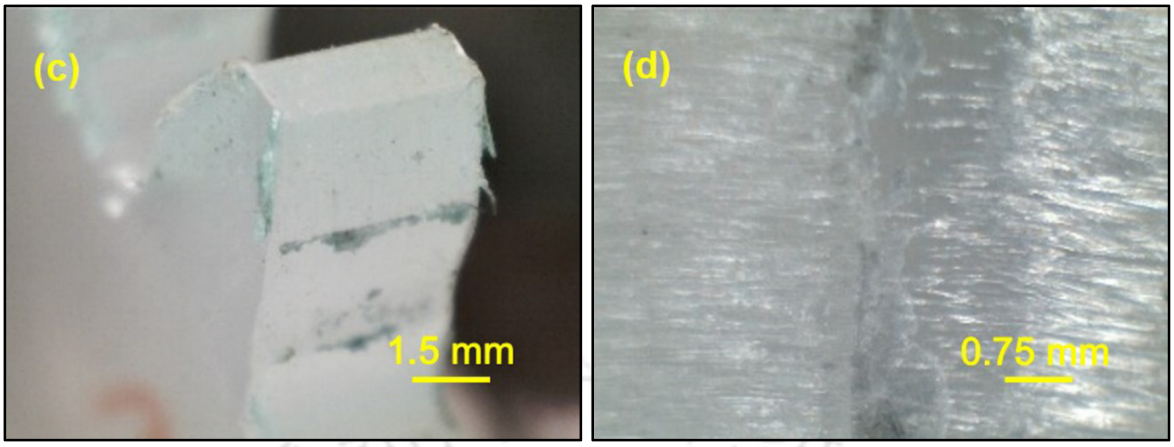

Figure 4.13 Surface of gear tested at 2.5 Nm after 7.2×10^5 cycles: (a) test gear without cooling, (b) close-up view of test gear without cooling, (c) test gear with cooling, and (d) close-up view of test gear with cooling

Figure 4.13(a–d) shows the worn out tooth surface when gears were tested to 2.5 Nm. Figure 4.13(a) and Figure 4.13(b) show the tooth of gears tested without cooling and Figure 4.13(c) and Figure 4.13(d) show the tooth of gears tested with cooling. Gears tested without cooling exhibited severe damage when compared to the gears tested with cooling. The change in the direction of sliding at the pitch as well as direction of sliding is distinctly visible. Figure 4.14(a–d) shows the worn out gear tooth surface when the gears were subjected to 3 Nm.

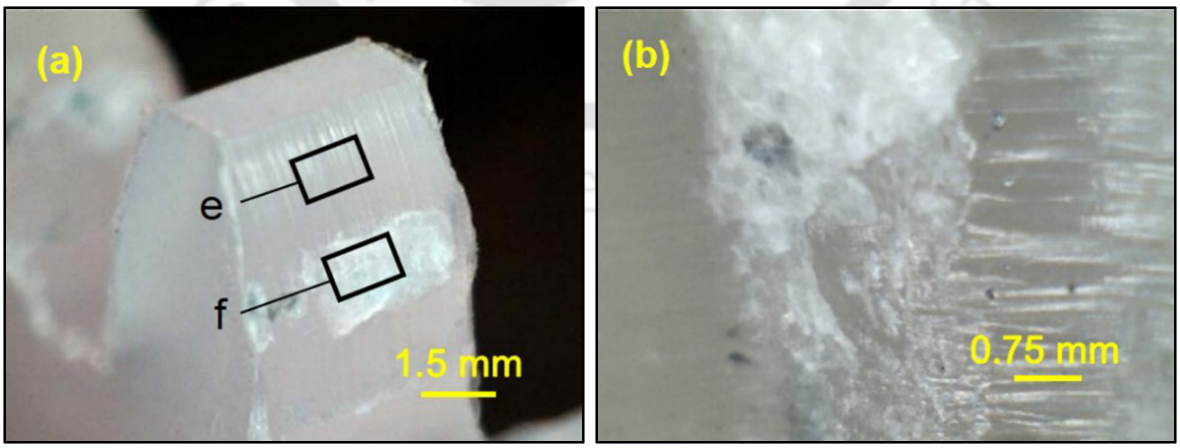

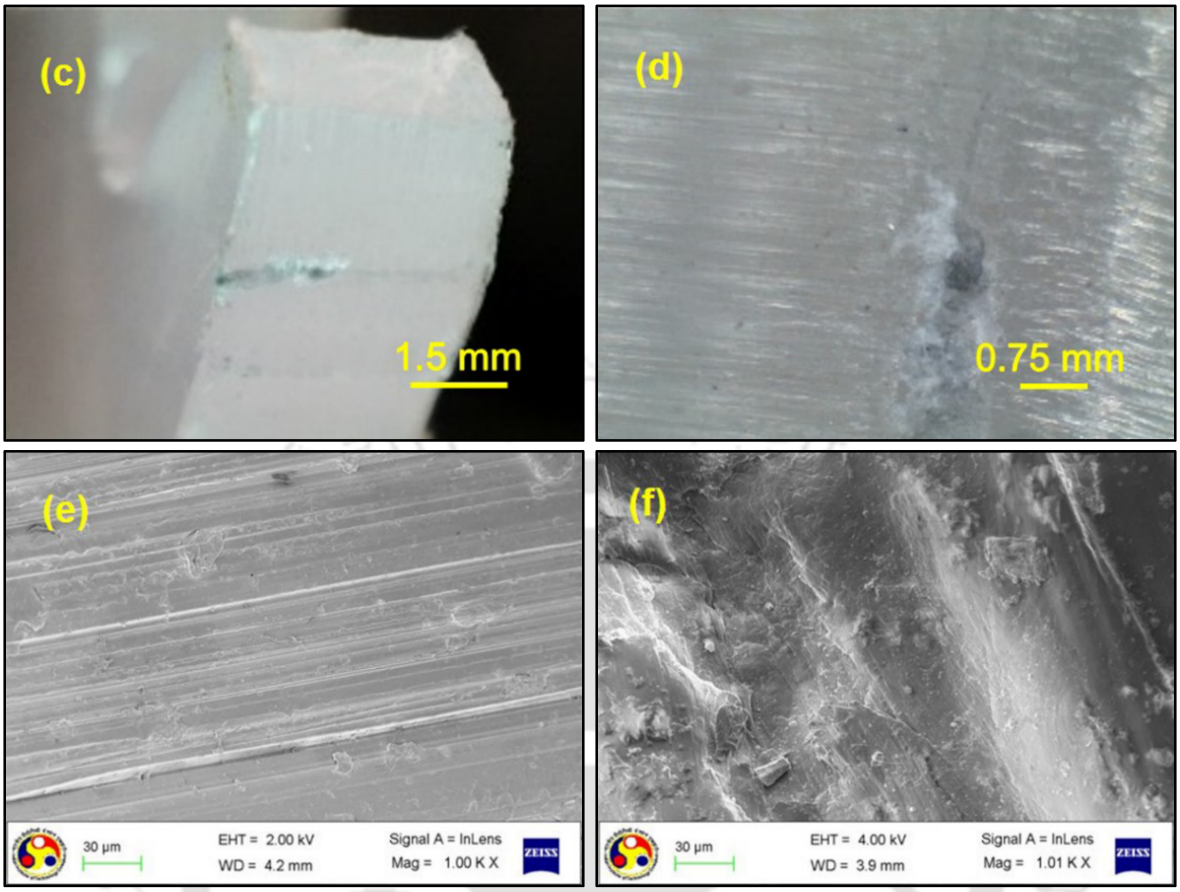

Figure 4.14 Surface of gear tested at 3 Nm after 1.4×10^5 cycles: (a) test gear without cooling, (b) close-up view of test gear without cooling, (c) test gear with cooling, (d) close-up view of test gear with cooling, (e) abrasive wear marks on gear tested without cooling, and (f) plastic deformation near the pitch region of gear tested without cooling

Figure 4.14(a) and Figure 4.14(b) correspond to the gears tested without cooling and Figure 4.14(c) and Figure 4.14(d) correspond to the gears tested with cooling. At this load condition, gears tested without cooling showed plastic flow due to its elevated temperature, whereas air cooling prevented these failures. Figure 4.14(e–f) shows the close-up view observed under scanning electron microscope (3 Nm without cooling). Figure 4.14(e) shows the abrasive marks above the pitch region and Figure 4.14(f) shows the plastic flow near the pitch region of the gear tooth.

4.5 TRANSMISSION EFFICIENCY

Gear transmission efficiency was evaluated to understand the effect of the gear tooth wear on the gear performance. The gear accuracy and frictional losses due to sliding and rolling motion of the gear teeth affected the power losses and transmission efficiency. In this work, only losses due to friction and wear were considered to evaluate the transmission efficiency. In the test rig, two bearings are used between the gear pair and torque sensors. For the simplicity, losses due to bearing and gear inaccuracy were neglected. Measured torque at the driver and driven end was used to compute the transmission efficiency with the following relation

$$Transmission\ efficiency = \frac{Inline\ torque\ measured\ at\ the\ driven\ gear\ shaft}{Inline\ torque\ measured\ at\ the\ driver\ gear\ shaft} \quad (4.3)$$

Figure 4.15(a–c) shows the transmission efficiency of the test gear with and without compressed air cooling at various loads (2–3 Nm) for a finite number (1.4×10^5) of cycles. For all the test conditions, transmission efficiency exhibits a little drop as the number of cycles increase.

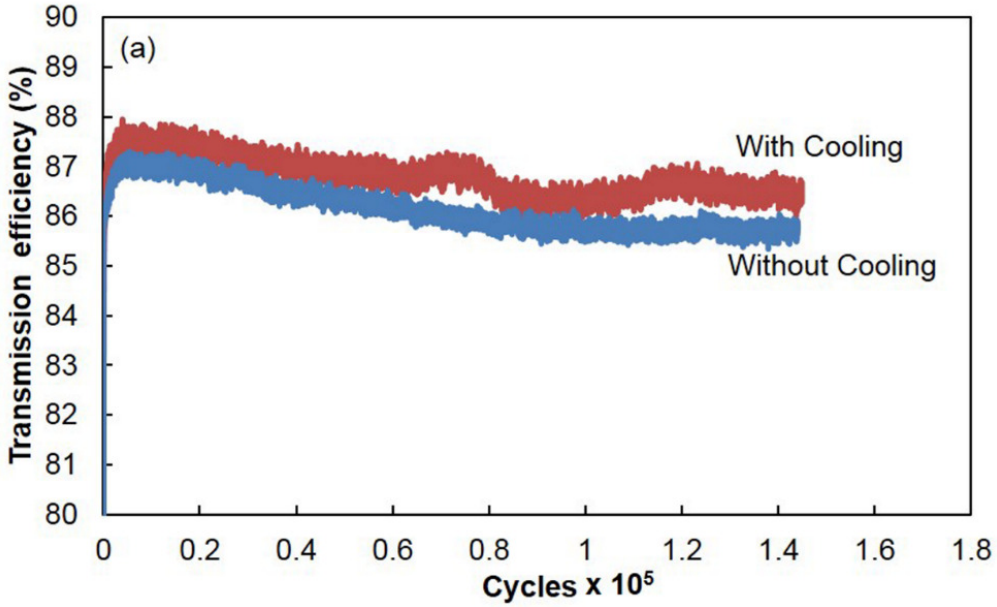

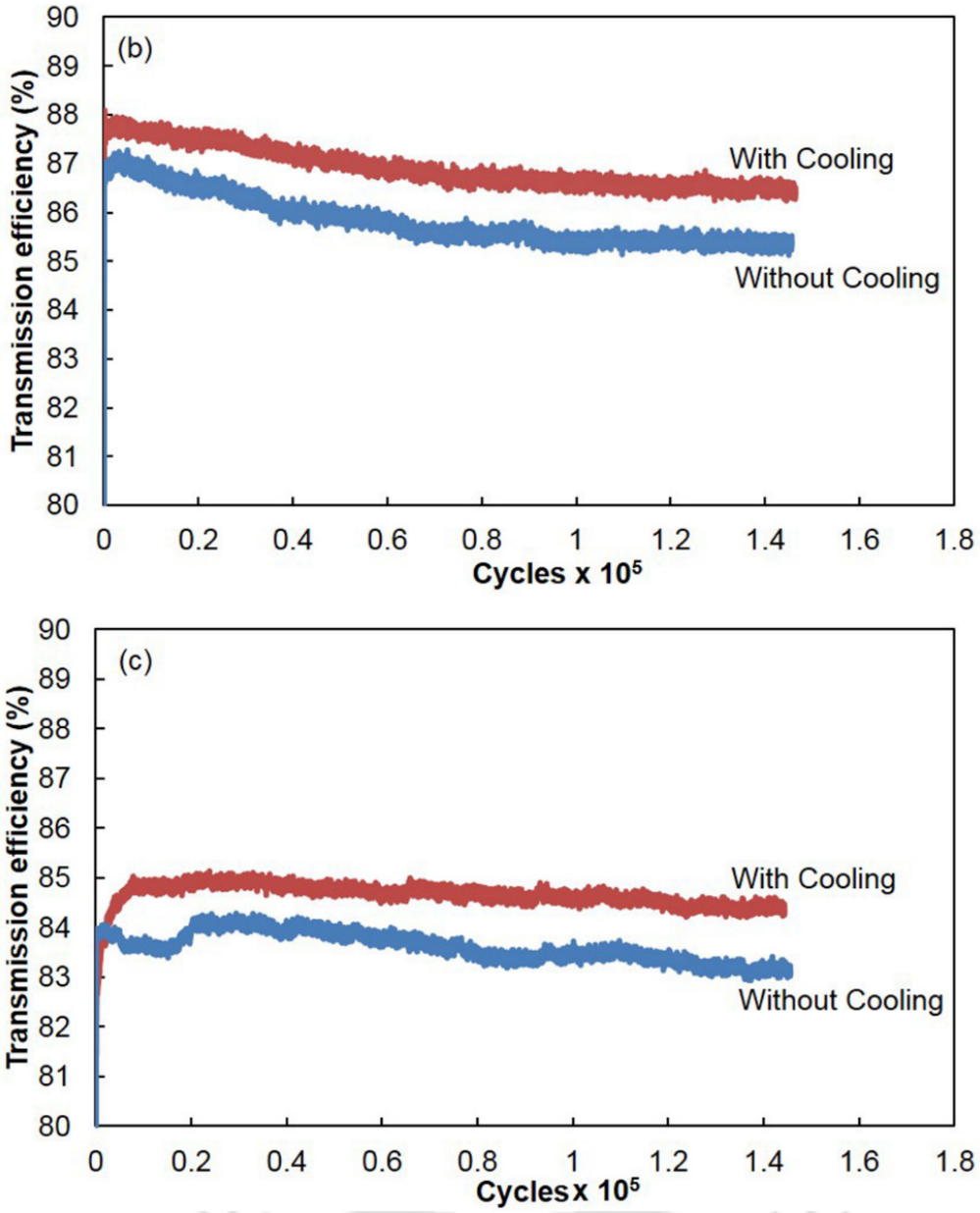

Figure 4.15 Transmission efficiency of test gear pair with and without cooling tested at (a) 2 Nm, (b) 2.5 Nm, and (c) 3 Nm

With increased number of cycles, progressive gear tooth wear contributes to the power loss and hence a slight drop in transmission efficiency is observed. Periodic measurement of gear tooth thickness (Figure 4.8) and worn out surface of the test gear (Figure 4.11) confirmed that the wear increased with the number of cycles. For all the considered test loads (2, 2.5, and 3 Nm), gear pairs

with cooling exhibited higher efficiency than that of the gear pairs without cooling (Figure 4.15(a–c)). Test gears loaded at 2, 2.5, and 3 Nm exhibited 1, 2, and 2% improvement of transmission efficiency respectively. Kirupasankar *et al.* (2012) measured the transmission efficiency of various thermoplastic composite spur gears. Gears made of higher elastic modulus exhibited low surface temperature and high efficiency. With the increased load, efficiency decreased for all the investigated materials.

4.6 SUMMARY

Injection-moulded test gears were subjected to various loads for a finite number of cycles to understand the wear performance, with and without compressed air and the following major conclusions were arrived,

- Continuous measurement of gear tooth surface temperature confirmed that the compressed air cooling reduced the net surface temperature by 15–23% for the test condition.
- Measurement of gear weight and tooth thickness confirmed that wear resistance of gears increased by 50–100% due to air cooling when they were loaded at 2 and 2.5 Nm.
- Tooth profile after finite number of cycles (10×10^5 and 7.2×10^5) at different loads (2 and 2.5 Nm) confirmed uniform wear across the face and flank region and superior wear resistance under air cooling.
- Worn out gear surface image after 10×10^5, 7.2×10^5, and 1.4×10^5 cycles when loaded at 2, 2.5, and 3 Nm confirmed the influence of air cooling in the wear resistance.
- Measured test gear pair transmission efficiency under air cooling condition exhibited about 2% enhanced performance than that of normal condition.

CHAPTER 5

EFFECT OF MATING STEEL GEAR MANUFACTURING PROCESS OVER THE PERFORMANCE OF INJECTION-MOULDED POLYPROPYLENE GEAR

5.1 INTRODUCTION

In the recent years, nonstandard gears including asymmetric gears (having different pressure angle at drive side and coast side) have drawn researcher's attention due to the advent of new manufacturing processes. Polymer based materials are generally used to manufacture nonstandard gears through injection-moulding as it involves only one complex profile die. These nonstandard polymer gears are generally paired with identical steel pinion due to the requirement of superior load carrying capacity. Thus, standard polymer gears are meshed with a hobbed steel gear, whereas nonstandard polymer gears are in mesh with a wire-cut electric discharge machining (WEDM) steel gear. Surface manufactured through WEDM possesses different surface characteristics when compared to that of machined surface. Additionally, unlike machined surface, WEDM surface of nonstandard gear cannot be processed by secondary finishing process like grinding. Polymer gear performance is slightly affected by the surface characteristics of mating steel gear (Akkurt, 1995).

Few researchers have investigated the effect of manufacturing processes over gear performance. Bergseth *et al.* (2012) manufactured gears by hobbing, green-shaving, honing, and grinding and investigated the influence of surface topography on the contact area and pressure using boundary element method. Green shaved gear and honed gear exhibited highest contact area ratio. Real

surface topography significantly affects wear, friction, and lubrication properties of the contact. Gupta and Jain (2014) manufactured miniature gears by WEDM and studied surface topography, bearing length parameters, microstructure, and micro hardness. At low discharge energy parameters, manufactured gear exhibited less profile and lead deviation with less surface roughness.

Nakatsuji and Mori (1999) examined surface durability of electrolytic polished gears and ground gears of same surface roughness. Electrolytic polishing generates micro pores which create lubricating films between the tooth surfaces and enhance resistance against pitting. Ali *et al.* (2010) manufactured miniature gears through micro WEDM and conventional WEDM. The average surface roughness of micro WEDM and conventional WEDM are found to be 50 nm and 2 µm. The range of dimensional accuracy exhibited by the micro WEDM and conventional WEDM are 0.1–1 µm and 2–3 µm respectively.

Few works have been carried out to understand the effect of electric discharge machining over surface and mechanical properties. Kumar *et al.* (2009) reviewed the phenomenon of surface modification by electric discharge machining (EDM) process. Surface layer produced by EDM contains a top white layer which crystallizes from the liquid cooled at high speed. White layers generated on a steel work piece have higher carbon content which resulted in increased resistance to abrasion and corrosion. Llanes *et al.* (2004) investigated the influence of surface finish by EDM on the flexural strength of tungsten carbide based materials. Four-point bending test was carried out and compared with conventional grinding and polishing process. From the investigation, it was concluded that the flexural strength of the material reduced due to EDM-induced flaws including surface residual stress. Bonny *et al.* (2008) prepared ZrO_2 based composites surface by wire-cut electric discharge machining and polishing to evaluate the tribological performance. The

coefficient of friction and wear rate of the composite machined by the WEDM were found to be higher when compared to that of the polished composite.

From the summary of the literature review, it is observed that the surface condition of the test gear significantly affects the surface durability of the gears. Friction and wear performance of the polymer based material is significantly affected by the counter surface topology. WEDM process alters the surface properties and no investigation was carried out to understand the surface durability of polymer gears against conventional machined and WEDM gear and this work attempts the same.

5.2 METHODOLOGY

Polypropylene (M110, Haldia Petrochemical Ltd.) was injection-moulded (Texair, JTS 40) to spur gears at 230 °C. Moulding conditions and test gears details, parameters are explained in the methodology Section 3.2 and 3.4 (CHAPTER 3). The gear tests were carried out at a constant speed of 800 rev/min and at various torques (2, 2.5, and 3 Nm). Polymer gear performance was evaluated by pairing with the standard stainless steel gears manufactured by conventional machining and WEDM process. The standard steel gear was manufactured by hobbing followed by grounding (conventional machining) and brass wire electrode was used for manufacturing stainless steel WEDM gear. Injection-moulded polymer gears and steel gears were measured for its accuracy. Injection-moulded gears are of DIN quality 10, WEDM and machined steel gears are of DIN quality 8 and 5 respectively. Polymer gears were paired with steel gear having larger face width, so that under any misalignment condition, the hard steel gear edge cannot contact and causes damage to the soft polymer gears. Mating steel gear tooth surface was observed under scanning electron microscope (Zeiss, Sigma) and noncontact three dimensional profiler (Taylor Hobson CCI MP) to understand its surface topology. Presence of elements on the manufactured mating steel

gear tooth surfaces was confirmed using XRD (PANalytical). The micro hardness of the mating steel gear tooth surface was measured (Buehler 1600) to understand its frictional characteristics. Noncontact three dimensional optical profiler was also used to obtain the bearing ratio curve of the gear tooth surface.

5.3 SURFACE MORPHOLOGY

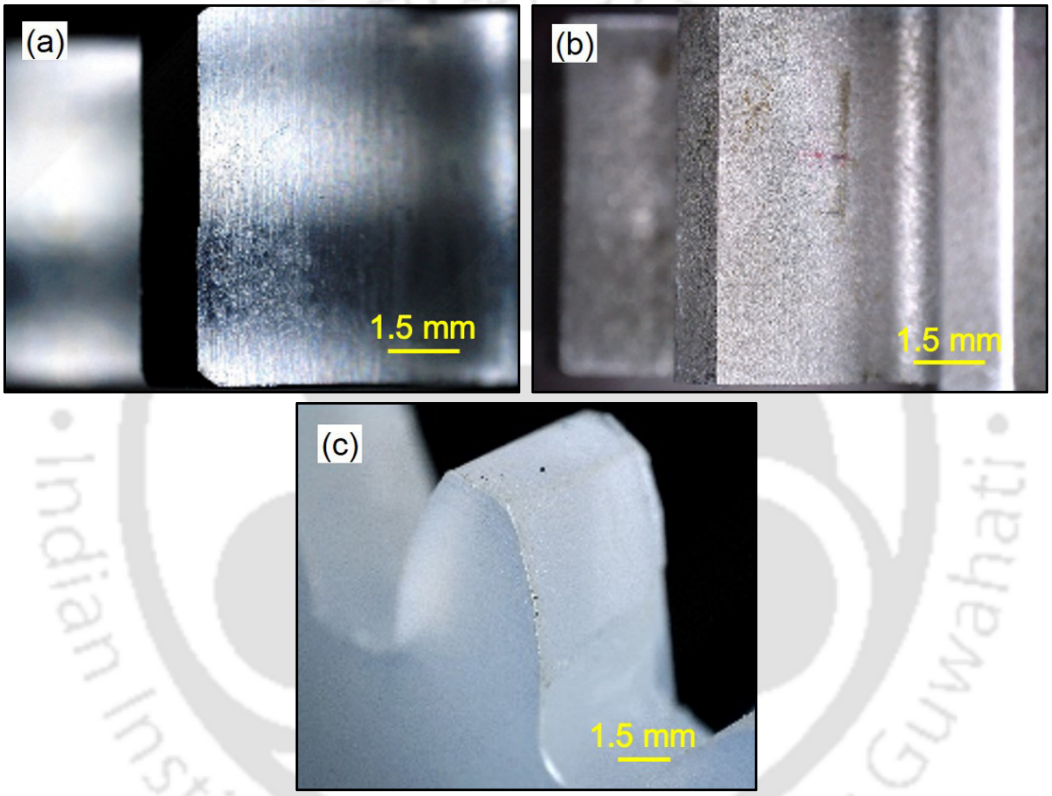

Figure 5.1 Mating gear tooth surface manufactured by (a) conventional machining, (b) wire-cut electric discharge machining, and (c) Injection-moulded polypropylene gear showing tooth profile

The gear surface of conventional machined gear, WEDM and injection-moulded polypropylene gear are shown in Figure 5.1. Figure 5.2(a–b) shows the tooth surface of a gear manufactured by conventional machining. Conventional machined surface was not exhibited any craters, pock marks and solidification layers of molten metal. In the WEDM, the spark produced the intense

heat and hence metal is melted and removed. Some of the molten metal was flushed out by dielectric fluid and remaining metal solidified and formed lumps of debris. This recast layer consists of crater, pock marks, and solidified spherical particles. The tooth surface of the gear manufactured by WEDM was observed under scanning electron microscope and shown in Figure 5.2(c–d). Tooth surface exhibited rough and porous texture with crater due to the collapse of plasma.

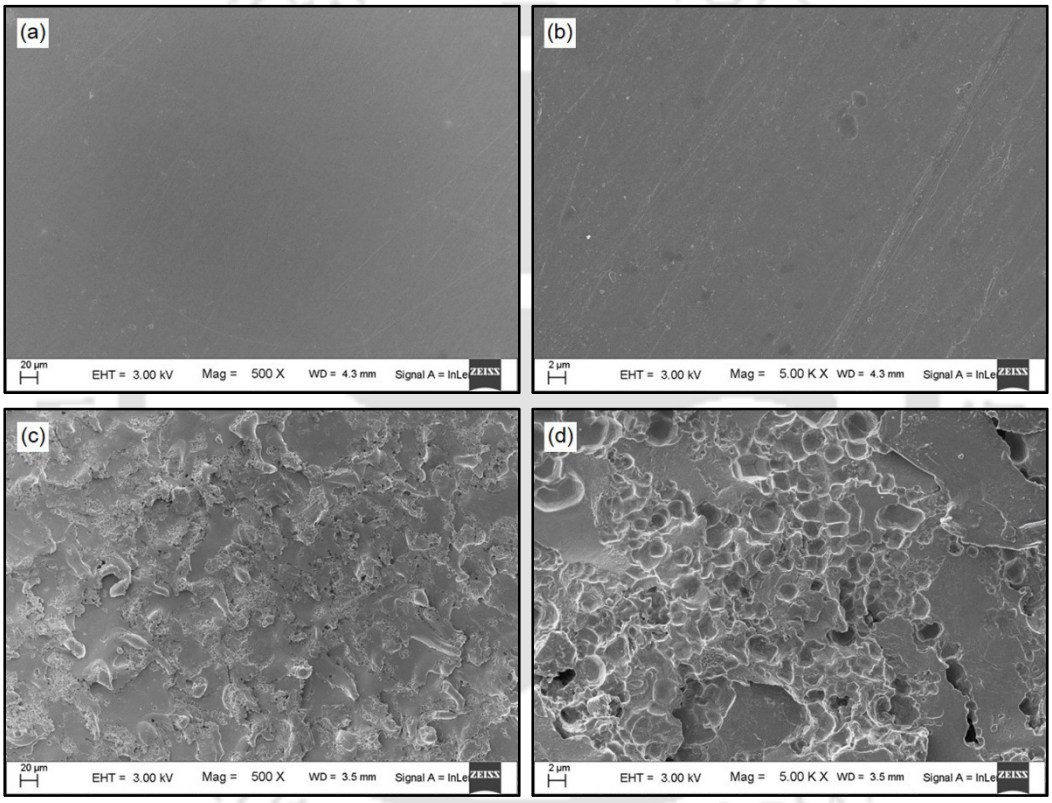

Figure 5.2 Scanning electron micrographs of gear tooth surface manufactured by (a–b) conventional machining and (c–d) wire-cut electric discharge machining

The elemental analysis of conventional machined and wire-cut EDM surfaces were carried out using XRD and shown in Figure 5.3. The XRD plot confirmed the presence of FCC γ-austenite phases in both the conventional machined and WEDM stainless steel surface determined from the plane orientation. From the XRD analysis, crystalline size of the machined and WEDM surface

was computed by using full width at half maximum using Scherrer's equation (Langford and Wilson, 1978).

$$a = \frac{\lambda}{\beta \cos\theta} \tag{5.1}$$

where a is the crystal size (nm), λ is the wave length of X-ray (0.15406 nm), β is the full-width at half maximum which is determined from XRD data (radian) and θ is the diffracted angle (deg). The average crystal size of all the planes for the conventional machined surface is 8.5 nm, whereas for the WEDM surface it is 15.2 nm. This increased crystal size is due to dynamic crystallization of planes at high temperature induced by EDM process.

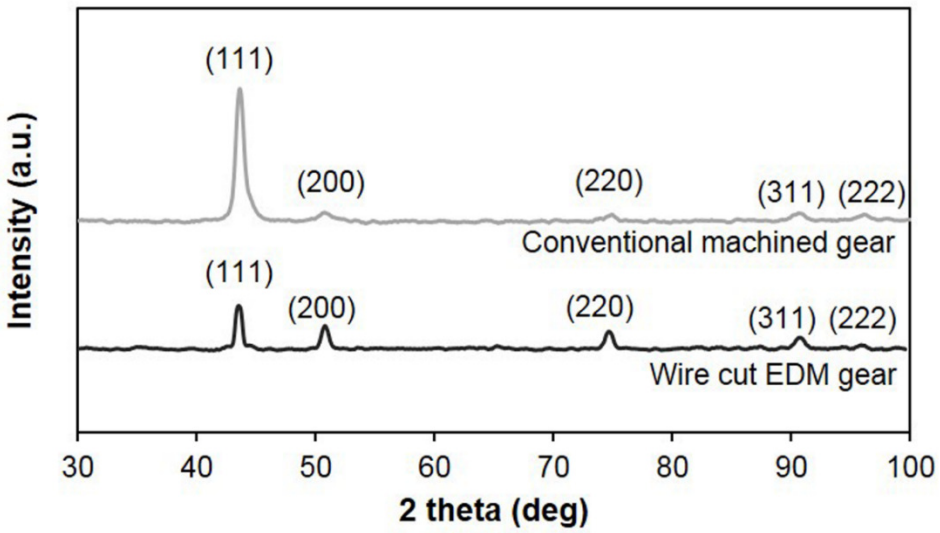

Figure 5.3 XRD spectrum of conventional machined and WEDM surface

Sidhom *et al.* (2013) also observed this dynamic recrystallization behaviour while evaluating white layer microstructure of AISI 316L stainless steel. Murray and Clare (2012) and Murray *et al.* (2014) also discussed similar kind of XRD plot for austenitic steel after EDM, pulsed electron beam irradiation and compared with machined surface.

Gear tooth machined surface and WEDM surfaces were prepared and investigated for the grain size and shown in Figure 5.4(a–d). Grain size of the WEDM surface was slightly smaller than that of machined surface. Extreme high temperature at short duration in the WEDM process contributes to reduce the grain size.

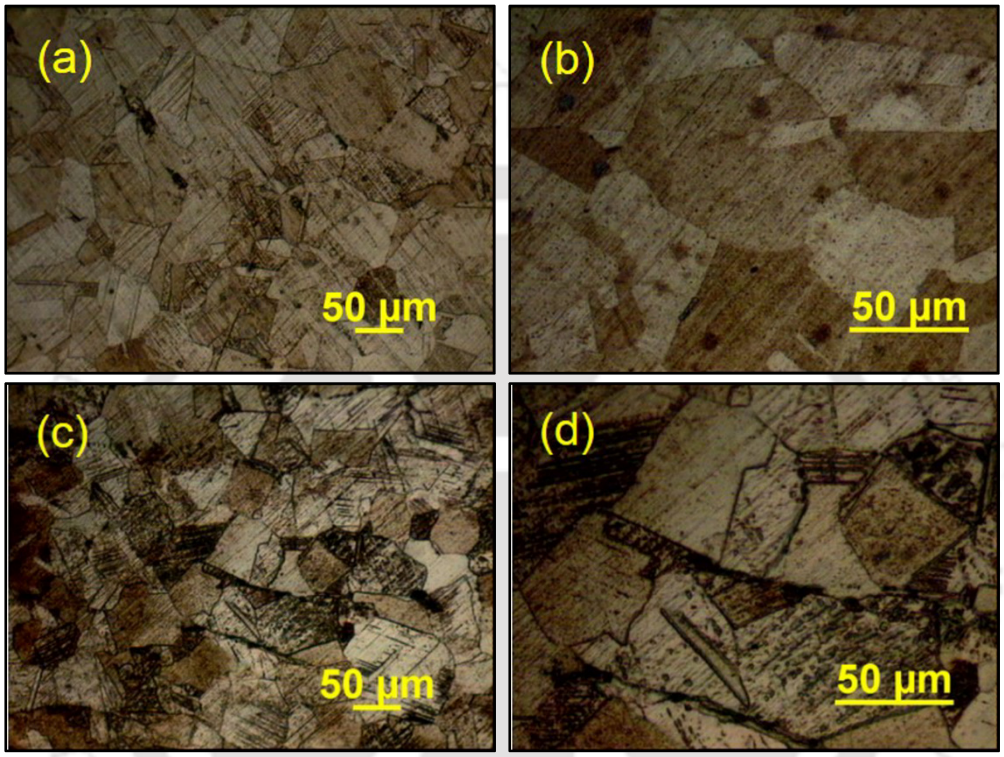

Figure 5.4 Micro graph of gear tooth surface (a–b) machined surface and (c–d) WEDM surface

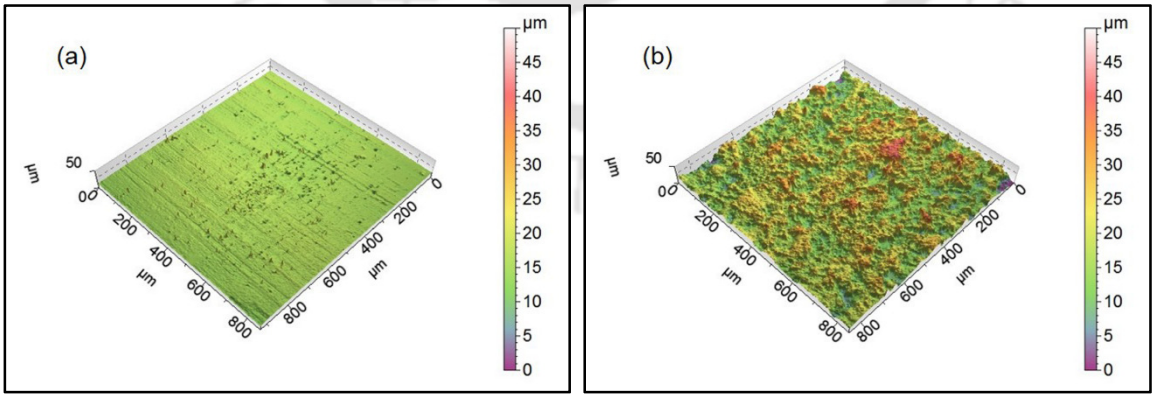

Figure 5.5 Three dimensional profiler image of (a) conventional machined gear tooth surface and (b) gear tooth surface manufactured by WEDM

Three dimensional surface profiler images of mating conventional machined and wire-cut EDM gears are shown in Figure 5.5. From the Figure 5.5 it is revealed that WEDM gear tooth surface exhibited more undulations when compared to that of conventional machining. Surface roughness (R_a) of the injection-moulded polypropylene gear was 2–2.6 µm.

The surface topography can be indexed by the bearing ratio. The bearing ratio curve of the mating metal steel gears is shown in Figure 5.6. Conventional machined gear tooth surface exhibited

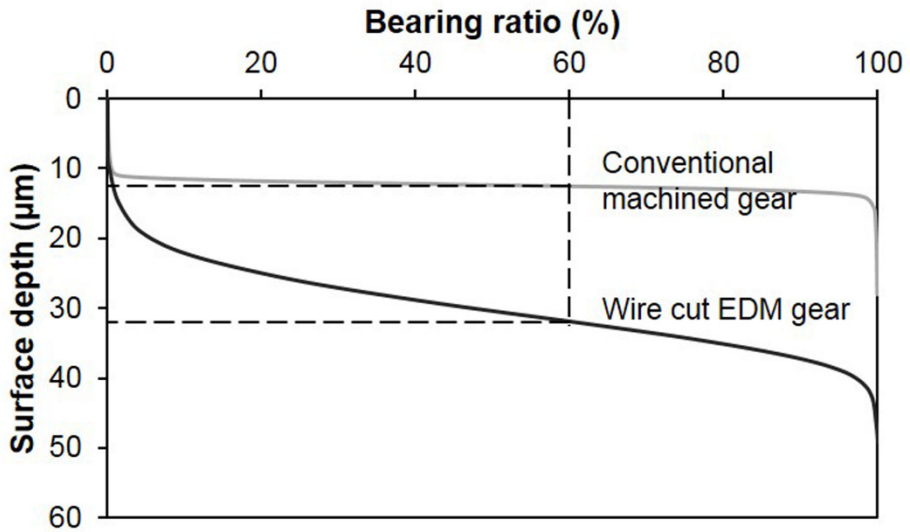

Figure 5.6 Bearing ratio curve of mating steel gears

superior load bearing capability at any considered surface depth. Bergseth *et al.* (2012) also reported similar kind of 3D surface profiler images and predicted the real area of contact and mean contact pressure exerted by the surface due to different manufacturing processes such as hobbing, grinding, honing, and green shaving. For the applied 2500 N normal load, the exerted mean contact pressures were 2800, 1500, 1200, and 1200 MPa for hobbing, grinding, honing, and green shaving respectively. Thus surface with higher surface roughness generate more contact pressure. In the present case, the average surface roughness of the conventional machined and wire cut EDM gear was in the range of 0.41–0.48 and 4.74–5.26 µm respectively. Thus gear manufactured by WEDM

would generate more contact pressure when paired with test polymer gear. Surface roughness (R_a) of the injection-moulded polypropylene gear was 2–2.6 µm.

5.4 MICRO HARDNESS

Surface hardness of the mating gear would play vital role in the friction behaviour with the test polymer gear. Both the machined and WEDM surface were mirror polished then the hardness was measured with the aid of Vickers hardness tester (Buehler 1600) using a diamond pyramid indenter. After indentation, the diagonal of the indentation was measured and the hardness (HV) was computed based on the following equation,

$$HV = \frac{1.854F}{d^2} \tag{5.2}$$

where F is the applied load (kgf) and d is the arithmetic mean of two diagonal (mm). Figure 5.7 shows the measured micro hardness of the conventional machined and WEDM surfaces. The breakdown of hydrocarbon from the electrode and dielectric fluid during EDM process increased

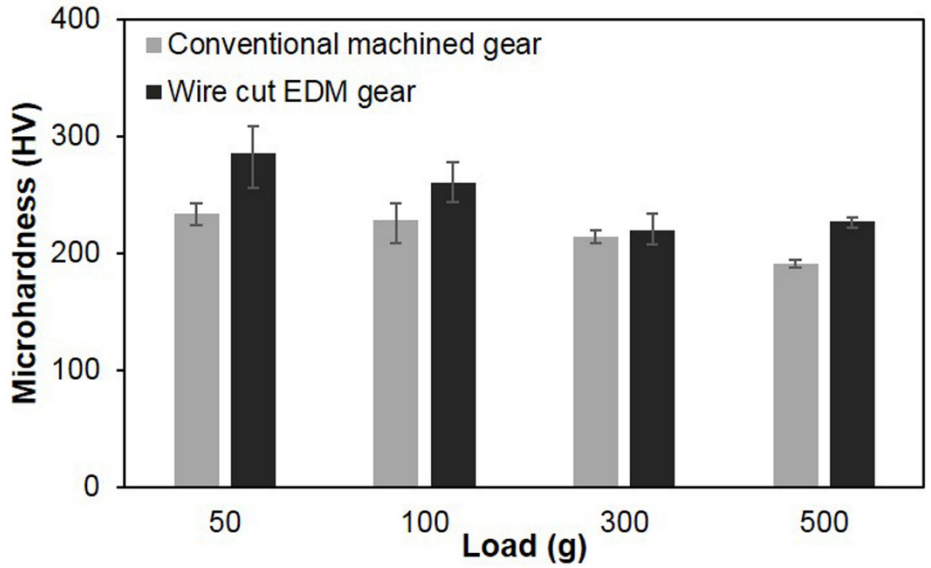

Figure 5.7 Measured micro hardness of the considered counter gear surface

the carbon content and the carbon enrichment, increased crystal size contributes for the increased hardness.

5.5 GEAR SURFACE TEMPERATURE

The gear tests were carried out (Section 3.4; CHAPTER 3) at a constant speed of 800 rev/min and at various loads (2, 2.5, and 3 Nm) against machined and WEDM gear. The net surface temperature of the polymer gear against conventional machined and wire-cut EDM gear at 2, 2.5, and 3 Nm is shown in Figure 5.8(a–c).

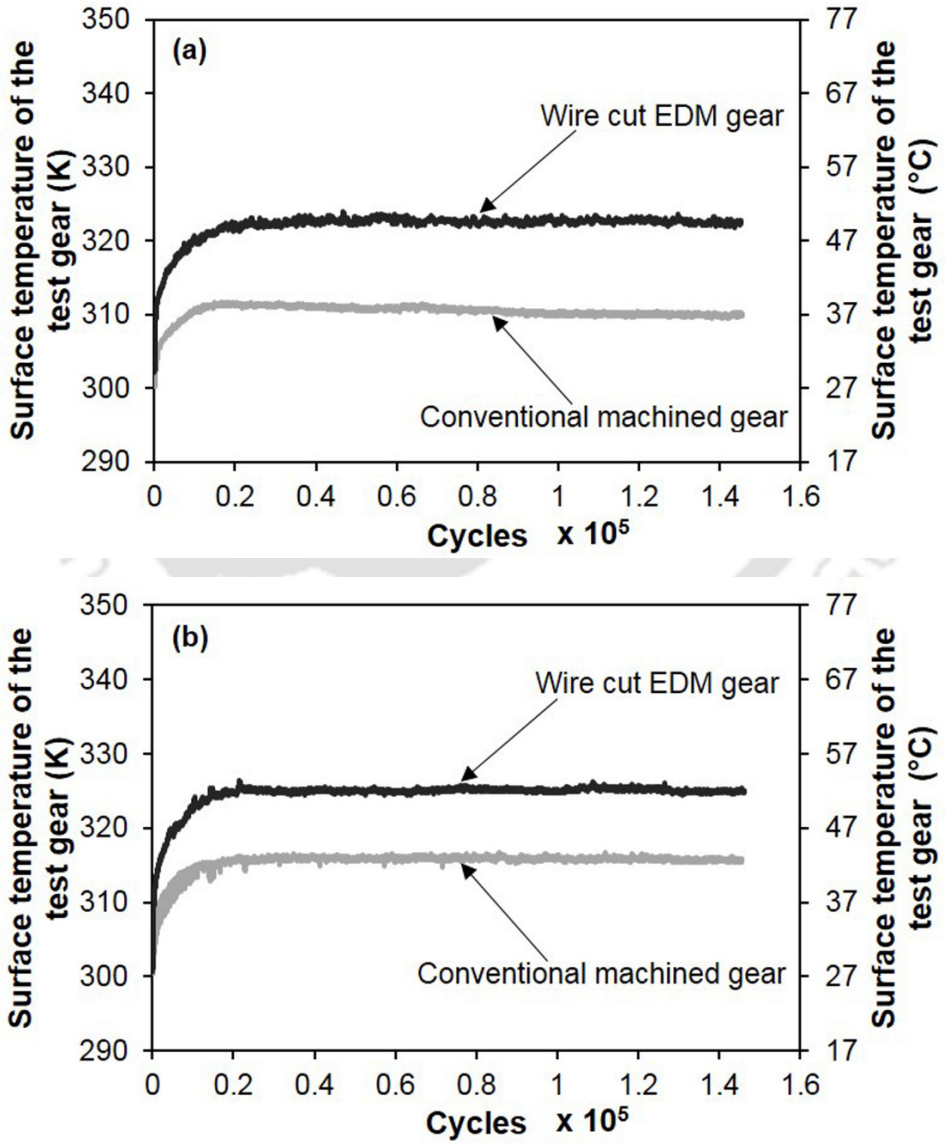

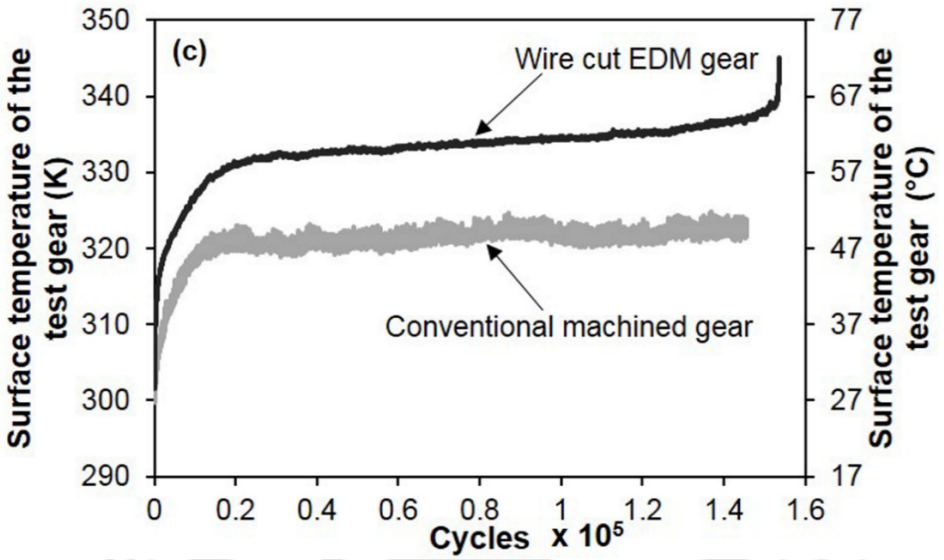

Figure 5.8 Measured surface temperature of the test gears when paired with conventional machined gear and WEDM gear at (a) 2 Nm, (b) 2.5 Nm, and (c) 3 Nm

Polymer gears exhibited a temperature rise of 10–15 °C while tested against wire-cut EDM gear when compared to conventional machined mating gear. The reason for this behaviour is explained as follows.

Mating steel gear manufactured through WEDM exhibited higher surface roughness and hardness when compared to that of conventional machined gear. A polymer test gear mate with a steel gear with poor surface roughness and higher hardness, more amount of heat is generated due to increased friction. Both hardness and surface roughness of the WEDM surface is increased when compared to the machined surface. It is to be noted, the hardness difference between steel and polymer gears are many orders different, however hardness increase due to recast layer is very less. Hence the increased surface temperature of polymer gear is predominantly due to the surface roughness. For all the gear tests, initially there was a gradual rise in temperature and then it reaches a steady state temperature due to the balance between heat generation and heat dissipation. The polymer gear tested against wire-cut EDM gear at 3 Nm causes thermal induced fatigue failure

confirmed by the sudden rise in surface temperature. However, there was no such sudden rise in temperature at 2 and 2.5 Nm load. The nominal contact stress at the pitch circle region was calculated based on Hertzian contact stress equation,

$$\sigma_C = \frac{2W_n}{\pi B b} \tag{5.3}$$

$$B = \sqrt{\frac{2W_n}{\pi b}\frac{\left(\frac{1-\gamma_1^2}{E_1}\right)+\left(\frac{1-\gamma_2^2}{E_2}\right)}{\left(\frac{1}{D_1}+\frac{1}{D_2}\right)}} \tag{5.4}$$

$$D_1(or)D_2 = d_1(or)d_2 \sin \emptyset_n \tag{5.5}$$

$$W_n = \frac{W_t}{cos\emptyset_n} \tag{5.6}$$

$$W_t = \frac{2T}{d_2} \tag{5.7}$$

where σ_C is the maximum contact stress of parallel axis cylinders (Pa), W_n is the load normal to the tooth (N), B is the semi-width of contact between cylinders (m), b is the gear face width (m), $\gamma_1 \; and \; \gamma_2$ is the poisson's ratio of the driver and driven, $E_1 \; and \; E_2$ is the young's modulus of gear and pinion (Pa), $D_1 \; and \; D_2$ is the contact diameter of driver and driven equivalent cylinders, $d_1(or)d_2$ is the pitch circle diameter (m) of the driver and driven gear, $\emptyset_n$ is the standard normal pressure angle (deg), W_t is the load tangential to the tooth (N), T is the torque on the driven gear (Nm).

The schematic view of the gear tooth contact at pitch point is shown in Figure 5.9. The contact stress at the pitch point of the test gear were found to be 35.9, 40.1, and 43.9 MPa respectively for the applied torques 2, 2.5, and 3 Nm. The young's modulus of the steel and polypropylene were assumed as 200 and 0.8 GPa. The poisson's ratio of steel and polypropylene were assumed as 0.3

and 0.4. The detail mechanical properties determination of polypropylene is explained in Subsection 8.3.1 (CHAPTER 8).

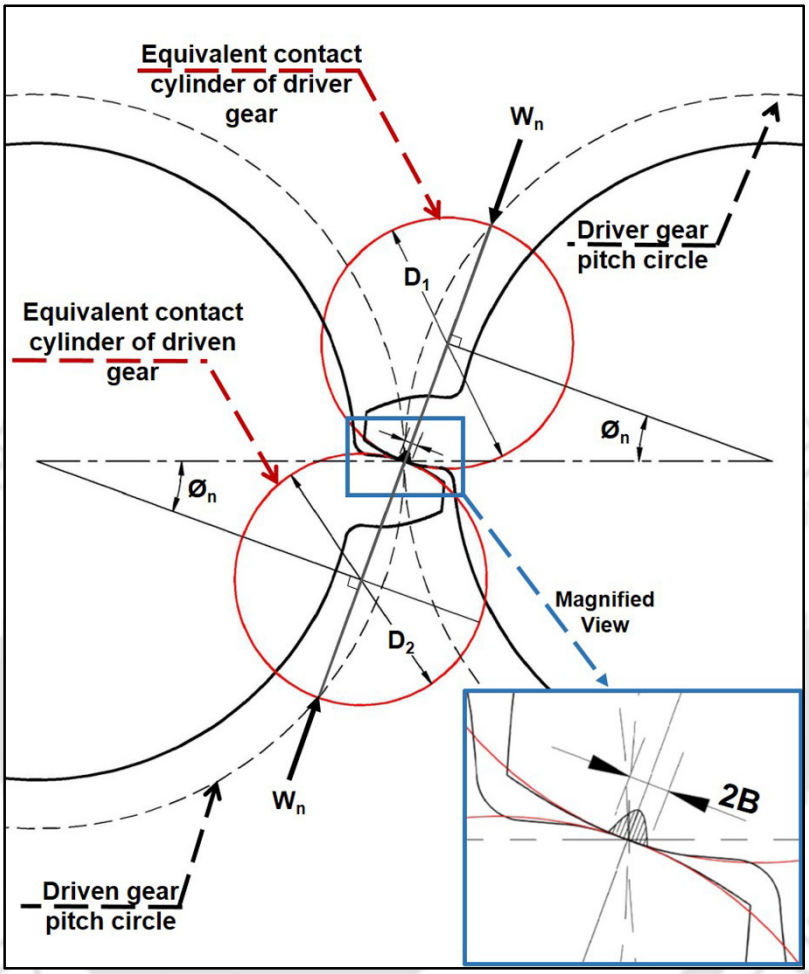

Figure 5.9 Schematic view of gear tooth contact stress

With the increase in applied load, the contact stress and tooth deformation increases which significantly increases the net surface temperature of the test gears. Guha and Chowdhuri (1996) reported that the effect of surface roughness on the surface temperature of a sapphire pin against carbon steel disc at 17 N and 2 m/s. The disc was machined by grinding, polishing, and shot-blasting to make a broad range of surface finish (0.05, 0.13, 0.23, 0.92, 1.47, and 3.01 µm). At 17

N and 2 m/s, the maximum surface temperature of 430 °C was obtained for 3.01 µm roughness disc and 378 °C surface temperature was obtained for 0.05 µm roughness disc.

5.6 GEAR TOOTH WEAR

The gear tooth thickness of the test gears was measured periodically (every 3 hours, 1.44×10^5 cycles) to understand the wear performance of test gears against conventional machined and wire-cut EDM gear. The gear tooth thickness of test polymer gears were measured across three teeth at 2 and 2.5 Nm and shown in Figure 5.10. The wear resistance of test gear decreased 78–84% against wire-cut EDM gear compared to test gear against conventional machined gear.

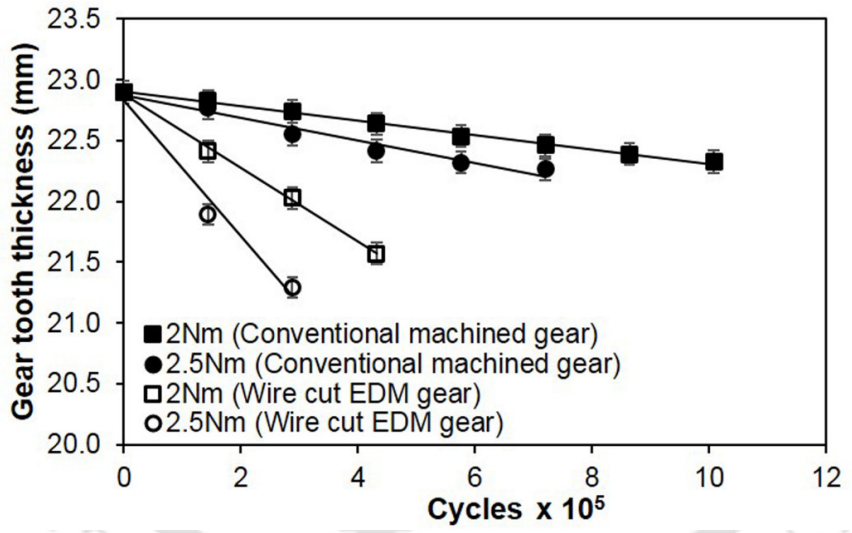

Figure 5.10 Measured gear tooth wear

At 2 and 2.5 Nm the test gears were run upto 10.05×10^5 and 7.2×10^5 cycles against conventional machined gear, whereas against wire-cut EDM gear, test gears were run only upto 4.32×10^5 and 2.88×10^5 cycles when subjected to 2 and 2.5 Nm load. Weight loss per 1×10^5 cycles of the test gear at 2 and 2.5 Nm load is shown in Figure 5.11. The percentage weight loss per 1×10^5 cycles of the polymer gears at 2 and 2.5 Nm against conventional machined gear is 0.3–0.4%, whereas against wire-cut EDM gear it is 1–2%. Akkurt (1995) observed the effect of surface roughness of

mating metal on the wear of acetal gears at 1000 rpm and 6.5 Nm. Wear loss of the acetal gear was maximum when the surface roughness of the mating metal gears was 0.56 µm and least at 0.09

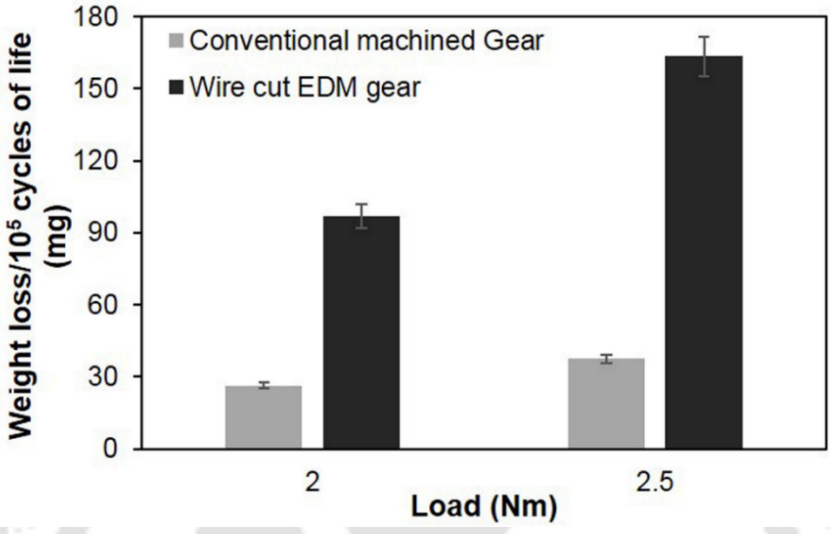

Figure 5.11 Measured weight loss of the polymer gear

µm roughness. Bonny *et al.* (2009) also investigated the influence of EDM process on the tribological behaviour of different surface finished tungsten carbide disc against tungsten carbide pins using pin-on-plate test rig for the test parameters of 15 N, 0.3 m/s, and 10 Km sliding distance. By varying the process parameters, the rough surfaces were made in the range of 2.08–2.37 µm (R_a) and the fine surfaces were made in the range of 0.19–0.27 µm (R_a). The wear rate was high (2.7×10^{-7} $mm^3/N/m$) for the rough surface compared to fine surface plate (4.6×10^{-9} $mm^3/N/m$). And also the rough surface causes pronounced ploughing component due to abrasion when compared to finer surface.

5.7 WORN OUT SURFACE MORPHOLOGY

The worn out surface of the test gears after finite number of cycles are shown in Figure 5.12–Figure 5.14. For all the test conditions, test gears are subjected to wear failures except the polymer gear against wire-cut EDM gear at 3 Nm (thermal induced tooth deformation as shown in (Figure 5.14(b)).

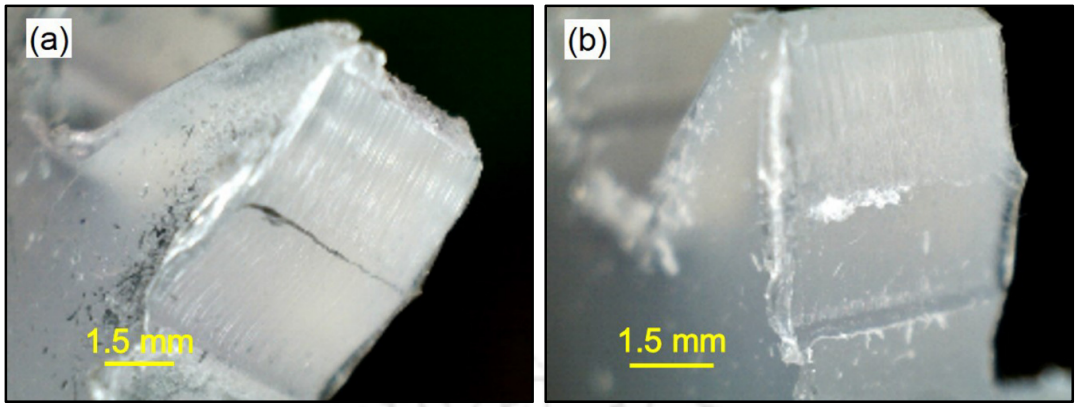

Figure 5.12 Worn out of test gear at 2 Nm against (a) conventional machined gear (after 10.08×10^5 cycles) and (b) WEDM gear (after 4.32×10^5 cycles)

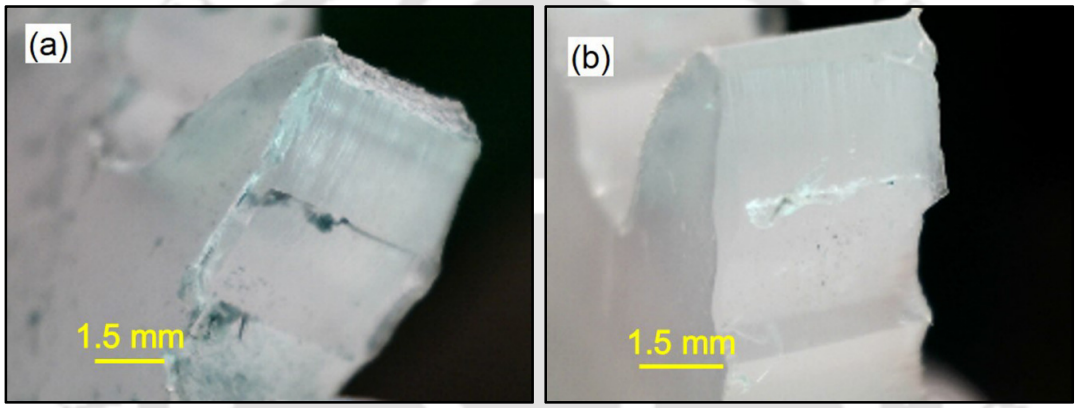

Figure 5.13 Worn out of test gear at 2.5 Nm against (a) conventional machined gear (after 7.20×10^5 cycles) and (b) WEDM gear (after 2.88×10^5 cycles)

Test gear paired with WEDM gear (Figure 5.12(b) and Figure 5.13(b)) exhibited excessive wear when compared to that of test gear paired with conventional machined gear (Figure 5.12(a) and Figure 5.13(a)). In addition, the service life exhibited by the polymer gear when paired with WEDM gear is considerably less when compared to the polymer gear when paired with conventional machined gear. Wear marks and change in the sliding direction (ridge at pitch region) are distinctly visible in all the test conditions. Mao *et al.* (2010) also reported the thermal induced bending failure of acetal–acetal gear pairs at the loads and speed of 10–16.10 Nm and 1000 rpm. Similarly, Senthilvelan and Gnanamoorthy (2006) observed thermal induced plastic deformation

of Nylon 66 gear against identical steel gear at the load and speed of 3 Nm and 1000 rev/min. During the engagement of dedendum (approach) the test gear with the metal gear, rolling direction opposes the sliding direction results in high wear in test gear dedendum. Subsequently formation of ridge occurred at the pitch region due to pure rolling. At the recess process, the coincidence of sliding with rolling direction causes lesser wear than that of wear at dedendum area.

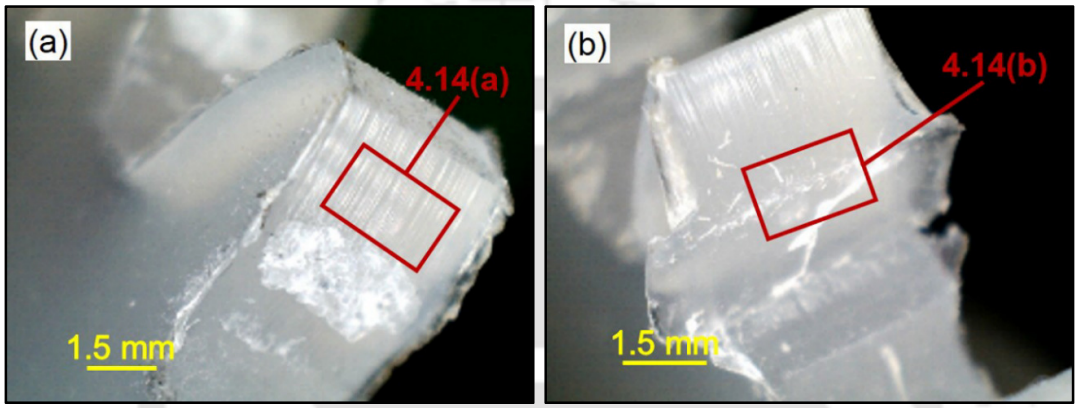

Figure 5.14 Worn out of test gear at 3 Nm against (a) conventional machined gear (after 1.44×10^5 cycles) and (b) WEDM gear (after 1.54×10^5 cycles)

Worn out polypropylene gears tested at 3 Nm against the machined steel gear and WEDM is shown in Figure 5.14(a–b). Wear failure was observed for polypropylene tested against machined steel gear whereas thermal induced tooth deformation was observed against WEDM gear.

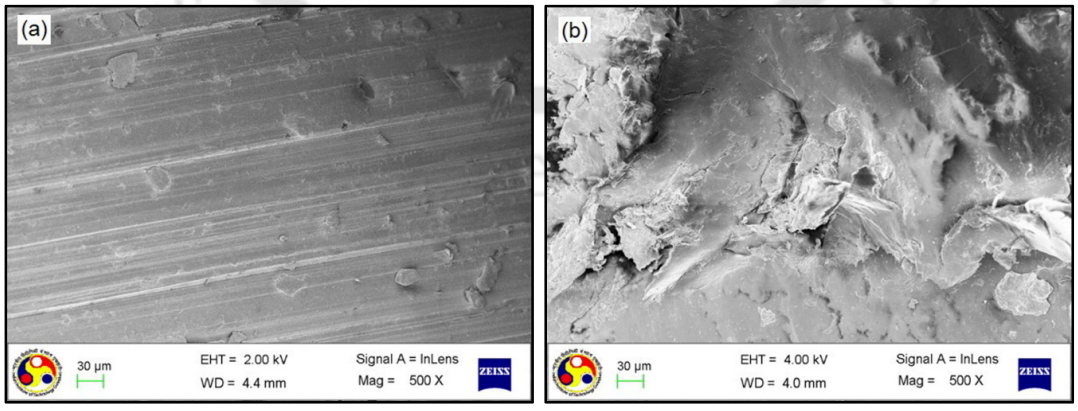

Figure 5.15 Close-up view of the test gear at 3 Nm against (a) conventional machined gear (after 1.44×10^5 cycles) and (b) WEDM gear (after 1.54×10^5 cycles)

Worn out polypropylene gears tested at 3 Nm against the machined steel gear and WEDM were further observed under scanning electron microscope. Polymer gear tested against machined steel gear showed dominant abrasive wear (Figure 5.15(a)). Polymer gears tested against WEDM showed dominant plastic deformation (Figure 5.15(b)).

5.8 SUMMARY

Durability of injection-moulded polypropylene gear was evaluated when paired with two types of steel gears (a) manufactured by gear hobbing followed by grinding and (b) wire-cut electric discharge machining process. Due to the difference in surface topology and hardness between these two mating gears, test polymer gears exhibited significantly different performance and the following major conclusions were arrived

- Polymer gears paired with a WEDM gear generates more heat due to the poor surface topology and increased hardness.
- Measured gear tooth thickness at lower loads (2–2.5 Nm) and inspection at various stages of service confirmed the superior performance of polymer gears when paired with hobbed gear compared to that of WEDM gear. 78% to 84% decreased wear resistance was observed for polymer gear paired with WEDM gear compared to that of hobbed gear.
- At higher loads, polymer gears exhibited thermal fatigue failure when paired with WEDM and only excessive wear was observed without any tooth deformation when polymer gears are parried with machined gear.

CHAPTER 6

EFFECT OF MATING STEEL GEAR SURFACE OVER THE PERFORMANCE OF INJECTION-MOULDED POLYPROPYLENE GEAR

6.1 INTRODUCTION

Extensive investigations have been carried out to understand the effect of gear material, gear parameters, and service conditions over polymer gear durability. However, the effect of the mating gear surface condition over the test gear performance has not been completely understood. Micro geometry of the metal gear can significantly influence the friction-wear performance of polymer gears due to their superior hardness. Previous chapter deals with the effect of manufacturing process including conventional machined & grounded and wire-cut EDM steel gear over the polypropylene gear performance whereas current chapter considered wire-cut EDM steel gear having different surface roughness over the polypropylene gear performance. In the present work both the mating and test gear are of nonstandard asymmetric gear. Asymmetric gears (having different pressure angles at drive and coast side) are being considered by the recent researchers to improve bending and contact load-carrying capacity. Additionally, these nonstandard asymmetric steel gears cannot be manufactured by the standard manufacturing process including hobbing and shaping, but can be developed by wire-cut electric discharge machining process. In addition, conventional secondary process including shaving and grinding cannot be utilized to improve this nonstandard gear quality including surface roughness. Thus, the effect of asymmetric mating steel

gear surface roughness over asymmetric polymer test gear has been reported and standard pin on disc test under different surface roughness condition was also carried out to correlate the surface roughness effect with the frictional force.

6.2 METHODOLOGY

Polypropylene (M110, Haldia Petrochemical Ltd.) was injection-moulded (Texair, JTS 40) to test gears are of 3 mm module, 18 numbers of teeth, and face width of 4 mm with drive and coast side pressure angles of 20° and 34° respectively. The gear parameters and details of the test gears are shown in Figure 6.1 and Table 6.1.

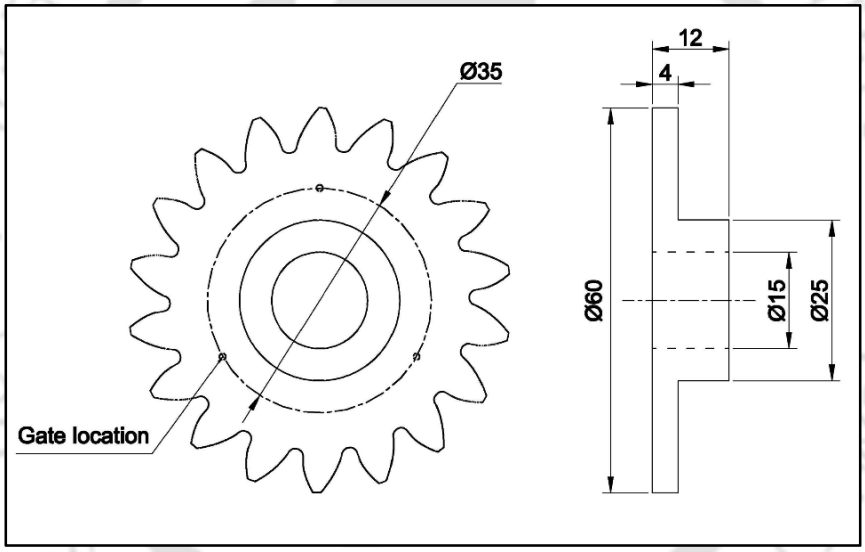

Figure 6.1 Test gear details

Table 6.1 Test gear parameters

Parameters	Value	
Pressure angle (°)	20	34
Module (mm)	3	
Number of teeth	18	
Pitch circle diameter (mm)	54	
Tip circle diameter (mm)	60	
Face width (mm)	4/12	
Root fillet radius (mm)	1.14	

The gear tests were carried out (Section 3.4; CHAPTER 3) at a constant speed of 800 rev/min and at various torques (2, 2.5, and 3 Nm). To understand the effect of surface roughness, the gears were run for the same fixed time cycles (3600 s). All the tests were carried out under the room conditions. Moulded test gears were meshed with stainless steel gears (SS 316) having identical gear parameters but of 12 mm face width, manufactured through the wire-cut electric discharge machining (Electronica, ULTIMA2010) process. The DIN quality of the injection-moulded and WEDM gear was reported in Section 5.2 (CHAPTER 5).

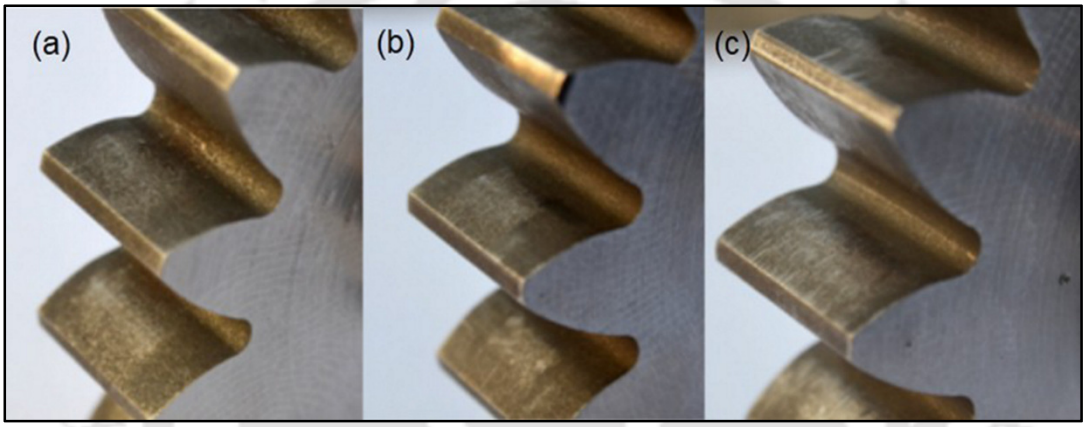

Figure 6.2 View of the machined steel gears (a) newly machined gear, (b) run against polymer gear for 5×10^5 cycles, and (c) run against polymer gear for 10×10^5 cycles

Stainless steel gears having different surface finish were used for the tests. Type A is a newly manufactured steel gear, type B is a steel gear run against the polymer gear for 5×10^5 cycles, and type C is a steel gear run against a polymer gear for 10×10^5 cycles. Figure 6.2 shows the close-up view of mating steel gears having different roughness. The hardness of the steel gear is 72–78 HRB and Shore D hardness of the injection-moulded polypropylene gear is 72. The surface roughness of the gear was measured with the aid of stylus type perthometer (Mitutoyo Surftest SJ-401). Noncontact three-dimensional optical profiler (Taylor Hobson CCI MP) was used to obtain three-dimensional image of the gear tooth surface and the bearing ratio curve.

Stainless steel discs were manufactured through the wire-cut electric discharge machining with different surface roughness. Wear performance of injection-moulded polypropylene was investigated with the aid of the pin on disc tribometer (DUCOM, TR-201) in accordance with ASTM G99. Before testing, pins were flattened for the uniform contact area and surface roughness by running against silicon carbide (SiC) abrasive paper. Test samples were weighed before and after test. Tests were carried out at a normal load of 20 N and at the surface velocity of 56.54 m/min. During testing, frictional force and wear were continuously measured and recorded.

6.3 SURFACE MORPHOLOGY OF GEARS

The tooth surface profile of the polymer and mating steel gears are shown in Figure 6.3(a–d). Surface roughness of at least three different regions was measured and its variation of R_a was shown as a range. The surface roughness of the injection-moulded polypropylene gear was 2–2.6 µm. The surface roughness of type A, type B, and type C gears were 3.5–3.9 µm, 2.5–2.9 µm, and 1.9–2.2 µm respectively.

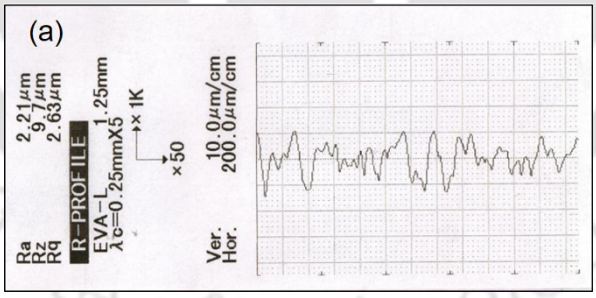

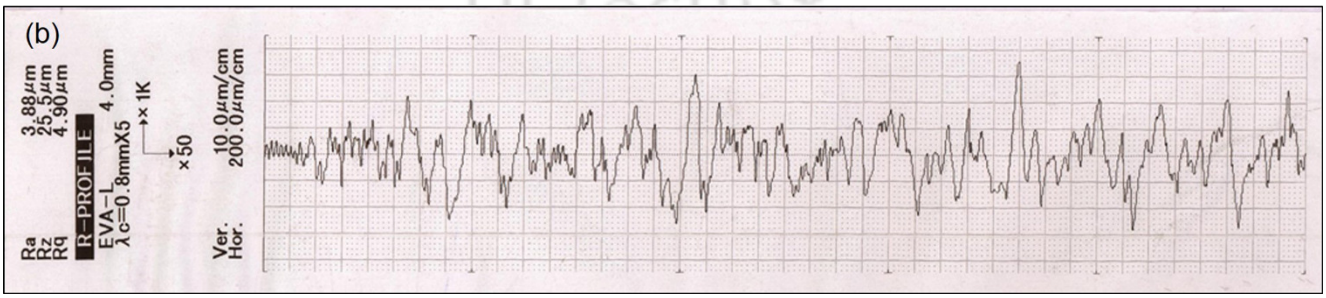

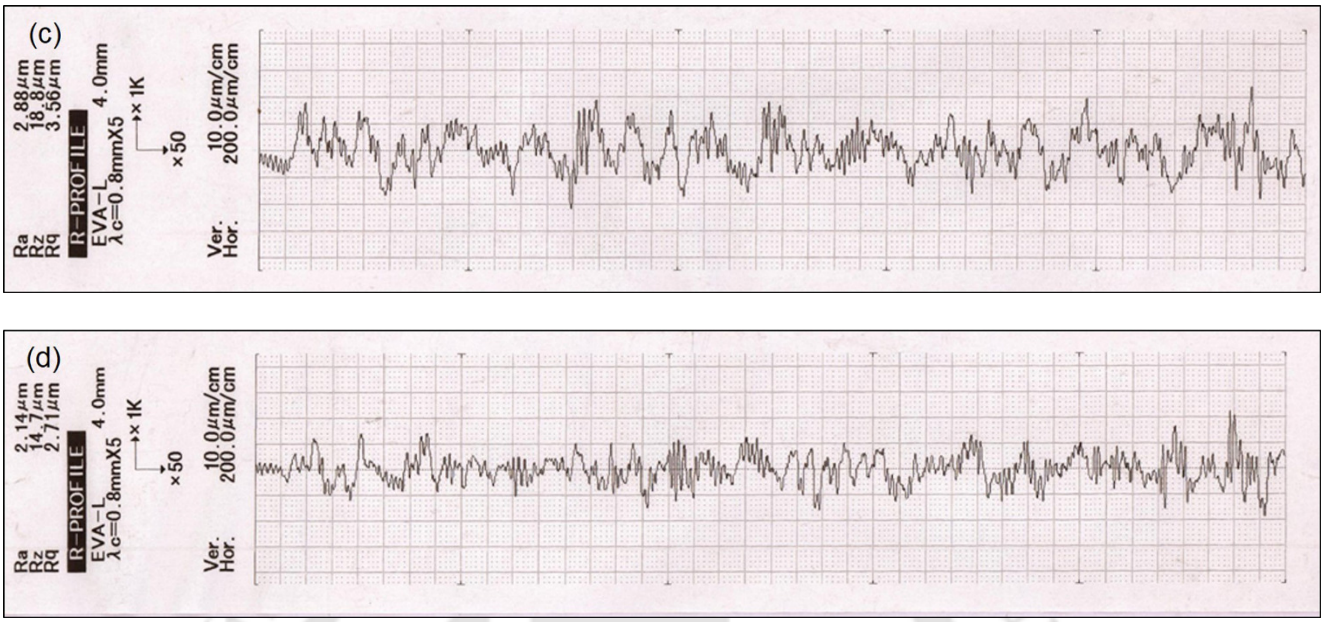

Figure 6.3 (a) Surface profile of injection-moulded polypropylene gear tooth, (b) surface profile of steel gear A tooth, (c) surface profile of steel gear B tooth, and (d) surface profile of steel gear C tooth

The surface of the mating steel gears was examined comprehensively, since polymer gear tooth surfaces are easily damaged. Hard asperities of the steel gear tooth surface can provide more resistance for the sliding of the polymer gear surface. Hard asperities of the steel surface can plow the polymeric surface, which can fracture, tear, and fragment the soft polymeric material.

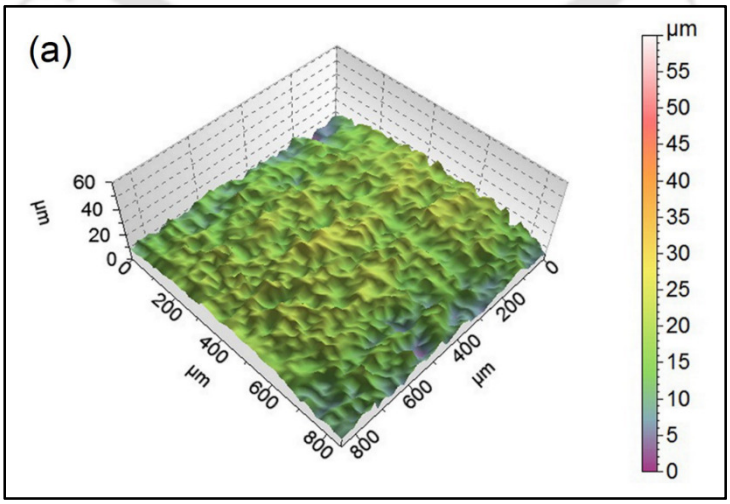

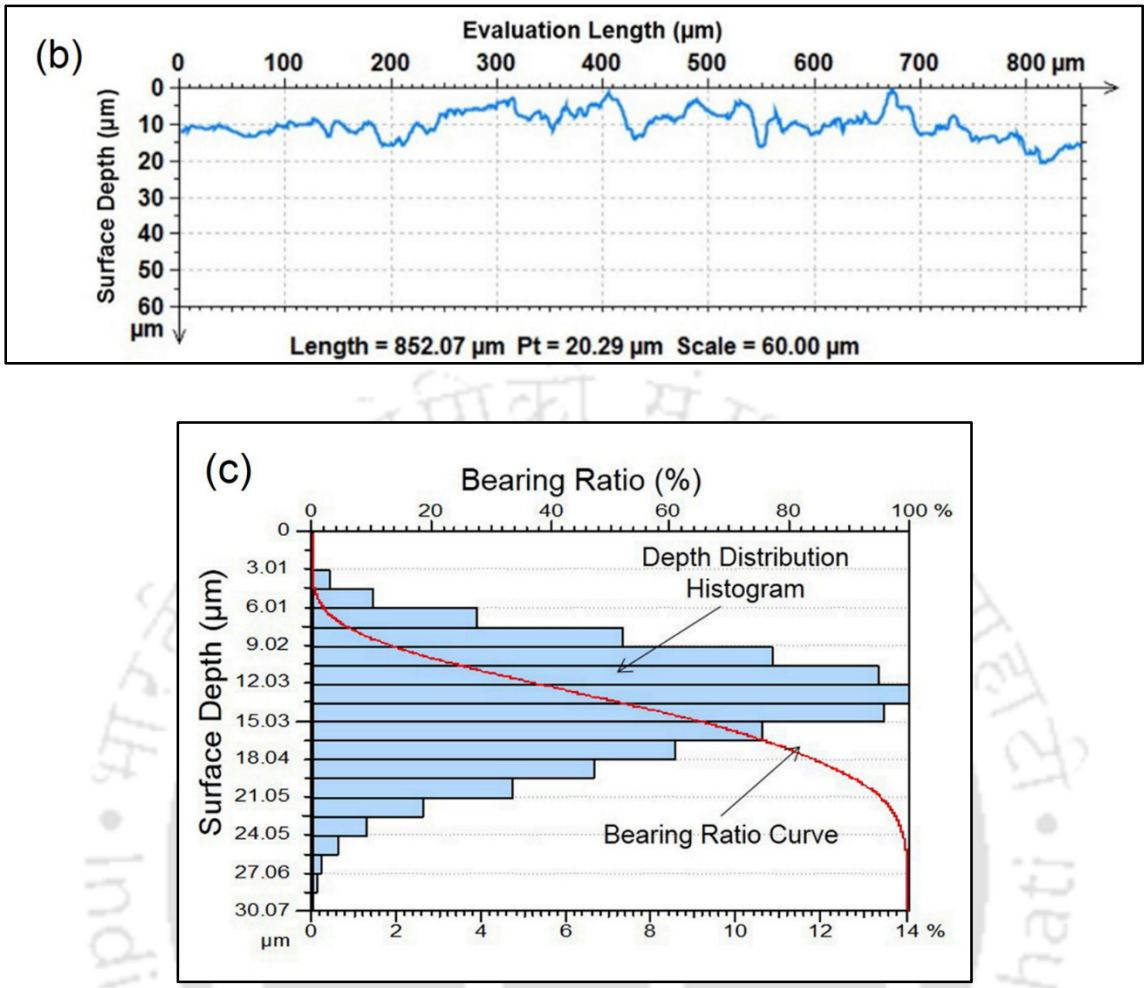

Figure 6.4 (a) Three-dimensional surface image of steel gear C tooth, (b) two-dimensional surface depth of steel gear C tooth, and (c) estimated bearing ratio curve of steel gear C tooth

Apart from the surface morphology, Abbott-Firestone (bearing-ratio) curve of steel gear tooth surfaces was also obtained to understand the friction and wear behaviour of polymer-steel gear performance. Figure 6.4(a) shows the three-dimensional surface image of the steel gear C. Figure 6.4(b–c) shows the extracted surface depth of gear tooth C and estimated bearing ratio curve of gear tooth C.

All the considered steel gears (A, B, and C) were observed under profiler and their bearing ratio curves are shown in Figure 6.5. It is revealed that for any particular depth of profile, the bearing

ratio can be obtained for a given gear tooth surface. For 15 µm surface depth of profile, gear A (3.5–3.9 µm) exhibited 13%, gear B (2.5–2.9 µm) exhibited 37%, and gear C (1.9–2.2 µm) exhibited 57% bearing ratio. For any given depth of the surface profile, the gear tooth surface having high surface roughness exhibited lesser bearing ratio. Contact pressure would increase with the reduction in bearing ratio, which will result in increased surface friction and frictional temperature.

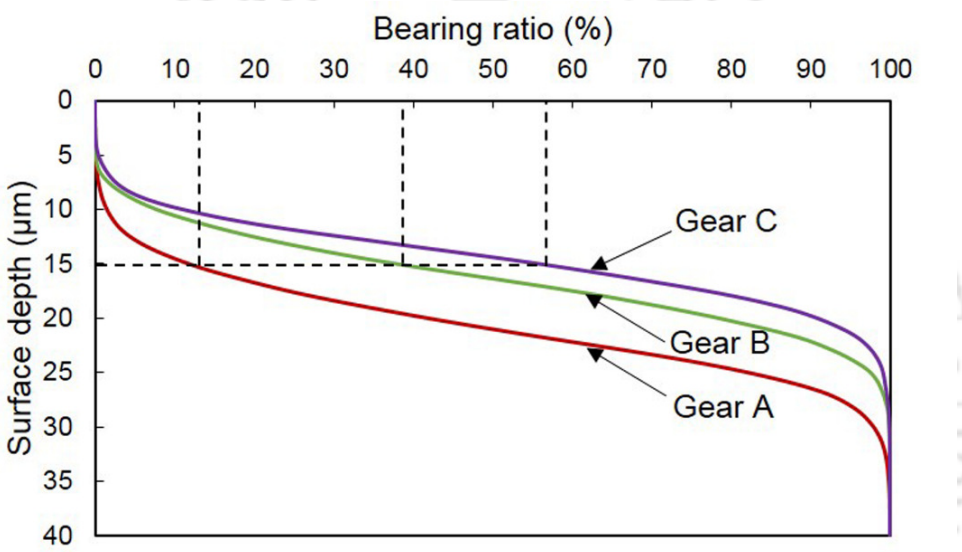

Figure 6.5 Bearing ratio curve of the steel gears A, B, and C tooth

Bergseth *et al.* (2012) also used three-dimensional surface measurements to measure the tooth surface of gears manufactured through various processes. From this measurement, real area of contact and mean contact pressures were predicted at desired normal loads. Gears manufactured by hobbing (R_a 1.1 µm), grinding (R_a 1.1 µm), honing (R_a 0.47 µm), and gear shaving (R_a 0.45 µm) exhibited mean contact pressures of 2800, 1500, 1200, and 1200 MPa for the considered 2500 N normal load.

6.4 GEAR SURFACE TEMPERATURE

Injection-moulded polypropylene gears were paired with steel gears at various loads (2, 2.5, and 3 Nm) and at 800 rev/min for 3600 s in the power absorption gear test rig. Under testing, gear tooth surface experienced a combination of rolling and sliding and generated frictional heat due to surface interaction. In addition, due to the visco-elastic nature of the thermoplastic material, repeated gear tooth deflection generated heat due to the material hysteresis. Part of the generated heat is dissipated by convection (due to the gear rotation) and conduction (through mating steel gears). The net surface temperature of test gear is continuously measured by the IR temperature sensor.

Figure 6.6(a) shows the net surface temperature of polypropylene gear paired with steel gears having different surface roughness at 2.5 Nm load. Initially, the surface temperature showed a gradual increase in temperature and then became stable. This behaviour is due to the following reason: Initially, a transfer layer of polymer film was formed on the counter steel surface. Subsequently, due to repeated interactions, the film got removed. The temperature due to friction increased until next layer formed and this process repeated till steady state was reached (Tzanakis

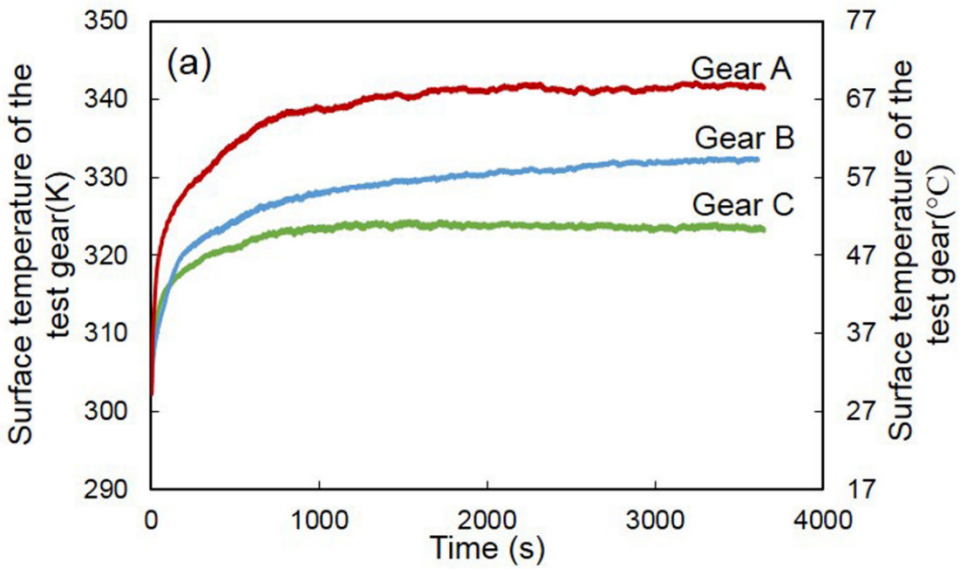

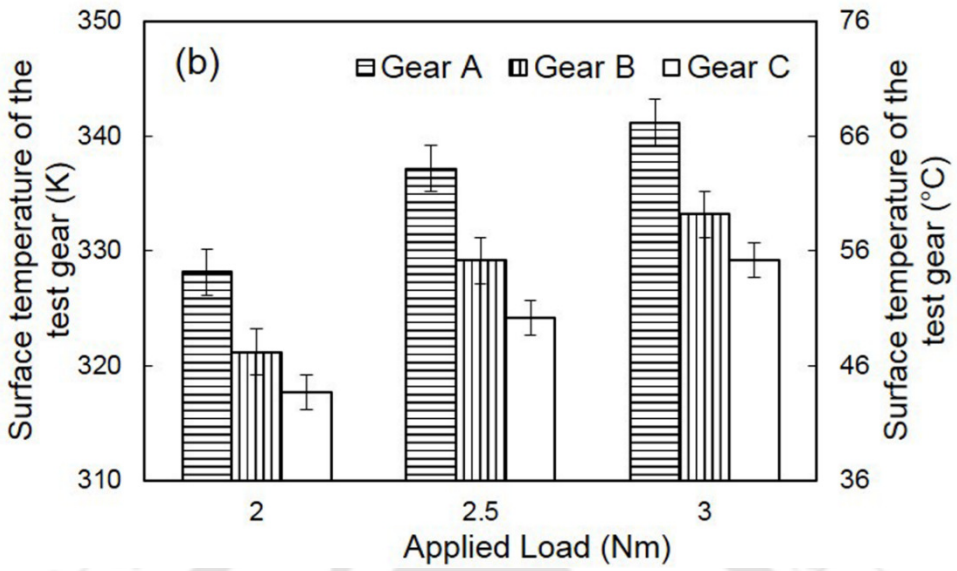

Figure 6.6 (a) Measured surface temperature of polymer gear at 2.5 Nm load and (b) maximum surface temperature of polymer gears when paired with different steel gears A, B, and C

et al., 2013). A similar behaviour of surface temperature was observed by other researchers as well (Hooke *et al.*, 1993; Breeds *et al.*, 1993; Kim, 2006; Duzcukoglu, 2009; Mao *et al.*,2010). As the normal load increased, the contact pressure increased, which resulted in increased surface temperature of the test gears.

The net surface temperature of test gear increased, when the mating steel gear surface roughness increased. Figure 6.6(b) shows the maximum surface temperature of test gears when paired with steel gears having different surface roughness. The test gear exhibited an increase of about 20 °C surface temperature, when the surface roughness of steel gears increased from 2 to 4 µm. Tzanakis *et al.* (2013) evaluated wear performance of PTFE composites against steel having different surface roughness (R_a= 0.12, 0.25,0.50, and 0.70 µm) in a reciprocating tribometer. With the increased surface roughness, the coefficient of friction and surface temperature initially increased and then decreased beyond 0.25 µm R_a.

6.5 GEAR TOOTH WEAR

Gear tooth thickness and gear weight after test were measured to understand the wear resistance of test gears. Figure 6.7 shows the tooth thickness reduction of polypropylene gear when paired with steel gears having different surface roughness. A reduction of about 200 µm tooth thickness was observed, when the surface roughness (R_a) of the mating steel gear decreased by 2 µm. At 2 Nm loading, the polypropylene gear exhibited a weight loss of 190, 108, and 27 mg when paired with A, B, and C steel gears respectively.

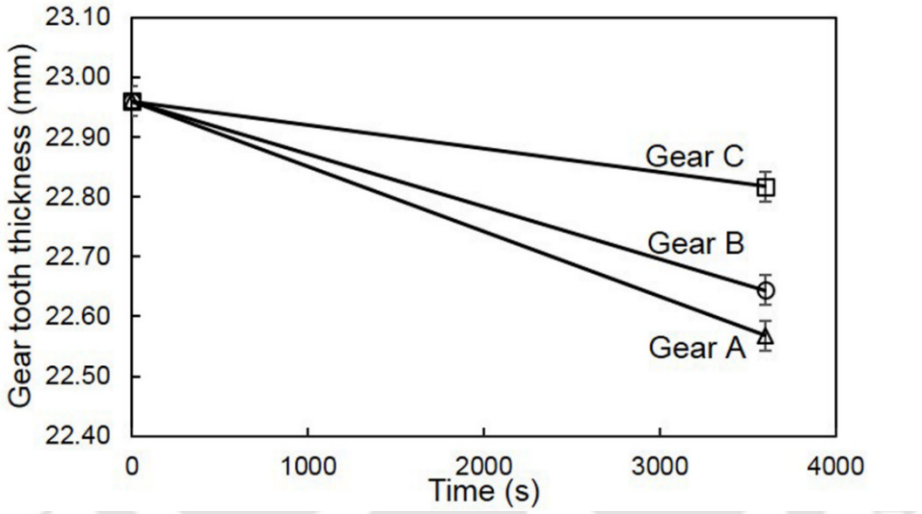

Figure 6.7 Gear tooth thickness reduction

Akkurt (1995) also observed an increase in wear resistance when the surface roughness of the mating steel gear decreased. The volume loss exhibited by the test gears after 4 h (6.5 Nm and 1000 rev/min) was 6, 3, 1.5, and 1 mm^3 when paired with metal gears having surface finish of 56, 26, 11, and 9 µm respectively.

6.6 WORN OUT SURFACE MORPHOLOGY

Worn out gear tooth surfaces were observed under digital microscope to quantify the surface damage. Figure 6.8–Figure 6.10 show the worn out and tooth deformation of polypropylene gears

when paired with steel gears at 2, 2.5, and 3 Nm loading. Figure 6.8(a–c) the worn out surface of the test gears, when paired with steel gears A (3.5–3.9 µm), B (2.5–2.9 µm), and C (1.9–2.2 µm) at 2 Nm respectively.

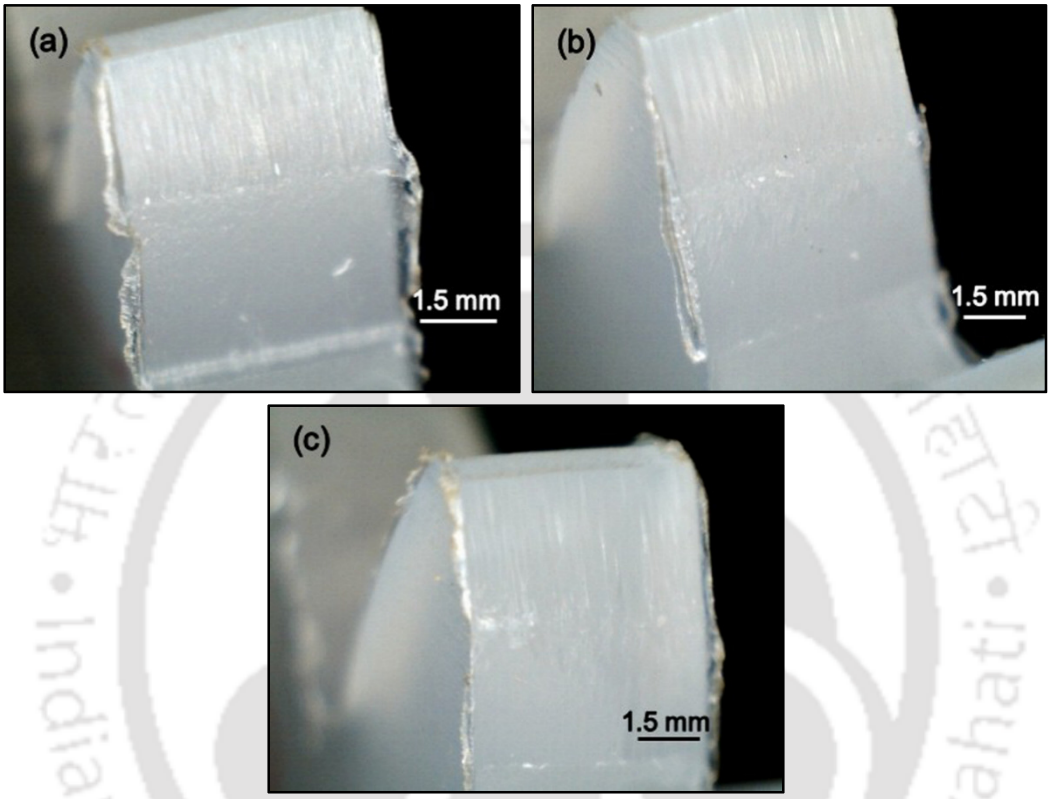

Figure 6.8 Worn out polymer gear when paired with (a) steel gear A, (b) steel gear B, and (c) steel gear C at 2 Nm after 48×10^3 cycles (3600 s and 800 rev/min)

Wear marks were distinctly observed and pitch location was also seen, where sliding direction changes. However, no difference was observed among the test gears when paired with the steel gears A, B, and C.

Figure 6.9(a–c) shows the worn out surface of gears when paired with steel gear A, B, and C at 2.5 Nm. In this load condition, gear paired with steel gear A exhibited severe surface damage near the pitch region. However, the gear paired with steel gear B exhibited lesser surface damage and the

gear paired with steel gear C exhibited least surface damage. At 2.5 Nm load, the gear exhibited significant influence of the mating steel gear surface finish.

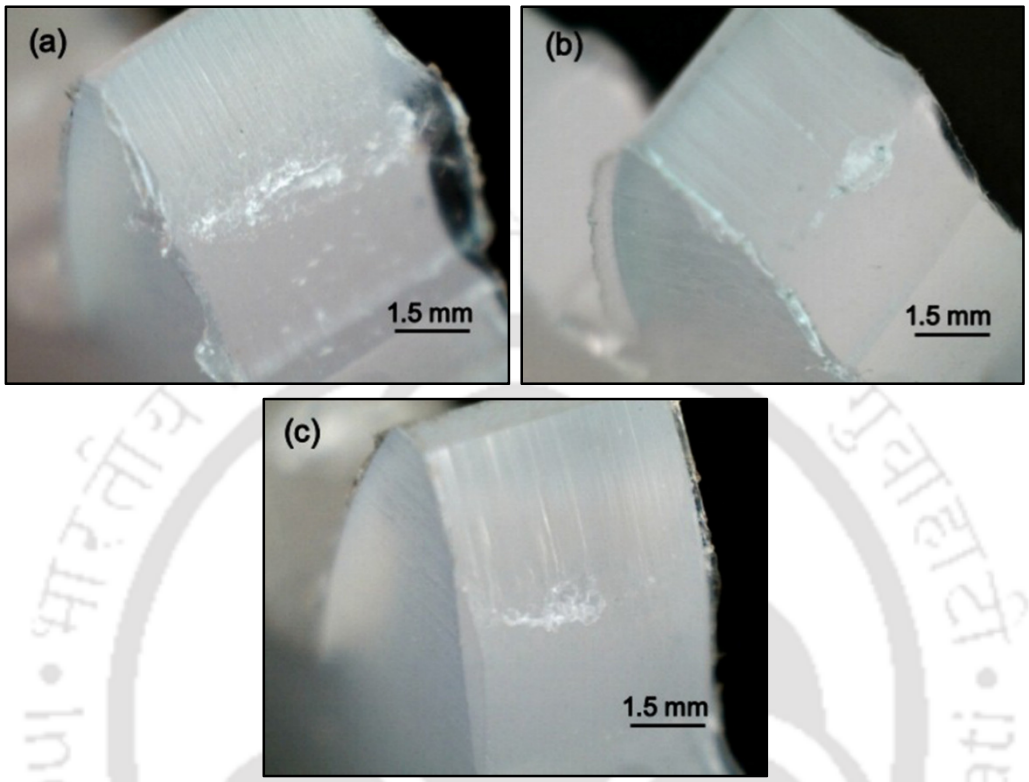

Figure 6.9 Worn out polymer gear when paired with (a) steel gear A, (b) steel gear B, and (c) steel gear C at 2.5 Nm after 48×10^3 cycles (3600 s and 800 rev/min)

Figure 6.10(a–c) shows the worn out gear tooth surface when paired with steel gear A, B, and C at 3 Nm. In this load, the effect of the mating steel gear surface finish was predominant due to the excessive surface temperature of the polymer gears.

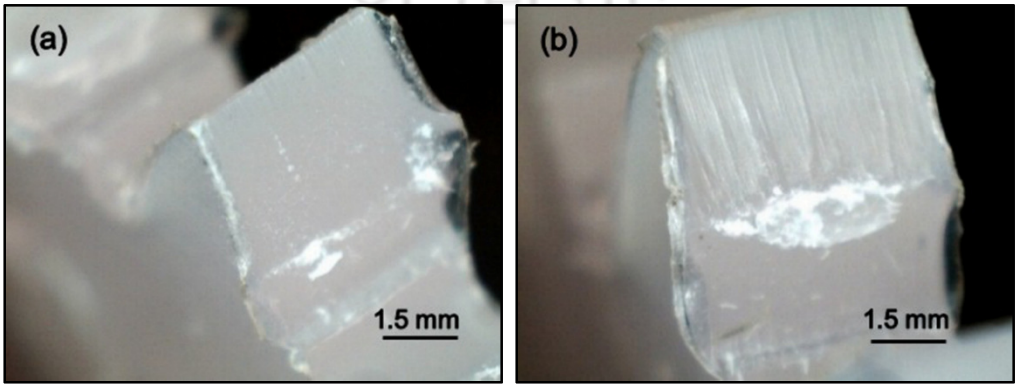

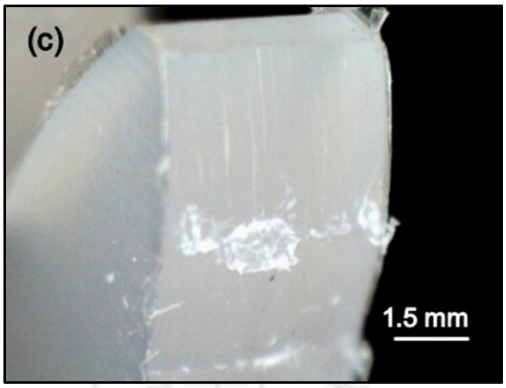

Figure 6.10 Worn out polymer gear when paired with (a) steel gear A, (b) steel gear B, and (c) steel gear C at 3 Nm after 48×10^3 cycles (3600 s and 800 rev/min)

The maximum measured surface temperatures of the polypropylene gear when paired with steel gears A, B, and C were 67, 59, and 52 °C respectively at 3 Nm. Due to this, plastic deformation of gear tooth was observed when paired with steel gears A and B; however, no such thermal failure was observed when paired with steel gear C.

6.7 FRICTION AND WEAR PERFORMANCE OF POLYPROPYLENE

In the durability evaluation of polymer gear, the effect of friction (net surface temperature, weight loss, tooth thickness reduction) was measured but frictional force/coefficient of friction could not be measured due to the complex sliding and rolling motion involved in the gear meshing. Hence, to confirm the surface roughness effect on the frictional behaviour, gear materials (polypropylene)

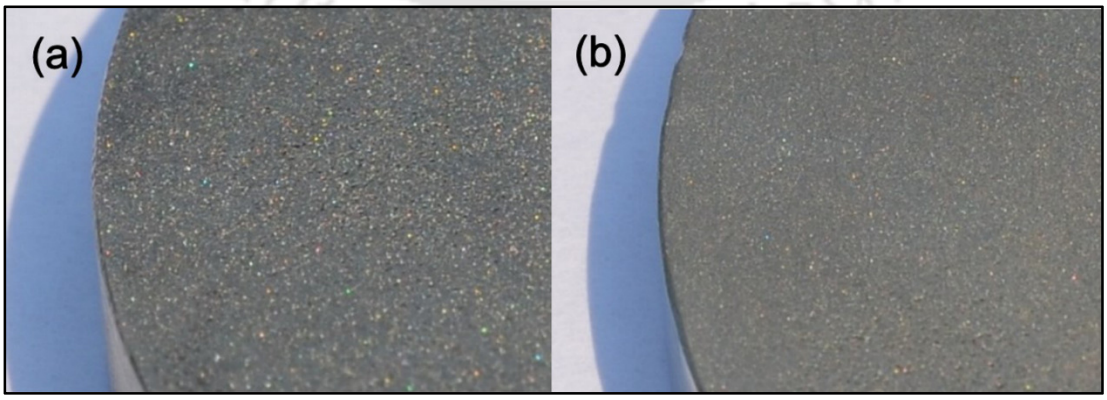

Figure 6.11 View of counter steel disc A and B

were injection-moulded into specimen and made to slide against two different steel discs (designated as disc A and disc B) having different surface roughness. Figure 6.11 shows the close-up view of counter steel discs having different roughness.

Figure 6.12(a–c) shows the surface profile of polypropylene specimen, disc A, and disc B. The initial surface roughness of the polypropylene specimen, disc A, and disc B were 0.5–0.8 µm, 4.7–5.4 µm, and 2.6–3.2 µm respectively.

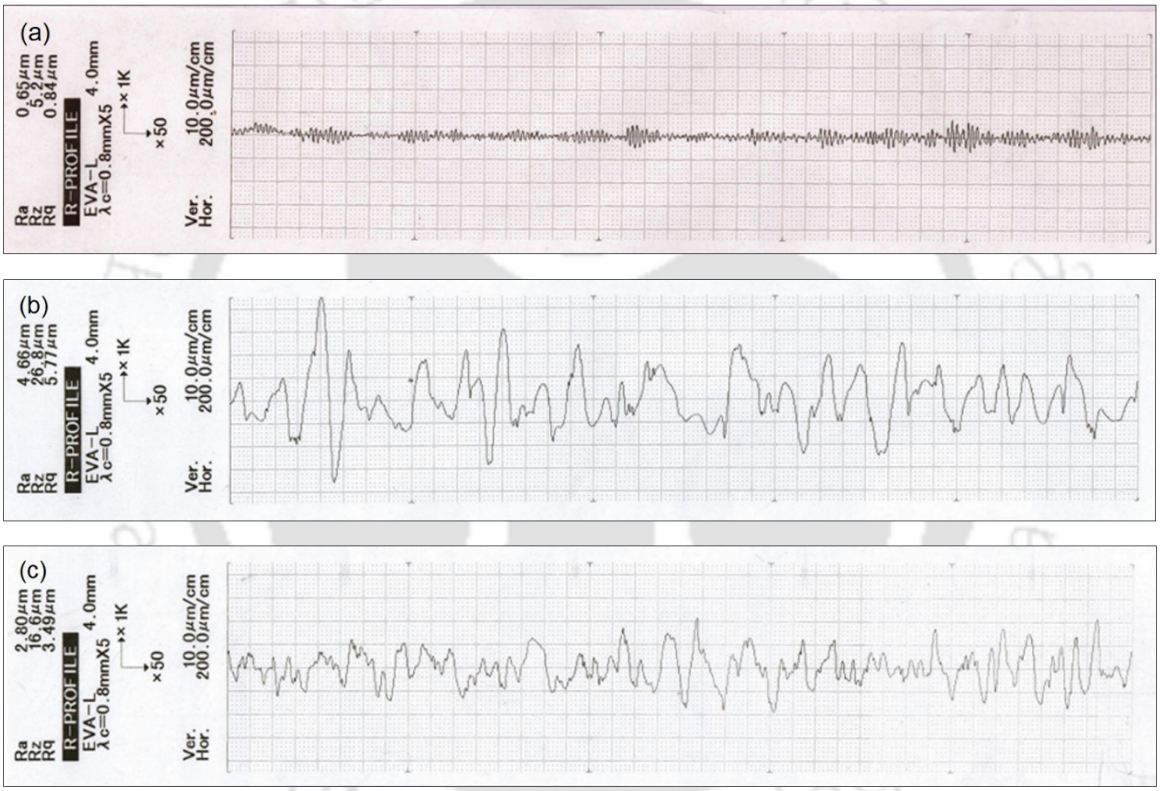

Figure 6.12 (a) Surface profile of injection-moulded polypropylene specimen, (b) surface profile of steel disc A, and (c) surface profile of steel disc B

To understand the surface of these discs, bearing ratio curves were obtained. Figure 6.13 shows the bearing ratio curve of considered counter disc. For a 30 µm surface depth, the bearing ratio exhibited by the disc A was 25%, whereas the bearing ratio exhibited by disc B was 80%. For any given depth of surface profile, the disc surface having high surface roughness (disc A) exhibited

lesser bearing ratio. Contact pressure would increase with the reduction in bearing ratio, which will result in increased surface friction and frictional temperature.

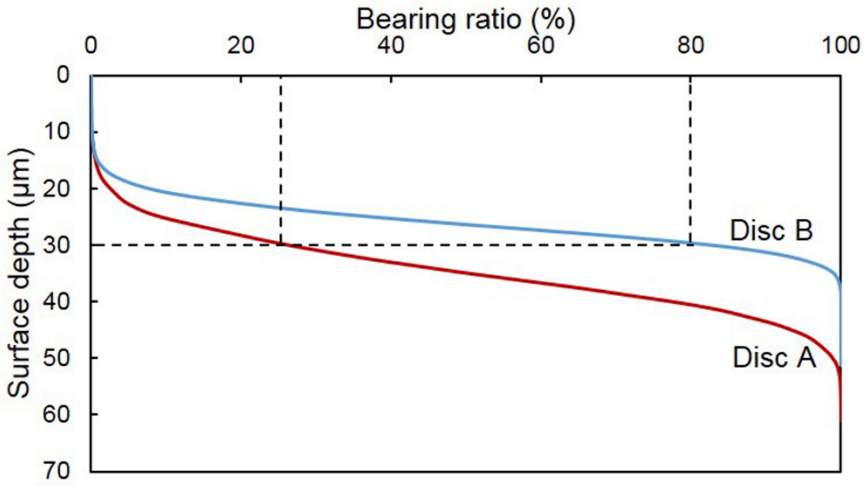

Figure 6.13 Bearing ratio curve of discs A and B

The measured surface temperature of the polypropylene specimen (Figure 6.14) confirmed this fact. The surface temperature of the polypropylene specimen showed an increase of 10 °C when the counter disc changed from disc B (R_a= 2.6–3.2 µm) to disc A (R_a= 4.7–5.4 µm).

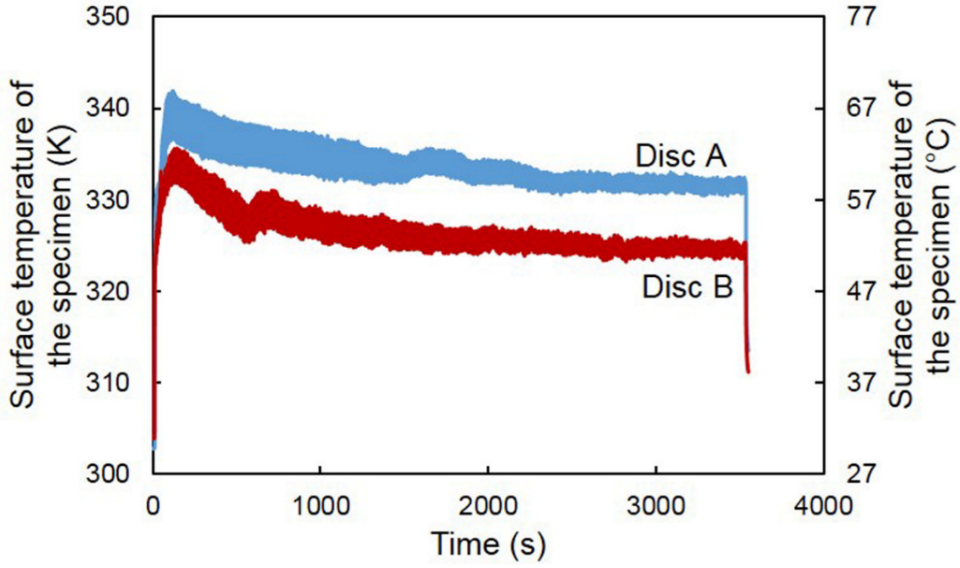

Figure 6.14 Net surface temperature of polypropylene pin when slid against steel disc A and B

Unlike the durability evaluation of gear, this test can quantify coefficient of friction/frictional force. Figure 6.15 shows the friction of polypropylene against different surface roughness steel disc. As expected, there was a gradual drop in friction with the increase in time due to the formation

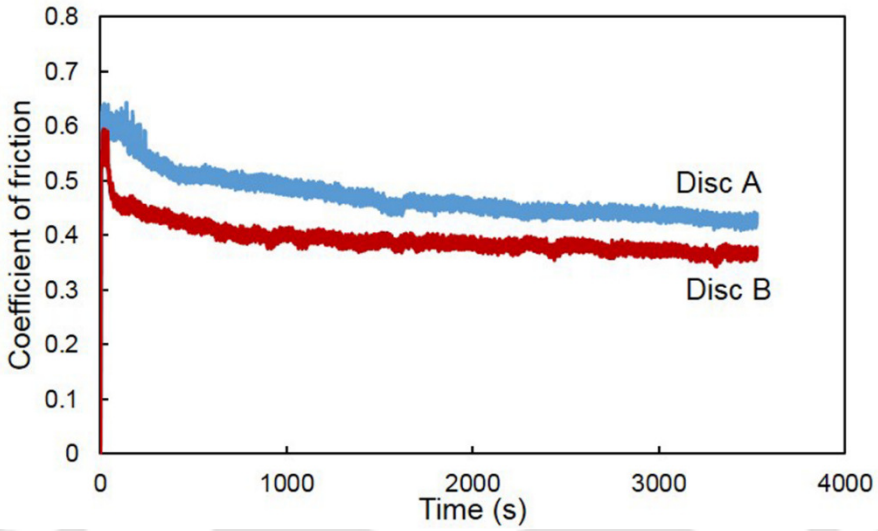

Figure 6.15 Friction coefficient of polypropylene pin against steel disc A and B

of polymer film on the counter steel disc. The co-efficient of friction gradually became stable. An increase of 0.1 coefficient of friction was observed, when the polypropylene slide against steel disc A when compared to that of disc B. Thus, a significant effect of surface roughness on frictional resistance is confirmed from these test results.

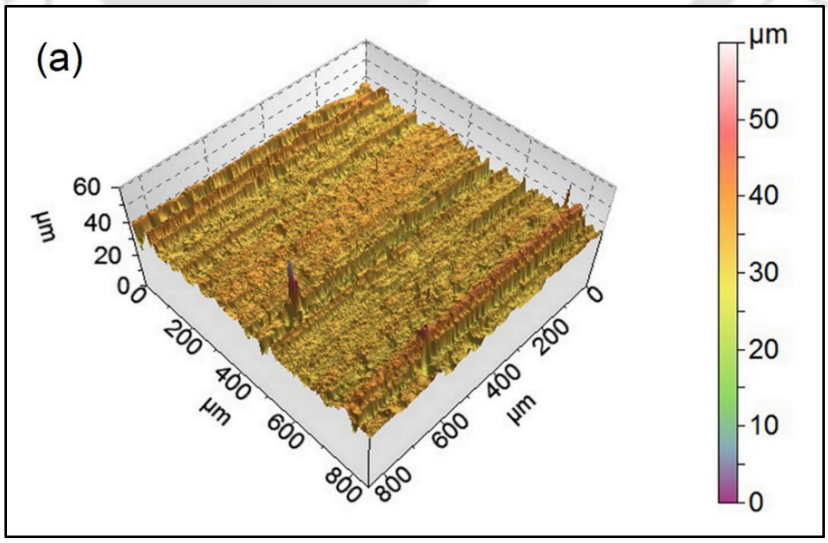

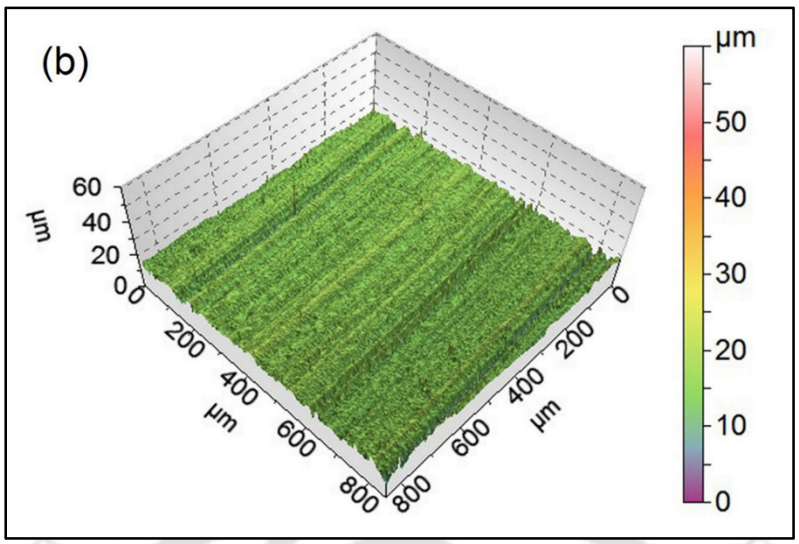

Figure 6.16 (a) Worn out surface of polypropylene pin when slid against steel disc A and (b) worn out surface of polypropylene pin when slid against steel disc B

Figure 6.16(a–b) show the worn out surface of the polypropylene pins observed under noncontact three-dimensional profiler, when sliding against steel discs A and B. Polypropylene specimen slide against steel disc A (4.7–5.4 μm) showed excessive ploughing marks when compared to specimen slide against steel disc B (2.6–3.2 μm). Thus, surface damage of the polypropylene pins also confirmed the effect of mating steel disc surface finish.

6.8 SUMMARY

Injection-moulded asymmetric polypropylene gears were evaluated by pairing with three asymmetric steel gears (newly manufactured steel gear, steal gear run against polymer gear for 5×10^5 cycles and steal gear run against polymer gear for 10×10^5 cycles having different surface roughness) and the following major conclusions were arrived

- The bearing ratio curve of the mating steel gear surface showed that the contact area reduced when steel gear having higher surface finish was paired with polypropylene gears.

- The net surface temperature of the polypropylene gears increased about 20 °C when the surface roughness of steel gears increased from 2 to 4 μm due to high contact pressure.
- Measurement of the gear weight and the tooth thickness confirmed that the wear resistance of polypropylene gear decreased with the increase in surface roughness of the mating steel gears.
- Friction and wear performance evaluation of polypropylene in the pin on disc configuration confirmed that the friction and wear increased with the increase in surface roughness of the steel disc.

CHAPTER 7

INJECTION-MOULDED ASYMMETRIC POLYPROPYLENE GEAR PERFORMANCE

7.1 INTRODUCTION

In the recent years, the importance of gears with advanced tooth forms have increased mainly due to the advancement in manufacturing process. By altering standard tooth forms, bending/contact load carrying capacity and tooth sliding characteristics can be altered as desired. In particular, gears manufactured through powder metallurgy and injection-moulding process can have desired nonstandard tooth forms including asymmetric tooth profile. Both sintered and injection-moulded gears required only one die, hence gear tooth of any complex profile can be economically manufactured.

In most of the engineering applications, gears are being rotated in only one direction; by altering other inactive coast side tooth profile, gear strength/gear dynamic forces can be altered as desired. In most of the applications, gears are operated unidirectional, i.e., only one side of the gear tooth profile is loaded. Asymmetric gears are being considered by researchers to enhance the gear performance for such unidirectional applications. For the past decade, significant numerical and analytical works have been carried out to understand the advantages and limitations of asymmetric gears. However, this chapter presents experimental performance evaluation of asymmetric gear.

7.2 METHODOLOGY

The asymmetric gears details and parameters are reported in the Section 6.2 (CHAPTER 6). Gears were moulded at an injection pressure of 9 MPa and temperature maintained in three zones of the barrel was 210, 230, and 250 °C. Injection-moulded test gears are shown in Figure 7.1. The moulded polypropylene gears were meshed with stainless steel gears having identical gear parameters but of 12 mm face width, manufactured through wire-cut electric discharge machining

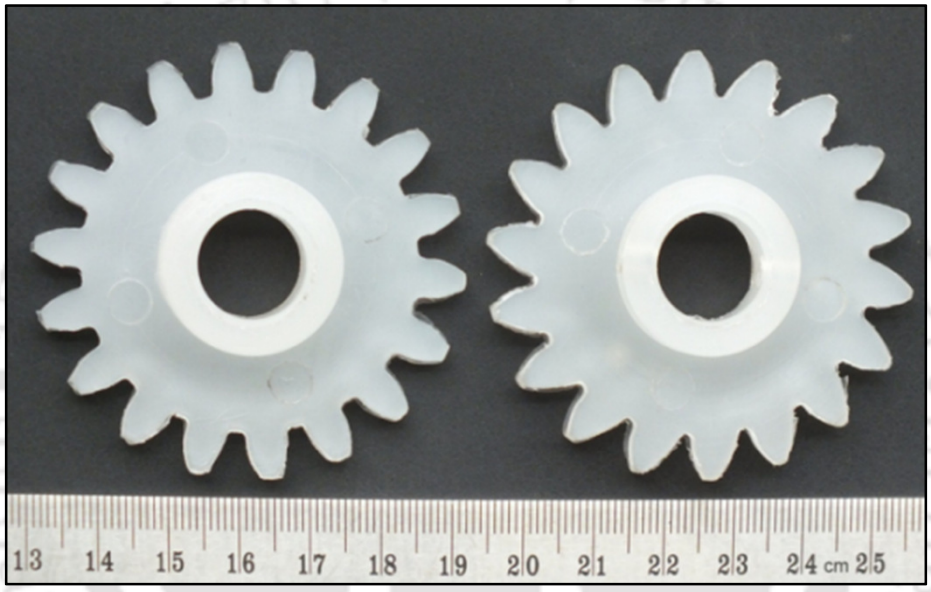

Figure 7.1 Injection-moulded symmetric and asymmetric test gears

(Eletronica, ULTIMA2010) process. The quality and hardness of both the gears (Polypropylene and Steel gear) are reported in the Section 5.2 (Chapter 5) and Section 6.2 (CHAPTER 6). The surface roughness of steel and polypropylene gears are 3.5–3.9 µm and 2–2.6 µm.

A test rig (Figure 7.2) was developed in-house to measure the gear tooth deflection under static loading. Test rig driving shaft was attached to the metal gear and polypropylene gear was attached to the driven shaft and the shafts were supported by bearings at a fixed centre distance. The bending resistance of the gear tooth was determined by applying the static load on the single tooth and the corresponding tooth deflection was measured by a rotary encoder. A pulley was attached to the

driver shaft to apply static torque and dead weights were added at the end of the rope which was wound around the pulley. Inline torque sensor (HBM, T20WN) was connected between the pulley and driver gear through below couplings (KBK, KB4C) to measure the applied torque. In the driven side, the polymer gear was firmly locked in a position at any desired roll angle/position

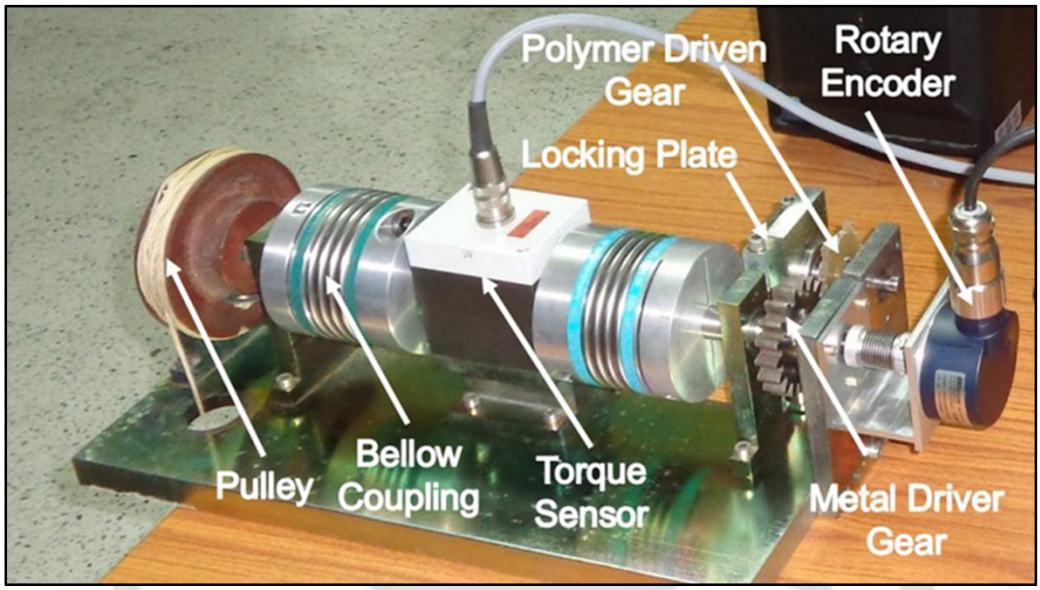

Figure 7.2 Gear tooth deflection test rig

with a steel gear by using a locking plate. Since test polymer gear was locked in a position, tooth deflection of polymer test gear was measured by the position of the steel gear by rotary encoder through steel gear shaft.

7.3 GEAR SURFACE TEMPERATURE

The gear tests were carried out (Section 3.4; CHAPTER 3) at a constant speed of 800 rev/min and at various loads (2, 2.5, 3, 3.5, 4, and 4.5 Nm). Figure 7.3(a) shows the measured surface temperature of test gears tested at 3–4.5 Nm. The rise in surface temperature is due to the repetitive gear tooth deflection and surface interaction at the face and flank region of test gear with the standard steel gear. In all the four loads, both symmetric and asymmetric gears exhibited almost same surface temperature.

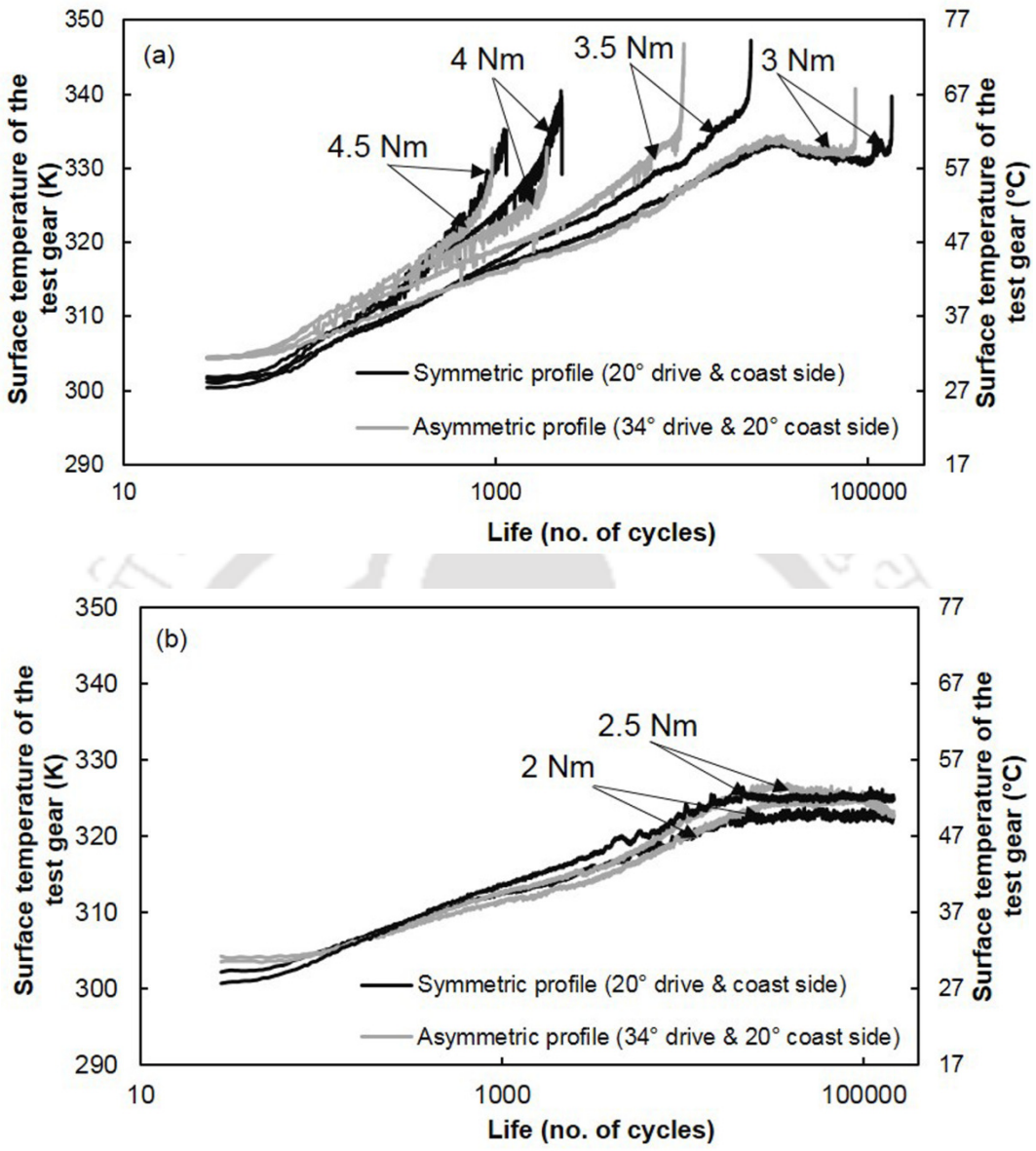

Figure 7.3 Measured surface temperature of the test gears at (a) 3–4.5 Nm and (b) 2–2.5 Nm

In both the test gears, when the load increased, the maximum surface temperature exhibited by the test gear increased. For 3–4.5 Nm loads, a sudden rise in surface temperature was exhibited by the test gears, which clearly revealed the thermal induced plastic tooth deformation. However, no such sudden rise was observed at gears, while tested at 2–2.5 Nm (Figure 7.3(b)).

7.4 GEAR TOOTH WEAR

Wear performance of the test gears were evaluated by measuring the tooth thickness of the test gears periodically (every 1.44×10^5 cycles, 3 h). Figure 7.4 shows the gear tooth thickness measured across three teeth of asymmetric and symmetric gears tested at 2 and 2.5 Nm.

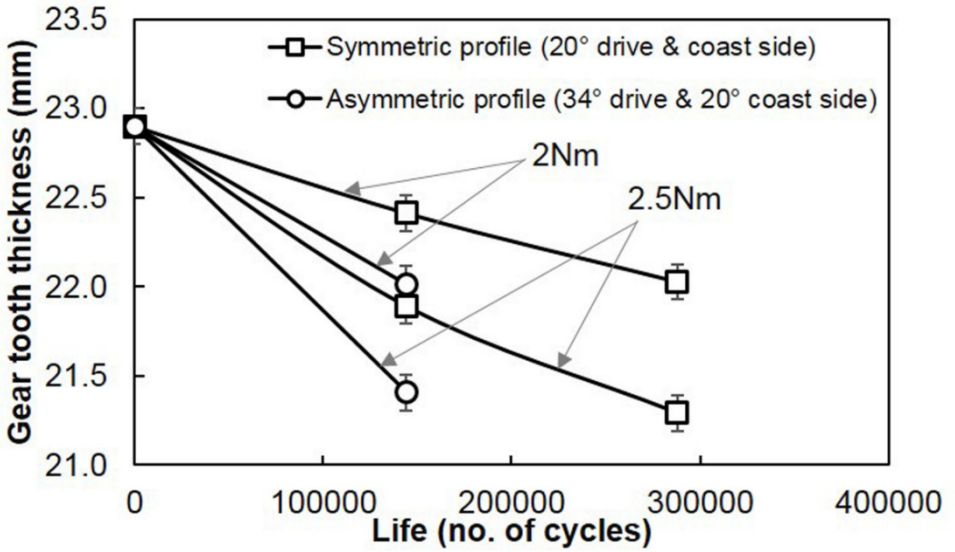

Figure 7.4 Measured gear tooth thickness across three teeth of the test gears

The symmetric gears were run upto 2.88×10^5 cycles when subjected to 2 and 2.5 Nm and asymmetric gears were run only upto 1.44×10^5 cycles at these loads. Weight loss of the test gears also confirmed the inferior wear resistance of asymmetric gear than that of symmetric gear. Weight loss of symmetric and asymmetric gears tested at 2 Nm load was 419 mg after 4.32×10^5 cycles and 273 mg after 1.44×10^5 cycles. Similarly, weight loss of symmetric and asymmetric gears tested at 2.5 Nm was 470 mg after 2.88×10^5 cycles and 406 mg after 1.44×10^5 cycles. The following section presented the reason for the inferior wear performance of the asymmetric gear.

7.4.1 Symmetric Vs Asymmetric – Tooth Wear

The influence of drive side pressure angle over the contact ratio of gear pair and its performance is briefed in this section. Figure 7.5(a–b) shows the beginning and end of the tooth engagement of a pair of symmetric and asymmetric gears. The angle of action in the symmetric gear is 28° and

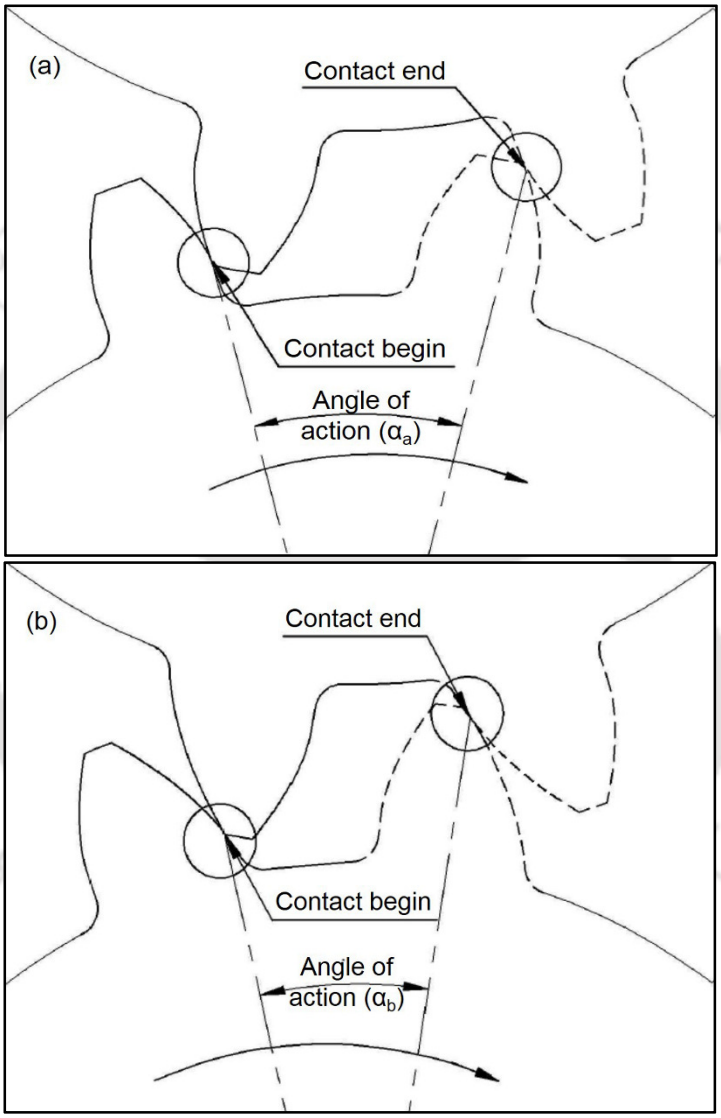

Figure 7.5 Gear tooth engagement of (a) symmetric gear pair and (b) asymmetric gear pair

21° in the asymmetric gear. Contact ratio is the ratio of the angle of action to the pitch angle and can be calculated using the following equation,

$$Contact\ ratio = \frac{Arc\ of\ contact}{Circular\ pitch} \tag{7.1}$$

$$Arc\ of\ contact = \frac{Path\ of\ contact}{cos\ \emptyset_n} \tag{7.2}$$

$$Path\ of\ contact = [\sqrt{R_a^2 - R^2 Cos^2 \emptyset_n} - Rsin\emptyset_n] + [\sqrt{r_a^2 - r^2 Cos^2 \emptyset_n} - rsin\emptyset_n] \tag{7.3}$$

where R_a and r_a are the addendum circle radius of the driver and driven gear (mm), R and r are the pitch circle radius of the driver and driven gears (mm), $\emptyset_n$ is standard normal pressure angle of gear (deg).

The increased pressure angle reduced the angle of action and contact ratio. The contact ratio of symmetric (20/20) and asymmetric gears (34/20) are 1.53 and 1.25 respectively. Due to this reduced contact ratio (18.3%), the load acting period on a single asymmetric gear tooth was longer compared to the symmetric gear for the same test conditions. Cavdar *et al.* (2005) examined the effect of various pressure angles (20°–40°) at the drive side with 20° at coast side. With the increase in pressure angle, increased single tooth contact period was observed. Karpat *et al.* (2008) considered various (20°–35°) pressure angles at the drive side with 20° coast side gears and evaluated static transmission errors. It was found that, with the increase in pressure angle at the drive side, the single tooth region increased. It was also found that the increased pressure angle causes increased dynamic force. Thus the reduced contact ratio and increased dynamic force contributed to the inferior wear performance of asymmetric gears.

7.4.2 Worn out Morphology of Test Gears

Figure 7.6(a–b) and Figure 7.7(a–b) show the symmetric and asymmetric gear tooth surface after finite number of cycles when loaded at 2 Nm and 2.5 Nm respectively.

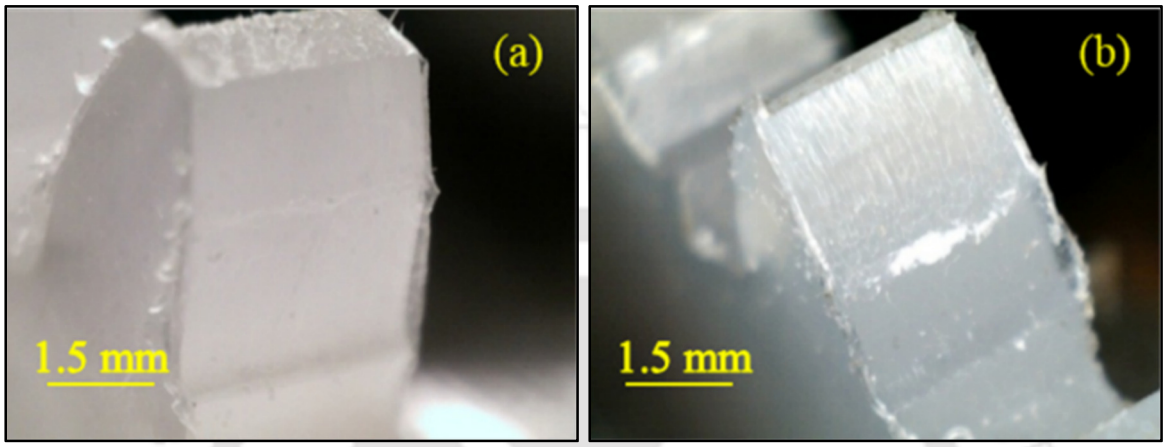

Figure 7.6 Worn out gear tooth surface of (a) symmetric gear and (b) asymmetric gear after 1.45×10^5 cycles, 2 Nm

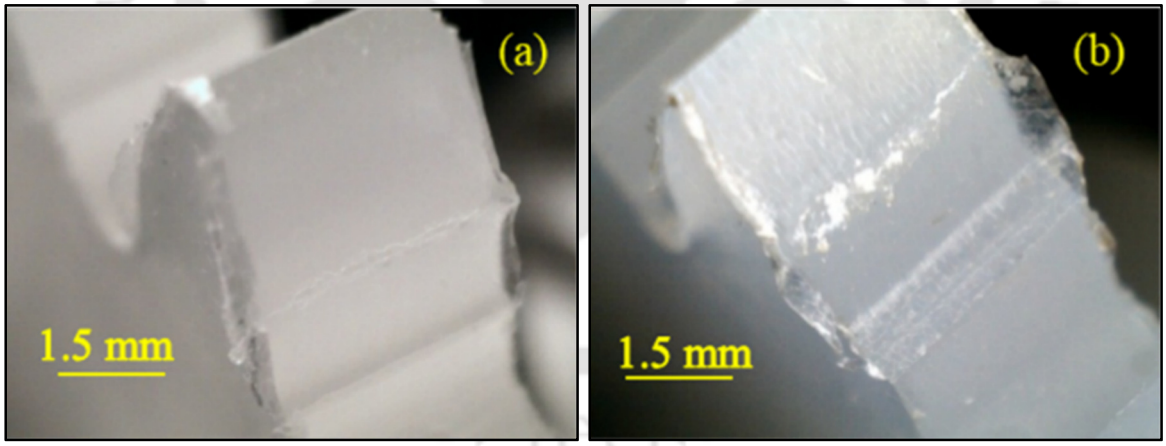

Figure 7.7 Worn out gear tooth surface of (a) symmetric gear and (b) asymmetric gear after 1.45×10^5 cycles, 2.5 Nm

Failure morphology also confirmed the inferior performance of asymmetric gear over symmetric gears. To understand, whether the wear has taken place on the coast side, the coast side of the test

gears were inspected under digital microscope. Figure 7.8(a–b) and Figure 7.9(a–b) confirms that for both the test loads (2 and 2.5 Nm), both the symmetric and asymmetric gears exhibited no wear on the coast side.

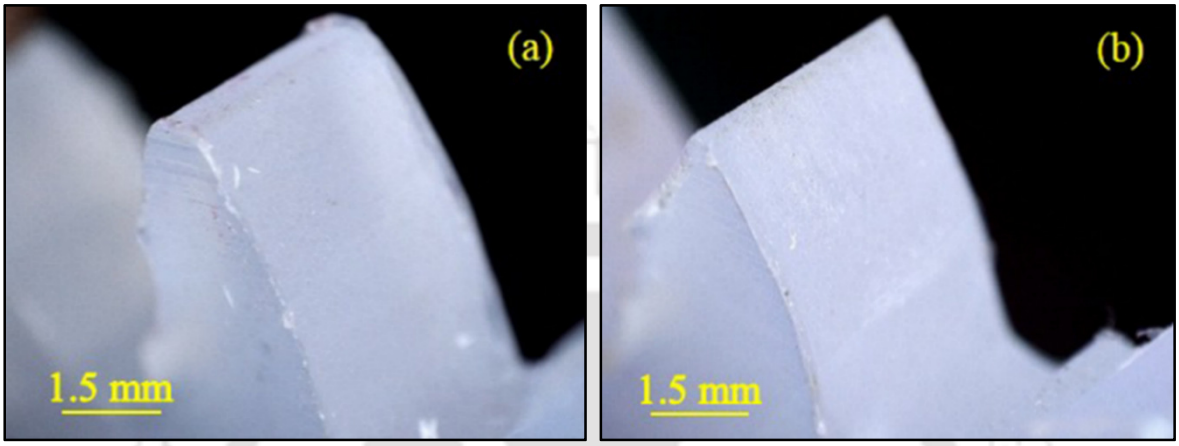

Figure 7.8 Coast side gear tooth surface of (a) symmetric gear after 4.32×10^5 cycles and (b) asymmetric gear after 1.45×10^5 cycles, 2 Nm

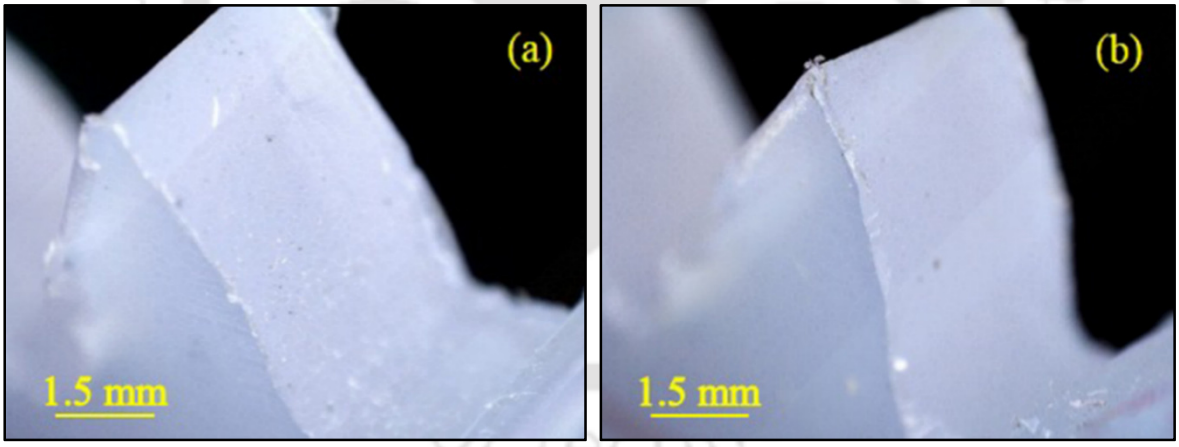

Figure 7.9 Coast side gear tooth surface of (a) symmetric gear after 2.88×10^5 cycles and (b) asymmetric gear after 1.45×10^5 cycles, 2.5 Nm

7.4.3 Gear Tooth Profile Wear

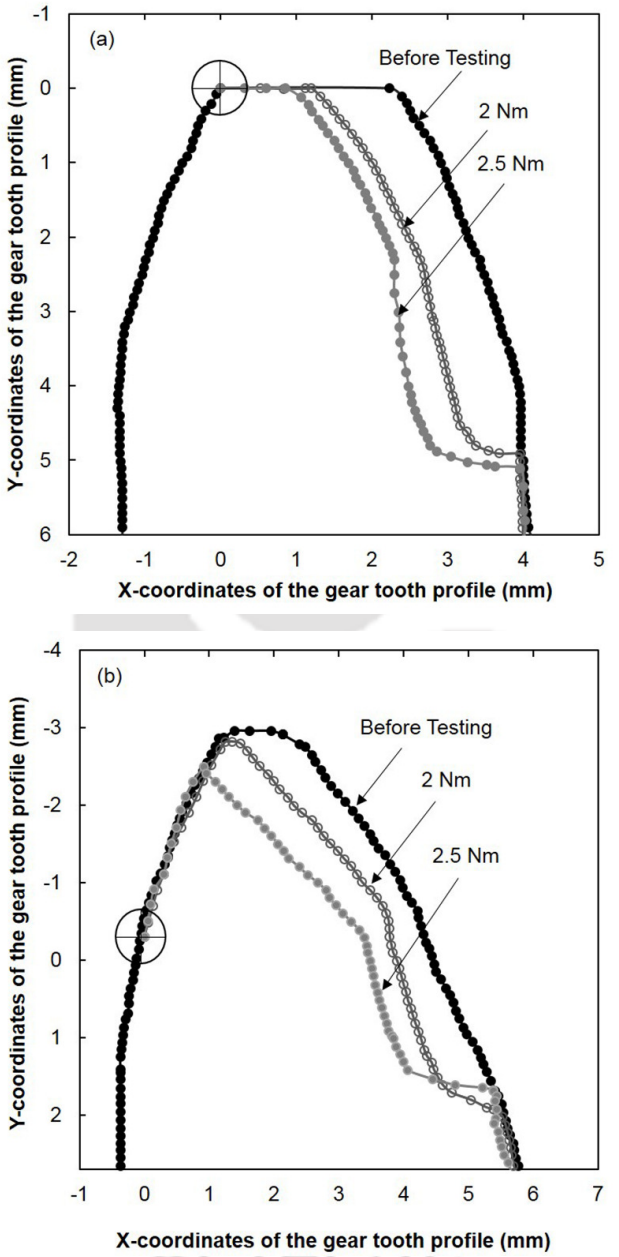

Figure 7.10 Final profile of the test gears (a) symmetric gear tooth profile tested at 2 and 2.5 Nm after 4.32×10^5 and 2.88×10^5 cycles; (b) asymmetric gear tooth profile tested at 2 and 2.5 Nm after 1.44×10^5 cycles

The wear depth in the profile of the symmetric and asymmetric tested gear was determined using optical profile projector and compared with untested gear. The wear depth was slightly less near

the pitch region when compared to tip and root region of polypropylene gears. Figure 7.10(a–b) shows the final involute profile of a symmetric and asymmetric gear tooth tested at 2 and 2.5 Nm. About 70 points were chosen to measure the coordinates from the coast side tip (for symmetric gear) or coast side pitch point (for asymmetric gear) to the drive side root of the involute profile. Profile of the injection-moulded gear before test was also taken to compare with the worn out surface. Symmetric gear loaded at 2 and 2.5 Nm after 4.32×10^5 and 2.88×10^5 cycles is shown in Figure 7.10(a). Similarly Figure 7.10(b) shows the profile of test asymmetric gear loaded at 2 and 2.5 Nm after 1.44×10^5 cycles. From both the test conditions, inferior wear resistance was observed for asymmetric gear and also, tooth wear increased with increase in load.

The relative sliding velocity of the asymmetric (0.82 m/s) and symmetric (1.13 m/s) gear was calculated from the following equation and it was maximum at the tip and root regions and thus the wear near these regions were maximum which was observed from the final profile of the test gears.

$$Maximum\ sliding\ velocity = (\omega_1 + \omega_2) \times (Path\ of\ appraoch/recess) \tag{7.4}$$

$$Path\ of\ approach/recess = \frac{Path\ of\ contact}{2} \tag{7.5}$$

where ω_1 *and* ω_2 is the angular velocity of the driver and driven gear (rad/s). But however, near the pitch region, the wear was minimum due to very less/ zero relative sliding velocity and thus wear was less near the pitch region.

7.5 PLASTIC DEFORMATION

The test gears (symmetric and asymmetric gears) exhibited abrupt temperature raise and subsequently failure by plastic deformation at 3–4.5 Nm loads. Figure 7.11(a–b) shows the tooth deformation of symmetric and asymmetric gears at 3 Nm. Close-up view of the tooth deformation

(Figure 7.11(c–d)) confirmed the thermal induced plastic tooth deformation. Plastic flow and traces of the molten gear materials were clearly observed. A sudden rise in the gear tooth temperature along with the repetitive cyclic load contributed to this severe tooth deformation. Figure 7.3(a) confirmed the sudden rise of gear tooth surface temperature at this load.

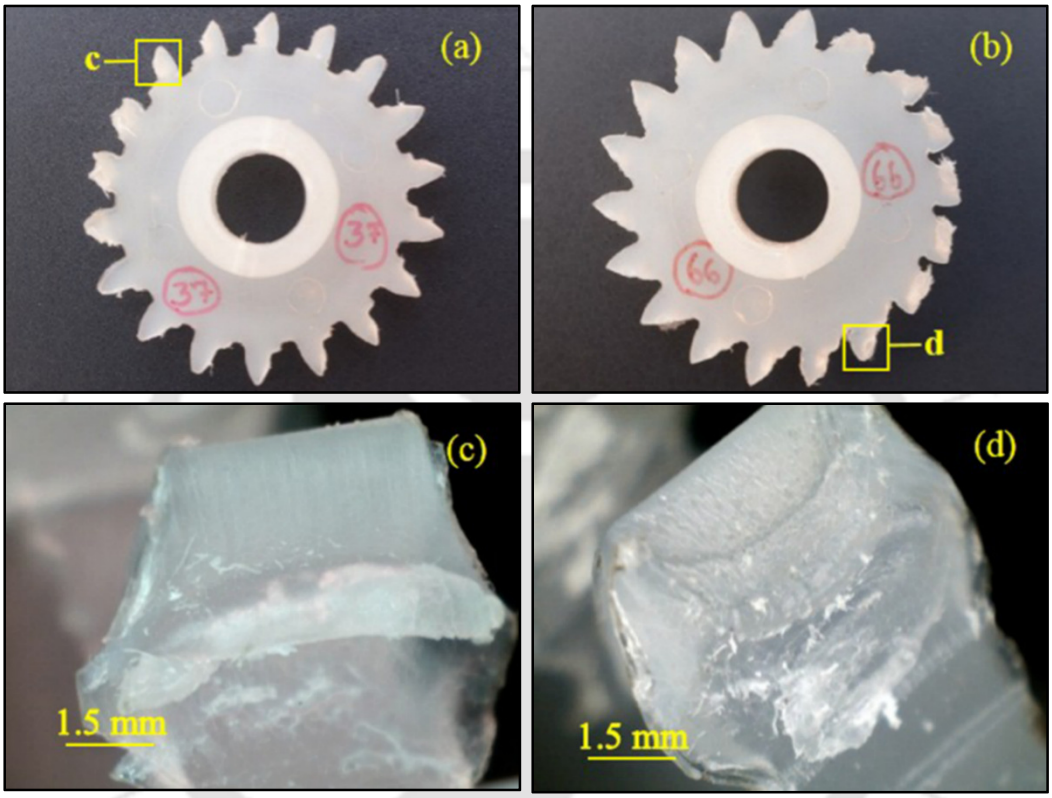

Figure 7.11 Failure morphology of (a) symmetric gear (1.34×10^5 cycles), (b) asymmetric gear (0.85×10^5 cycles) at 3 Nm, (c) close-up view of Figure 7.11(a) showing tooth deformation, and (d) close-up view of Figure 7.11(b) showing tooth deformation

Similarly, tooth deformation of the symmetric and asymmetric gears at higher loads (3.5–4.5 Nm) are shown in the Figure 7.12–Figure 7.14. The gear tooth deformation observed in the test gears confirmed the thermal induced plastic tooth deformation. For all the test loads, asymmetric gears exhibited inferior performance than that of symmetric gears. However, Cavdar *et al.* (2005) and

Karpat *et al.* (2008) reported reduced bending stress in the asymmetric gear. The reason for the inferior performance of asymmetric gears over the symmetric gear is explained below.

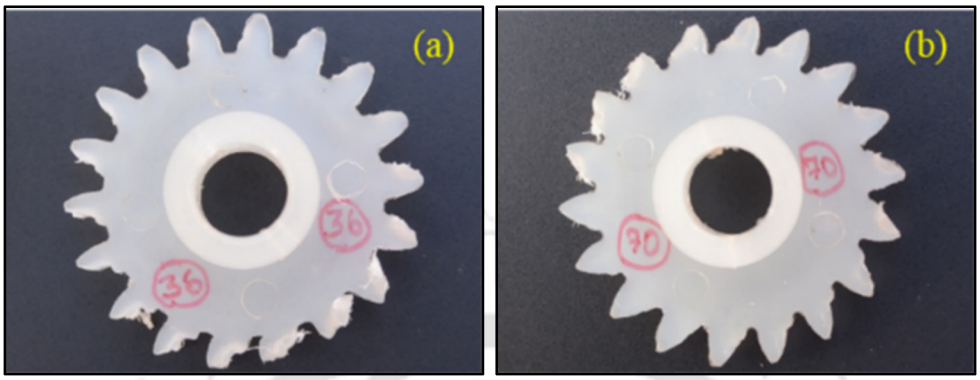

Figure 7.12 Failure morphology of (a) symmetric gear (23.44×10³ cycles) and (b) asymmetric gear (10.23×10³ cycles) at 3.5 Nm

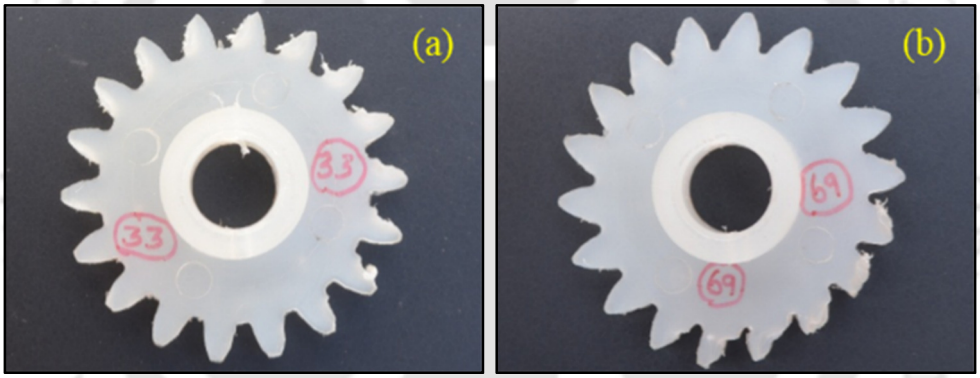

Figure 7.13 Failure morphology of (a) symmetric gear (2.67×10³ cycles) and (b) asymmetric gear (1.88×10³ cycles) at 4 Nm

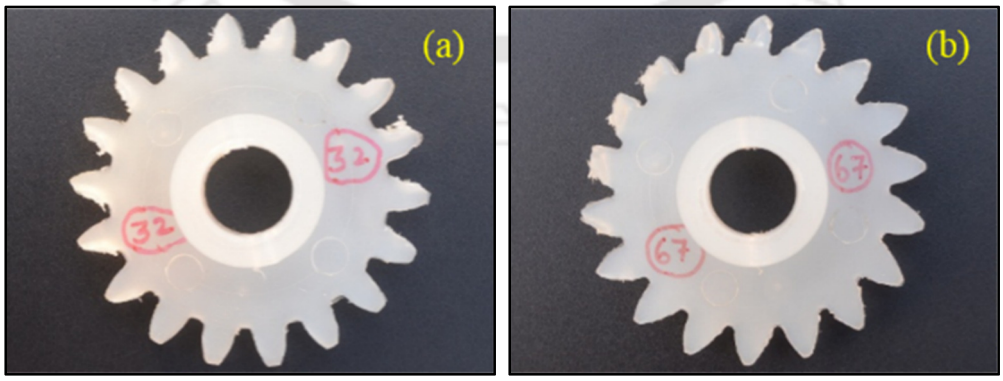

Figure 7.14 Failure morphology of (a) symmetric gear (1.14×10³ cycles) and (b) asymmetric gear (0.96×10³ cycles) at 4.5 Nm

7.5.1 Symmetric Vs Asymmetric – Plastic Deformation

The inferior performance of the asymmetric gear was due to the change in loading condition. The highest point single tooth contact (HPSTC) is the worst load position for the bending failure (Figure 7.15). The location of the highest point single tooth contact was calculated from the following equation (AGMA 908-B89).

$$Location\ of\ HPSTC\ (C_4) = \left[C_r\ sin\ \emptyset_r - \sqrt{r_a^2 - r_b^2}\right] + P_b \tag{7.6}$$

$$\emptyset_r = cos^{-1}\left[\frac{R_b + r_b}{C_r}\right] \tag{7.7}$$

$$P_b = \frac{2\pi R_b}{Z_1} \tag{7.8}$$

where C_r is the operating centre distance (mm), $\emptyset_r$ is the operating transverse pressure angle (deg), R_a and r_a is the addendum radius of driver and driven gear (mm), P_b is the transverse base pitch (mm), R_b and r_b is the base radius of driver and driven gear (mm) and Z_1 is the number of driver gear teeth.

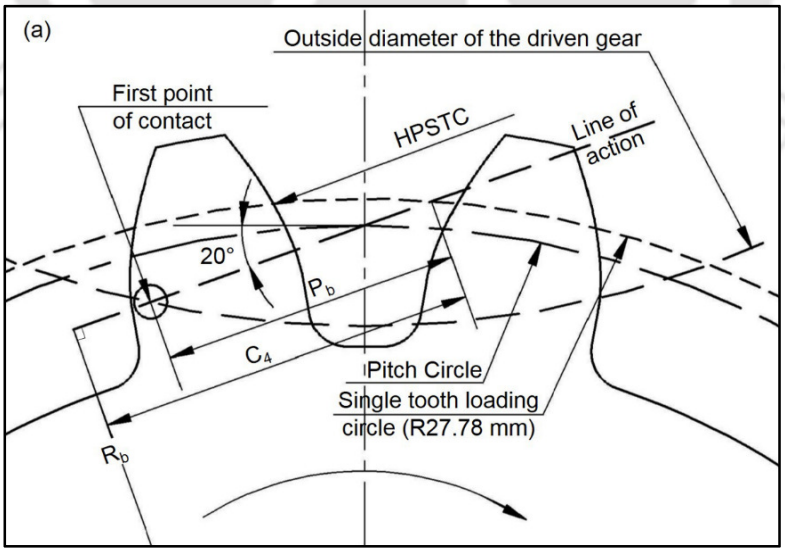

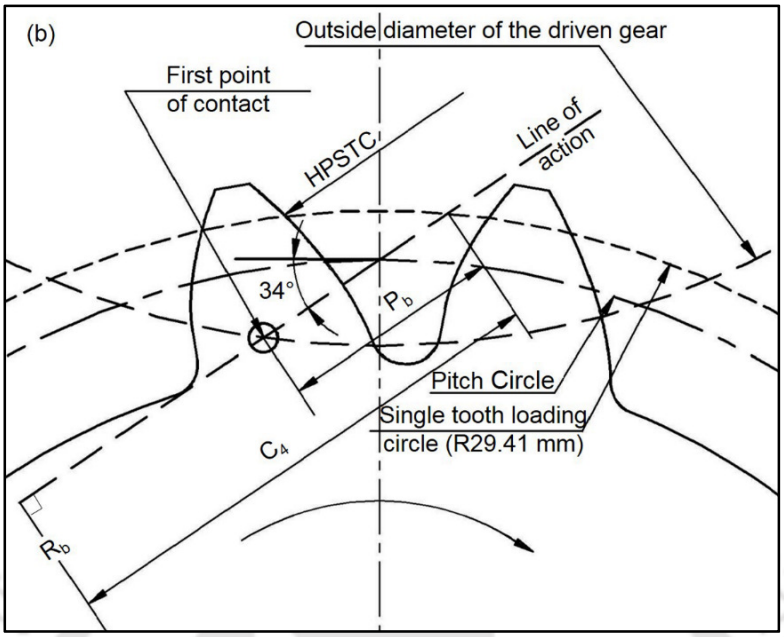

Figure 7.15 HPSTC load position of (a) symmetric gear and (b) asymmetric gear

The pressure angle varies with respect to the load application point (Figure 7.16). The pressure angle and load angle of the HPSTC can be determined by,

$$\emptyset_{nW} = \tan^{-1}\left[\frac{C_4}{r_{nb}}\right] \tag{7.9}$$

$$\emptyset_{nL} = \tan\emptyset_{nW} - \tan\emptyset_n + \emptyset_n - \frac{S_n}{2r_n} \tag{7.10}$$

The radius at which the HPSTC and virtual load can be calculated by using the following equation,

$$r_{nW} = \frac{r_{nb}}{\cos\emptyset_{nW}} \tag{7.11}$$

$$r_{nL} = \frac{r_{nb}}{\cos\emptyset_{nL}} \tag{7.12}$$

where r_{nb} is the virtual base radius (mm), $\emptyset_{nW}$ is the pressure angle at the load application point (radian/deg), $\emptyset_{nL}$ is the load angle (radian), $\emptyset_n$ is the standard normal pressure angle (radian), S_n

is the normal circular tooth thickness (mm), r_{nW} is the HPSTC radius (mm) and r_{nL} is the virtual load radius (mm).

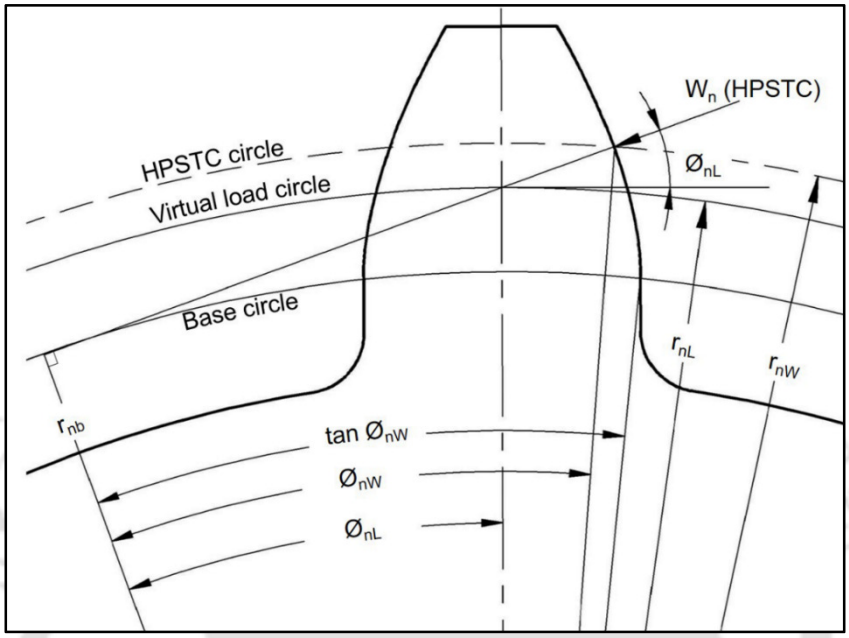

Figure 7.16 Load angle and load radius

The load angle at HPSTC of symmetric and asymmetric gears are 20.26° and 42.05° respectively. The radial distance of the HPSTC point for the asymmetric and symmetric gear tooth are 29.41 mm and 27.78 mm respectively. This increased load radius along with thermal softening could have contributes to the inferior performance of asymmetric gear. However, many researchers revealed the improved bending load carrying capacity of asymmetric gear tooth profile (Cavdar *et al.*, 2005; Karpat *et al.*, 2008; Muni *et al.*, 2007) wherein only pure static bending load at fixed position (either pitch or HPSTC positions) was considered. Wear failure is predominant in polymer gears, however root cracking and pitting failure are very unusual (Senthilvelan and Gnanamoorthy, 2004; Mao, 2007; Senthilvelan and Gnanamoorthy, 2007; Pogacnik and Tavcar, 2015). During the initial period of test, polymer gear surface interaction causes wear and material hysteresis causes increased surface temperature resulted in gear tooth softening. The material loss and thermal

softening combined with increased loading radius contributes to the earlier failure (plastic deformation) of the asymmetric gears compared to the symmetric gear.

7.6 PERFORMANCE

The performance of asymmetric gear was quantified in terms of useful life from the test and compared with symmetric gear. Figure 7.17 shows the life of symmetric and asymmetric polymer

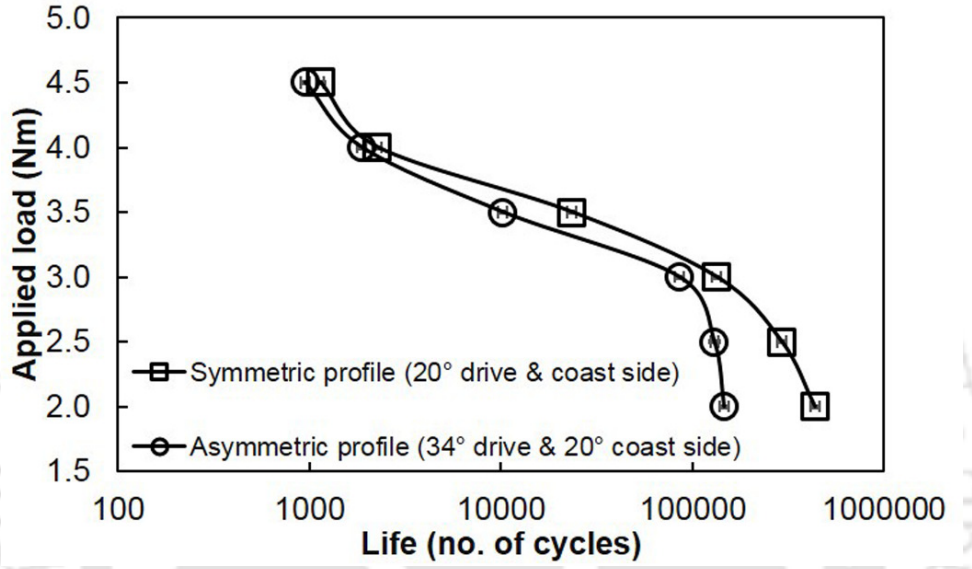

Figure 7.17 Life of the symmetric and asymmetric gears at various loads

gears subjected to various loads (2, 2.5, 3, 3.5, 4 and 4.5 Nm). As reported in earlier section, test gears subjected to 2–2.5 Nm exhibited wear failure and gears subjected to 3–4.5 Nm exhibited plastic tooth deformation failure. Each test condition was repeated for three times and the average life cycle of polymer gears was calculated and the deviations are found to be well within 5%. Thus the asymmetric gear exhibited slightly less performance due to the decreased contact ratio and increased bending moment (loading radius from 27.78 mm to 29.41 mm) compared to the symmetric gear.

7.7 STATIC GEAR TOOTH DEFLECTION

For all the considered loads, asymmetric gears exhibited inferior performance than that of symmetric gears. This inferior performance of asymmetric gear was unexpected in spite of the reduced bending stress as reported by the Cavdar *et al.* (2005) and Karpat *et al.* (2008). To validate this fact, the gear tooth deflection was evaluated by in-house developed gear tooth deflection test rig. Deflection of both asymmetric gear and symmetric gear tooth deflection was measured (Figure

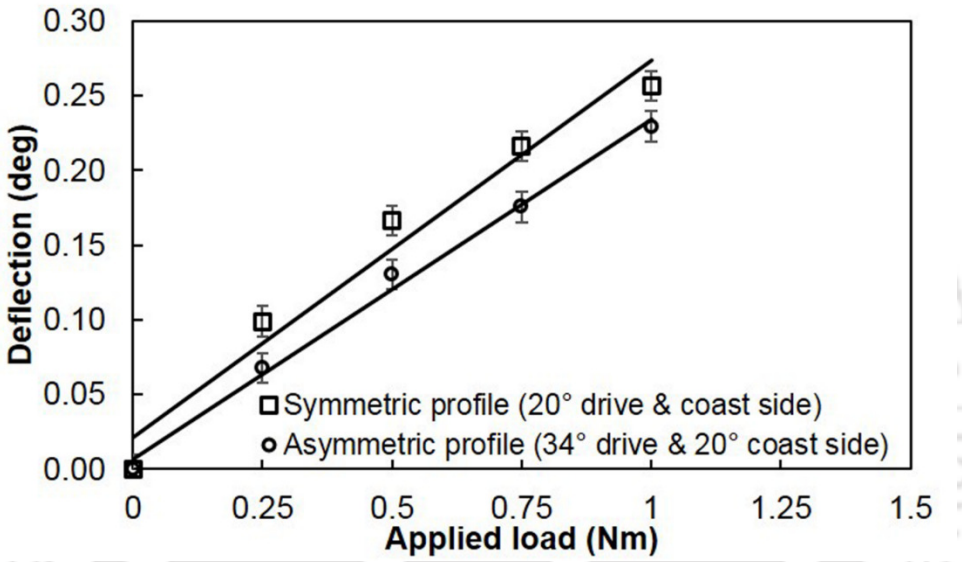

Figure 7.18 Gear tooth deflection of symmetric gear and asymmetric gear

7.18). From the Figure 7.18, it is revealed that deflection of the asymmetric gear tooth is less (10–30%) than that of symmetric gear tooth. Thus the bending resistance of asymmetric gear tooth is superior. Less gear tooth deflection of asymmetric gear confirmed the superior bending resistance when compared to that of symmetric gear. Failure morphology of both symmetric and asymmetric gears not revealed any pure bending failure, no root cracks were observed on any of the test gears. Test gears exhibited excessive gear tooth wear at lower loads (2–2.5 Nm) and plastic tooth deformation due to thermal assisted fatigue. This failure morphology revealed contact fatigue as the contributing mechanism. Thus reduction of contact ratio contributed to the inferior fatigue performance of asymmetric gear over symmetric gear for the test condition.

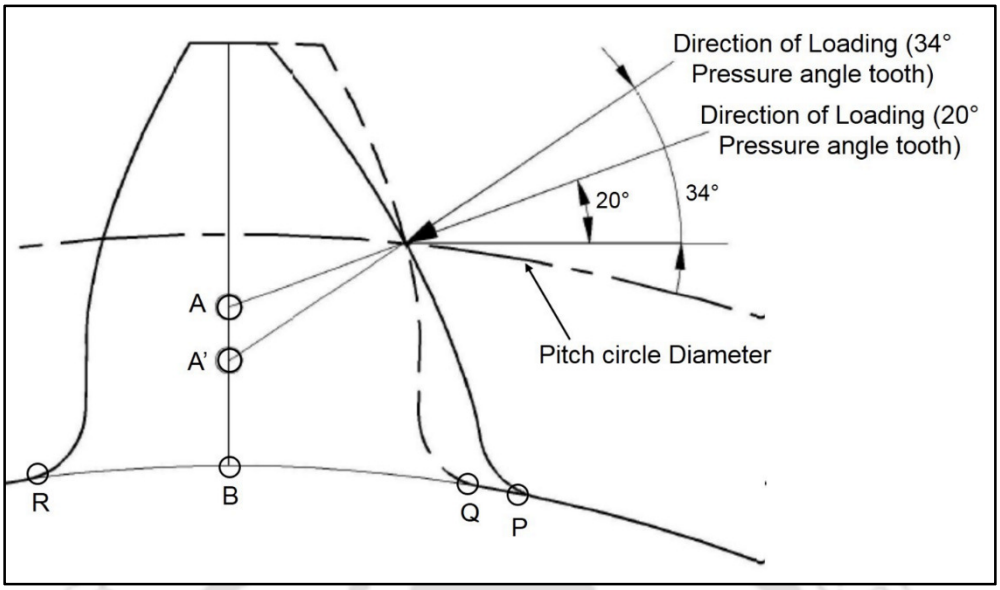

Figure 7.19 Schematic of symmetric gear and asymmetric gear with loading

Figure 7.19 shows the schematic of symmetric and asymmetric gear with load acting on the pitch circle configuration. The effective cantilever length of the gear tooth decreased from BA to BA' when the pressure angle is increased from 20° to 34°.This reduced cantilever length contributes to the reduction of gear tooth bending moment.

7.8 SUMMARY

This chapter deals with the performance evaluation of injection-moulded symmetric and asymmetric spur gears for its durability in the power absorption gear test rig and following major conclusions were arrived.

- Test gears (both symmetric and asymmetric gears) exhibited tooth wear failure at lower loads (2–2.5 Nm) and plastic tooth deformation at higher loads (3–4.5 Nm).
- The radial distance of the HPSTC point increased for the asymmetric gear (29.41 mm) compared to the symmetric gear (27.88 mm) and the contact ratio of symmetric and asymmetric gears are 1.53 and 1.25 respectively.

- The reduced contact ratio and increased radial distance of the HPSTC point contributes for the inferior performance of asymmetric gear at all the tested conditions (2–4.5 Nm).
- Asymmetric gear with 34° pressure angle at drive side exhibited superior capability to carry bending load than that of symmetric gear with 20° pressure angle at both the sides.

CHAPTER 8

MECHANICAL AND TRIBOLOGICAL PERFORMANCE OF CNT–PP COMPOSITES

8.1 INTRODUCTION

Temperature-sensitive mechanical properties of the polypropylene limit its applications and, therefore, reinforced polypropylene materials are being considered to widen the applications. The addition of CNT improves the mechanical (Yang *et al.*, 2008; Kim *et al.*, 2009; Kang *et al.*, 2010; Suresha *et al.*, 2010; Chen *et al.*, 2011; Liu *et al.*, 2013), tribological (Chen *et al.*, 2003; Cai *et al.*, 2004; Yang *et al.*, 2005; Yang *et al.*, 2005; Wang *et al.*, 2008; Cho, 2008; Park *et al.*, 2013; Solonin *et al.*, 2014; Roy *et al.*, 2015) and shrinkage (Prashantha *et al.*, 2009) properties of polymers. And also the self-lubrication and better thermal conductivity of CNT improves the thermal characteristics (Zaikov *et al.*, 2010; Xin and Li, 2012) of its reinforced polymer. This chapter investigated the mechanical and tribological performance of the CNT–PP (0.5, 1.0, 3.0 and 5.0 wt%) composites developed using the melt compounding technique. The developed composites were injection-moulded into tensile specimens and pins to evaluate the mechanical and tribological properties of the composites.

8.2 METHODOLOGY

In the present investigation, a 20 wt% CNT–PP master batch (PLASTICYL PP 2001, Nanocyl) was used. Various CNT–PP composites (0.5 1.0, 3.0, and 5.0 wt%) were developed by adding polypropylene (M110, Haldia) with the master batch using melt compounding technique.

Developed CNT–PP composites were then injection-moulded into tensile and pin specimens. The material processing and moulding conditions are explained in Section 3.2 (CHAPTER 3). Figure 8.1(a–b) shows the tensile and pin specimens of the considered test materials.

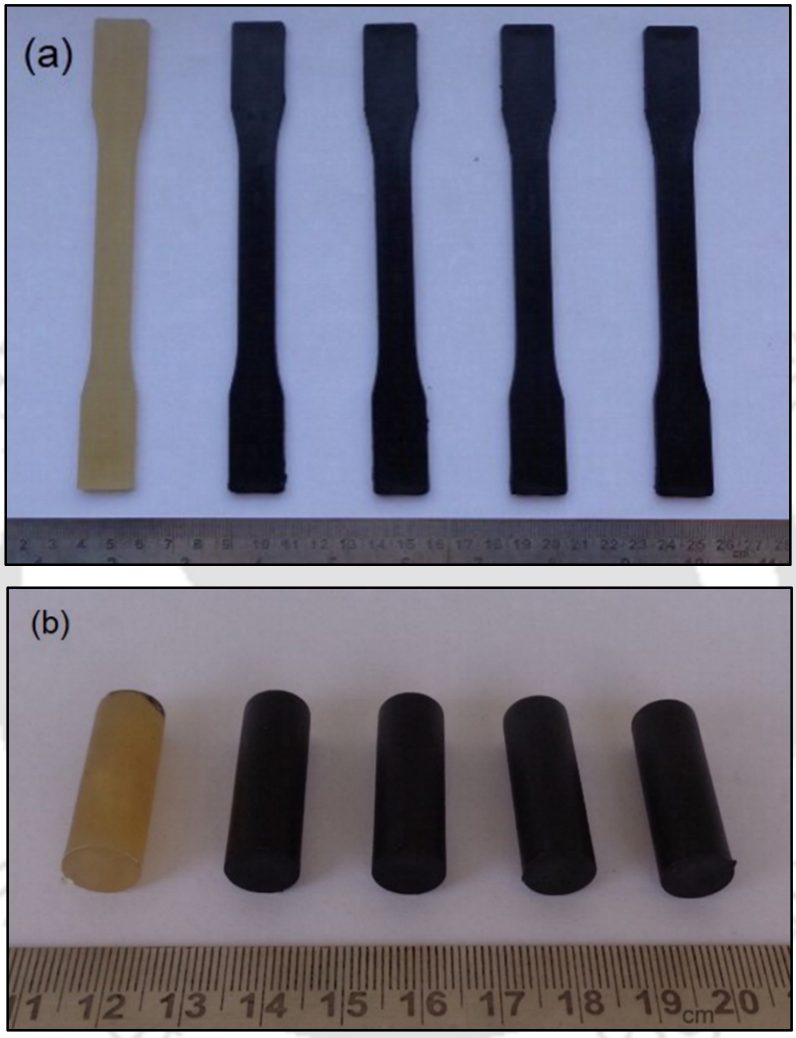

Figure 8.1 (a) Tensile and (b) pin specimens of polypropylene, 0.5, 1, 3, 5 wt% CNT–PP composites

The performance evaluation of the developed CNT–PP composites are explained in Section 3.3 (CHAPTER 3). The tensile strength of the developed materials was measured at room temperature with the aid of a servo hydraulic test machine. Injection-moulded tensile specimens were made according to ASTM D638 and tested at a crosshead speed of 20 mm/min. At least three specimens

were measured for each condition. The hardness of the injection-moulded sample was measured as per ASTM D2240 with the aid of a Shore-D-Durometer. Approximately, 10 readings at different locations were taken and the average value was reported.

The friction and wear characteristics of the test materials were evaluated with the aid of a pin-on-disc apparatus. Test specimens with a 10 mm diameter were slid against a hardened steel disc. The initial surface roughness and hardness of the counter disc were 2.6–3.2 µm (Figure 8.2) and 80–81.5 HRB. The root mean square (R_q) was 3.24–3.54 µm and the maximum height of the profile (R_z) was 15.8–16.6 µm.

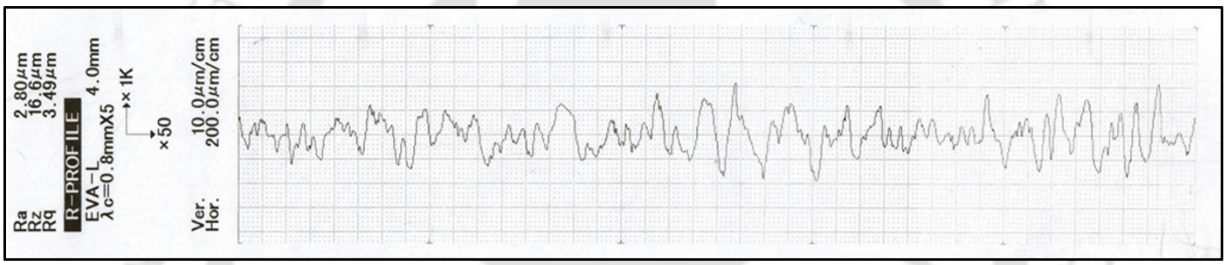

Figure 8.2 Surface profile of counter steel disc

Before testing, pins were flattened to form a uniform contact area and a surface roughness of 0.5–0.8 µm at the contact area was achieved by rubbing the pin against SiC abrasive paper. Tests were performed at a normal load of 50 N and at a sliding speed of 56.54 m/min in accordance with ASTM G99.

8.3 MECHANICAL PROPERTIES

8.3.1 Structural Properties

Stress–strain curve obtained for the test materials using servo hydraulic test machine and shown in Figure 8.3. The presence of CNT limits the movement of the polymer molecules, and thus, the percentage elongation of the polypropylene decreased as the CNT percentage increased.

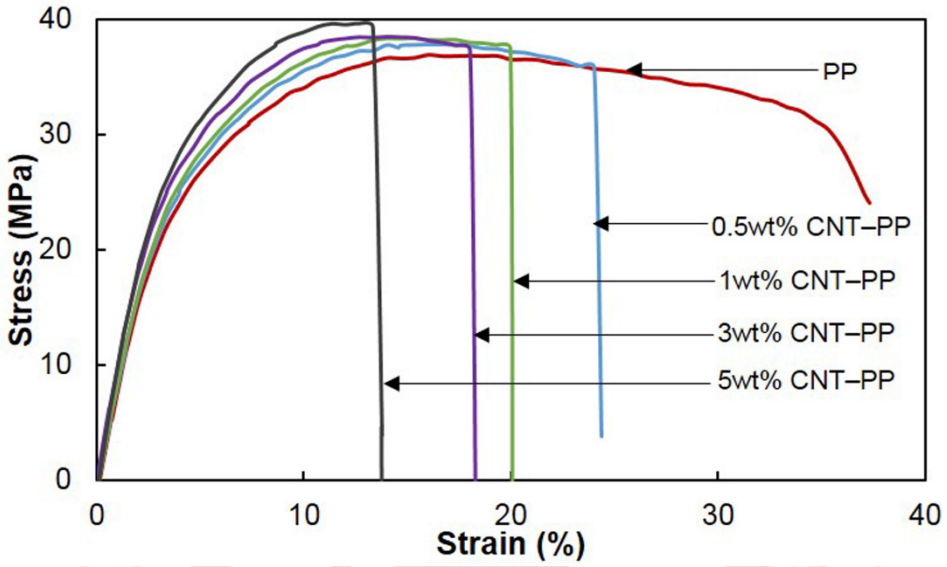

Figure 8.3 Stress–strain plot of the tested CNT–PP composites

Figure 8.4 summarizes the measured yield strength and Young's modulus of the test materials. The yield strength and tensile modulus increased and ductility decreased as the CNT content increased. The interface between the polymer and CNT is strong; therefore, the external load applied to the composite is efficiently transferred across the interface, which resulted in increased tensile strength.

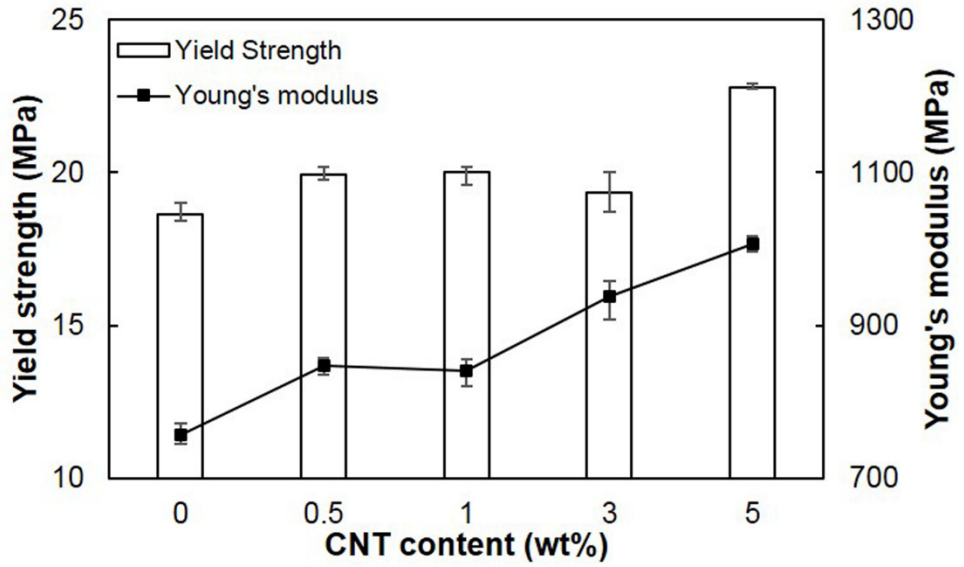

Figure 8.4 Yield strength and Young's modulus of the CNT–PP composites

Many researchers (Kim *et al.*, 2009; Park *et al.*, 2013; Prashantha *et al.*, 2008; Roy *et al.*, 2015) also observed an increased strength as the CNT content increased. Kim *et al.* (2009) investigated the mechanical properties of CNT (0.5–1.5 wt%) reinforced thermotropic liquid crystal polyester (TLCP) prepared using the melt blending method. The tensile strength and modulus of the CNT–TLCP composites increased by 41% and 34% respectively, for the 1.5 wt% CNT–TLCP composite compared to the pristine TLCP. Park *et al.* (2013) investigated the tensile properties of a CNT–UHMWPE (2.5–10 wt%) nano-composite prepared using the melt blending method and compared the materials with in-situ polymerized nanocomposites. An increased yield strength (30%) was observed for 10 wt% CNT–UHMWPE. Prashantha *et al.* (2008) investigated the mechanical properties of CNT–PP (1–5 wt%) composites. As the CNT content increased, the tensile modulus and yield stress of the developed composite increased by 68% and 25% respectively. Roy *et al.* (2015) investigated the mechanical behaviour of a CNT-reinforced (0.4–1.2 wt%) nylon 12 processed by plasma treatment. A significant improvement in the tensile strength, Young's modulus, elongation at break, and storage modulus were observed due to the addition of 1.2 wt% CNT because of strong interfacial adhesion and homogeneous dispersion.

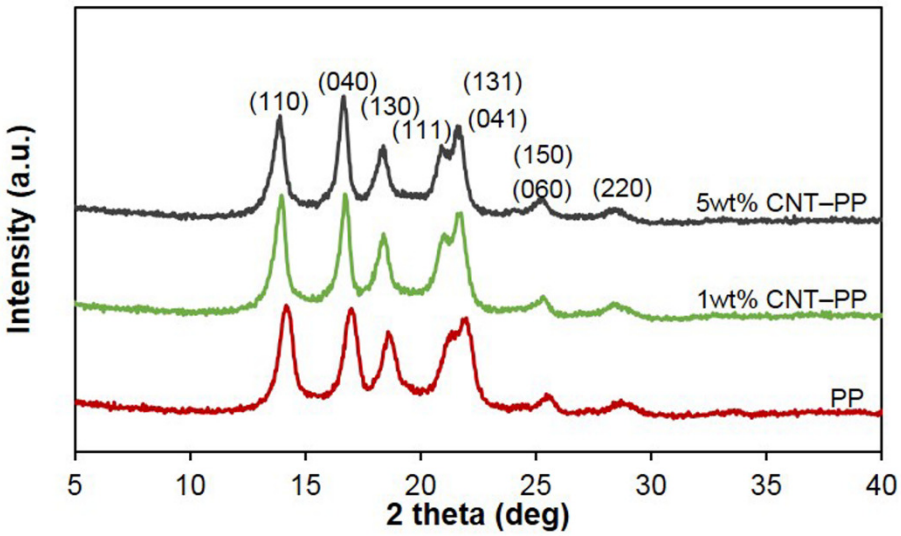

Figure 8.5 XRD plot of the CNT–PP composites

Addition of CNT to the polypropylene matrix altered the material crystallinity and hence improved the mechanical properties. X-ray diffraction (XRD) was performed on the test materials to understand the effect of addition the CNTs on the material crystallinity. The XRD pattern of the developed CNT–PP composites is shown in Figure 8.5. The major and minor peaks were observed at angles of 14.1°, 17.0°, 18.6°, 21.1°, 21.7°, 25.52°, and 28.82°. The planes of orientation are (110), (040), (130), (111), (131) and (041), (150) and (060), and (220) which form an α-monoclinic crystal structure for the unit cell of the polypropylene. A similar XRD plot and plane orientation were reported by Yang *et al.* (2008), Paik and Kar (2009), and Yang *et al.* (2013). The crystalline size of the CNT–PP composites was calculated using the Scherrer's equation mentioned in Equation 5.1 (Section 5.3; Chapter 5). The average crystal size of the polypropylene, 1 wt% CNT–PP, and 5 wt% CNT–PP composites are 12.8, 14.6, and 15.1 nm respectively. Marginal improvement in the crystalline size was observed due to the addition of the CNT.

8.3.2 Fractography of Tensile Specimen

Fractography is used to determine the cause of failure and prevent the recurrence. The fractured surface of 1 wt% CNT–PP and 5 wt% CNT–PP tensile specimens (Figure 8.6(a) and Figure 8.7(a) respectively) were observed using a scanning electron microscope to check the agglomerates that developed in the composite. The fractured surface of 1 wt% CNT–PP material exhibited very few agglomerates because the shear energy involved in the compounding conditions broke the agglomerates. Figure 8.6(a) shows the fractured surface, where the agglomeration surfaces are enclosed in circles, in which more CNTs existed as exfoliates. However, the 5 wt% CNT–PP fractured surface exhibited significant agglomeration (Figure 8.7(a)) because of strong van der waals forces of attraction and the compounding conditions are not sufficient to break these agglomerates. More circles indicated more agglomerations, as shown in the Figure 8.7(a), with

less CNTs as exfoliates. With higher magnification, the fractured surface of 1 wt% CNT–PP and 5 wt% CNT–PP tensile specimens (Figure 8.6(b) and Figure 8.7(b) respectively) were observed using a scanning electron microscope to check the dispersion of the CNTs. Good CNT dispersion in the polypropylene would translate the intrinsic properties of the CNTs to the composite.

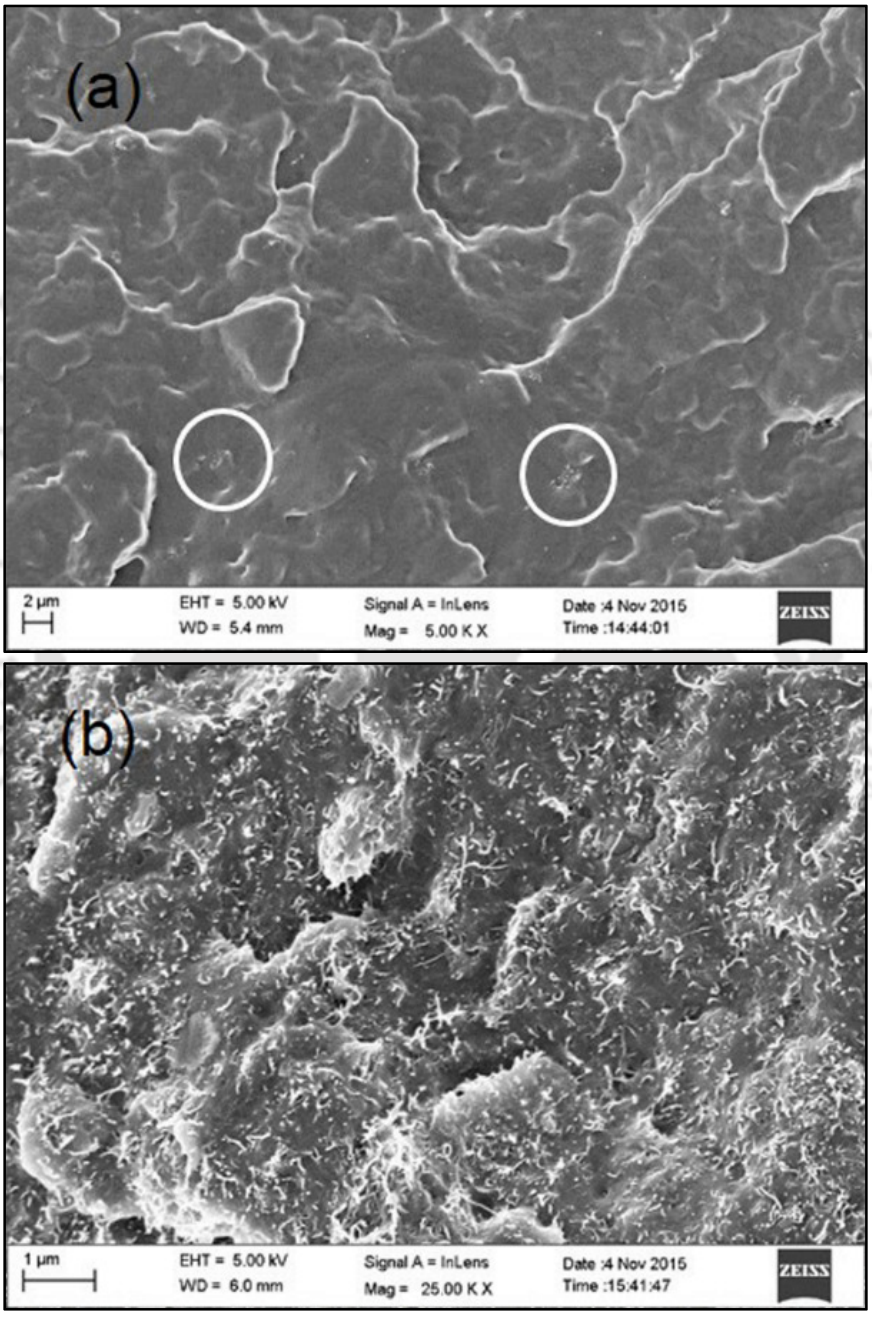

Figure 8.6 Fractured surface of the 1wt% CNT–PP that shows (a) agglomerates and (b) the dispersion of CNTs in the PP

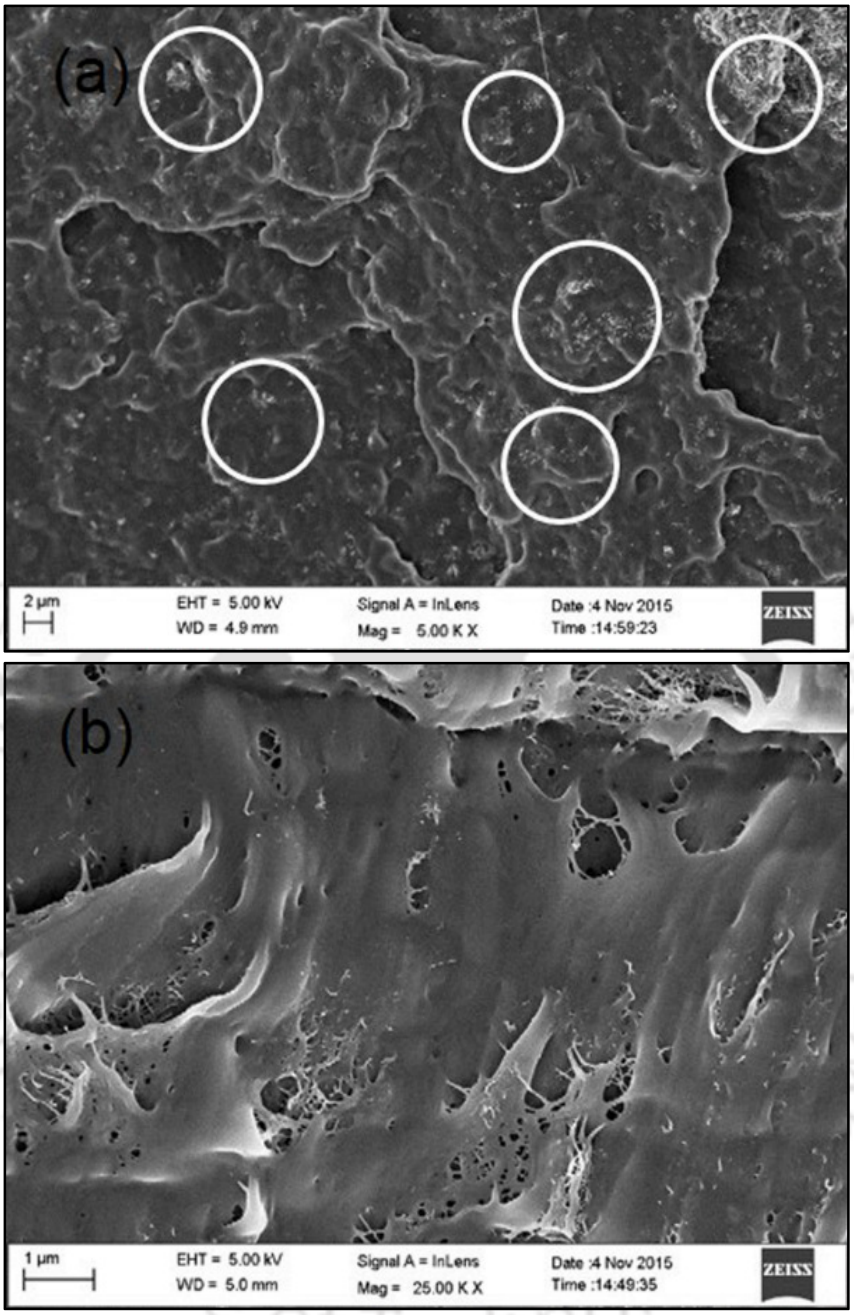

Figure 8.7 Fractured surface of the 5wt% CNT–PP that shows (a) agglomerates and (b) the dispersion of CNTs in the PP

Figure 8.7(b) shows the separation of the surface due to the voids formation around the nucleating agent. In both composites (Figure 8.6(b) and Figure 8.7(b)), the polypropylene matrix wrapped

around the CNTs. The polymer matrix wrapping around the CNTs is a sign of improved interaction (hydrogen bonding) between the CNTs and polymer matrix (Yazdani-Pedram *et al.*, 2010).

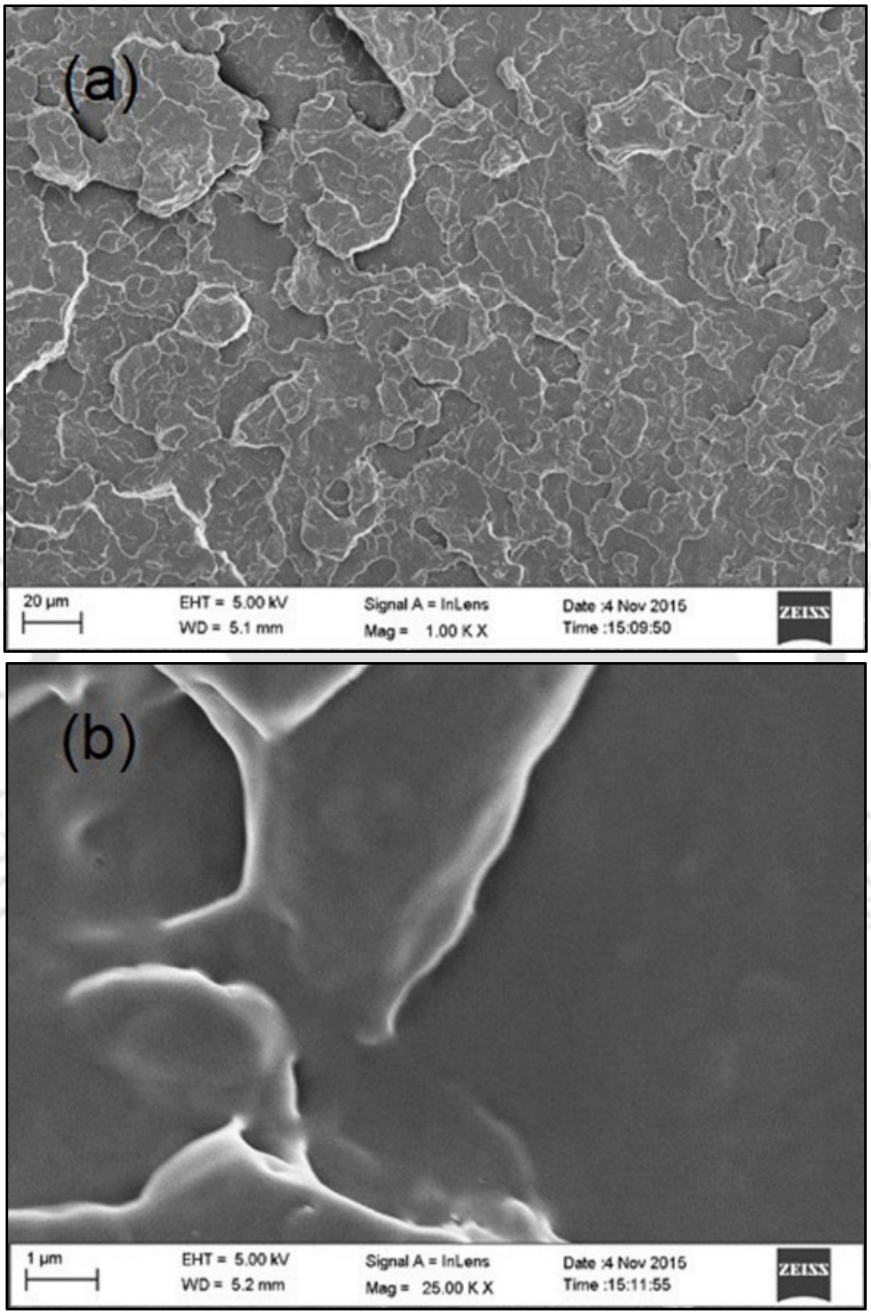

Figure 8.8 Fractured surface of the polypropylene that shows no agglomerates

Pan *et al.* (2010) reported failure morphology for 3 and 10 wt% CNT–PP. About 3 wt% CNT–PP exhibited a certain amount of CNT aggregates. However, 10 wt% CNT–PP, exhibited a larger

amount of aggregates and less CNTs existed as exfoliates. The fractured surface of the unreinforced polypropylene specimen (cryo-treated) was also observed at the same magnification (Figure 8.8(a–b)) where no agglomerates were observed.

8.3.3 Hardness

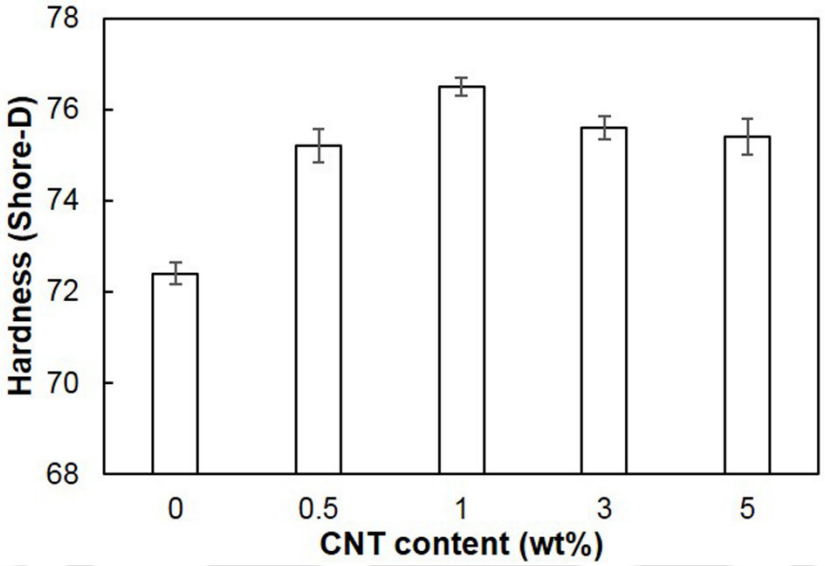

Figure 8.9 Hardness of the considered CNT–PP composites

Hardness is the measure of relative resistance to the permanent indentation and durometer is used to determine the hardness of various grade of polymers. The Shore-D hardness of the 0, 0.5, 1, 3, and 5 wt% CNT–PP composites were 72.4, 75.2, 76.50, 75.6, and 75.4 Shore-D respectively with ±0.4% deviation (Figure 8.9). The hardness of the composites increased proportionally upto 1 wt%, and beyond 1 wt%, the hardness decreased slightly due to agglomeration of the CNTs in the polypropylene. Yang *et al.* (2005) observed an increased micro hardness of the PMMA-CNT composite upto 1%, and decreased hardness beyond that threshold. Yang *et al.* (2005) observed an increased micro hardness of the PS–CNT composite upto 1.5% CNT content, and a decreased

hardness beyond that threshold. Wang *et al.* (2008) observed an increased microhardness of AMMA–CNT composite upto 1.5 wt% and decreased beyond that threshold.

8.4 TRIBOLOGICAL PROPERTIES

8.4.1 Friction and Wear Measurements

The polymers are susceptible to wear, hence evaluation of its tribological performance is important when they are used for contact applications. The developed CNT–PP composite is proposed to use in gear application which involves both rolling and sliding motion. Hence, the sliding friction performance of the developed composites were evaluated and compared with unreinforced polypropylene. The friction coefficient and wear of unreinforced polypropylene and CNT–PP composites were evaluated at a normal load of 50 N and at a sliding speed of 56.54 m/min. Online wear of the test materials (Figure 8.10) revealed two distinct wear behaviours (slopes): an initial transient run-in wear followed by a steady-state wear. Unreinforced polypropylene showed transient run-in wear upto 430 s/465 µm wear. Beyond 430 s, no significant change in wear rate was observed among all of the tested materials. 1 wt% CNT–PP exhibited transient run-in wear upto 150 s/175 µm wear. Other CNT–PP materials (0.5, 3, and 5 wt%) also exhibited transient run-in wear upto 220–230 s/325–360 µm wear. Thus, the addition of the CNTs to the polypropylene reduced the transient run-in wear. All the considered test materials including unreinforced polypropylene exhibited an approximately 0.2 µm/s wear rate, which confirmed the CNTs had very little effect in this region. The role of the CNTs was obvious only in the initial transient run-in wear region. The addition of the CNTs to the polypropylene has slightly increased the wear resistance of the developed composite.

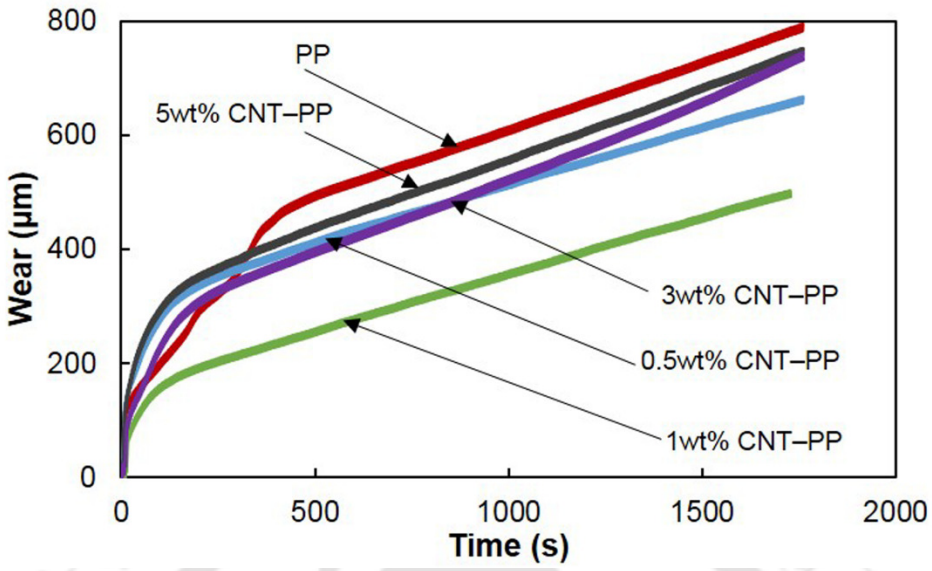

Figure 8.10 Online wear of the tested CNT–PP composites

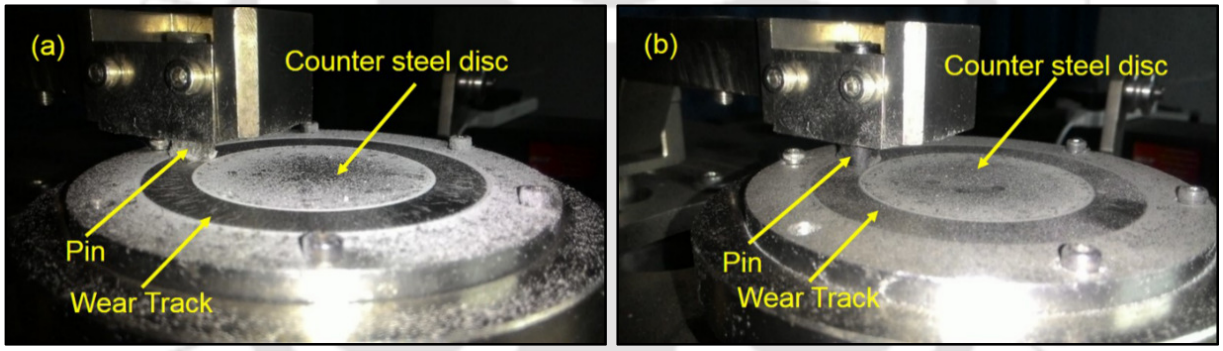

Figure 8.11 Surface of the counter disc after test (a) polypropylene and (b) 1 wt% CNT–PP

The wear of the considered test materials did not exhibit saturation because of insufficient formation of a transfer layer on the counter disc material. Figure 8.11(a–b) confirmed worn out debris away from the wear track, and no formation of adhesive layer. To differentiate the wear resistance of the CNT–PP, wear rate of the polypropylene and CNT–PP composites were calculated based on the following equation (Yang *et al.*, 2005) and shown in Figure 8.12,

$$\omega = \frac{V}{NL} \tag{8.1}$$

where ω is the wear rate in $mm^3N^{-1}m^{-1}$; V is the wear volume loss in mm^3; N is the applied load in N; and L is the sliding distance in m.

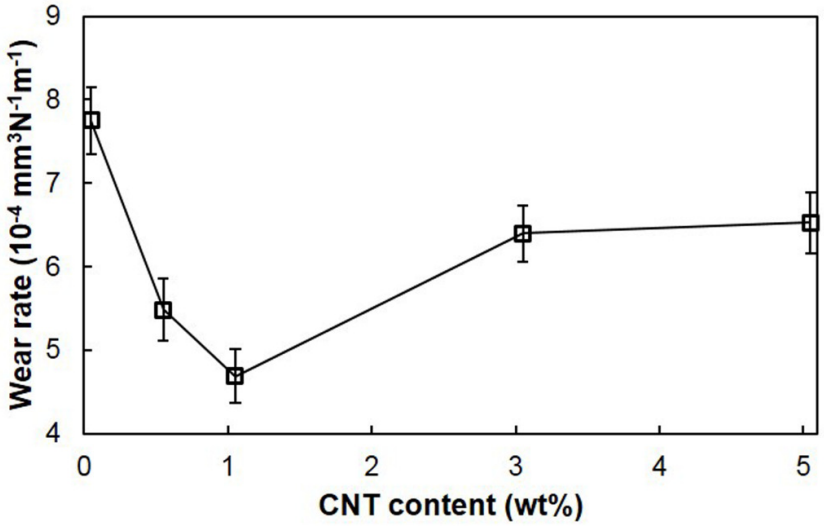

Figure 8.12 Wear rate of the considered CNT–PP composites

Among the considered test materials, 1 wt% CNT–PP composite exhibited highest wear resistance and unreinforced polypropylene exhibited lowest wear resistance. The wear rate of 0, 0.5, 1, 3, and 5 wt% CNT–PP for the considered load condition was 7.8, 5.5, 4.8, 6.4, and 6.5 (10^{-4} $mm^3N^{-1}m^{-1}$) respectively.

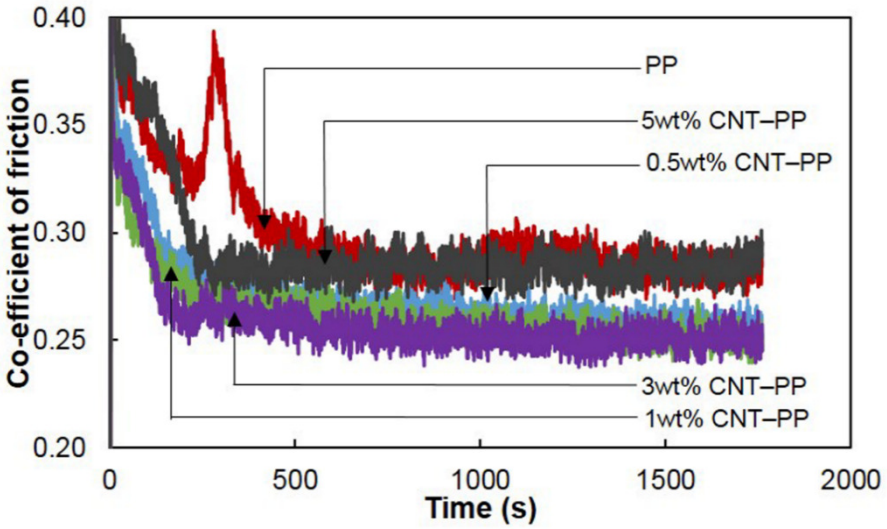

Figure 8.13 Friction coefficient of the tested CNT–PP composites

Figure 8.13 shows the coefficient of friction of the test materials; all test material showed an increased coefficient, which drops after a certain amount of time (500 s). This behaviour is due to the nonuniform contact between the pin and the counter disc. After a certain time (500 s), the contact between the disc and specimen becomes uniform, so the coefficient of friction becomes stable. The measured coefficient of friction (Figure 8.13) also confirmed this fact. 1 wt% CNT–PP composite had the smallest coefficient of friction and the unreinforced polypropylene had the maximum coefficient of friction for the test conditions. The improved mechanical strength of the CNT–PP results in improved wear resistance compared to unreinforced polypropylene. The addition of 3 and 5 wt% CNT reduced the wear resistance compared to 1 wt% CNT–PP because of the presence of agglomerations, which weaken the fibre–matrix interface.

At least, three trials were performed on each composite material and the average of the friction coefficient and weight loss are plotted in Figure 8.14. The experimental results revealed that the friction coefficient decreased as the CNT content increased upto 3 wt% CNT–PP and then increased, whereas, the wear and weight loss decreased upto 1 wt% CNT–PP and then increased significantly. Chen *et al.* (2003) investigated the wear performance of CNT–PTFE. As the CNT content increased, the wear rate decreased upto 20% volume content, beyond which the wear rate increased. Yang *et al.* (2005) observed a decreased wear rate of the PS–CNT composite upto 1.5 wt% of the CNT and an increased rate beyond this amount. Yang *et al.* (2005) observed a decreased wear rate of the PMMA–CNT composite upto 1.5 wt% and an increased rate beyond this amount. Wang *et al.* (2008) investigated the tribological behaviour of an AMMA–CNT composite. As the CNT content increased, the wear resistance increased and coefficient of friction decreased upto 1.5 wt%, and beyond this amount both the wear rate and coefficient of friction increased. This

behaviour is due to good dispersion of the CNT upto 1.5 wt% and poor dispersion when the content is greater than 1.5 wt%.

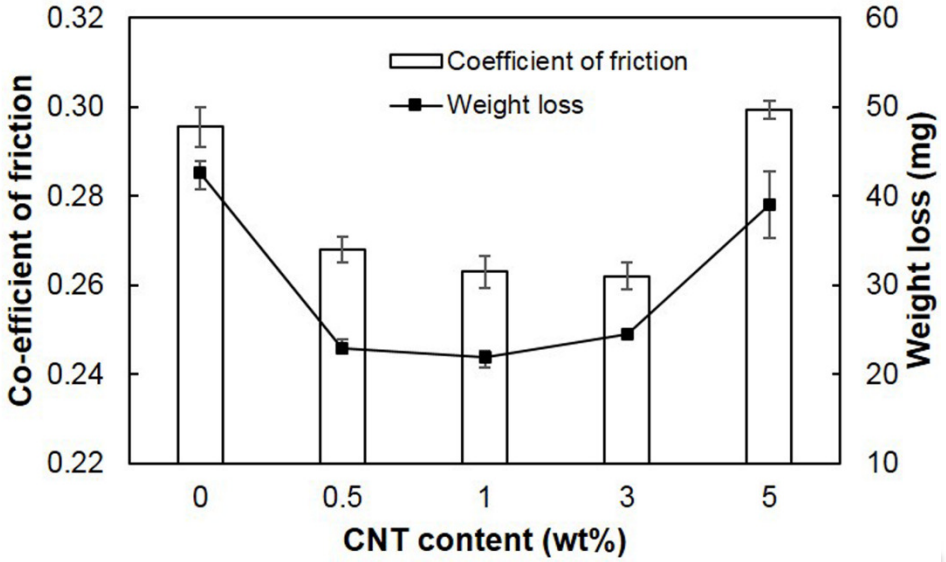

Figure 8.14 Average friction coefficient and weight loss of the CNT–PP composites

8.4.2 Wear Morphology

After the wear tests, the worn out unreinforced polypropylene and 1 wt% CNT–PP specimens were observed using a scanning electron microscope to understand the wear mechanism. The hard and sharp asperities of the steel disc plough the specimen, which caused microcracks and furrows, and forms abrasive and adhesive wear marks on the unreinforced polypropylene (Figure 8.15(a–b)). However, there were considerably fewer plucked and ploughed marks on the worn out surface of 1 wt% CNT–PP (Figure 8.16(a–b)). Both the test materials showed wear marks in the direction of sliding. The unreinforced polypropylene had deeper ploughing marks compared to 1 wt% CNT–PP composite. Similar worn out surface morphologies were observed by Suresha *et al.* (2010) on nano-clay, graphite, and a short fibre filled PA66/PP blend in which reinforcements reduced the wear rate.

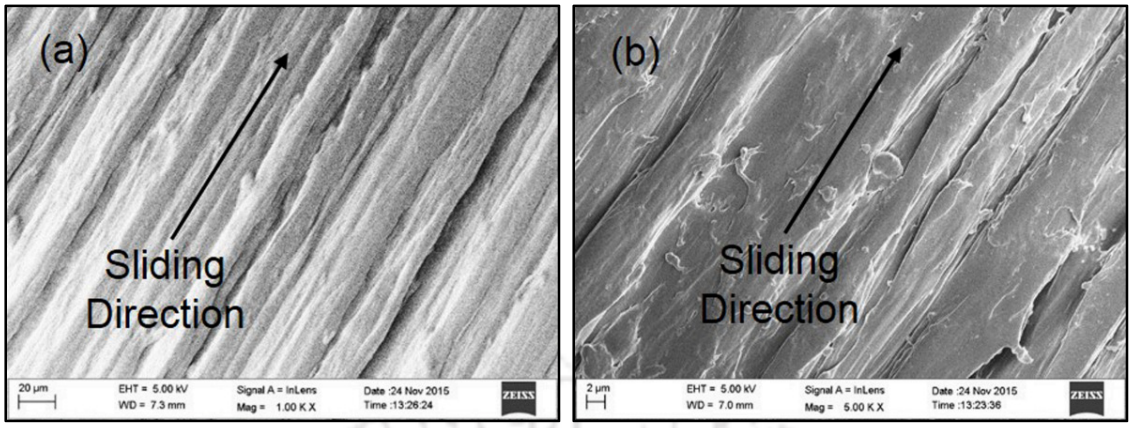

Figure 8.15 Worn out surface of the polypropylene material that shows the sliding direction and deeper wear tracks

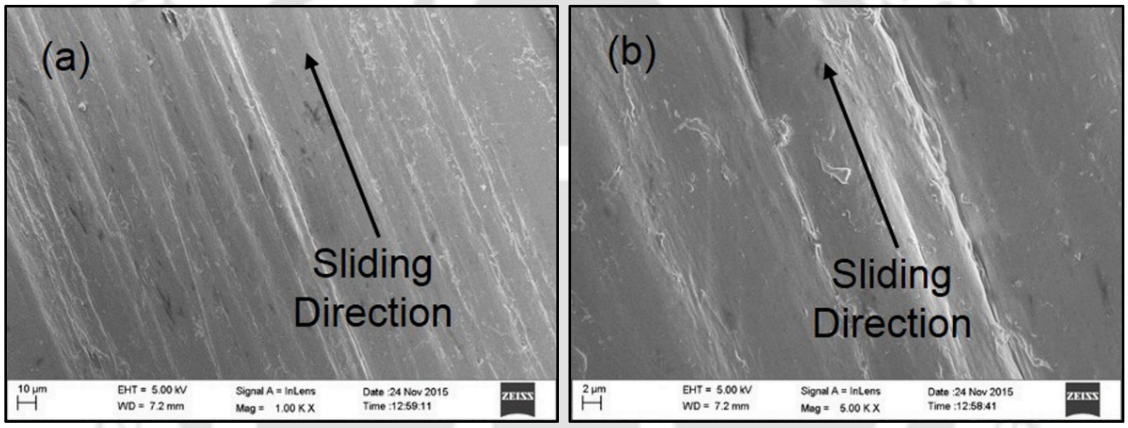

Figure 8.16 Worn out surface of the 1wt% CNT–PP composite that shows the sliding direction and mild wear tracks

Chen *et al.* (2003) observed wear morphology of the PTFE and CNT-PTFE composites. The worn out surface of the PTFE was rough, which confirmed adhesive wear and ploughing. However, the worn out surface of the CNT–PTFE composite was smooth. Cai *et al.* (2004) investigated the wear morphology of PI–CNT composites. The worn out surface of the unreinforced PI revealed significant adhesion and abrasive wear traces when compared to the PI–CNT composites. Wang *et al.* (2008) observed the worn surface of the pure AMMA and AMMA–CNT composites. The pure AMMA showed plucked and ploughed marks, which are indicative of adhesive wear and

ploughing. The worn out surface of the 1.5 wt% AMMA–CNTs composite showed a relatively smooth, uniform, and compact surface. Park *et al.* (2013) observed the worn out surfaces of neat UHMWPE, mechanically blended CNT and in-situ polymerized composite. Wear tracks of the neat UHMWPE in the sliding direction revealed ploughing wear. The blended composite showed a wider width abrasive wear because of the agglomeration and poor interfacial adhesion with the polyethylene matrix. The in-situ polymerized composite did not have any abrasive wear marks.

The worn out surface morphology of the test specimens (Figure 8.17(a–c)) was observed using a noncontact profiler to quantify the surface damage. Hard asperities of the mating steel disc plough the surface and mainly abrasive wear was observed. The 1 wt% CNT–PP exhibited the least surface damage (Figure 8.17(b)) and the maximum surface damage was observed on the unreinforced polypropylene (Figure 8.17(a)). The worn out surface of the unreinforced polypropylene is predominantly red and orange colour, and corresponds to a depth of 12.5–17.5 µm, as shown on the scale. 1 wt% CNT–PP worn out surface prominently shows wear marks with a green colour that corresponds to a depth of 2.5–7.5 µm.

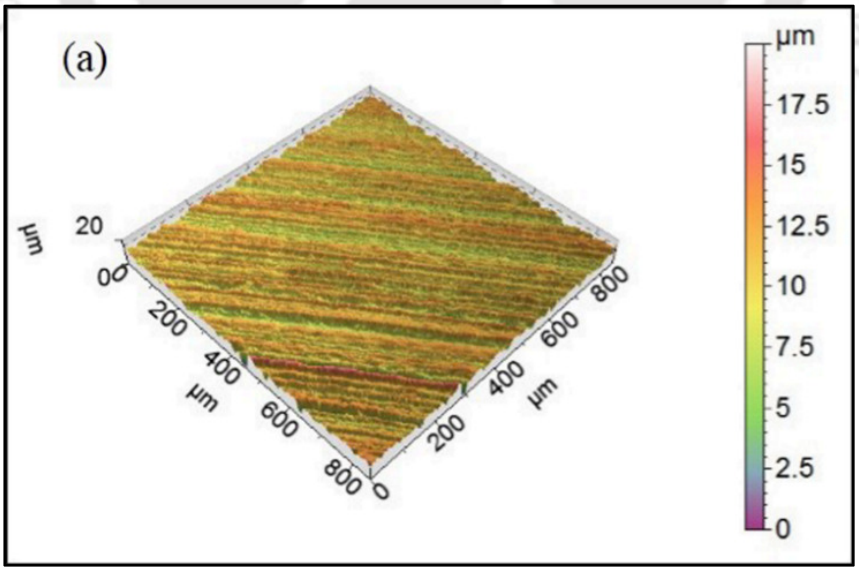

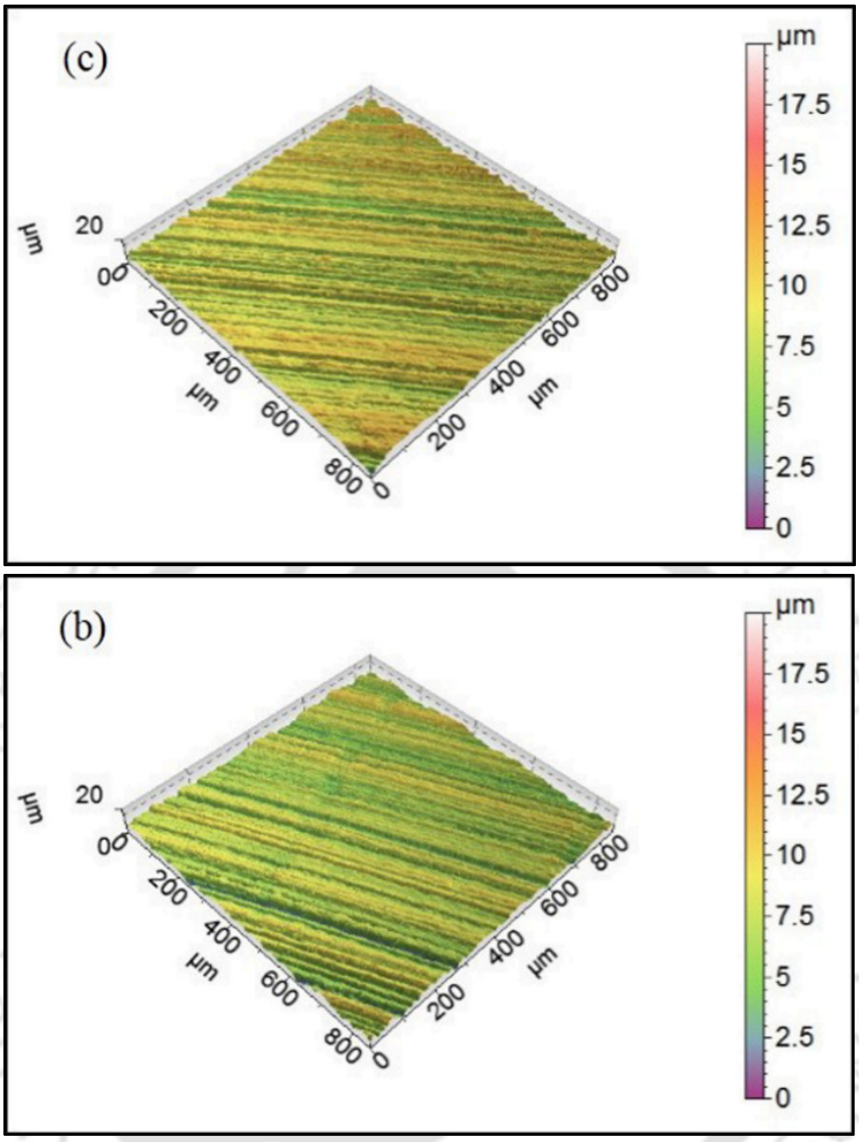

Figure 8.17 Optical profilometer image of the worn out surface of (a) unreinforced polypropylene, (b) 1wt% CNT–PP, and (c) 5wt% CNT–PP

The 5 wt% CNT–PP worn out surface (Figure 8.17(c)) with green and yellow colours corresponds to a depth of 5–10 μm. The worn out surface with the deepest wear marks was quantified as severe damage. Cho (2008) also reported similar three-dimensional surfaces of CNT–PPS composites with the aid of atomic force microscope (AFM). A uniform worn pin surface was observed in 0.2% CNT–PPS due to the uniform low wear, whereas 10% CNT–PPS composite exhibited poor surface because of the higher wear rate caused by the CNT agglomeration.

8.4.3 Frictional Heating

During sliding, an IR camera was used to measure the surface temperature of the test specimen near the contact area. The measured temperature data was analysed by extracting the temperature from three different locations: (a) close to the contact interface, (b) close to the disc surface, and (c) away from the contact surface. The temperature from these locations was extracted and plotted for the test duration. Figure 8.18(a–b) shows the measurement locations and an actual thermograph (5 wt% CNT–PP) of the test materials respectively.

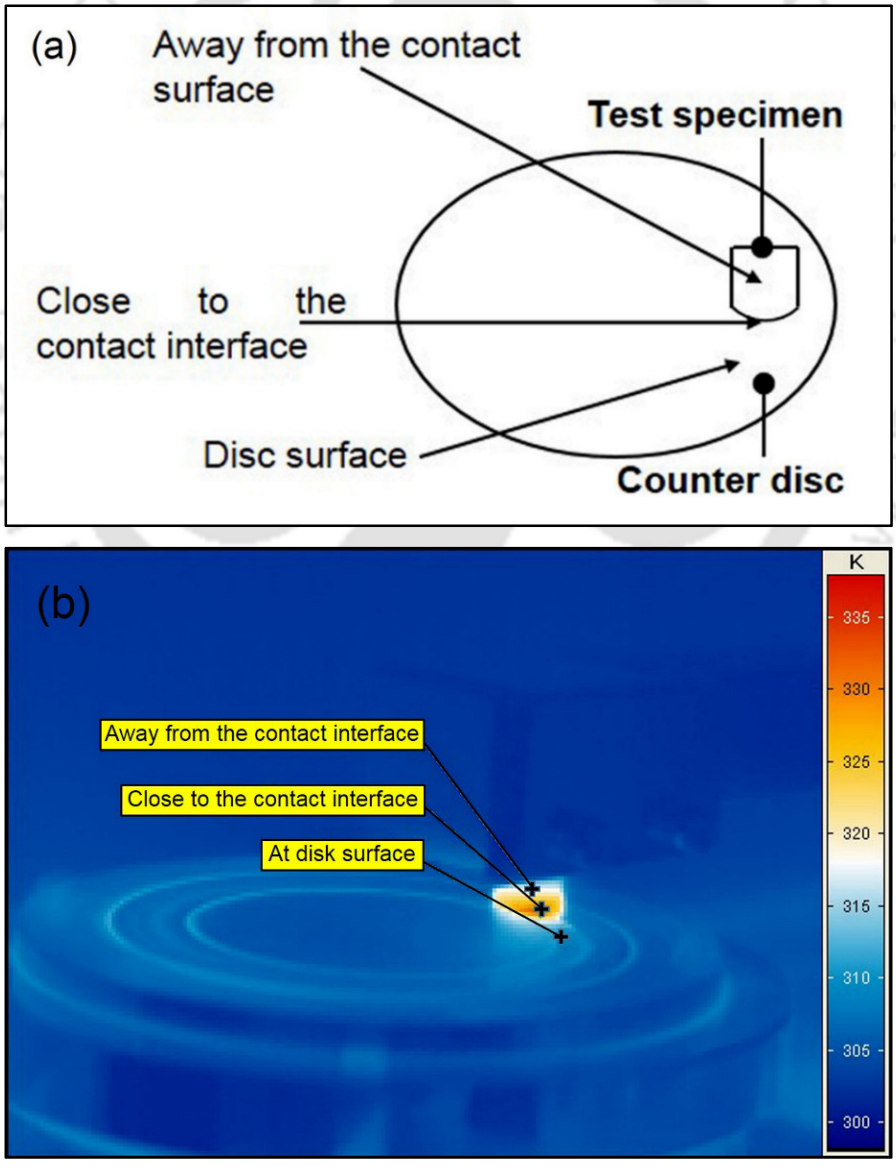

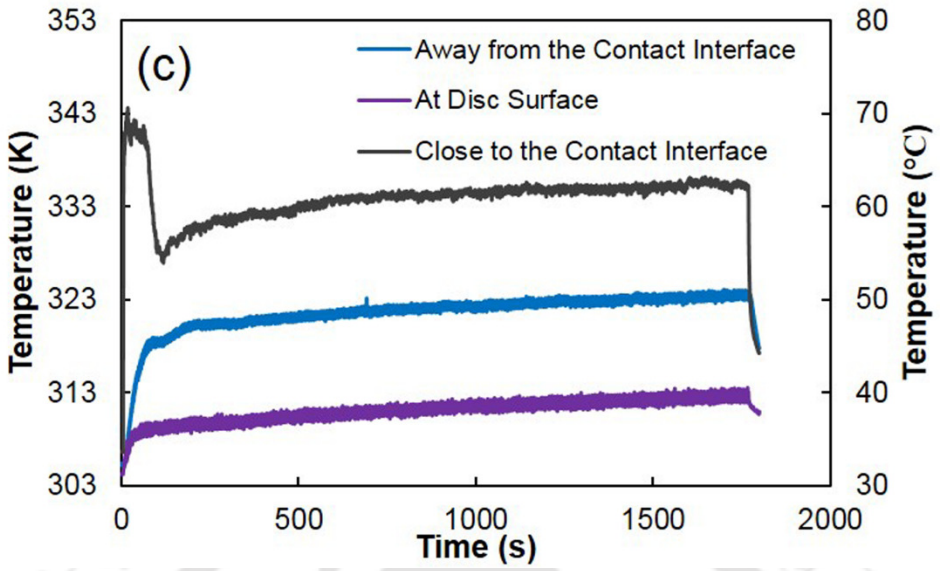

Figure 8.18 (a) Schematic of the test specimen with the temperature measurement locations, (b) Various regions of the temperature measurement during sliding wear of 5 wt% CNT–PP, and (c) Measured temperatures at various regions of the 5 wt% CNT–PP while sliding

Figure 8.18(c) shows the extracted temperature at these locations for the test duration. The measured temperature stabilized after several minutes. The stable temperature showed significant temperature differences at various locations, while repeatability of temperature measurements was good. Abbasi *et al.* (2014) also utilized an IR camera to measure the specimen's surface temperature under sliding wear in the pin-on-disc test configuration.

The thermograph was acquired for 0, 1, and 5 wt% CNT–PP composites and shown in Figure 8.19. The location close to the contact interface was selected and the corresponding temperature was extracted for further analysis. The maximum temperature data were extracted from the IR-thermograph (specimen–disc interface) and plotted with reference to the test duration (Figure 8.20). Similar to the coefficient of friction, a sudden raise in temperature was observed initially. After approximately 500 s, the temperature stabilized because of the uniform contact between the counter disc and test specimens.

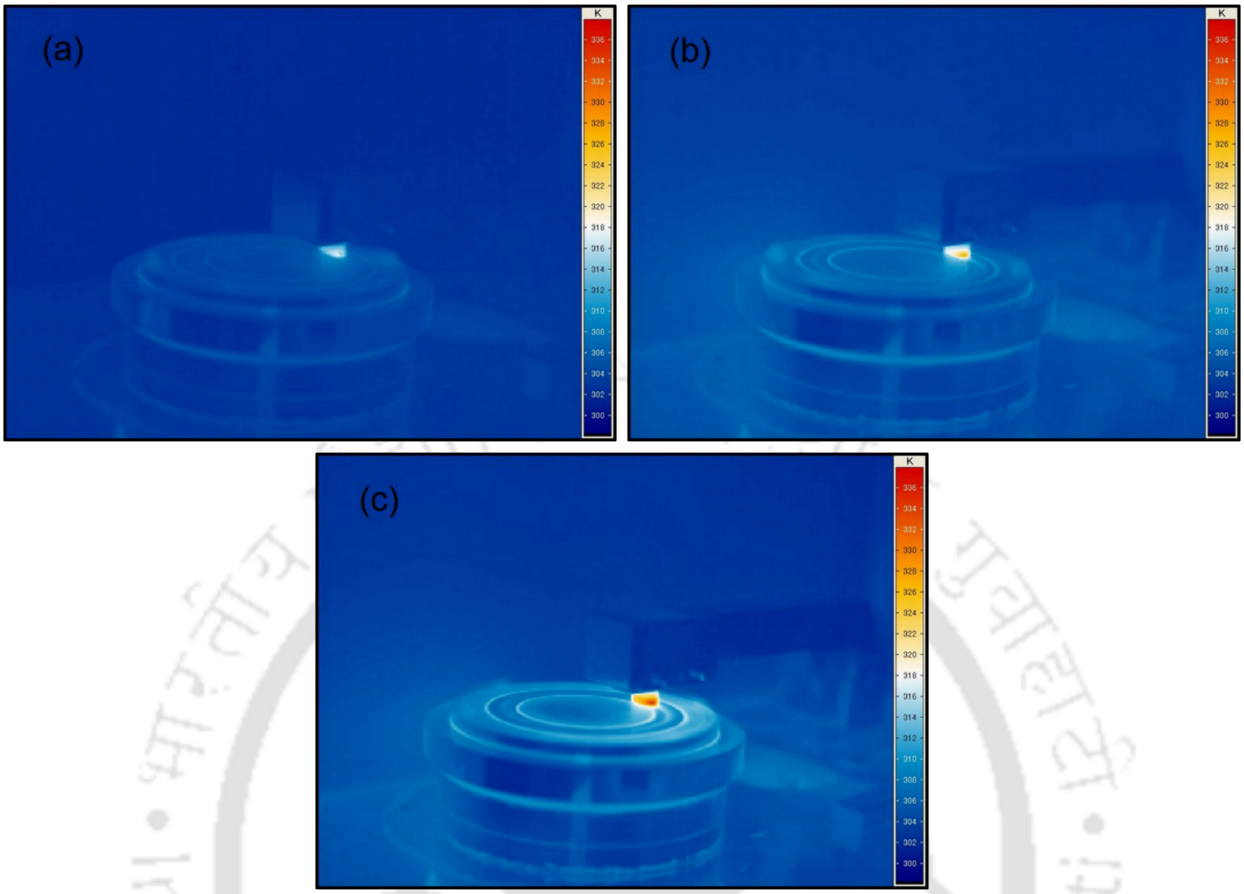

Figure 8.19 Thermograph of (a) polypropylene, (b) 1 wt% CNT–PP, and (c) 5 wt% CNT–PP at 50 N load and sliding speed of 56.54 m/min

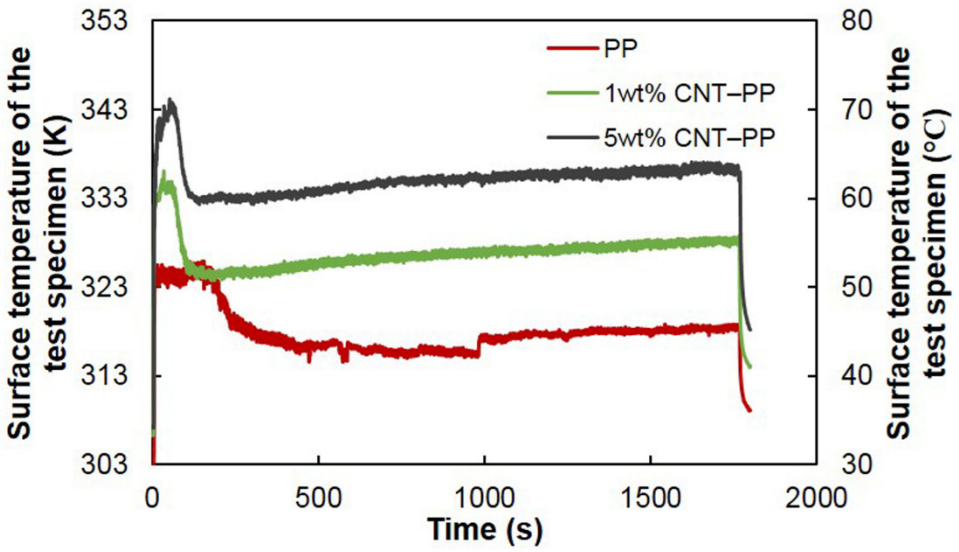

Figure 8.20 Surface temperature of the tested CNT–PP composites while sliding

Every test condition was repeated three times and the average surface temperature of the test material with standard error is shown in Figure 8.21. It is observed that the measured surface temperature of the test specimens increased as the CNT content increased.

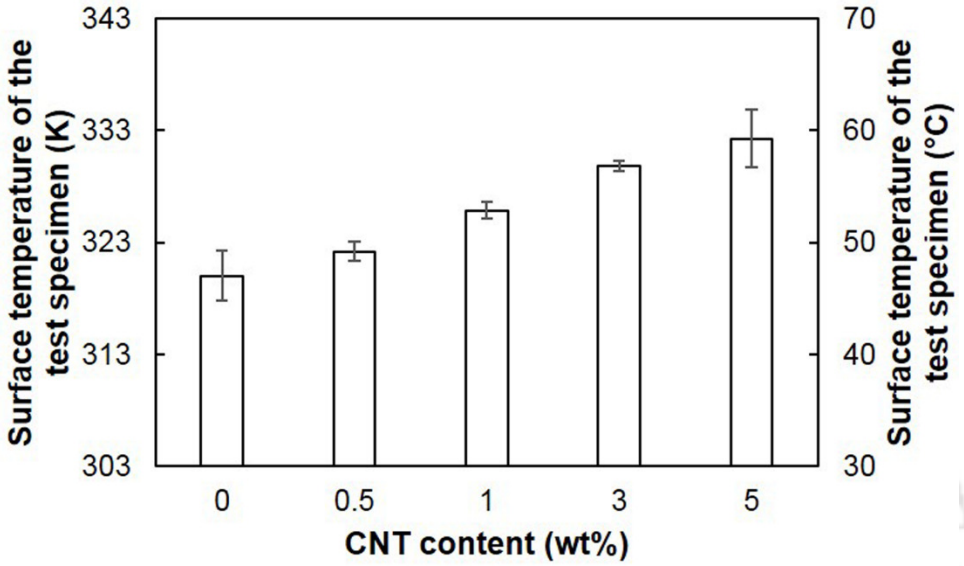

Figure 8.21 Measured surface temperature of the tested CNT–PP composites

The measured surface temperature of the 1 wt% CNT–PP composite is higher than that of unreinforced polypropylene material. The addition of the CNTs to the polypropylene has increased the strength, modulus, and thermal conductivity of the composite. The increased thermal conductivity increases the dissipating capability of CNT–PP. However, the measured surface temperature of the test specimen was the instantaneous temperature (i.e. the temperature was measured continuously while testing). It is not the net surface temperature after completely dissipating the generated heat. The addition of the CNTs to the polypropylene material has created more interfaces. Under sliding with some normal load, the CNT–PP materials with additional interfaces might have promoted more internal collisions/friction among the polymer molecules. Because of this increased internal friction, the surface temperature of the CNT–PP materials had higher temperatures.

Unal and Mimaroglu (2012) as well as Kim *et al.* (2012) observed that the increased surface temperature of the composites was caused by the reinforcement in the sliding wear test. Unal and Mimaroglu (2012) investigated the friction and wear performance of polyamide 6 and graphite composites. The addition of graphite (5–15 wt%) reduced the coefficient of friction (30%–60%) and wear rate. However, the measured surface temperature increased (20%–85%) for the test conditions (50–100 N – normal load, 0.4–1.6 m/s – sliding velocity and 4,000 m – sliding distance). Kim *et al.* (2012) investigated the friction and wear performance of polyamide and glass fibre composites to understand the orientation of reinforced fibres. The addition of glass fibres (10–50 wt%) reduced the coefficient of friction (15%–30%) and the wear rate. However, the surface temperature measured with an IR thermometer confirmed an increase in the temperature (10–15%) due to the addition of the glass fibres for the test conditions (100–900 N – normal load, 23.6 cm/s – sliding velocity and 7,000 m – sliding distance).

8.5 THERMAL CHARACTERISTICS

Thermal characteristics of gear materials need to be understand, as the polymer gears are susceptible to thermal failure. Figure 8.22 shows the melting behaviour of polypropylene, 1, and 5 wt% CNT–PP composites. The change in the physical state transformation occurred because it is an endothermic material that absorbs the heat and changes its physical state from the solid to liquid phase. The heat flux increased from the baseline; then, it returned to the baseline at the end of the transformation. The highest point of heat flux indicates the melting point of the material. The melting temperature of the polypropylene was almost same when the CNT was increased from 0 to 1 to 5 wt%. The area under the polypropylene curve (Figure 8.22) appeared to be larger because the peak of the polypropylene curve is larger than the 1 wt% CNT–PP curve. However,

the spread of the 1 wt% CNT–PP curve is greater, therefore, the 1 wt% CNT–PP has a larger area when compared to the polypropylene.

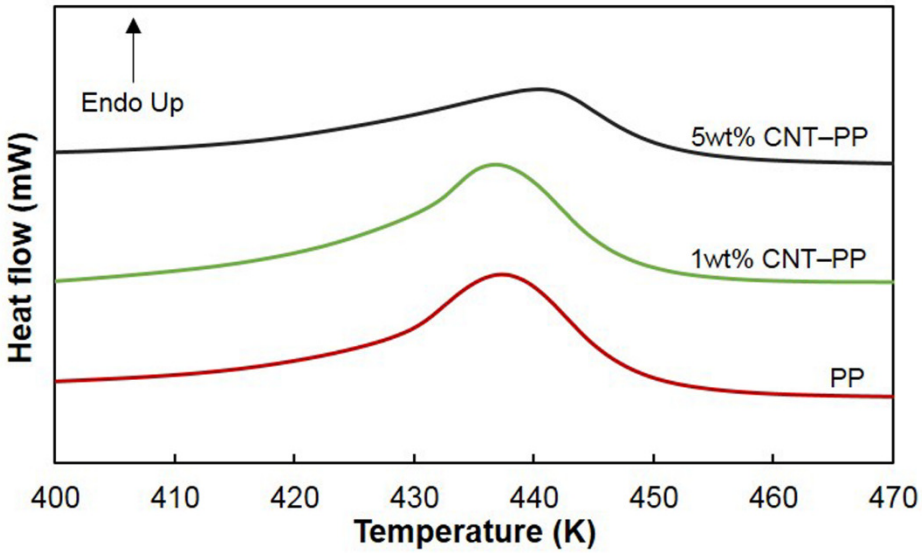

Figure 8.22 DSC melting curve of polypropylene and CNT–PP composites

The test material curve was analysed using Perkin-Elmer, STA 8000 software and the area under the curve (ΔH_m) was computed and used to calculate the degree of crystallinity. The degree of crystallinity was also determined from the melting curve by using the following equation (Xin and Li, 2012)

$$X_c = \frac{\Delta H_m}{(1 - W_f)\Delta H_m^\circ} \times 100 \qquad (8.2)$$

where X_c is the percentage crystallinity; ΔH_m is the measured heating enthalpy (J/g); ΔH_m° is the melting enthalpy of 100% crystalline polypropylene (209 J/g); and W_f is the weight fraction of the filler. The degree of crystallinity of the polypropylene increased from 47.7% to 52.5% when the CNT percentage increased from 0 to 1 wt% because the CNTs formed nucleating sites, but at 5 wt%, the degree of crystallinity decreased to 43.7%. This behaviour is because the CNTs restricted

the polypropylene chains mobility and acted as barriers to the crystal growth. Xin and Li (2012) investigated the crystallization properties of CNT–PP (0, 1, 3, 5, 8, and 10 wt%) composites using melting enthalpy. The degree of crystallinity increased from 41.9% to 42.2% when the CNT increased from 0 to 1 wt%, whereas above 1 wt%, the degree of crystallinity decreased to 38.2% (10 wt% CNT–PP). Ersoy and Onder (2013) also reported the percentage of crystallinity of the CNT–PP (0, 1.8, 4.6, and 8wt%) composites using the DSC cooling curve. The degree of crystallinity increased from 39.7% to 44.7% when the CNT percentage increased from 0 to 4.6 wt%, and above 1 wt%, it decreased (42% at 8 wt% CNT–PP).

The thermogravimetric analysis (TGA) plot of 1 and 5 wt% CNT–PP is shown in Figure 8.23 and compared with unreinforced polypropylene. From the Figure 8.23, it is observed that the temperature of the polypropylene is 617 K. The onset thermal degradation behaviour of 1 wt%

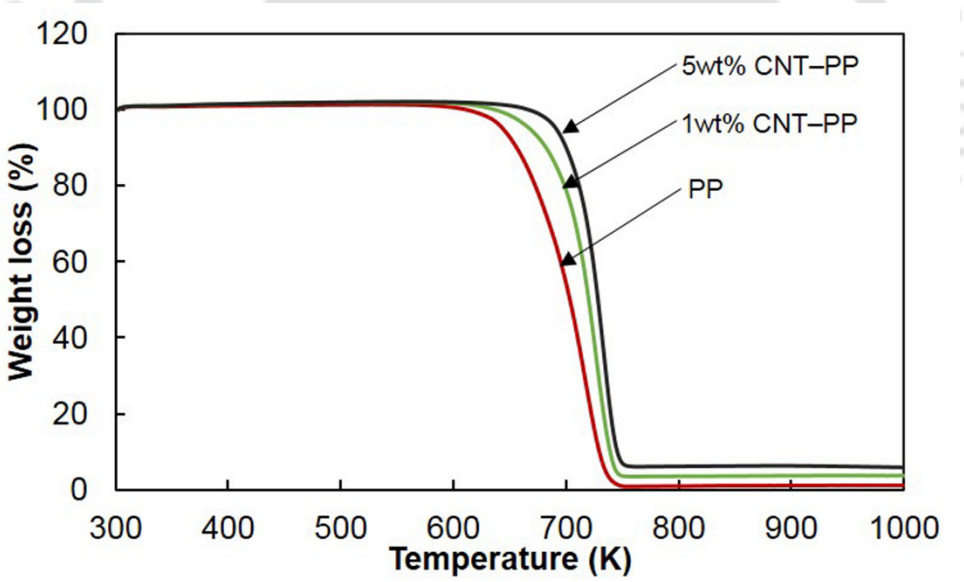

Figure 8.23 TGA plot of the CNT–PP composites

CNT–PP and 5 wt% CNT–PP are 646 and 671 K respectively. For the tested CNT–PP, the decomposition temperature was approximately 29–54 K higher and, thus, the thermal stability increased due to the addition of the CNTs. Zaikov *et al.* (2010) reported a similar thermal

degradation behaviour of the polypropylene and MWCNT–PP (1, 3, and 5 wt%) composites. An approximately 60 °C increase in the onset thermal degradation temperature was observed for the 5 wt% CNT–PP composite compared to the unreinforced polypropylene material. Yazdani-Pedram *et al.* (2013) evaluated the thermal properties using the TGA and reported that the initial decomposition temperature of the polypropylene and 1 wt% CNT–PP were 335 °C and 360 °C respectively.

8.5.1 Thermal Conductivity

The thermal conductivity of the developed CNT–PP composites was measured with the aid of a thermal property analyser (Decagon, KD2 Pro) with an accuracy of ±0.01 W/mK. The measured average thermal conductivity of the 0, 0.5, 1, 3, and 5 wt% CNT–PP composites (Figure 8.24) was 0.216, 0.253, 0.271, 0.279, and 0.325 W/mK respectively, with ±2% deviation. The thermal conductivity of the CNT–PP composite increased as the CNT content increased. The improved thermal stability and conductivity of the developed composite prevented thermal damage during sliding wear, as shown in Figure 8.15 and Figure 8.16. Zaikov *et al.* (2010) observed an increased

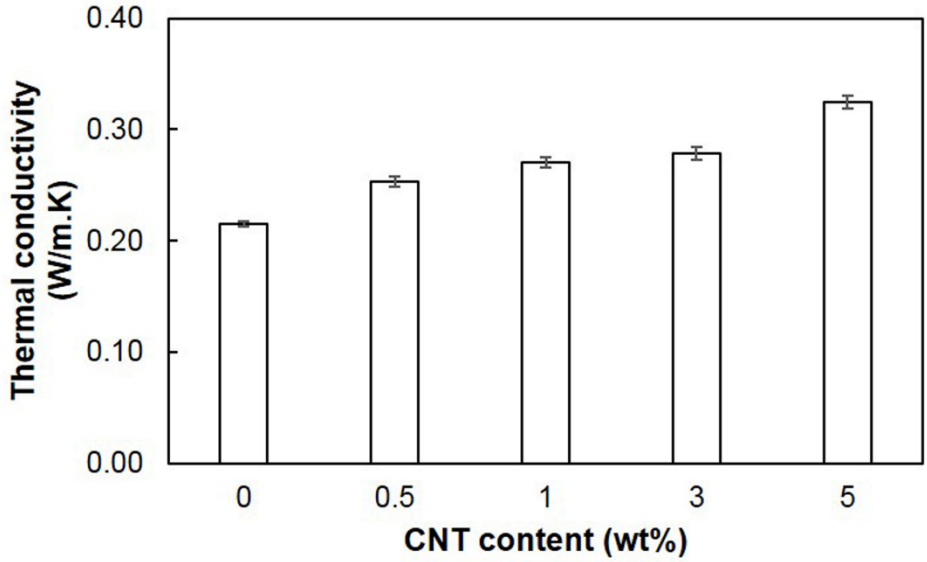

Figure 8.24 Thermal conductivity of the considered CNT–PP composites

(30–35%) thermal conductivity for CNT–PP composites as the CNT content increased (0 to 5 wt%). Park *et al.* (2013) also reported an increased (66% to 366%) thermal conductivity of a UHMWPE polymer when the CNT content increased upto 10 wt%.

8.6 SUMMARY

Injection-moulded CNT–PP composites (0.5–5 wt%) were developed using the melt compounding technique. Developed composites were evaluated for their tensile properties, tribological behaviours, thermal characteristics and the following major conclusions were arrived

- The tensile strength and modulus of the CNT–PP composites increased as the CNT content increased. Among the materials tested, 5 wt% CNT–PP composite exhibited superior strength and modulus.
- The addition of CNTs beyond 1 wt% CNT–PP caused more agglomeration and thus hardness and crystallinity decreased beyond 1 wt% CNT–PP.
- The addition of CNTs to the PP slightly increase the wear resistance of the developed composite.
- The addition of CNTs to the polypropylene increased the thermal stability and conductivity of the CNT–PP composite and increased the surface temperature.

CHAPTER 9

SURFACE DURABILITY OF INJECTION-MOULDED CARBON NANOTUBE–POLYPROPYLENE SPUR GEARS

9.1 INTRODUCTION

Polymer composite gears are replacing metallic gears in many applications owing to their noise reduction, self-lubrication, mass production capability, lower weight, and cost. Short fibre reinforced thermoplastics are being considered for light and medium duty engineering applications because of their improved mechanical strength combined with cost-effective advantages. In recent years, the carbon nanotube (CNT) reinforced thermoplastics are being preferred over the short fibre reinforced thermoplastics because of the absence of directional shrinkage characteristics (Prashantha *et al.*, 2009), directional mechanical (Sandler *et al.*, 2007; Prashantha *et al.* 2008; Prashantha *et al.*, 2009; Thiebaud and Gelin, 2009) and tribological (Gandhi *et al.*, 2013) properties. This chapter investigated the performance of CNT–PP (1 wt%) composite gear developed using the melt compounding technique. The developed composites were injection-moulded into spur gear and evaluated for their durability behaviour and compared with unreinforced polypropylene spur gear.

9.2 METHODOLOGY

The 1 wt% CNT–PP composite gear was developed using twin-screw extruder and injection-moulding machine. The gear processing, moulding conditions, test gear details and parameters are

explained in Section 3.2 and Section 3.4 (CHAPTER 3). Injection-moulded polypropylene and 1 wt% CNT–PP gears are shown in Figure 9.1.

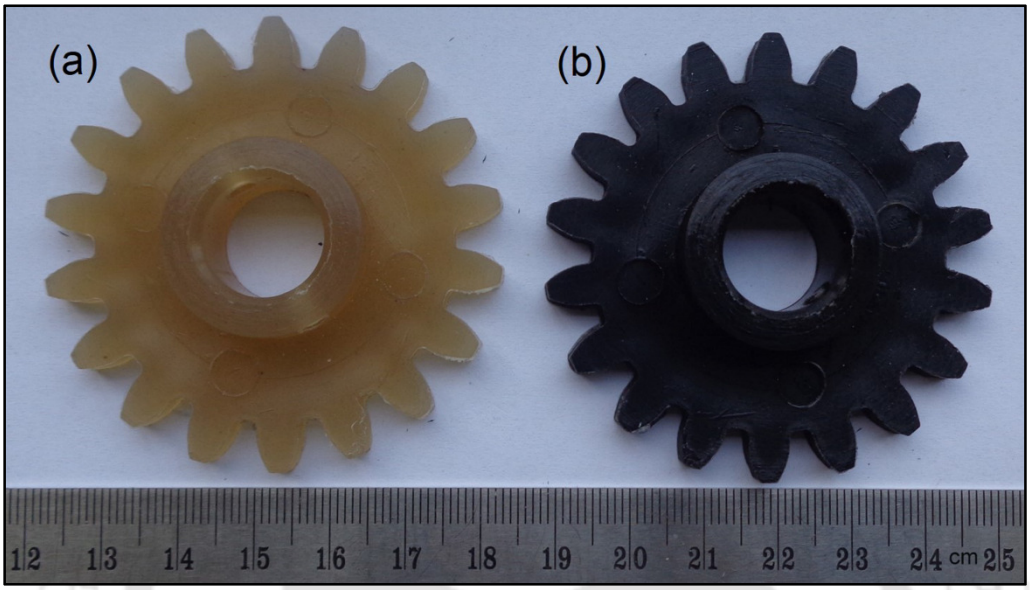

Figure 9.1 Injection-moulded polypropylene and 1 wt% CNT–PP gears

The gear performance was evaluated using in-house developed power absorption gear test rig. The sensor, data acquisition and performance evaluation details of the developed CNT–PP composite gear is explained in Subsection 3.4.1–3.4.2 (CHAPTER 3). The gear tests were performed at a constant speed of 800 rev/min and at various loads (2, 2.5, 3, 3.5, 4, and 4.5 Nm) until failure or 8.6×10^5 cycles, whichever occurred first. Depending on the test gear and loading conditions, 3–8 trials were conducted for each test condition. The tests were repeated until at least three gears exhibited the same life within ±5% deviation. The average lives of three trials were used for the results and discussion.

9.3 PROPERTIES OF TEST GEAR MATERIALS

The mechanical and thermal properties of the developed composites were measured according to ASTM D638 and ASTM D5930. The yield strength, Young's modulus, and the thermal

conductivity of the developed nanocomposites are summarized in the Table 9.1. The addition of CNTs increased the material strength, modulus and thermal conductivity. Detail mechanical and tribological properties of unreinforced and various CNT–PP composites (0.5–5 wt%) is reported in CHAPTER 8.

Table 9.1 Mechanical and thermal properties of the test gear materials

	Polypropylene	**1 wt% CNT–PP**
Yield strength (MPa)	18.64 ± 0.39	20.00 ± 0.40
Young's modulus (MPa)	757.43 ± 15	839.98 ± 19
Thermal conductivity (W/m.K)	0.0215 ± 0.002	0.270 ± 0.004

Among the materials tested, 1 wt% CNT–PP composite exhibited the least frictional resistance and maximum wear resistance. The average coefficient of friction of 1 wt% CNT–PP and unreinforced polypropylene materials were 0.26–0.27 and 0.29–0.30 respectively, against the steel surface under sliding conditions (50 N and 56.54 m/min). It should be noted that the contact is conformal in this sliding wear test configuration. However, the contact is nonconformal in the gear mesh and the relative motion is a combination of rolling and sliding. Despite this basic difference, the coefficient of friction against a steel surface under sliding indicates the relative frictional characteristics of test gear materials. Thus, the presence of CNTs help to reduce the coefficient of friction when it slides against the steel surface.

9.4 GEAR SURFACE TEMPERATURE

The measured temperature is the net surface temperature of the test gear during gear testing. Figure 9.2 shows the net surface temperature of test gears (Polypropylene and 1 wt% CNT–PP) at lower load (2–2.5 Nm) conditions. The test gear temperature gradually increases in the beginning and stabilizes at approximately 50,000 cycles. Initially, the heat generation caused by the surface

interaction and material hysteresis was higher than the heat dissipation. As the gear rotates, increased heat dissipation resulting from convection caused the temperature increase to saturate. Both of the test gears exhibited an increased temperature (approximately 5 °C) when the load was increased from 2 to 2.5 Nm. However, at the same load conditions, both polypropylene and CNT–PP gears exhibited almost same temperature. The test gears exhibited only tooth wear, and no tooth deformation was observed.

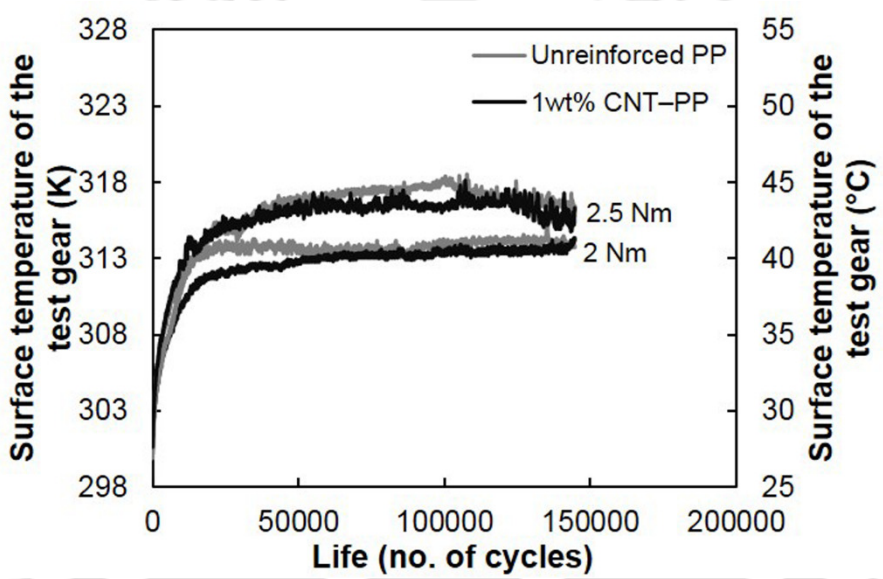

Figure 9.2 Measured surface temperature of test gear at 2 and 2.5 Nm

The test gears exhibited 5–10 °C higher temperature when the load was increased from 2.5 to 3 Nm (Figure 9.3). At this load (3 Nm), the polypropylene gear exhibited approximately 5 °C higher temperatures compared to the 1 wt% CNT–PP gear; however, neither test gear exhibited plastic deformation. Both the polypropylene and CNT–PP gears exhibited an abrupt temperature increase, which confirmed the occurrence of plastic deformation at the load of 3.5 Nm (Figure 9.3). The abrupt temperature increase of the CNT–PP gear occurred after 1.2×10^5 cycles, whereas the polypropylene gear exhibited a temperature increase after 0.8×10^5 cycles. Thus, CNT–PP gears exhibit lower surface temperature and improved performance compared to polypropylene gears.

This behaviour is because of enhanced mechanical strength (7.3% higher yield strength), reduced friction (10% lower coefficient of friction), and improved thermal properties (26% higher thermal conductivity) of the CNT–PP material. Mao *et al.* (2010) observed less wear (0.06 to 1 mm) when

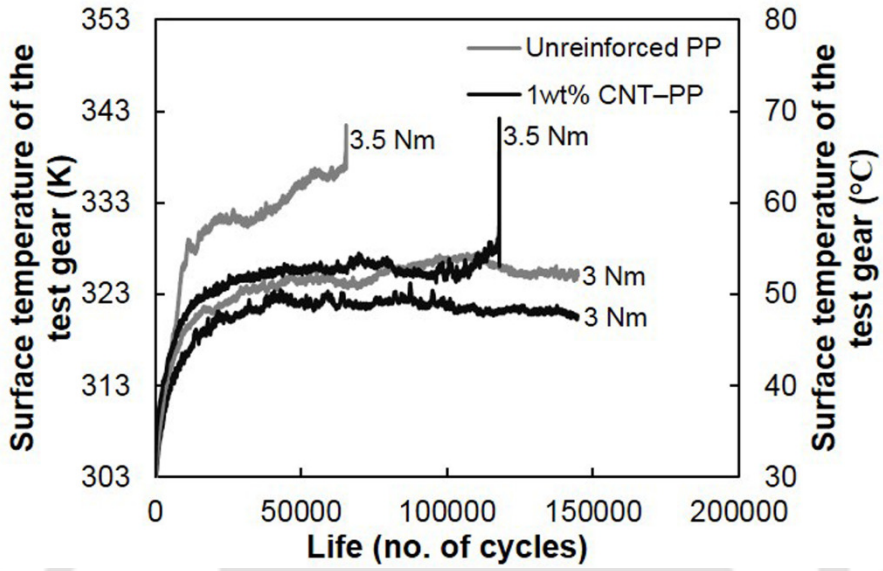

Figure 9.3 Measured surface temperature of test gear at 3 and 3.5 Nm

acetal gears were subjected to 7 to 9 Nm loads. Beyond this critical load, wear increased considerably as a result of increase in operating temperature (100 °C to 120 °C). Lee *et al.* (2014) investigated the frictional behaviour of various CNT–PA composites having different lengths of reinforcement. The CNT–PA exhibited lower surface temperature (188 °C to 168 °C) as a result of its superior thermal conductivity (0.334 to 0.405 W/mK).

At higher loads (4 and 4.5 Nm), the test gears exhibited plastic deformation (Figure 9.4). Both the polypropylene and CNT–PP gears exhibited an abrupt temperature increase. At these loads, the test gear exhibited a temperature increase very early compared to the lower load (3.5 Nm). The polypropylene gear exhibited an early temperature increase compared to the CNT–PP gear for the same load condition. Thus, the CNT–PP material used in the gears resulting in increased stiffness, higher thermal conductivity and reduced coefficient of friction. Mao (2007) also observed wear failure at lower loads and fatigue failure at higher loads while investigating the durability of POM

and PA gears. At higher speeds and loads, the test gears exhibited tooth bending failure; at lower speeds and loads, the test gears exhibited tooth wear. Pogacnik and Tavcar (2015) also observed similar durability improvement caused by the addition of reinforcement while investigating PA and POM gears.

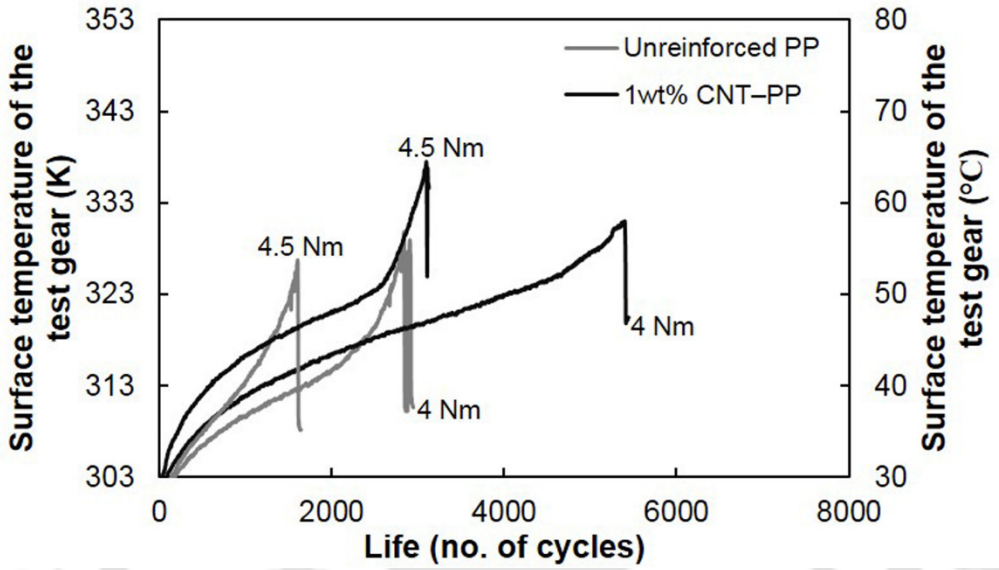

Figure 9.4 Measured surface temperature of test gear at 4 and 4.5 Nm

9.5 TRANSMISSION EFFICIENCY

Two inline torque sensors were used to measure the transmitted torque between the driver and driven shafts. The bearing losses and gear inaccuracies were neglected for simplicity; the transmission efficiency of the gear pair was calculated using the Equation 4.3 reported in Section 4.5 (Chapter 4). The transmission efficiency of polypropylene and 1 wt% CNT–PP gear at 2.5 Nm is shown in Figure 9.5. It is observed that the 1 wt% CNT–PP composite gear exhibited approximately 1%–1.5% enhancement in transmission efficiency. Kirupasankar *et al.* (2012) also observed transmission efficiency improvement (92.2% to 95.6%) while investigating nanoclay

reinforced polyamide (0% to 5%) spur gears. The higher elastic modulus and the lower surface temperature enhanced the transmission efficiency.

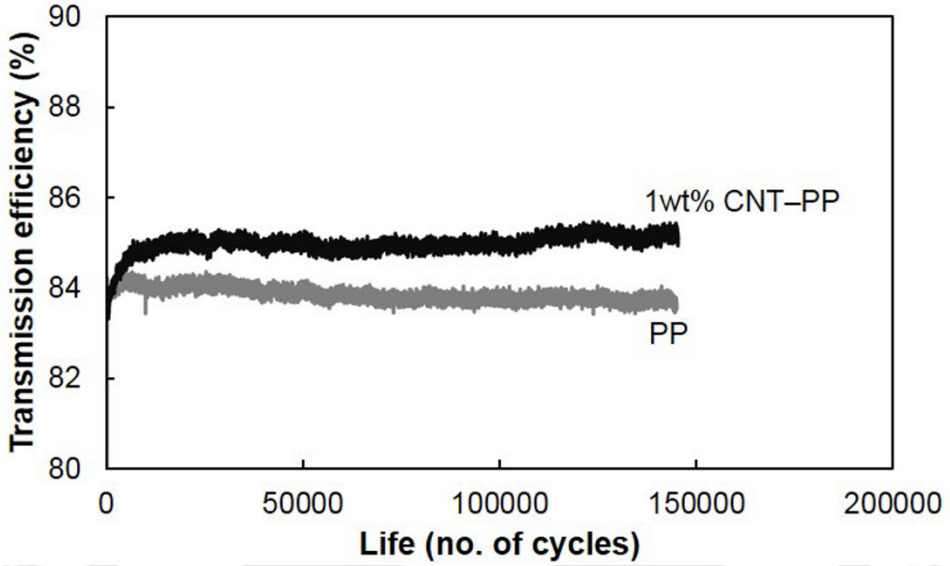

Figure 9.5 Transmission efficiency of test gear at 2.5 Nm

9.6 GEAR TOOTH WEAR

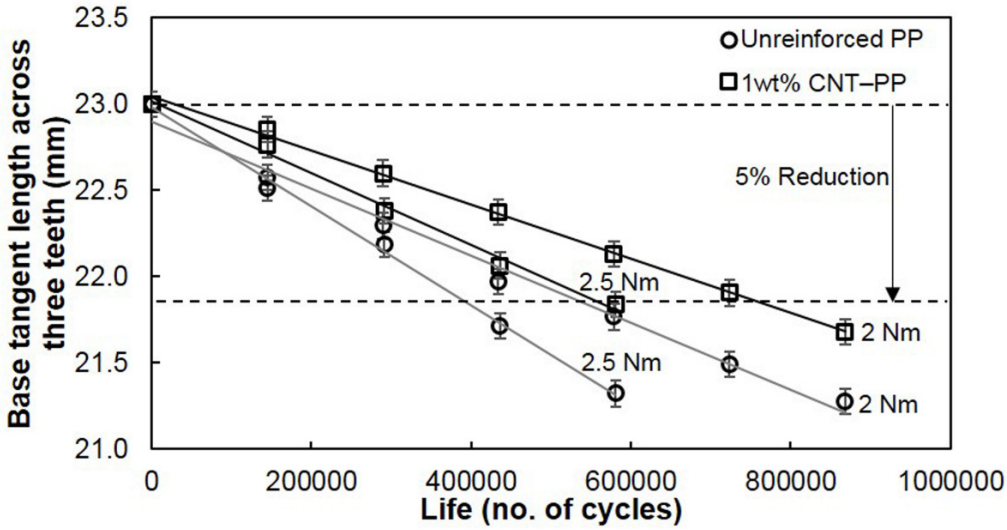

Figure 9.6 Measured gear tooth thickness across three teeth of the test gears

At lower loads (2–2.5 Nm), the polypropylene and CNT–PP gears exhibited only tooth wear, and no tooth deformation was observed. The test gear wear was predominantly abrasive; the wear

tracks in the direction of sliding confirmed this fact. The gear tooth thickness was measured periodically after every 3 h (1.4×10^5 cycles) by measuring the base tangent length across the three teeth using a gear tooth micrometre (1 µm accuracy) and shown in Figure 9.6. A 5% reduction of base tangent length was considered as a wear failure. As the number of cycles increased, both polypropylene and CNT–PP gears showed increased linear wear. The wear rate (slope of the line) was lower for the CNT–PP gears compared to the polypropylene gears. At 2 and 2.5 Nm loading, CNT–PP gears were run upto 7.6×10^5 and 5.6×10^5 cycles to attain 5% reduction in wear, whereas polypropylene gears were run for only 5.4×10^5 and 4.0×10^5 cycles respectively. Yousef *et al.* (2013) also observed similar behaviour; CNT–POM gears exhibited 12%–15% reduced weight loss compared to the POM gears. Hoskins *et al.* (2014) investigated the rolling contact fatigue performance of PEEK material. As the load increased, both the coefficient of friction and temperature increased. At higher load conditions, surface melting and contact fatigue failures were predominant.

9.7 GEAR TOOTH PROFILE WEAR

The gear tooth profile wear was measured using an optical profile projector and are shown in Figure 9.7 and Figure 9.8(a–b). The gear tooth profile was observed under the vertical profile projector at 20X magnification. Approximately 70 points were chosen to measure the coordinates from the tip to root of the involute profile. The origin was considered to be the coast-side tip of the gear for the measurement of worn out gear tooth surface. A profile of an injection-moulded gear before testing was measured and plotted as the reference. The worn out surfaces of polypropylene and 1 wt% CNT–PP gears subjected to 2 Nm load after 1.4×10^5 cycles are shown in Figure 9.7. The relative sliding velocity was calculated from the Equation (7.3)–Equation (7.5) (Section 7.4; Chapter 7) and it was maximum (1.135 m/s) at the tip and root regions. However, the wear was

minimum near the pitch region, as the relative sliding velocity is less at the pitch region. Among the evaluated test gears, CNT–PP gears exhibited less wear than polypropylene gears.

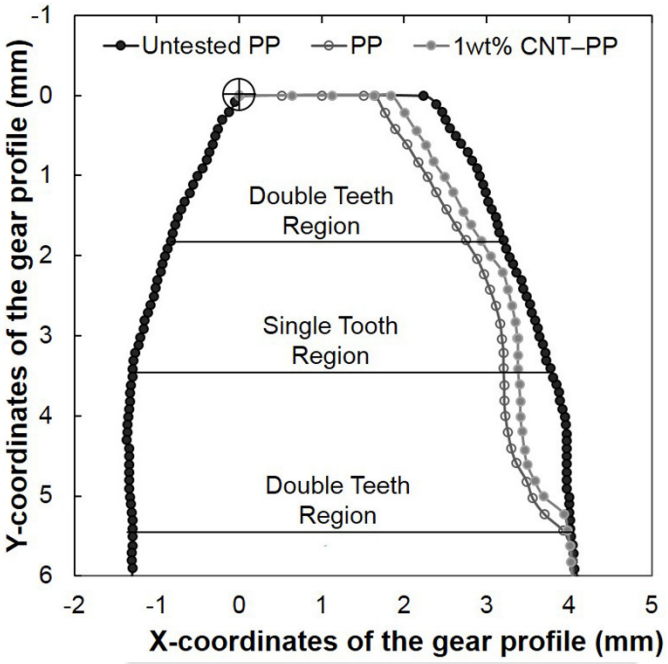

Figure 9.7 Worn out gear profile of test gear at 2 Nm after 1.4×10^5 cycles

Duzcukoglu (2009) also observed similar nonuniform wear behaviour along the tooth profile while investigating the surface durability of tooth width modified PA 66 spur gears. The wear of the standard unmodified PA gears near tip (1.84 mm) and root (2.42 mm) were higher compared to the region near the pitch point (0.69 mm). This behaviour is due to the effect of higher sliding velocity at the root and tip of the standard unmodified gear tooth.

However, as the number of cycle increases, this nonuniform wear along the tooth profile could not be identified even at this low load (2 Nm) condition. Figure 9.8(a) revealed uniform wear on the worn out gear tooth profile at 2 Nm after 8.64×10^5 cycles. At higher loads as well, only uniform wear along the profile was identified (Figure 9.8(b)). At higher loads and after many cycles of testing, excessive wear and ridges near the root region were observed. This excessive wear and the

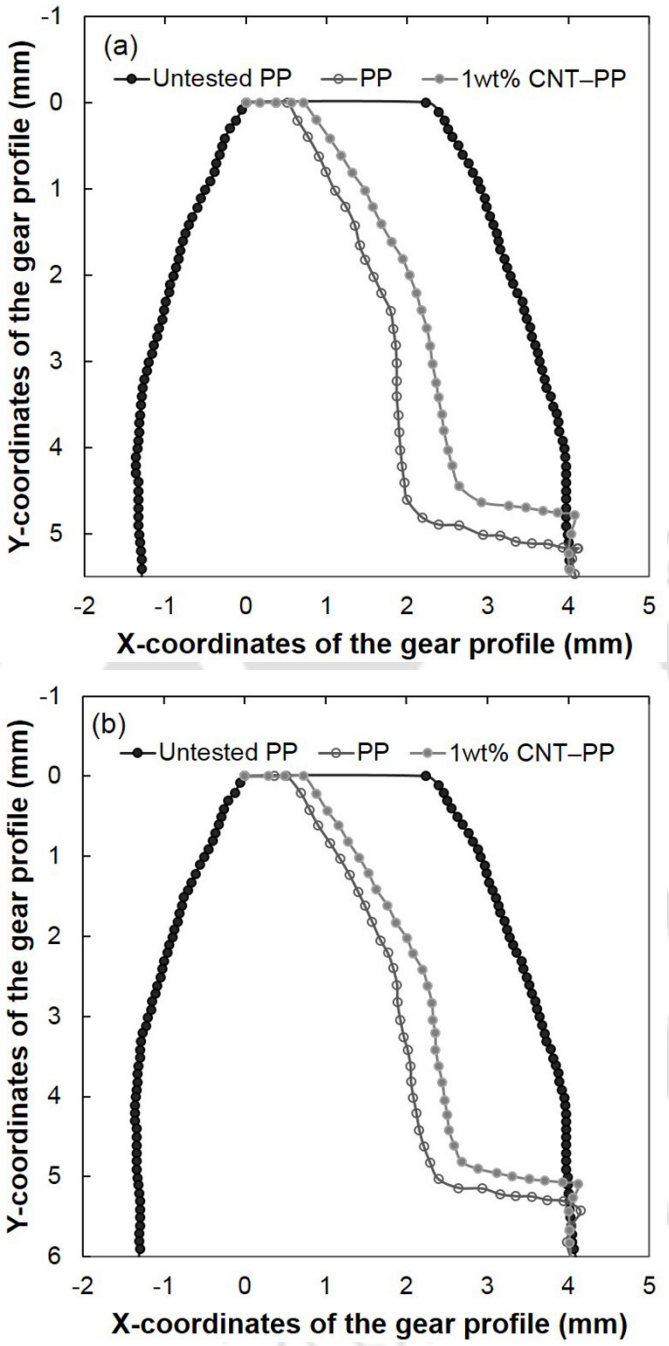

Figure 9.8 Worn out tooth profile of test gear at (a) 2 Nm after 8.64×10^5 cycles and (b) 2.5 Nm after 5.76×10^5 cycles

formation of ridges were also confirmed by the failure images of the test gears (Figure 9.10(c–d) and Figure 9.11(c–d)). This behaviour is attributed to the increased gear tooth deflection of the polymer gear at the higher load and higher cycles of testing. The tip of the mating steel gear

removed the flank region of the polymer gear as a result of the nonconjugate action and contact stress (35.9 MPa corresponds to 2 Nm torque). The CNT–PP gears exhibited less wear compared to the polypropylene gears for both of the evaluated loads. Wright and Kukureka (2001) also observed this excessive wear near the root region of polyamide gears using a coordinate measuring machine. The worn out gear tooth profile exhibited ridges near the root region resulting from premature contact. Senthilvelan and Gnanamoorthy (2004) also observed this excessive wear and ridge formation caused by the premature contact in nylon gears at higher loads. Karimpour *et al.* (2010) numerically modelled the contact behaviour of POM–POM gear pair. The kinematic behaviour of polymeric gear predicted the premature and extended contacts of the meshing cycle because of the large tooth deflections experienced by the polymer gear teeth in a gear pair.

9.8 PERFORMANCE

The performance of both the test gears (Polypropylene and CNT–PP) at various test loads (2–4.5 Nm) is summarized in Figure 9.9. This plot consolidates both tooth wear and tooth deformation

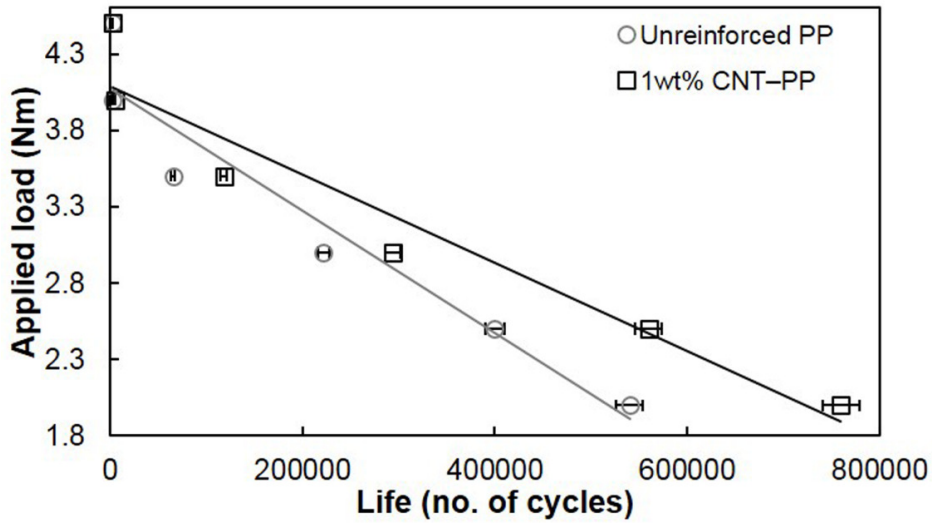

Figure 9.9 S-N curve of polypropylene and 1 wt% CNT–PP gears at various loads

failure modes. At lower loads (2–2.5 Nm), test gears exhibited tooth wear; at higher loads (3–4.5 Nm), gears exhibited tooth deformation. The CNT–PP gears exhibited superior performance

compared to polypropylene gears for the evaluated load range, and domination is higher when the failure criterion was tooth wear. Thus, it can be concluded that the CNT played a predominant role in wear resistance and resistance against plastic deformation. For the evaluated test loads, 1 wt% CNT–PP gears exhibited approximately 30% to 80% life improvement compared to the polypropylene gears.

Bravo *et al.* (2015) presented various damage modes of plastic gears comprehensively; wear and plastic deformation were identified as the predominant failure modes. Loos *et al.* (2013) investigated the performance of PU and CNT–PU. In the low stress regime, CNT–PU exhibited poor performance compared to the PU. This could be due to the CNT–matrix interface damage. However, in the high stress regime, CNT–PU exhibited superior performance (240% increase) compared to the PU gears.

9.9 GEAR DAMAGE MORPHOLOGY

Figure 9.10 and Figure 9.11 shows the gear tooth surfaces subjected to lower loads (2–2.5 Nm) at various stages. Figure 9.10(a–b) shows the polypropylene and 1 wt% CNT–PP gear tooth surface after 1.44×10^5 cycles at 2.5 Nm. Wear marks clearly indicated the direction of sliding; a change in the direction of sliding at the pitch line was also observed.

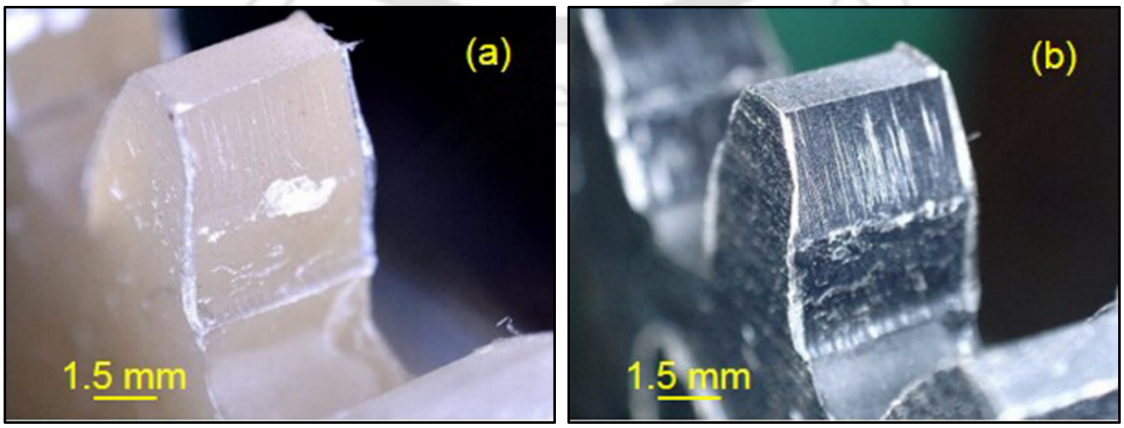

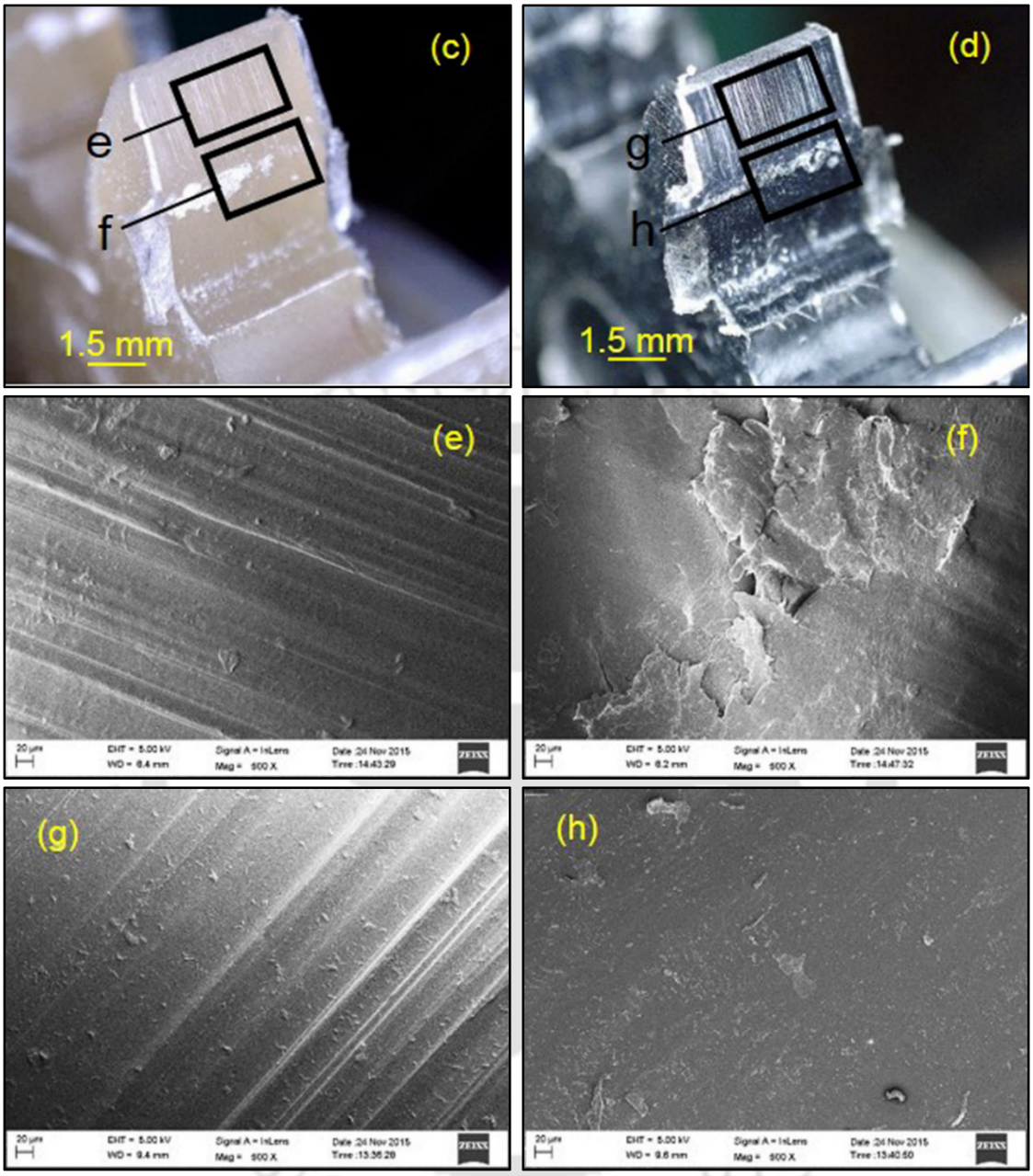

Figure 9.10 Tooth surface of test gear subjected to 2.5 Nm (a) polypropylene after 1.44×10^5 cycles, (b) 1 wt% CNT–PP after 1.44×10^5 cycles, (c) polypropylene after 5.76×10^5 cycles, (d) 1 wt% CNT–PP after 5.76×10^5 cycles, (e–f) SEM image of polypropylene gear after 5.76×10^5 cycles, and (g–h) SEM image of 1 wt% CNT–PP after 5.76×10^5 cycles

Figure 9.10(c–d) shows the polypropylene and 1 wt% CNT–PP test gear surfaces after 5.76×10^5 cycles at 2.5 Nm. Figure 9.10(e–f) and Figure 9.10(g–h) shows the scanning electron micrographs

of polypropylene and CNT–PP test gears displaying plastic deformation and uniform wear. For the same test load conditions, polypropylene gears exhibited severe wear, whereas CNT–PP gear exhibited only mild wear. Deeper wear marks were observed on the polypropylene gear compared to the CNT–PP gear. The improved mechanical strength, thermal stability and reduced friction improved the performance of CNT–PP gear. The net surface temperature of the CNT–PP gear was lower compared to the polypropylene gear because of the improved thermal conductivity and lower coefficient of friction. The CNT–PP gear did not exhibit plastic deformation, whereas the polypropylene gear exhibited plastic deformation at the same load condition.

Mao *et al.* (2015) investigated the wear behaviour of machine-cut polymer gears. The adhesive wear was dominant, and the wear at the tooth pitch region was low compared to root and tip regions. Mertens and Senthilvelan (2015) investigated the effect of air cooling on the durability of polypropylene gears. Gears tested without cooling exhibited severe damage compared to the gears tested with cooling.

Figure 9.11(a–b) shows the worn out tooth surface of polypropylene and 1 wt% CNT–PP tested at 2 Nm after 1.44 $\times 10^5$ cycles. Figure 9.11(c–d) shows the tooth of polypropylene and 1 wt% CNT–PP gears tested at 2 Nm after 5.76×10^5 cycles.

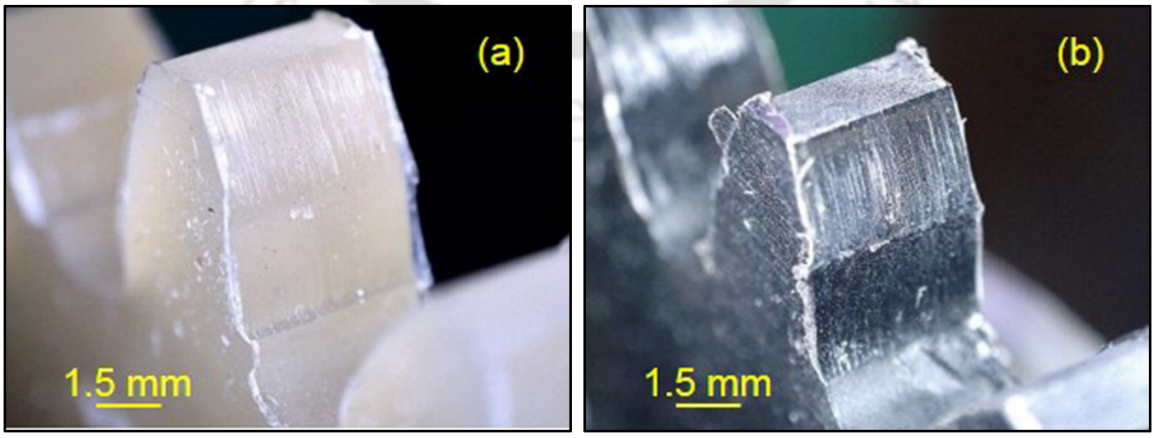

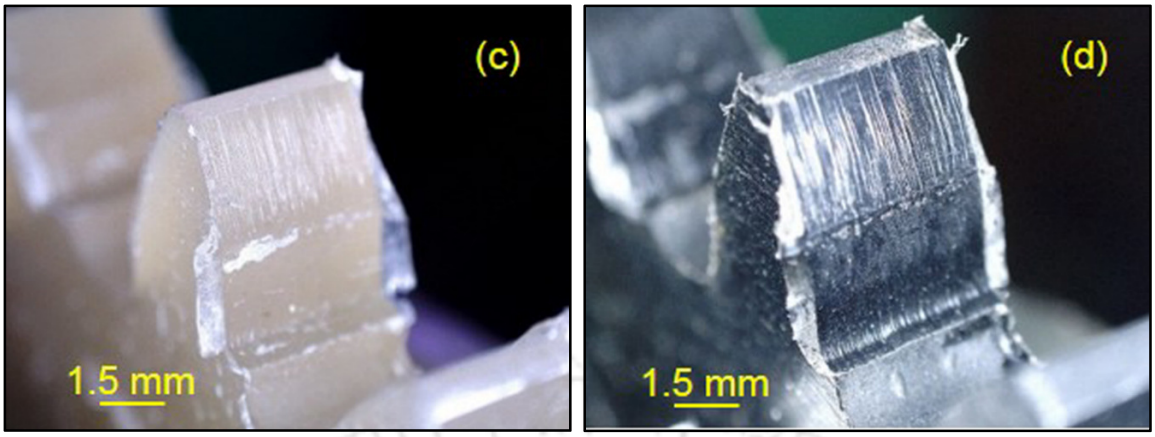

Figure 9.11 Tooth surface of test gear subjected to 2 Nm (a) polypropylene after 1.44×10^5 cycles, (b) 1 wt% CNT–PP after 1.44×10^5 cycles, (c) polypropylene after 5.76×10^5 cycles, and (d) 1wt% CNT–PP after 5.76×10^5 cycles

In both test conditions, mild wear marks were observed at the initial stage (1.44×10^5 cycles). However, as the cycle passes, severe wear marks showed the sliding direction and pitch point where the change in direction of sliding takes place. The polypropylene gears exhibited tooth deformation; however, the CNT–PP gears exhibited only tooth wear towards the end of the test (5.76×10^5 cycles).

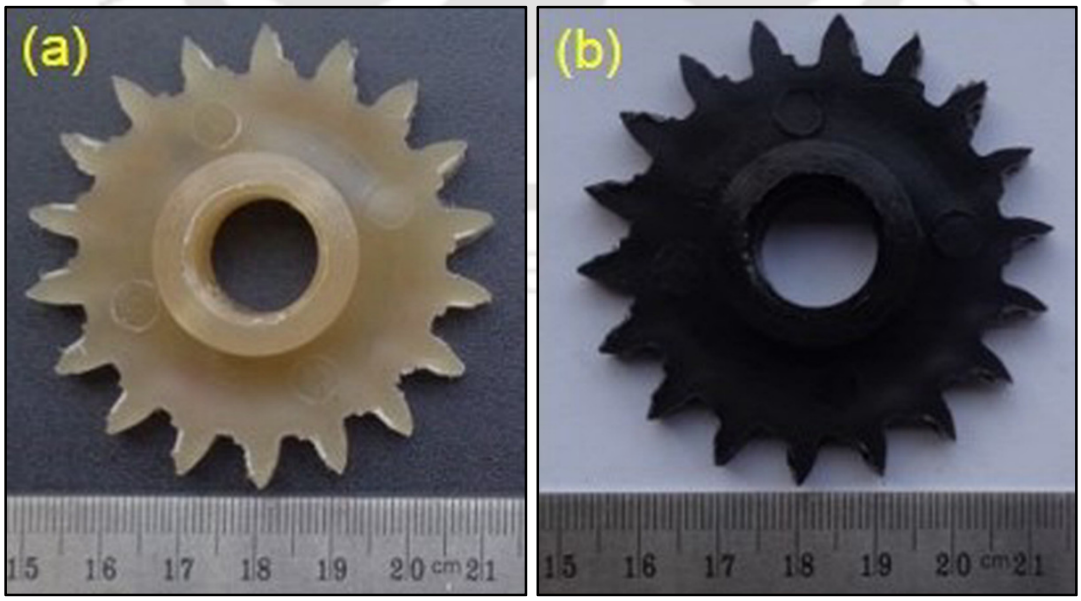

Figure 9.12 Test gear failure showing all teeth, 2 Nm: (a) polypropylene and (b) 1 wt% CNT–PP

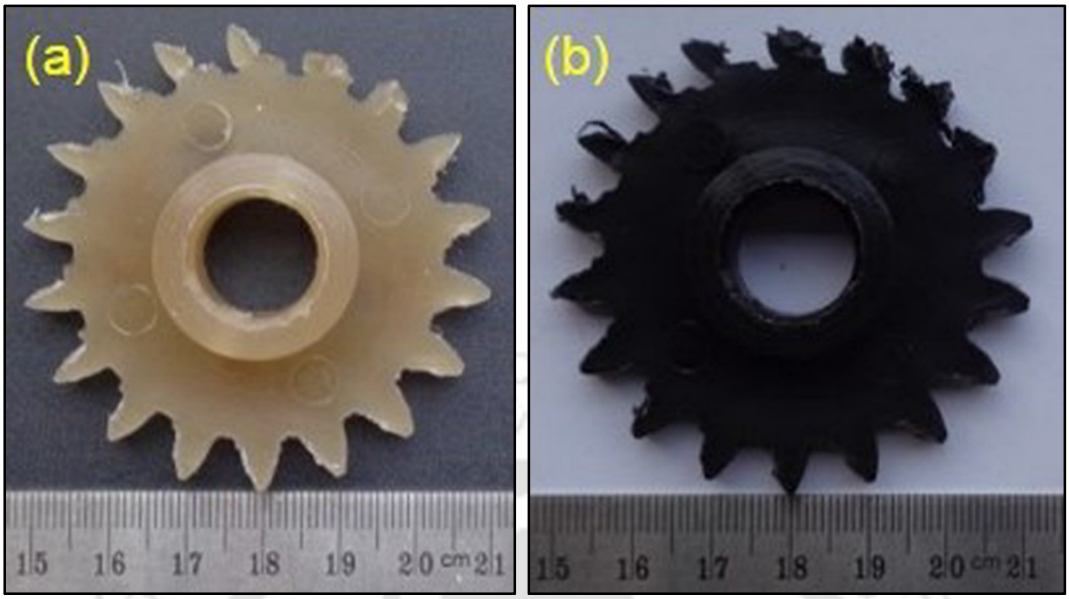

Figure 9.13 Test gear failure showing all teeth, 3 Nm: (a) polypropylene and (b) 1 wt% CNT–PP

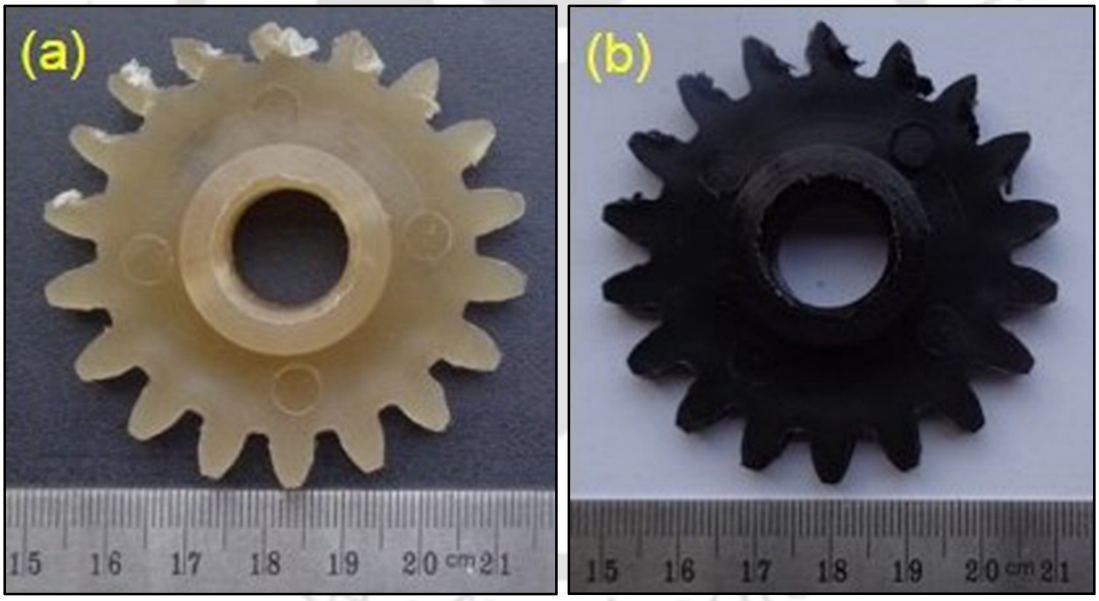

Figure 9.14 Test gear failure showing all teeth, 4 Nm: (a) polypropylene and (b) 1 wt% CNT–PP

Figure 9.12–Figure 9.14 shows the test gear failure at various loads. At lower loads (2 Nm) all the tooth exhibited almost uniform wear (Figure 9.12(a–b)). However, at higher loads (3 and 4 Nm), tooth deformation was observed in consecutive teeth (Figure 9.13(a–b) and Figure 9.14(a–b)). Soon after the failure commencement (indicated by the change in sound and abrupt temperature

increase), the tests were stopped. The repetitive tooth deformation and magnitude of loading caused tooth deformation at higher loads (3–4 Nm).

9.10 SUMMARY

Injection-moulded unreinforced and CNT–PP composite (1 wt%) gear was developed using the melt compounding technique. The durability of the developed unreinforced and composite gear was evaluated using power absorption test rig and the following major conclusions were arrived

- Injection-moulded polypropylene and CNT–PP gears exhibited tooth wear at lower loads (2–2.5 Nm) and tooth deformation at higher loads (3–3.5 Nm).
- Injection-moulded CNT–PP gears did not exhibit any measurable variation of gear surface temperature at lower loads (2–2.5 Nm) compared to polypropylene gears. However, the wear resistance of CNT–PP gears was higher than polypropylene gears.
- In the initial testing stage, both test gears (polypropylene and CNT–PP) exhibited less wear near the pitch region and more wear near the tip and root regions caused by the increased sliding velocity at these regions.
- The transmission efficiency of the CNT–PP gear with the steel gear increased by 1%–1.5% for the test conditions.
- CNT–PP gears exhibited a surface temperature drop of 5–10 °C at higher loads (3–3.5 Nm) and exhibited 30%–80% increased life compared to the polypropylene gears.

CHAPTER 10

SUMMARY AND CONCLUSIONS

10.1 SUMMARY

Performance evaluation of injection-moulded symmetric and asymmetric polypropylene gears were carried out using in-house developed power absorption gear test rig. The effect of manufacturing process and surface roughness of mating gear and environment was evaluated on the performance of polypropylene gear. The net surface temperature of test gears and torque available at both test and standard gears were continuously measured. Periodically gear tooth thickness was measured. Weight and surface roughness of the test gear before and after test was measured. Worn out gear tooth surfaces and failure morphology of the test gears were analysed. Various carbon nano-tube reinforced polypropylene composites were developed, mechanical, tribological, and thermal properties were evaluated. Following major conclusion were drawn from these investigations.

10.2 CONCLUSIONS

- Injection-moulded polypropylene gears exhibited improved performance under compressed air environment. A significant reduction (15–23%) of gear tooth surface temperature and improved wear resistance (50–100%) and slightly improved (2%) transmission efficiency was observed.
- Injection-moulded polypropylene gears were paired with conventional hobbed steel gear and wire-cut electric discharge machined (WEDM) steel gear. Recast layer formed on the surface of WEDM gear generated more heat due to the poor surface topology and increased

hardness. Consequently, wear resistance of polypropylene gear decreased by 78%–84% when paired with WEDM gear compared to the hobbed gear. At higher loads, polypropylene gears exhibited thermal fatigue failure and excessive wear when paired with WEDM and hobbed steel gear respectively.

- Injection-moulded asymmetric polypropylene gears were evaluated by pairing with three asymmetric steel gears (newly manufactured steel gear, steal gear run against polymer gear for 5×10^5 cycles and steal gear run against polymer gear for 10×10^5 cycles having different surface roughness). The net surface temperature of the polypropylene gears increased about 20 °C when the surface roughness of steel gears increased from 2 to 4 μm.
- Both symmetric (20/20) and asymmetric (34/20) gears exhibited wear failure at lower loads (2–2.5 Nm) and plastic tooth deformation at higher loads (3–4.5 Nm). The contact ratios of symmetric and asymmetric gears are 1.53 and 1.25 respectively. The radial distance of the HPSTC point increased for the asymmetric gear (29.41 mm) compared to the symmetric gear (27.88 mm). This reduced contact ratio and increased radial distance of the HPSTC point contributes for the inferior performance of asymmetric gear at all the tested conditions (2–4.5 Nm). Static gear tooth deflection revels superior bending load carrying capability of asymmetric gear compared to the symmetric gear.
- The yield strength and Young's modulus increased with the increase in CNT content. However, 1 wt% CNT–PP material exhibited superior hardness, least friction, and wear loss compared to the investigated test materials. Beyond this CNT amount, agglomeration contributes to deteriorate poor tribological performance.
- Injection-moulded polypropylene and 1 wt% CNT–PP gears exhibited wear failure at lower loads (2–2.5 Nm) and plastic tooth deformation at higher loads (3–4.5 Nm). 1 wt% CNT–

PP gears exhibited 30%–80% increased life compared to the polypropylene gears. 1 wt% CNT–PP gears exhibited lower surface temperature (5–10 °C), and slightly higher transmission efficiency (1–1.5%) compared to the polypropylene gears.

10.3 FUTURE SCOPE

- In the present investigation, surface durability of injection-moulded polypropylene gear was evaluated under dry condition using power absorption gear test rig. In future, this test rig can be modified to run under liquid lubricant condition, so that effect of lubrication can be evaluated.
- In the present investigation, static load was applied in the gear tooth deflection test rig to evaluate bending load carrying capacity of symmetric and asymmetric gears. In the future, this test rig can be modified to apply fatigue load so that the bending fatigue performance can be evaluated.

REFERENCES

1. **Abbasi S, Teimourimanesh S, Vernersson T, Sellgren U, Olofsson U and Lunden R** (2014) Temperature and thermoelastic instability at tread braking using cast iron friction material. *Wear*, Elsevier **314**(1-2): 171–180.
2. **AGMA 908-B89** (1989) *AGMA information sheet*.
3. **Akkurt S** (1995) On the effect of surface roughness on wear of acetal-metal gear pairs. *Wear*, **184**(2): 107–109.
4. **Ali MY, Karim ANM, Adesta EYT, Ismail AF, Abdullah AA and Idris MN** (2010) Comparative study of conventional and micro WEDM based on machining of meso/micro sized spur gear. *International Journal of Precision Engineering and Manufacturing*, **11**(5): 779–784.
5. **Alipiev O** (2011) Geometric design of involute spur gear drives with symmetric and asymmetric teeth using the Realized Potential Method. *Mechanism and Machine Theory*, **46**(1): 10–32.
6. **Barrett TS, Stachowiak GW and Batchelor AW** (1992) Effect of roughness and sliding speed on the wear and friction of ultra-high molecular weight polyethylene. *Wear*, **153**(2): 331–350.
7. **Bergseth E, Sjoberg S and Bjorklund S** (2012) Influence of real surface topography on the contact area ratio in differently manufactured spur gears. *Tribology International*, **56**: 72–80.
8. **Bernasconi A, Davoli P, Basiole A and Filippi A** (2007) Effect of fibre orientation on the fatigue behaviour of a short glass fibre reinforced polyamide-6. *International Journal of Fatigue*, **29**(2): 199–208.

9. **Bernasconi A, Conrado E and Hine P** (2015) An experimental investigation of the combined influence of notch size and fibre orientation on the fatigue strength of a short glass fibre reinforced polyamide 6. *Polymer Testing*, **47**: 12–21.
10. **Bonny K, Baets PD, Vleugels J, Salehi A, Van der Biest O, Lauwers B and Liu W** (2008) Influence of electrical discharge machining on tribological behavior of ZrO2-TiN composites. *Wear*, **265**(11-12): 1884–1892.
11. **Bonny K, Baets PD, Ost W, Vleugels J, Huang S, Lauwers B and Liu W** (2009) Influence of electrical discharge machining on the reciprocating sliding friction and wear response of WC-Co cemented carbides. *Wear*, **266**(1-2): 84–95.
12. **Bravo A, Koffi D, Toubal L and Erchiqui F** (2015) Life and damage mode modeling applied to plastic gears. *Engineering Failure Analysis*, **58**(1): 113–133.
13. **Breeds AR, Kukureka SN, Mao K, Walton D and Hooke CJ** (1993) Wear behaviour of acetal gear pairs. *Wear*, **166**(1): 85–91.
14. **Cai H, Yan F and Xue Q** (2004) Investigation of tribological properties of polyimide/carbon nanotube nanocomposites. *Materials Science and Engineering A*, **364**(1-2): 94–100.
15. **Cavdar K, Karpat F and Babalik FC** (2005) Computer aided analysis of bending strength of involute spur gears with asymmetric profile. *Journal of Mechanical Design*, **127**(3): 477–484.
16. **Chen D, Wang R, Tjiu WW and Liu T** (2011) High performance polyimide composite films prepared by homogeneity reinforcement of electrospun nanofibers. *Composites Science and Technology*, **71**(13): 1556–1562.
17. **Chen WX, Li F, Han G, Xia JB, Wang LY, Tu JP and Xu ZD** (2003) Tribological

behavior of carbon-nanotube-filled PTFE composites. *Tribology Letters*, **15**(3): 275–278.

18. **Cho M** (2008) The Flexural and tribological behavior of multi-walled carbon nanotube–reinforced polyphenylene sulfide composites. *Materials Transactions*, **49**(12): 2801–2807.
19. **Cirino M, Friedrich K and Pipes RB** (1988) The effect of fiber orientation on the abrasive wear behavior of polymer composite materials. *Wear*, **121**(2): 127–141.
20. **Costopoulos T and Spitas V** (2009) Reduction of gear fillet stresses by using one-sided involute asymmetric teeth. *Mechanism and Machine Theory*, **44**(8): 1524–1534.
21. **Crippa G and Davoli P** (1995) Comparative fatigue resistance of fiber reinforced nylon 6 gears. *Journal of Mechanical Design*, **117**(1): 193–198.
22. **Dixit US, Sarma DK and Davim JP** (2012) *Environmentally friendly machining*. *Springer-Verlag New York*.
23. **Duan Y, Cong P, Liu X and Li T** (2009) Friction and wear of polyphenylene sulphide (PPS), polyethersulfone (PES), and polysulfone (PSU) under different cooling conditions. *Journal of Macromolecular Science, Part B: Physics*, **48**(3): 604–616.
24. **Duzcukoglu H** (2009) PA 66 spur gear durability improvement with tooth width modification. *Materials and Design*, **30**(4): 1060–1067.
25. **Duzcukoglu H** (2009) Study on development of polyamide gears for improvement of load-carrying capacity. *Tribology International*, **42**(8): 1146–1153.
26. **Eiss NS, Wood KC, Herold JA and Smyth KA** (1979) Model for the transfer of polymer to rough , hard surfaces. *Journal of Lubrication Technology*, **101**(78): 212–218.
27. **Ekwaro-Osire S, Durukan I and Alemayehu FM** (2011) Experimental and probabilistic analysis of asymmetric gear tooth. In: *Proceedings of the SEM Annual Conference*, 207–212.

28. **Ersoy MS and Onder E** (2013) Mechanical and thermal behaviors of polypropylene - multi-walled carbon nanotube nanocomposite monofilaments. *Fibres and Textiles in Eastern Europe*, **21**(2(98)): 22–27.

29. **Franklin SE and Kraker A De** (2003) Investigation of counterface surface topography effects on the wear and transfer behaviour of a POM-20% PTFE composite. *Wear*, **255**(1-6): 766–773.

30. **Gandhi RA, Palanikumar K, Ragunath BK and Davim JP** (2013) Role of carbon nanotubes (CNTs) in improving wear properties of polypropylene (PP) in dry sliding condition. *Materials and Design*, **48**: 52–57.

31. **Goel A, Chawla KK, Vaidya UK, Chawla N and Koopman M** (2009) Characterization of fatigue behavior of long fiber reinforced thermoplastic (LFT) composites. *Materials Characterization*, **60**(6): 537–544.

32. **Guha D and Chowdhuri SKR** (1996) The effect of surface roughness on the temperature at the contact between sliding bodies. *Wear*, **197**(1-2): 63–73.

33. **Gupta K and Jain NK** (2014) On surface integrity of miniature spur gears manufactured by wire electrical discharge machining. *International Journal of Advanced Manufacturing Technology*, **72**(9): 1735–1745.

34. **Hakimian E and Sulong AB** (2012) Analysis of warpage and shrinkage properties of injection-molded micro gears polymer composites using numerical simulations assisted by the Taguchi method. *Materials and Design*, **42**: 62–71.

35. **Hisakado T** (1977) The influence of surface roughness on abrasive wear. *Wear*, **41**(1): 179–190.

36. **Hohn B-R, Michaelis K and Kreil O** (2006) Influence of surface roughness on pressure

distribution and film thickness in EHL-contacts. *Tribology International*, **39**(12): 1719–1725.

37. **Hooke CJ, Mao K, Walton D, Breeds AR and Kukureka SN** (1993) Measurement and prediction of the surface temperature in polymer gears and its relationship to gear wear. *Journal of Tribology*, **115**(1): 119–124.
38. **Hoskins TJ, Dearn KD, Chen YK and Kukureka SN** (2014) The wear of PEEK in rolling-sliding contact - Simulation of polymer gear applications. *Wear*, **309**(1-2): 35–42.
39. **Hossan MR and Hu Z** (2008) Strength evaluation of polymer composite spur gear by finite element analysis. In: *Proceedings of IMECE2008*, 66617 (1–8).
40. **Imrek H** (2009) Performance improvement method for Nylon 6 spur gears. *Tribology International*, **42**(3): 503–510.
41. **Kang CH, Yoon KH, Park Y-B, Lee D-Y and Jeong S-S** (2010) Properties of polypropylene composites containing aluminum/multi-walled carbon nanotubes. *Composites Part A: Applied Science and Manufacturing*, **41**(7): 919–926.
42. **Kapelevich A** (2000) Geometry and design of involute spur gears with asymmetric teeth. *Mechanism and Machine Theory*, **35**(1): 117–130.
43. **Karimpour M, Dearn KD and Walton D** (2010) A kinematic analysis of meshing polymer gear teeth. *Proceedings of the Institution of Mechanical Engineers, Part L: Journal of Materials Design and Applications*, **224**(3): 101–115.
44. **Karpat F and Ekwaro-Osire S** (2008) Influence of tip relief modification on the wear of spur gears with asymmetric teeth. *Tribology Transactions*, **51**(5): 581–588.
45. **Karpat F, Ekwaro-Osire S, Cavdar K and Babalik FC** (2008) Dynamic analysis of involute spur gears with asymmetric teeth. *International Journal of Mechanical Sciences*,

50(12): 1598–1610.

46. **Karpat F, Ekwaro-Osire S and Khandaker MPH** (2008) Probabilistic analysis of MEMS asymmetric gear tooth. *Journal of Mechanical Design*, **130**(4): 042306 (1–6).
47. **Kim CH** (2006) Durability improvement method for plastic spur gears. *Tribology International*, **39**(11): 1454–1461.
48. **Kim JY, Kim DK and Kim SH** (2009) Effect of modified carbon nanotube on physical properties of thermotropic liquid crystal polyester nanocomposites. *European Polymer Journal*, **45**(2): 316–324.
49. **Kim SH, Shin MC, Byun JW, Hwan OK and Chu CN** (2012) Efficiency prediction of worm gear with plastic worm wheel. *International Journal of Precision Engineering and Manufacturing*, **13**(2): 167–174.
50. **Kim SS, Shin MW and Jang H** (2012) Tribological properties of short glass fiber reinforced polyamide 12 sliding on medium carbon steel. *Wear*, Elsevier B.V. **274-275**: 34–42.
51. **Kirupasankar S, Gurunathan C and Gnanamoorthy R** (2012) Transmission efficiency of polyamide nanocomposite spur gears. *Materials and Design*, **39**: 338–343.
52. **Koffi D, Gauvin R and Yelle H** (1985) Heat generation in thermoplastic spur gears. *Journal of Mechanisms Transmissions and Automation in Design*, **107**(1): 31–36.
53. **Kumar P, Kommogi RK and Senthilvelan S** (2009) Injection molded asymmetric spur gear - development and preliminary performance evaluation. *International Journal of Plastics Technology*, **13**(2): 186–192.
54. **Kumar S, Singh R, Singh TP and Sethi BL** (2009) Surface modification by electrical discharge machining: A review. *Journal of Materials Processing Technology*, **209**(8): 3675–

3687.

55. **Kumar VS, Muni DV and Muthuveerappan G** (2008) Optimization of asymmetric spur gear drives to improve the bending load capacity. *Mechanism and Machine Theory*, **43**(7): 829–858.

56. **Kurokawa M, Uchiyama Y and Nagai S** (1999) Performance of plastic gear made of carbon fiber reinforced poly- ether-ether-ketone. *Tribology International*, **32**(9): 491–497.

57. **Kurokawa M, Uchiyama Y and Nagai S** (2000) Performance of plastic gear made of carbon fiber reinforced poly-ether-ether-ketone: Part 2. *Tribology International*, **33**(10): 715–721.

58. **Kurokawa M, Uchiyama Y and Nagai S** (2000) Tribological properties and gear performance of polyoxymethylene composites. *Journal of Tribology*, **122**(4): 809–814.

59. **Kurokawa M, Uchiyama Y, Iwai T and Nagai S** (2003) Performance of plastic gear made of carbon fiber reinforced polyamide 12. *Wear*, **254**(5-6): 468–473.

60. **Langford JI and Wilson AJC** (1978) Scherrer after sixty years: A survey and some new results in the determination of crystallite size. *Journal of Applied Crystallography*, **11**(2): 102–113.

61. **Lee SM, Shin MW and Jang H** (2014) Effect of carbon-nanotube length on friction and wear of polyamide 6,6 nanocomposites. *Wear*, **320**: 103–110.

62. **Letzelter E, Guingand M, Vaujany JPD and Schlosser P** (2010) A new experimental approach for measuring thermal behaviour in the case of nylon 6/6 cylindrical gears. *Polymer Testing*, **29**(8): 1041–1051.

63. **Li W, Wood A, Weidig R and Mao K** (2011) An investigation on the wear behaviour of dissimilar polymer gear engagements. *Wear*, **271**(9-10): 2176–2183.

64. **Lin A-D and Kuang JH** (2008) Dynamic interaction between contact loads and tooth wear of engaged plastic gear pairs. *International Journal of Mechanical Sciences*, **50**(2): 205–213.

65. **Litvin FL, Lian Q and Kapelevich AL** (2000) Asymmetric modified spur gear drives-reduction of nosise, localiztion of contact, simulation of meshing and stress analysis. *Computer Methods in Applied Mechanics and Engineering*, **188**(1-3): 363–390.

66. **Litwin W** (2011) Influence of surface roughness topography on properties of water-lubricated polymer bearings: experimental research. *Tribology Transactions*, **54**(3): 351–361.

67. **Liu M, Zhang C, Tjiu WW, Yang Z, Wang W and Liu T** (2013) One-step hybridization of graphene nanoribbons with carbon nanotubes and its strong-yet-ductile thermoplastic polyurethane composites. *Polymer*, **54**(12): 3124–3130.

68. **Llanes L, Casas B, Idanez E, Marsal M and Anglada M** (2004) Surface integrity effects on the fracture resistance of electrical-discharge-machined WC-Co cemented carbides. *Journal of the American Ceramic Society*, **87**(9): 1687–1693.

69. **Loos MR, Yang J, Feke DL, Manas-Zloczower I, Unal S and Younes U** (2013) Enhancement of fatigue life of polyurethane composites containing carbon nanotubes. *Composites: Part B*, **44**(1): 740–744.

70. **Mao K** (2007) A new approach for polymer composite gear design. *Wear*, **262**(3-4): 432–441.

71. **Mao K, Li W, Hooke CJ and Walton D** (2010) Polymer gear surface thermal wear and its performance prediction. *Tribology International*, **43**(1-2): 433–439.

72. **Mao K, Langlois P, Hu Z, Alharbi K, Xu X, Milson M, Li W, Hooke CJ and Chetwynd**

D (2015) The wear and thermal mechanical contact behaviour of machine cut polymer gears. *Wear*, **332-333**: 822–826.

73. **Marimuthu P and Muthuveerappan G** (2014) Effect of addendum height and teeth number on asymmetric normal contact ratio spur gear based on load sharing. *Universal Journal of Mechanical Engineering*, **2**(4): 132–136.
74. **Marimuthu P and Muthuveerappan G** (2014) Influence of pressure angle on load sharing based stresses in asymmetric normal contact ratio spur gear drives. *Applied Mechanics and Materials*, **465-466**: 1229–1233.
75. **Marimuthu P and Muthuveerappan G** (2016) Design of asymmetric normal contact ratio spur gear drive through direct design to enhance the load carrying capacity. *Mechanism and Machine Theory*, **95**: 22–34.
76. **Marimuthu P and Muthuveerappan G** (2016) Investigation of load carrying capacity of asymmetric high contact ratio spur gear based on load sharing using direct gear design approach. *Mechanism and Machine Theory*, **96**: 52–74.
77. **Menezes PL, Kishore and Kailas S V.** (2008) Influence of roughness parameters on coefficient of friction under lubricated conditions. *Sadhana - Academy Proceedings in Engineering Sciences*, **33**(3): 181–190.
78. **Mertens AJ and Senthilvelan S** (2015) Durability enhancement of polymer gear using compressed air cooling. *Proceedings of the Institution of Mechanical Engineers, Part L: Journal of Materials: Design and Applications*, **230**(2): 515–525.
79. **Mohan NA and Senthilvelan S** (2014) Preliminary bending fatigue performance evaluation of asymmetric composite gears. *Mechanism and Machine Theory*, **78**: 92–104.
80. **Moorthy V and Shaw BA** (2013) An observation on the initiation of micro-pitting damage

in as-ground and coated gears during contact fatigue. *Wear*, **297**(1-2): 878–884.

81. **Muller MT, Krause B, Kretzschmar B and Potschke P** (2011) Influence of feeding conditions in twin-screw extrusion of PP/MWCNT composites on electrical and mechanical properties. *Composites Science and Technology*, **71**(13): 1535–1542.
82. **Muni DV, Kumar VS and Muthuveerappan G** (2007) Optimization of asymmetric spur gear drives for maximum bending strength using direct gear design method. *Mechanics Based Design of Structures and Machines*, **35**(2): 127–145.
83. **Murray JW and Clare AT** (2012) Repair of EDM induced surface cracks by pulsed electron beam irradiation. *Journal of Materials Processing Technology*, **212**(12): 2642–2651.
84. **Murray JW, Walker JC and Clare AT** (2014) Nanostructures in austenitic steel after EDM and pulsed electron beam irradiation. *Surface and Coatings Technology*, **259**: 465–472.
85. **Nakatsuji T and Mori A** (1999) Pitting durability of electrolytically polished medium carbon steel gears - succeeding report. *Tribology Transactions*, **42**(2): 393–400.
86. **Novais RM, Simon F, Paiva MC and Covas JA** (2012) The influence of carbon nanotube functionalization route on the efficiency of dispersion in polypropylene by twin-screw extrusion. *Composites Part A: Applied Science and Manufacturing*, **43**(12): 2189–2198.
87. **Ovaert TC and Ramachandra S** (1995) The effect of controlled counterface topography on polymer transfer and wear. *International Journal of Machine Tools and Manufacture*, **35**(2): 311–316.
88. **Paik P and Kar KK** (2009) Polypropylene nanosphere: particle size and crystal structure. *International Journal of Plastics Technology*, **13**(1): 68–82.

89. **Pan Y, Li L, Chan SH and Zhao J** (2010) Correlation between dispersion state and electrical conductivity of MWCNTs/PP composites prepared by melt blending. *Composites Part A: Applied Science and Manufacturing*, **41**(3): 419–426.

90. **Park HJ, Kim J, Seo Y, Shim J, Sung MY and Kwak S** (2013) Wear behavior of in situ polymerized carbon nanotube/ultra high molecular weight polyethylene composites. *Macromolecular Research*, **21**(9): 965–970.

91. **Patti A, Barretta R, Sciarra FMD, Mensitieri G, Menna C and Russo P** (2015) Flexural properties of multi-wall carbon nanotube/polypropylene composites : Experimental investigation and nonlocal modeling. *Composite Structures*, **131**: 282–289.

92. **Pedersen NL** (2010) Improving bending stress in spur gears using asymmetric gears and shape optimization. *Mechanism and Machine Theory*, **45**(11): 1707–1720.

93. **Blau PJ (Ed.)** (1992) *ASM Handbook-Friction, Lubrication, and Wear Technology*. *ASM International*,.

94. **Pogacnik A and Tavcar J** (2015) An accelerated multilevel test and design procedure for polymer gears. *Materials and Design*, **65**: 961–973.

95. **Prashantha K, Soulestin J, Lacrampe MF, Claes M, Dupin G and Krawczak P** (2008) Multi-walled carbon nanotube filled polypropylene nanocomposites based on masterbatch route: Improvement of dispersion and mechanical properties through PP-g-MA addition. *Express Polymer Letters*, **2**(10): 735–745.

96. **Prashantha K, Soulestin J, Lacrampe MF, Krawczak P, Dupin G and Claes M** (2009) Masterbatch-based multi-walled carbon nanotube filled polypropylene nanocomposites: Assessment of rheological and mechanical properties. *Composites Science and Technology*, **69**(11-12): 1756–1763.

97. **Prashantha K, Soulestin J, Lacrampe MF, Lafranche E, Krawczak P, Dupin G and Claes M** (2009) Taguchi analysis of shrinkage and warpage of injection-moulded polypropylene/multiwall carbon nanotubes nanocomposites. *Express Polymer Letters*, **3**(10): 630–638.

98. **Roy S, Das T, Zhang L, Li Y, Ming Y, Ting S, Hu X and Yue CY** (2015) Triggering compatibility and dispersion by selective plasma functionalized carbon nanotubes to fabricate tough and enhanced Nylon 12 composites. *Polymer*, **58**: 153–161.

99. **Sandler J, Broza G, Nolte M, Schulte K, Lam Y-M and Shaffer MSP** (2003) Crystallization of carbon nanotube and nanofiber polypropylene composites. *Journal of Macromolecular Science, Part B*, **42**(3-4): 479–488.

100. **Sarma DK and Dixit US** (2007) A comparison of dry and air-cooled turning of grey cast iron with mixed oxide ceramic tool. *Journal of Materials Processing Technology*, **190**(1-3): 160–172.

101. **Senthilvelan S and Gnanamoorthy R** (2004) Damage mechanisms in injection molded unreinforced, glass and carbon reinforced nylon 66 spur gears. *Applied Composite Materials*, **11**(6): 377–397.

102. **Senthilvelan S and Gnanamoorthy R** (2004) Wear characteristics of injection-moulded unfilled and glass-filled nylon 6 spur gears. *Proceedings Of The Institution Of Mechanical Engineers, Part J: J. Engineering Tribology*, **218**(6): 495–502.

103. **Senthilvelan S and Gnanamoorthy R** (2006) Damping characteristics of unreinforced, glass and carbon fiber reinforced nylon 6/6 spur gears. *Polymer Testing*, **25**(1): 56–62.

104. **Senthilvelan S and Gnanamoorthy R** (2006) Effect of gear tooth fillet radius on the performance of injection molded Nylon 6/6 gears. *Materials and Design*, **27**(8): 632–639.

105. **Senthilvelan S and Gnanamoorthy R** (2006) Fiber reinforcement in injection molded nylon 6/6 spur gears. *Applied Composite Materials*, **13**(4): 237–248.

106. **Senthilvelan S and Gnanamoorthy R** (2007) Effect of rotational speed on the performance of unreinforced and glass fiber reinforced Nylon 6 spur gears. *Materials and Design*, **28**(3): 765–772.

107. **Senthilvelan S and Gnanamoorthy R** (2008) Influence of reinforcement on composite gear metrology. *Mechanism and Machine Theory*, **43**(9): 1198–1209.

108. **Senthilvelan S and Gnanamoorthy R** (2009) Efficiency of injection-moulded polymer composite spur gears. *Proceedings Of The Institution Of Mechanical Engineers, Part J: J. Engineering Tribology*, **223**(6): 925–928.

109. **Sharma VS, Dogra M and Suri NM** (2009) Cooling techniques for improved productivity in turning. *International Journal of Machine Tools and Manufacture*, **49**(6): 435–453.

110. **Sidhom H, Ghanem F, Amadou T, Gonzalez G and Braham C** (2013) Effect of electro discharge machining (EDM) on the AISI316L SS white layer microstructure and corrosion resistance. *International Journal of Advanced Manufacturing Technology*, **65**(1-4): 141–153.

111. **Solonin YM, Nenakhov A, Kostornov AG, Danilenko NI, Gorban VF and Karpets M** (2014) Fluoroplastic-multi-walled carbon nanotube composites: Structural, mechanical and tribotechnical characteristics. *Powder Metallurgy and Meatl Ceramics*, **52**(11-12): 620–631.

112. **Spitas V, Spitas C and Costopoulos T** (2009) Reduction of tooth fillet stresses using novel one-sided involute asymmetric gear design. *Mechanics Based Design of Structures and Machines*, **37**(2): 157–182.

113. **Sung N-H and Suh NP** (1979) Effect of fiber orientation on friction and wear of fiber

reinforced polymeric composites. *Wear*, **53**(1): 129–141.

114. **Suresha B, Ravi Kumar BN, Venkataramareddy M and Jayaraju T** (2010) Role of micro/nano fillers on mechanical and tribological properties of polyamide66/polypropylene composites. *Materials and Design*, **31**(4): 1993–2000.

115. **Taburdagitan M and Akkok M** (2006) Determination of surface temperature rise with thermo-elastic analysis of spur gears. *Wear*, **261**(5-6): 656–665.

116. **Teisuke B, Hiroshi S and Taku A** (2001) Wear of plastic spur gear made by injection molding. *Journal of Japanese Society of Tribologists*, **46**(11): 889–896.

117. **Thiebaud F and Gelin JC** (2009) Multiwalled carbon nanotube/polypropylene composites: Investigation of the melt processing by injection molding and analysis of the resulting mechanical behaviour. *International Journal of Material Forming*, **2**: 149–152.

118. **Torrance AA** (1997) A simple datum for measurement of the Abbott curve of a profile and its first derivative. *Tribology International*, **30**(3): 239–244.

119. **Tung SC and Cheng W** (1998) Simulation test of grease-lubricated steel-polymer interface of worm gear. *Tribology Transactions*, **41**(4): 537–542.

120. **Tzanakis I, Conte M, Hadfield M and Stolarski TA** (2013) Experimental and analytical thermal study of PTFE composite sliding against high carbon steel as a function of the surface roughness, sliding velocity and applied load. *Wear*, **303**(1-2): 154–168.

121. **Unal H and Mimaroglu A** (2012) Friction and wear performance of polyamide 6 and graphite and wax polyamide 6 composites under dry sliding conditions. *Wear*, **289**: 132–137.

122. **Walton D, Cropper AB, Weale DJ and Meuleman PK** (2002) The effciency and friction of plastic cylindrical gears Part 1: Influence of materials. *Proceedings of the Institution of*

Mechanical Engineers, Part J: Journal of Engineering Tribology, **216**(2): 75–78.

123. **Walton D, Cropper AB, Weale DJ and Meuleman PK** (2002) The effciency and friction of plastic cylindrical gears Part 2 : Influence of tooth geometry. *Proceedings of the Institution of Mechanical Engineers, Part J: Journal of Engineering Tribology*, **216**(2): 93–104.

124. **Wang C, Dong B, Gao GY, Xu MW and Li HL** (2008) A study on microhardness and tribological behavior of carbon nanotubes reinforced AMMA-CNTs copolymer nanocomposites. *Materials Science and Engineering A*, **478**(1-2): 314–318.

125. **Wang ZJ, Kwon DJ, Gu GY, Kim HS, Kim DS, Lee CS, DeVries KL and Park JM** (2013) Mechanical and interfacial evaluation of CNT/polypropylene composites and monitoring of damage using electrical resistance measurements. *Composites Science and Technology*, **81**: 69–75.

126. **Weale DJ, White J and Walton D** (1999) The effect of fiber orientation and distribution on the tooth stiffness of a polymer composite gear. *Journal of Reinforced Plastics and Composites*, **18**(5): 454–463.

127. **Wieleba W** (2002) The statistical correlation of the coefficient of friction and wear rate of PTFE composites with steel counterface roughness and hardness. *Wear*, **252**(9-10): 719–729.

128. **Wright NA and Kukureka S.** (2001) Wear testing and measurement techniques for polymer composite gears. *Wear*, **251**(1-12): 1567–1578.

129. **Xiao L, Bjorklund S and Rosen BG** (2007) The influence of surface roughness and the contact pressure distribution on friction in rolling/sliding contacts. *Tribology International*, **40**(4): 694–698.

130. **Xin F and Li L** (2012) The role of silane coupling agent in carbon nanotube/polypropylene composites. *Journal of Composite Materials*, **46**(26): 3267–3275.

131. **Yang BX, Shi JH, Pramoda KP and Goh SH** (2008) Enhancement of the mechanical properties of polypropylene using polypropylene-grafted multiwalled carbon nanotubes. *Composites Science and Technology*, **68**(12): 2490–2497.

132. **Yang HS, Kiziltas A and Gardner DJ** (2013) Thermal analysis and crystallinity study of cellulose nanofibril-filled polypropylene composites. *Journal of Thermal Analysis and Calorimetry*, **113**(2): 673–682.

133. **Yang Z, Dong B, Huang Y, Liu L, Yan FY and Li HL** (2005) A study on carbon nanotubes reinforced poly(methyl methacrylate) nanocomposites. *Materials Letters*, **59**(17): 2128–2132.

134. **Yang Z, Dong B, Huang Y, Liu L, Yan FY and Li HL** (2005) Enhanced wear resistance and micro-hardness of polystyrene nanocomposites by carbon nanotubes. *Materials Chemistry and Physics*, **94**(1): 109–113.

135. **Yazdani-Pedram M, Menzel C, Toro P, Quijada R, May-Pat A and Aviles F** (2013) Mechanical and thermal properties of multiwalled carbon nanotube/polypropylene composites using itaconic acid as compatibilizer and coupling agent. *Macromolecular Research*, **21**(2): 153–160.

136. **Yousef S, Khattab A, Zaki M and Osman TA** (2013) Wear characterization of carbon nanotubes reinforced polymer gears. *IEEE Transactions on Nanotechnology*, **12**(4): 616–620.

137. **Yousef S, Osman TA, Abdalla AH and Zohdy GA** (2015) Wear characterization of carbon nanotubes reinforced acetal spur, helical, bevel and worm gears using a TS universal test rig.

The Journal of The Minerals, Metals & Materials Society, **67**(12): 2892–2899.

138. **Yousef SS, Burns DJ and McKinlay W** (1973) Techniques for assessing the running temperature and fatigue strength of thermoplastic gears. *Mechanism and Machine Theory*, **8**(2): 175–185.

139. **Zaikov GE, Rakhimkulov AD, Lomakin SM, Dubnikova IL, Shchegolikhin AN and Davidov EY** (2010) Thermal degradation and combustion behavior of polypropylene/MWCNT composites. *AIP Conference Proceedings*, **1255**: 1–3.

LIST OF PUBLICATIONS BASED ON THE RESEARCH WORK

Refereed Journals

1. **A. Johnney Mertens** and **S. Senthilvelan**, Durability enhancement of polymer gear using compressed air cooling, *Proceedings of the Institution of Mechanical Engineers, Part L: Journal of Materials: Design and Applications*, **230**(2), 2016, 515–525.
2. **A. Johnney Mertens** and **S. Senthilvelan**, Durability of polymer gear- paired with steel gear manufactured by wire cut electric discharge machining and hobbing, *International Journal of Precision Engineering and Manufacturing*, **17**(2), 2016, 181–188.
3. **A. Johnney Mertens** and **S. Senthilvelan**, Durability of injection moulded asymmetric involute polymer spur gears, *International Journal of Powertrains*, **5**(3), 2016, 264–280.
4. **A. Johnney Mertens, Prateek Kumar** and **S. Senthilvelan**, The effect of the mating gear surface over the durability of injection-molded polypropylene spur gears, *Proceedings of the Institution of Mechanical Engineers, Part J: Journal of Engineering Tribology,* **230**(12), 2016, 1401–1414.
5. **A. Johnney Mertens and S. Senthilvelan**, Mechanical and tribological properties of carbon nanotube reinforced polypropylene composites, *Proceedings of the Institution of Mechanical Engineers, Part L: Journal of Materials: Design and Applications, Published online before print April 4, 2016, doi:10.1177/1464420716642620.*
6. **A. Johnney Mertens and S. Senthilvelan**, Surface durability of injection-moulded PP-CNT spur gear, *Proceedings of the Institution of Mechanical Engineers, Part L: Journal of Materials: Design and Applications, Published online before print June 12, 2016, doi:10.1177/1464420716654308.*

PRESENTATION IN CONFERENCES

1. **Saurav Verma, A. Johnney Mertens** and **S. Senthilvela**n, A new method to improve service life of polymer based gears, APA International Conference on Polymers: Vision & Innovations APA-2014, India Habitat Centre, New Delhi, February 19-21, 2014 (Poster Presentation).

2. **A. Johnney Mertens** and **S. Senthilvelan**, Adhesive wear performance of PP/MWCNT composites, International Conference on Advances in Manufacturing and Materials Engineering, AMME 2014, National Institute of Technology Karnataka, Surathkal, March 27-29, 2014, CD Proceedings. ***Also published in Procedia Materials Science, 5, 2014, 1192-1197.***

3. **A. Johnney Mertens** and **S. Senthilvelan**, Abrasive wear performance of CNT/PP composites, International Mechanical Engineering Congress 2014, National Institute of Technology Tiruchirappalli, June 13-15, 2014. ***Also Published in Applied Mechanics and Materials, 592-594, 2014, 1262-1266.***

4. **A. Johnney Mertens** and **S. Senthilvelan**, Effect of mating metal gear surface texture on the polymer gear surface temperature, 4th International Conference on Materials Processing and Characterization, Gokaraju Rangaraju Institute of Engineering and Technology, Hyderabad, March 14-15, 2015. **Also Published in *Material Today: Proceedings*, 2, 2015, 1763-1769.**

CURRICULUM VITAE

1. Name : **A. Johnney Mertens**

2. Date of Birth : 22.06.1989

3. Permanent Address : 82, J. J. Mansion,
Uppu Keni Vinayagar Kovil (via),
AARTHI Theatre Road
Y. M. R. Patty,
Dindigul – 624001
Ph. No.: +91-8473994769, +91-9566377564
Email: johnneymertens@gmail.com

4. Educational Qualifications:

2006–2010	**:**	**Bachelor of Engineering**
Institution	:	Panimalar Engineering College, Chennai–600123, India.
Specialization	:	Mechanical Engineering
2010–2012	**:**	**Master of Engineering**
Institution	:	Kongu Engineering College, Erode–638052, India
Specialization	:	Engineering Design
2012–2016	**:**	**Doctor of Philosophy**
Institution	:	Indian Institute of Technology Guwahati, Guwahati–781039, India
Registration Date	:	30.07.2012
Thesis Submission Date	:	15.07.2016
Defence Date	:	11.11.2016

DOCTORAL COMMITTEE

Guide	:	**Dr. S. Senthilvelan** Associate Professor Department of Mechanical Engineering
Chairperson	:	**Prof. P. S. Robi** Professor Department of Mechanical Engineering
Members	:	**Dr. S. Kanagaraj** Associate Professor Department of Mechanical Engineering
		Prof. G. Pugazhenthi Professor Department of Chemical Engineering